ESSAYS ON RIVER MECHANICS

Presented by the Graduate Students
in CE 717 River Mechanics (Spring 1986)

Instructor: P.Y. Julien

May 1986

CER 85 - 86 PYJ-28

FOREWORD

I am pleased to honor the work of my graduate students in this report. This semester, the evaluation was split in two major parts: 1) one final test, and 2) one major project. The requirements for the second part were as follows:

1) select a topic relevant to river mechanics and sediment transport,

2) conduct a mini literature review including papers published in the past five years,

3) compare new methodologies with those detailed in textbooks on either a theoretical basis or through comparison with an appropriate data set,

4) write a 40 page report and discuss the major findings in a 30-45 minute oral presentation,

5) summarize the analysis and results in a 12 page paper following the ASCE editorial standards.

The purpose of this project was to meet the following objectives:

1) familiarize with the recent literature and new methodologies not available in textbooks,

2) compare new and older methods and judge of the advancement of engineering technology or this topic,

3) structure the material,

4) develop skills to point out the most important elements of one's analysis,

5) share interesting results with the other students through an oral presentation and a written paper enclosed herein.

Not only the students showed greated enthusiasm in this class but the reader will certainly agree with me that the objectives were met with great success. I am personally very impressed with the overall quality of the work presented and can only encourage them to pursue advanced studies in this field.

P. Y. Julien

TABLE OF CONTENTS

MEANDERING AND BRAIDING OF RIVERS

by Mohsen M. Ahmed[1]

ABSTRACT: A hydrodynamic stability analysis is presented by a two-dimensional mathematical model for a dune-covered bed of an alluvial channel with a nonerodible bank material to investigate the instability of an originally straight channel and its tendency to meander or braid. The model predicts whether the channel meanders, braids, or remains straight.

Introduction

Channel patterns straight, meandering, and braided have attracted the attention of those who are conscious of their natural environment. In particular, scientists have been fascinated and puzzelled as to why straight alluvial streams tend to meander its course.

Meander initiation in alluvial rivers has been analyzed by some investigators as an instability problem. Callander (1) concluded that channels with loose boundaries are unstable, with the possible exception of channels just beyond the threshold of grain movement. Engelund and Skovgaard (5) presented a three-dimensional model for a flow in a fixed wall rectangular channel with its bed formed of non-cohesive sediment. Their analysis indicated that for given hydraulic resistance and depth, the river will exhibit meandering if the width is smaller than some threshold value B_*, while a wider river will braid in two or more courses. Olesen (9) in his mathematical model for horizontal two-dimensional flow showed that the depth width ratio has a decisive influence on the development of alternate bars with a wavelength of about 3-4 times the width.

---

[1]Graduate Student, Civil Engineering Department, Colorado State University, Fort Collins, Colorado.

Presented herein is a linearized stability analysis that has been introduced by Fredsøe (8) for a two-dimensional flow in a wide, shallow, straight alluvial stream with a nonerodible bank material which is a crude assumption for the discussion of meander initiation. The mathematical model was based on the assumption that the migration velocity of the developing alternate bars is very small and the flow adapts relatively fast to bed level changes, i.e., quasi-steady flow. The sediment transport model differentiated between sediment which is transported as a bed load, and that transported as a suspended load, the model includes, as well, the effect of transverse bed slope. Results of the linear stability analysis classified channels as either stable or unstable, i.e., tend to meander or braid.

Basic Flow Equations

If the flow is considered to be taking place on a perturbed bed, i.e., the plane bed is deformed to a position h above its original position. The character of meandering requires a double-periodic disturbance, so that h is given by

$$h = h_0 \cos(k_3 x_3) \exp(ik_1 x_1) = h_0 E \quad \ldots\ldots(1)$$

in which x_1 and x_3 are the longitudinal and transverse directions, respectively; h_0 is the amplitude of the perturbation, and k_1 and k_3 are the wave numbers in the x_1 and x_3 directions.

For steady-state condition, the following constitute the system of governing equations:

Momentum equation, x_1-direction

$$U_1(\partial U_1/\partial x_1)+U_3(\partial U_1/\partial x_3) = gI_0-\tau/\rho y-g(\partial(h+y)/\partial x_1) \quad \ldots\ldots(2)$$

Momentum equation, x_3-direction

$$U_1(\partial U_3/\partial x_1)+U_3(\partial U_3/\partial x_3) = -(U_3/U_1)(\tau/\rho y)-g(\partial(h+y)/\partial x_3) \quad \ldots\ldots(3)$$

Flow continuity equation

$$\partial/\partial x_1(U_1 y)+\partial/\partial x_3(U_3 y) = 0 \quad \ldots\ldots(4)$$

where U_1 and U_3 are the velocity components in the x_1 and x_3 directions, y is the local depth, g the acceleration of gravity, ρ is the density of water, I_0 the undisturbed slope of the channel, and τ the local bed shear stress in the x_1-direction. The pressure term in Eq. (3) has been corrected as $g(\partial(h+y)/\partial x_3)$ instead of $g(\partial(h+y)/\partial x_1)$ as it was shown in

the original paper. The basic flow equations were based on the assumptions:

1) the velocity is uniformly distributed through depth of flow and the vertical component is zero.
2) the bed shear stress is parallel to the resultant velocity, V, these two assumptions imply that secondary currents have been ignored.
3) the pressure distribution is hydrostatic.

Eqs. (2)-(4) were linearized by introducing the following eqs.

$$U_1 = U+u_1,\ U_3 = u_3,\ y = D+\eta,\ \tau = \tau_b+\bar{\tau} \quad \ldots\ldots(5)$$

where U is flow velocity, D the depth of flow, and τ_b the bed shear stress in the unperturbed flow, while u_1, u_3, and $\bar{\tau}$ are perturbed terms which were assumed to be very small quantities and can be written as

$$u_1 = u_{10}E,\ \eta = \eta_0 E,\ \tau = \tau_0 E,\ u_3 = u_{30}\tan(k_3 x_3)E \quad \ldots\ldots(6)$$

substitution of Eqs. (1), (5), and (6) back into Eqs. (2)-(4) gives

$$Uik_1u_{10} = (\tau_b/\rho D)(\eta_0/D)-\tau_0/\rho D-ik_1g(h_0+\eta_0) \quad \ldots\ldots(7)$$

$$Uik_1u_{30} = -(u_{30}/U)(\tau_b/\rho D)+k_3g(h_0+\eta_0) \quad \ldots\ldots(8)$$

$$Uik_1\eta_0+Dik_1u_{10}+Du_{30}k_3 = 0 \quad \ldots\ldots(9)$$

In order to solve Eqs. (7)-(9) the author (8) suggested the following empirical relationship between the shear stress and some other hydraulic parameters in the form

$$\tau_0/\tau_b = \alpha(u_{10}/U) + \beta(\eta_0/D) \quad \ldots\ldots(10)$$

the coefficients and β will be defined in the next section. By making use of Eq. (10), Eqs. (7)-(9) were rewritten in the dimensionless forms as

$$(u_{10}/U)(F^2ik_1D+\alpha I_0)+(\eta_0/D)(ik_1D+I_0(\beta-1))+(h_0/D)(ik_1D) = 0 \quad \ldots\ldots(11)$$

$$(u_{30}/U)(F^2ik_1D+I_0)-(\eta_0/D)(K_3D)-(h_0/D)(k_3D) = 0 \quad \ldots\ldots(12)$$

$$(u_{10}/U)(ik_1D)+(u_{30}/U)(k_3D)+(\eta_0/D)(ik_1D) = 0 \quad \ldots\ldots(13)$$

in which $F^2 = U^2/gD$ is the Froude number. From Eqs. (11)-(13), the flow field can be calculated for given hydraulic parameters.

Hydraulic Resistance of Alluvial Channels

Alluvial channels are characterized by the formation of bed form, the most common one of which is the dunes which have a considerable sizes that they cannot be neglected as compared with the flow depth.

Dunes are also migrating downstream, their change in size and shape causes a continuous variation in the flow with time.

In that sense, flow in alluvial channels cannot be considered as either steady or uniform unless some basic assumptions are made. If dunes are considered as roughness elements, and the minor fluctuations of the cross-section are neglected, then the flow can be considered as uniform. Also, if the downstream migration which is causing a continuous variation to the flow is considered to be very slow, then the flow can be considered as steady. With these assumptions in mind, the problem was formulated using the fundamental concepts of steady uniform flow in open channels to derive the equations of resistance for a dune-covered bed as were introduced by Engelund and Hansen (4) by

$$\theta' = 0.06 + 0.4\,\theta^2 \qquad (14)$$

where θ' is the effective Shields parameter and θ is the Shields parameter which were given in the forms

$$\theta = \tau/(s-1)gd, \qquad \theta' = \theta\, y'/y \qquad (15)$$

in which s is the relative density of the sediment and d the diameter of the grains. y' was calculated by Einstein (2) as:

$$U/(gy'I)^{1/2} = 6 + 2.5 \ln (y'/k) \qquad (16)$$

where k is the sand roughness which was set equal to 2.5 d.

The coefficients α and β in Eq. (10) were found by the author as:

$$\alpha = (0.4\theta^2/\theta' + (1-0.8\theta^2/\theta')K)^{-1}, \quad \beta = K\alpha \qquad (17)$$

in which K was given by

$$K = -2.5(6+2.5 \ln(D'/2.5\alpha))^{-1}$$

Sediment Transport Model

The sediment transport model which Fredsøe used in his analysis differentiated between bed load and suspended load because the effect of the transverse slope acts only on the bed load, as the action of gravity on suspended particles has no transverse component. The model was originally presented by Engelund and Fredsøe (7) based on Bagnold's (1954) approach to the problem by introducing the concept of the tractive shear stress which, if exceeds a certain critical value, all particles in the upper layer are peeled off simultaneously and are dispersed in the fluid, some may go into suspension while others will be

transported as bed load, and similarly the subsequent layers, so that a stable bed could not exist.

The non-dimensional bed load transport, Φ_b, was found in this model under the assumption that the bed load is the transport of a certain fraction P(=probability) of the particles in a single layer to be

$$\Phi_b = \frac{q_b}{((s-1)gd^3)^{1/2}} = 5P(\theta'^{1/2} - 0.7\theta_c^{1/2}) \quad \ldots\ldots(18)$$

the expression for P was found to be

$$P = (1+(\frac{\pi/6 \tan \phi}{\theta' - \theta_c})^4)^{1/4} \quad \ldots\ldots(19)$$

in which tan ϕ is the dynamic friction coefficient, and the dynamic friction angle ϕ is usually taken as 27° for ordinary sand.

The vertical distribution of the concentration of suspended load has been introduced by Rouse (10) as

$$\frac{c}{c_a} = (\frac{D - x_2}{x_2} \cdot \frac{a}{D - a})^z \quad \ldots\ldots(20)$$

in which z is the Rouse number and is equal to $w/0.4U_f'$, c is the concentration of suspended sediment at x_2 from the bed, c_a is the concentration at reference level $x_2 = a$, and w is the fall velocity of the sediment particles. The main drawback of this formula is that c_a has to be known in advance before applying the formula.

The model predicts an expression for c_a as

$$c_a = 0.65/(1+\lambda_a^{-1})^3 \quad \ldots\ldots(21)$$

in which λ_a was defined as the linear concentration and given by

$$\lambda_a = (\frac{\theta' - \theta_c - \pi/6 \tan(\phi)P}{0.027 \, s \, \theta'})^{1/2} \quad \ldots\ldots(22)$$

It has to be noticed from Eqs. (21) and (22) that for a fixed value of θ_c, ϕ, and s, c_a depends only on θ' and this relationship is shown in Fig. 1, which indicates that c_a becomes too small for $\theta' < 0.1$ and approaches a constant value of 0.32 for large values of θ'.

When c_a is known, the transport rate q_s can be found from

$$q_s = \int_a^D cU \, dx_2 \quad \ldots\ldots(23)$$

where a was suggested to be taken equal to 2d.

From Eqs. (20) and (23), the suspended load was found by Einstein (2) to be

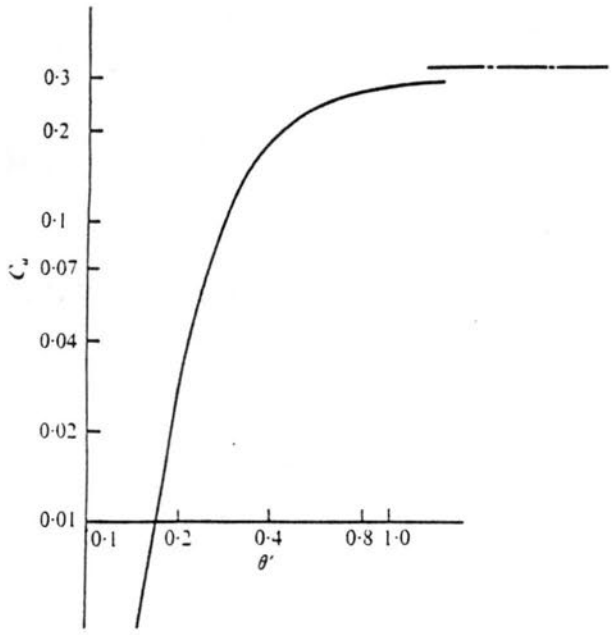

FIG. 1. Bed Concentration c_a versus θ', assuming s=2.65, θ_c = 0.05, and 0.27°. (After Engelund and Fredsøe, 1976).

$$q_s = 11.6\, c_a\, a\, U_f' \,(I_1 \ln(30D/k) + I_2) \quad \ldots\ldots(24)$$

where I_1 and I_2 are taken from the work charts published by Einstein.

Suspended Load Distribution

The non-uniform distribution of sediment concentration used in the stability analysis was based on the model introduced by Engelund (3) as an equilibrium between settling and diffusion under the assumption that the coefficient of eddy viscosity, ε, considered to be constant over the whole depth which is not true near the bed.

The unsteady, uniform distribution of sediment can be expressed by the continuity equation in the form

$$\frac{dc}{dt} = \omega \frac{\partial c}{\partial x_2} + \varepsilon \nabla^2 c \quad \ldots\ldots(25)$$

in which

$$\frac{dc}{dt} = \frac{\partial c}{\partial t} + U_1 \frac{\partial c}{\partial x_1} + U_2 \frac{\partial c}{\partial x_2} + U_3 \frac{\partial c}{\partial x_3} ,$$

$$\nabla^2 c = \frac{\partial^2 c}{\partial x_1^2} + \frac{\partial^2 c}{\partial x_2^2} + \frac{\partial^2 c}{\partial x_3^2} ,$$

ε is the eddy viscosity coefficient, given by $\varepsilon = 0.077 U_f\, y$.

In the case of steady, uniform flow Eq. (25) reduces to a single ordinary differential equation in the form

$$\omega c_o + \varepsilon \frac{dc_o}{dx_2} = 0 \qquad (26)$$

The distribution of the volume concentration c_o is then given by the solution of Eq. (26) in the form

$$c_o = c_{bo} \exp(-\omega x_2/\varepsilon) \qquad (27)$$

where c_{bo} is the nominal concentration at the bed level, and x_2 is the vertical coordinate. The values of c_o determined from Eq. (27) will be generally smaller than the actual concentrations because of the assumption of neglecting the vertical variation of the coefficient of eddy viscosity.

When the uniform flow is perturbed, the concentration is given by

$$c = c_o + \bar{c} \qquad (28)$$

where $\bar{c}$ is assumed to be very small quantity and given by

$$\bar{c} = \phi(x_2/D) \qquad (29)$$

Eq. (29) has been corrected by replacing $\bar{c}$ instead of c as it appeared in the original paper because it is not possible to come up with a negative value for c.

Substitute Eq. (28) into (25) and within the frame of first-order theory, Eq. (25) reduces to

$$U \frac{\partial \bar{c}}{\partial x_1} + u_2 \frac{\partial c_o}{\partial x_2} = \omega \frac{\partial \bar{c}}{\partial x_2} + \varepsilon \nabla^2 \bar{c} \qquad (30)$$

the first term in the right-hand side has been corrected to $\omega \frac{\partial \bar{c}}{\partial x_2}$ instead of $\omega \frac{\partial \bar{c}}{\partial x_3}$.

Put $u_2 = dh/dt = \partial h/\partial t + U(\partial h/\partial x_1)$ and set $(\partial h/\partial t)$ equal to zero for steady flow, and by making use of Eqs. (1), (28), and (29), Eq. (30) becomes

$$\phi'' + \frac{\omega D}{\varepsilon}\phi' - \phi\left(i\frac{Uk_1D^2}{\varepsilon} + (k_1D)^2 + (k_3D)^2\right) = -\frac{iUh_ok_1D^2c_o}{\varepsilon^2} \qquad (31)$$

It has to be noticed that there is a ϕ missing in the third term in the left-hand side of the equation in the original paper. Eq. (31) is a second-order ordinary differential equation with constant coefficients,

7

its solution will lead to two unknown constants which were determined by introducing the following two boundary conditions

i) the vertical sediment flux must vanish at the surface, which yields

$$\varepsilon\frac{\partial\bar{c}}{\partial x_2} + \omega\bar{c} = 0 \quad \text{at } x_2 = y,$$

$$\phi'(1) + (\omega D/\varepsilon)\phi(1) = 0 \qquad (32)$$

ii) the variation in the correct value c_a of the bed concentration with the local flow conditions can be calculated from (21) and (22) as

$$dc_a/d\theta = f(\theta')c_a \, d\theta'/d\theta$$

where

$$f(\theta') = \frac{3}{2(\lambda_a^3 + \lambda_a^2)\ 0.027s}\left(\frac{\theta_c}{\theta^2} - \frac{\pi}{6}\tan\phi\frac{\theta\ \partial p/\partial\theta - p}{\theta^2}\right)$$

in which

$$\partial p/\partial\theta = \frac{(\pi/6\tan\phi)^4}{(\theta - \theta_c)^5}\,.p^5$$

The variation in the nominal bed concentration was then determined by the definition of c_{bo} as

$$q_s = \int_0^D Uc_{bo}\exp\left(\frac{\omega}{\varepsilon}x_2\right) \simeq U\,\frac{\varepsilon}{\omega}\,c_{bo}\,\left(1-\exp\left(\frac{\omega D}{\varepsilon}\right)\right)$$

where q_s is given by Eq. (24). A relation between c_{bo} and c_a from this was found to be

$$c_a\,U_f' = k\,c_{bo}\,U$$

where k is a constant. By differentiating this expression with respect to θ

$$\frac{1}{c_a}\frac{dc_a}{d\theta} = \frac{U_f'}{U}\frac{d}{d\theta}\left(\frac{U}{U_f'}\right) + \frac{1}{c_{bo}}\frac{dc_{bo}}{d\theta}$$

based on Eq. (16) the first term in the right-hand side can be neglected. This leads to the following boundary condition at the bed

$$c_b = c_{bo} + h(dc_o/dx_2) + \bar{c} = c_{bo}(1 + \theta f(\theta')(d\theta'/d\theta)(\bar{\tau}/\tau_0))$$

which yields

$$\phi(o) = C_{bo}\left(\frac{\omega D}{\varepsilon} + \theta f(\theta')\frac{d\theta'}{d\theta}\frac{\tau_o}{\tau_b}\right) \qquad (33)$$

The function ϕ can be calculated from Eq. (31) using the two boundary conditions defined by Eqs. (32) and (33).

The Stability Analysis

So far, the assumption of steady flow over a stationary bed has been considered, which is in fact, unrealistic for the investigation of meander developing. However, it has been accepted based on the assumption that the downstream migration velocity was considered to be very small as stated before.

If the continuity equation for the sediment motion is expressed in the form

$$\frac{\partial q_1}{\partial x_1} + \frac{\partial q_3}{\partial x_3} = -(1 - n)\frac{\partial h}{\partial t} \quad \ldots\ldots(34)$$

in which q_1 and q_3 are the total volumetric sediment transport rates per unit width (bed load and suspended load) in the x_1 and x_3 directions, respectively; and n is the porosity of the sand. The standard factor $\exp(iK_1x_1)$, which was used to describe the periodicity, should consequently be replaced by

$$h = h_o \cos(K_3x_3) \exp[iK_1(x - at)] \quad \ldots\ldots(35)$$

where a is the complex migration velocity of the sand waves, its real part denotes the velocity of propagation of the wave in the x_1-direction; whereas its imaginary part determines the degree of damping, or amplification, depending on its sign, negative for damping, and positive for amplification. In connection with the stability analysis, the imaginary part of the complex migration velocity plays the rule.

The main point in the stability analysis is to determine the complex migration velocity, and this can be easily found by calculating all terms in Eq. (34) as follows

$$\frac{\partial q_1}{\partial x_1} = \frac{\partial q_{b1}}{\partial x_1} + \frac{\partial q_{s1}}{\partial x_1}$$

in which

$$\frac{\partial q_{b1}}{\partial x_1} = [(s-1)gd^3]^{1/2}\frac{\partial \Phi_{b1}}{\partial x_1} = q_b \cdot g(\theta')\frac{\partial \theta'}{\partial x_1} \quad \ldots\ldots(36)$$

where

$$g(\theta') = \frac{(\frac{\pi}{6}\tan\phi)^4}{(\theta' - \theta_c)^5}\left[1+\left(\frac{\pi/6\tan\phi}{\theta' - \theta_c}\right)^4\right]^{-1} + \frac{1}{2\theta'^{1/2}(\theta'^{1/2} - 0.7\theta_c^{1/2})},$$

and the longitudinal transport of suspended sediment was found from the expression

$$q_{s1} = \int_h^D C\,U_1\,dx_2 = \int_h^D (U + u_1)(c_o + \tilde{c})\,dx_2 \quad \ldots\ldots(37)$$

9

by linearization

$$q_{s1} = -h\, c_{bo}\, U + q_{so} + EUDG$$

in which,

$$G = \int_0^1 [\phi + \frac{U_{10}}{U} C_{bo} \exp(-\frac{\omega D}{\varepsilon} \frac{x_2}{D})]\, d\, (\frac{x_2}{D})$$

and q_{so} denotes the transport rate for the basic flow and given by

$$q_{so} = \int_0^D U c_o\, dx_2$$

similarly for the transverse direction

$$\frac{\partial q_3}{\partial x_3} = \frac{\partial q_{b3}}{\partial x_3} + \frac{\partial q_{s3}}{\partial x_3}$$

Engelund (6) has discussed the problem of the motion of a bed particle in a flow where the bed is sloping in the transverse direction, and it was found that due to the helicity which characterizes the flow around channel bends, the direction of the bed shear stress will deviate from the direction of the main flow, and q_{b3} was found to be

$$q_{b3} = q_b[\frac{u_3}{U} - \frac{1}{\tan \phi} \frac{\partial h}{\partial x_3}]$$

Hence,

$$\frac{\partial q_{b3}}{\partial x_3} = q_b\, [(K_3 D)\, \frac{U_{30}}{U} + \frac{(K_3 D)}{\tan \phi}\,]\, E \qquad (38)$$

The transverse rate of transport of suspended sediment is

$$q_{s3} = \int_h^D U_3\, (c_o + \tilde{c})\, dx_2 = q_{so} \frac{U_{30}}{U} E \qquad (39)$$

It has to be noticed that the suspended sediment has been calculated by integration with h as the lower limit of integration. Since h represents the height of perturbation for the case of perturbed flow, this implies that the sediment is transported in suspension only, i.e., the thickness of the bed layer was not considered.

Substitute Eqs. (36), (37), (38), and (39) into Eq. (34) where $\frac{\partial h}{\partial t}$ can be obtained directly by differentiating Eq. (35), also making use of the relation

$$\frac{\omega D}{\varepsilon} = \frac{\omega D}{0.077 U_f Y} = 13\, (\frac{4(s-1)gd}{3C_D U_f^2})^{1/2} = 13(\frac{4}{3\theta C_D})^{1/2} \qquad (40)$$

where C_D is the drag coefficient of the grains, the complex migration velocity $a = a_r + i a_i$ can be obtained as a function of a number of a non-dimensional quantities as

$$a = a(\theta, c_D, S, \frac{D}{d}, K_1 D, K_3 D) \qquad (41)$$

The flow will be considered unstable if the imaginary part a_i of a is positive which means that the perturbation will grow exponentially with amplification factor $K_1D\ a_i$.

If the imaginary parts of the resulting expression, which has the form of Eq. (41), are set equal to each other, the normalized amplification factor $a_i\ K_1D$ which will be given in the form, $\frac{(1-n)a_iK_1D}{\Phi_T}$, where Φ_t is the total dimensionless rate of sediment transport and will be called the amplification coefficient, A, which for a given condition of θ, C_D, S, and $\frac{D}{d}$ was found to be a function of (K_1D) which characterizes the meander wavelength, and (K_3D) which characterizes the channel width, i.e., the amplification coefficient, A, relates the meander wavelength to the channel width for a given geometry and flow condition.

The variation in the amplification coefficient, A, with K_1D was plotted for given values of K_3D, θ, S, and C_D as shown in Fig. 2, which indicated that for a given value of K_3D, the amplification coefficient has a maximum value which corresponds to a certain value of K_1D. This maximum determines the wavelength of the developing meander as was mentioned by Callander (1).

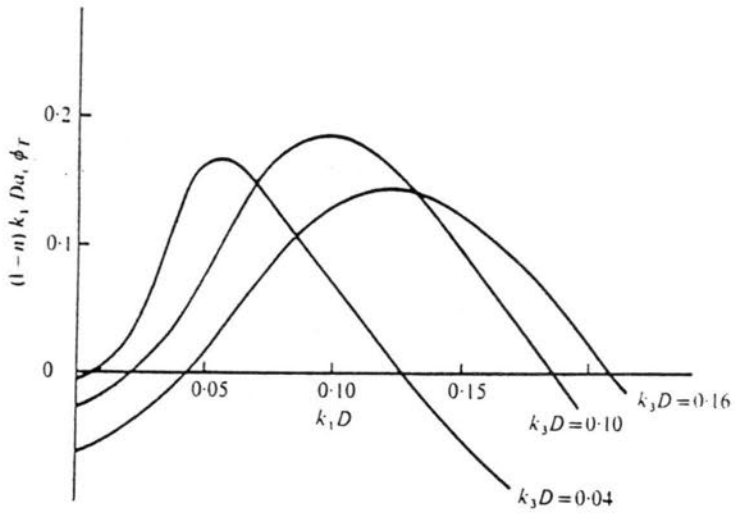

FIG. 2.-Variation in the Amplification factor A with K_1D and K_3D. θ = 0.2, S = 2.65, and C_D = 7 (after Fredsøe).

11

Further, this maximum has been plotted for different values of K_3D as shown in Fig. 3 which showed that for a given value of K_3D greater than a critical value, the maximum amplification coefficient is negative which means that the channel will remain stable, i.e., straight, and if the value of K_3D is less than the critical value, the maximum amplification coefficient will be positive which means that the channel is unstable, i.e., the channel will meander or braid.

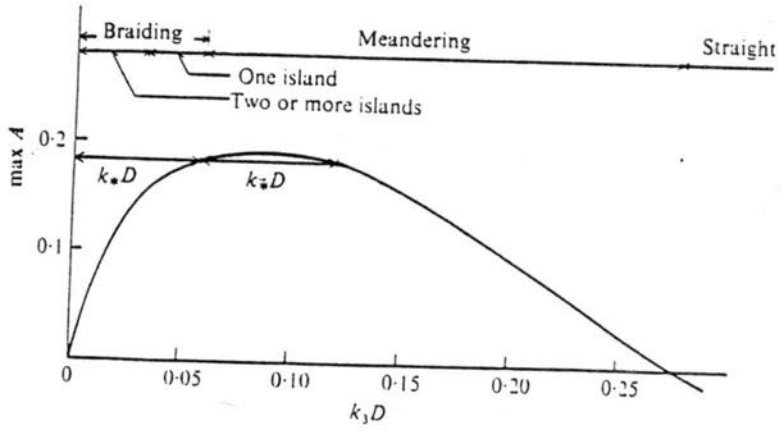

FIG. 3.-Variation in the Maximum Amplification Factor with K_3D (after Fredsøe, 1978).

The particular abscissa K_*D for which the maximum amplification coefficient is the same as for $2K_*D$ indicated that if K_3D is smaller than K_*D, the river will braid into one or more islands as mentioned by Engelund and Skovgaard (5). A stability diagram has been constructed for the case of dune-covered bed as shown in Fig. 4, which showed the value of $K_3D = \frac{\pi D}{B}$ at which the river will remain straight, meander, or braid as a function of Shield's parameter, θ. where B is the river width. The lower dotted line in the diagram indicates the transition from one to two braids. This stability diagram has been constructed for given values of $\frac{D}{d}$, S, and c_D. The author (8) has examined the effect of the sediment in suspension by constructing a stability diagram by incorporating the bed load alone into the analysis as shown in Fig. 5.

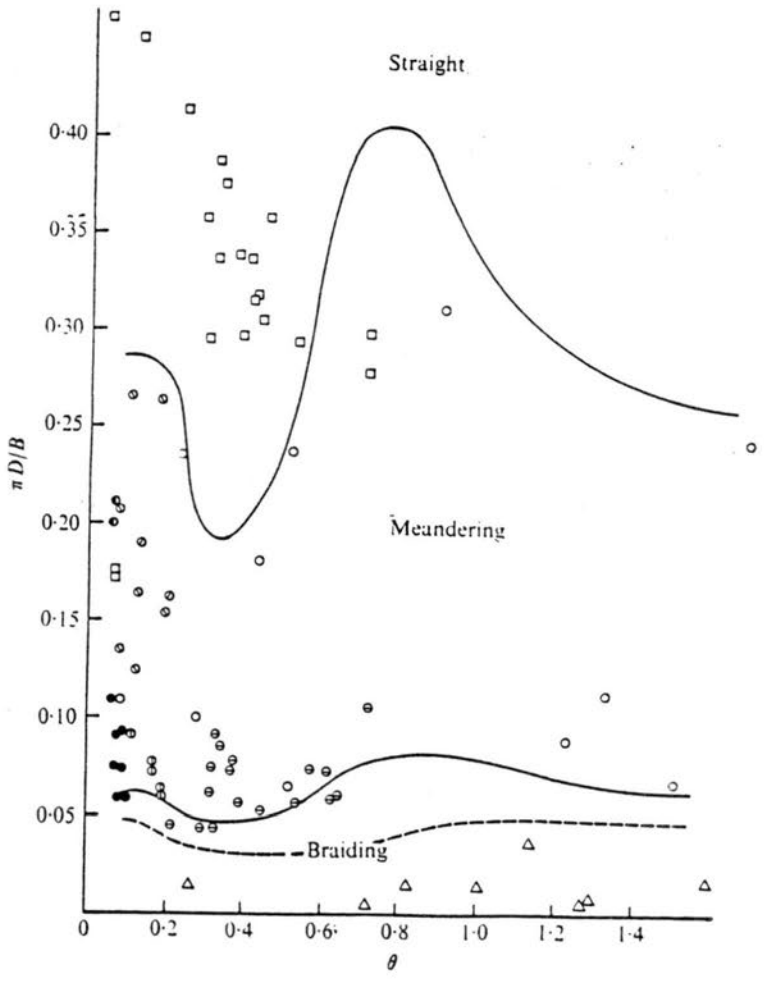

FIG. 4.-Stability Diagram for Dune-Covered Bed River. $S = 2.65$, $\frac{D}{d} = 1{,}000$, $c_D = 7$. The rectangles indicate straight data, the circles meandering and the triangles braiding (after Fredsøe, 1978).

The stability limits from this diagram has been changed from those shown in Figure 4. Figure 5 showed that when suspension is neglected, the bed will remain stable if θ is greater than about one.

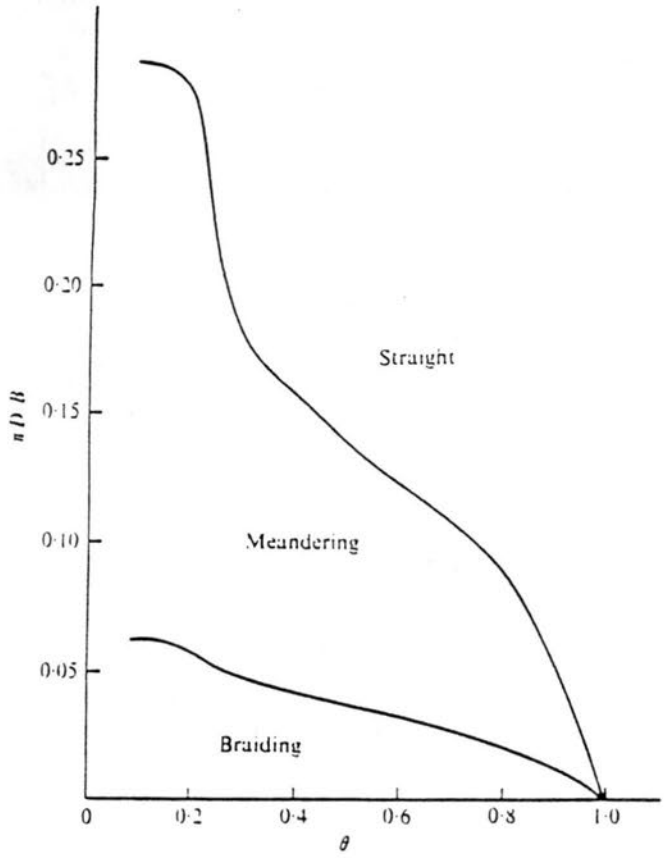

FIG. 5.-Stability Diagram for a Dune-Covered Bed Where the Suspended Load Has Been Neglected (after Fredsøe, 1978).

In Figure 6, another stability diagram has been constructed under the assumption that the bed is flat. This yields stability limits which differ from those in Figure 4.

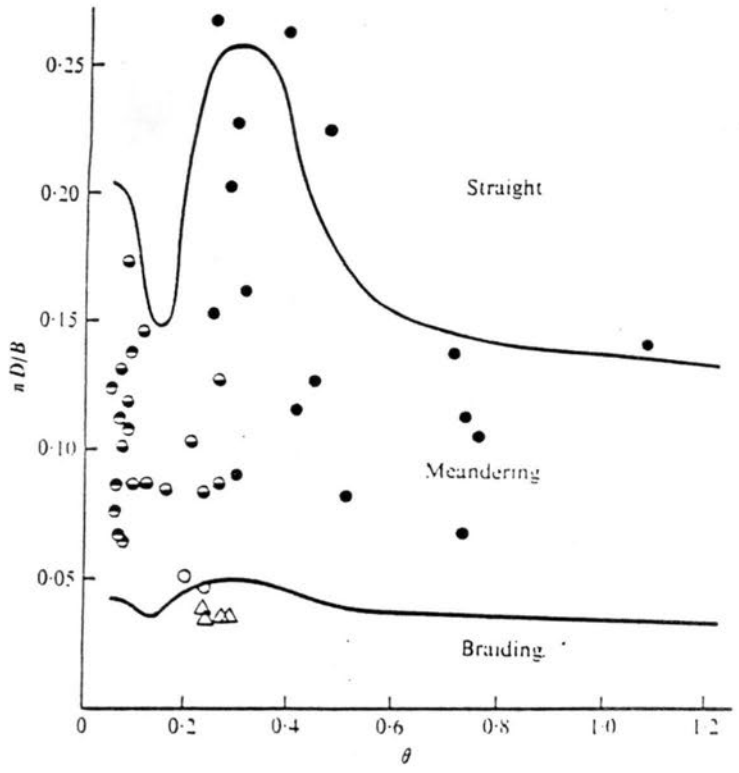

FIG. 6.-Stability Diagram for Originally Flat Bed (after Fredsøe, 1978).

Conclusion

The results of the stability analysis showed that a river will always remain straight if its width is smaller than 8 times its depth. Further, the river will braid if its width is larger than about 60 times its depth. These values are slightly dependent on the values of the Shield's parameter. It has to be noticed that the analysis has no explanation for whether the ratio B/D is the cause or the effect of the results of the analysis.

The assumptions that have been considered in this analysis are discussed below.

1) The assumption of constant eddy viscosity ε over the whole depth was just considered to avoid very complicated calculations. However, it will lead to different values of nominal bed concentration from what is actually occurring.

2) The assumption of having a fixed impermeable side walls is completely unrealistic for the discussion of meander initiation.

3) The calculations of the suspended load q_{s1} and q_{s3} from Eqs. (37) and (39) using the height of perturbation, h, as the lower limit of integration neglected the thickness of the bed layer.

4) A stability diagram has been constructed discussing the tendency of the river to meander, braid, or remain straight for the case of originally flat bed as shown in Figure 6, which contradicts with the theory introduced as the developing of meander or braid as a result of small perturbation superposed on the original plane bed.

5) There have been mistakes in some of the equations in the original paper which have been corrected. Eqs. (3), (29), (30), and (31) are the correct forms of (3), (30), (31), and (32) in the original paper.

Acknowledgment

This paper has been prepared as a partial fulfillment of the CE-717, River Mechanics. The student expresses his appreciation to his adviser and course instructor, Dr. P.Y. Julien, Assistant Professor of Civil Engineering, for his continuous encouragement during the preparation of this paper.

Appendix I.-References

1. Callander, R.A., "Instability and River Channels," Journal of Fluid Mechanics, Vol. 36, 1969, pp. 465-480.
2. Einstein, H.A., "The Bed Load Function for Sediment Transport in Open Channel Flow," U.S. Department of Agriculture, Tech. Bulletin No. 1026, 1950.
3. Engelund, F., "Instability of Erodible Beds," Journal of Fluid Mechanics, Vol. 42, 1971, pp. 225-244.
4. Engelund, F., and Hansen, E., "A Monograph on Sediment Transport in Alluvial Streams," Copenhagen: Technical Press, 1972.
5. Engelund, F., and Skovgaard, O., "On the Origin of Meandering and Braiding in Alluvial Streams," Journal of Fluid Mechanics, Vol. 57, Part 2, 1973, pp. 289-302.
6. Engelund, F., "Flow and Bed Topography in Channel Bends," Journal of Hydraulics Division, ASCE, Vol. 100, (HY11), 1974, pp. 1631-1648.

7. Engelund, F., and Fredsøe, J., "A Sediment Transport Model for Straight Alluvial Channels," Nordic Hydrology, Vol. 7, 1976, pp. 293-306.

8. Fredsøe, J., "Meandering and Braiding of Rivers," Journal of Fluid Mechanics, Vol. 84, 1978, pp. 609-624.

9. Olesen, K.W., "Alternate Bars In and Meandering of Alluvial Rivers," In River Meandering, Proceedings of the Conference Rivers' 83, 1984, pp. 873-884.

10. Rouse, H., "Modern Conceptions of the Mechanics of Turbulence," Transactions, ASCE, Vol. 102, 1937, pp. 463-505.

11. Simons, D.B., and Sentürk, F., Sediment Transport Technology, Water Resources Publications, 1977, 807 p.

Appendix II.-Notations

The following symbols are used in this paper.

A	=	amplification coefficient
a	=	complex migration velocity
β	=	channel width
c_{bo}	=	nominal concentration at the bed
c_D	=	drag coefficient
D	=	depth of unperturbed flow
d	=	grain mean fall diameter
g	=	acceleration due to gravity
h_o	=	amplitude of the perturbation
I_o	=	undisturbed slope of the channel
K_1, K_3	=	wave numbers in the x_1 and x_3 directions
K	=	sand roughness
q_b	=	bed load transport
q_s	=	suspended load
q_{so}	=	transport rate for the basic flow
U_1, U_2, U_3	=	velocity components in x_1, x, and x_3 directions
U_f	=	friction velocity
u_1, u_2, u_3	=	velocity components due to perturbation
x_1	=	co-ordinate in the flow direction
x_2	=	vertical co-ordinate
x_3	=	transverse co-ordinate

y = local water depth

θ = Shield's parameter

θ' = effective Shield's parameter

θ_c = critical Shield's parameter

λ_a = linear concentration

ε = eddy viscosity

ρ = density of water

τ = local bed shear stress in x_1-direction

τ_b = bed shear stress in the unperturbed flow

η_o = water surface deviation from the unperturbed level

S = relative density of the solid particles

n = porosity of sand grain

w = fall velocity of the solid particles.

AN EVALUATION OF CRITERIA FOR PREDICTING MORPHOLOGICAL PATTERNS IN ALLUVIAL RIVERS

By William G. Stubblefield

Abstract: Methods of predicting the morphological patterns of alluvial rivers developed by Lane, Leopold and Wolman, and Parker are evaluated using a recently published data set by Michael Church. The results indicate that none of the methods is very effective over a wide range of data. Lane's relation is verified by restricting the data set to those with bed material in the sand-size range.

INTRODUCTION

River channels have probably been given more attention than any other landform on earth, and there is nearly an infinite variety of stream forms. Rivers have been classified according to their age, as youthful, mature, or old (4). They have been classified according to the history of their development on a land surface, as antecedent, superposed, consequent and subsequent (5). In addition rivers may be classified according to their size, slope, velocity, discharge, type and quantity of sediment load, or they may be divided into two groups depending on their freedom to adjust their shape and gradient, as bedrock-controlled or alluvial channels. Bedrock-controlled channels are confined between outcrops of rock and the nature of the rock determines the shape of the channel. Alluvial channels, on the other hand, are free to adjust their dimensions, shape, pattern and gradient (3).

Alluvial rivers have also been grouped various ways. Schumm has classified alluvial rivers according to type of sediment moved through the system as bed-load, mixed-load, and suspended-load. A bed-load channel is defined as one that transports more than 11% bed load; a suspended-load channel is one that transports less than 3% bed load, and a mixed-load channel is in between these two (7). Probably the most obvious way of classifying alluvial channels is by pattern. The number of different patterns recognized varies from investigator to investigator from 2 to about 16.

Five basic bed-load channel patterns of alluvial rivers are recognized by Schumm. These vary from straight channels with low energy, slope, and bed transport to meandering channels, to straight braided channels with high energy, slope and bed transport.

Brice (1) recognized 4 major planform characteristics of alluvial rivers and 4 major types of rivers with commonly occurring combinations of these planforms.

The most used classification of alluvial rivers by form is into three categories: straight, meandering, or braided (8).

Experiments by Friedkin (2), Leopold and Wolman (8), Parker (12), and Lane (10) indicate that there are threshold values of slope and mean annual discharge or mean annual flood at which meandering and braided stream patterns change. In addition, it has been suggested by Lane (10), Quraishy (14) and others and confirmed by Edgar (6) and by Ackers and Charlton (11) that at very low slopes another threshold exists between straight and meandering stream patterns. The results of some of these investigators are

presented graphically by Schumm and Khan (9) on Fig. 1. Parker (12) also divides stream morphology into braided, meandering and straight patterns and has developed a procedure to predict morphology based on a two-dimensional math model.

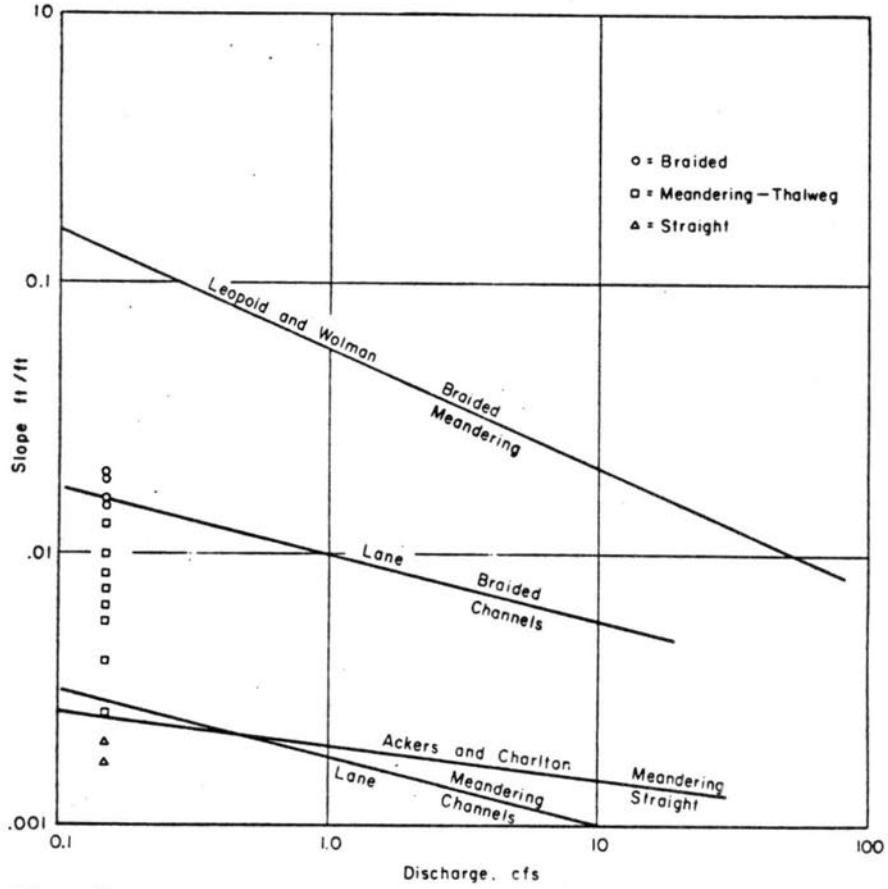

Fig. 1. Relation between slope and discharge and threshold slopes at each discharge, as defined by Lane (1957), Leopold and Wolman (1957), and Ackers and Charlton (1971). Symbols show position of experimental channels. (From Schumm and Khan, 1973.)

Church (13) has found that very few of the hydraulic data sets used by various investigators have had the consistency and homogeneity required to perform accurate comparison and analysis. He notes that the data may appear to be equivalent, but different methods of measurement and varying criteria are largely ignored. The variance in the results of different investigators may be attributed to inconsistent measurement between data sources, inappropriate comparisons of channels of different type, or a truly large range of variability of channel data. Most students generally attribute the varied results of different investigators to variable channel responses without a critical analysis of data.

Because of the variability in the data used to evaluate alluvial river channel regime, Church collected and published in 1983 an extensive data set he considered appropriate for comparative riverine hydraulic studies.

OBJECTIVE.—It is the purpose of this paper to use the recent data collected by Church to evaluate the general effectiveness or accuracy of the methods devised by Lane, Leopold and Wolman, and Parker to predict the probable morphology of alluvial river channels.

The emphasis of the paper will be on the difference between meandering and braided channels. Although it has been repeatedly demonstrated experimentally that a threshold between straight and meandering patterns exists, there are very few natural channels with combinations of discharge, sediment, and slope exhibiting a natural straight pattern. It is, therefore, not investigated in this paper.

PROCEDURE.—The general procedure will be to use the equations given by Lane, Leopold and Wolman, and Parker to predict the channel pattern. The pattern will be compared to the observed pattern according to Church for verification. An analysis of the results will provide information on the reliability of the methods. A description of each method will be independently presented prior to an analysis of the data. The data will be plotted and trends analyzed.

METHOD BY LANE

Lane (10) identified 8 separate variables that have a deterministic effect on channel form, but most of these were difficult to use, either because they could not be easily quantified, such as vegetation, or because there was no extensive data readily available for use. He further concluded that there were some variables which did not exert as much influence on channel pattern as others. Using these criteria, he settled on slope, discharge and bed-bank material as the variables which could be used to analyze channel patterns. Channel sinuosity was not included basically because of time and money limitations. Sediment type and load were not included because they were assumed to be determined by discharge, slope and bed-bank material and are, thus, dependent variables.

Recognizing the difficulty of relating the four variables discharge, slope, bed-bank material, and channel form with a single solution, Lane eliminated two of the variables by first selecting only streams having one pattern and one material size.

MEANDERING STREAMS.—Using the meandering pattern and grain sizes found in the lower Mississippi River a relation between slope and discharge was established. This relation is:

$$S = \frac{0.0017}{\sqrt[4]{Q}} \quad \ldots\ldots\ldots\ldots\ldots\ldots\ldots\ldots\ldots\ldots \quad (1)$$

where
S = slope in ft./ft.
Q = discharge in c.f.s.
This equation was generalized in the form:

$$S = \frac{K}{\sqrt[4]{Q}} \quad \ldots\ldots\ldots\ldots\ldots\ldots\ldots\ldots\ldots\ldots \quad (2)$$

with K = 0.0017.
This curve is plotted on Fig. 1.

Lane explained the variation of his data points by the fact that all the bed material sizes were not the same and the degree of meandering was different for each river. Despite this variation, however, Lane concluded that Eq. 1 very accurately represents the relation between slope and discharge for all meandering streams under equilibrium conditions with sediment size and sinuosity approximately equal to that found in the Lower Mississippi River.

BRAIDED STREAMS.—Lane evaluated the slope-discharge relation in braided streams by using only data from sand streams having steep slopes. Using data from 7-8 braided streams and a highly braided physical model of the Lower Colorado River, a slope-discharge relation was determined by regression analysis to be of the form:

$$S = \frac{0.01}{4\sqrt{Q}} \quad \ldots\ldots\ldots\ldots\ldots\ldots\ldots\ldots\ldots\ldots \quad (3)$$

with terms defined as before. This curve is also plotted on Fig. 1. This relation is not as accurate as the relation for meandering streams, possibly because it was more difficult to establish the degree of braiding than the degree of meandering and possibly because of the manner in which the rivers were formed.

Lane states that rivers braid for two different reasons: (1) overload of sediment and (2) steep slope. These physical situations are not necessarily related. This accounts for some of the scatter in the data.

METHOD BY LEOPOLD AND WOLMAN

The authors of this method (8) identified at least 8 interrelated hydraulic parameters affecting the shape and characteristics of natural rivers and streams. Some of the variables are noted to occur in repeating associations. Two of the more important variables, slope and discharge, were plotted for a variety of natural streams. It was observed that this data could be separated by stream morphology into patterns of straight, meandering, or braided streams. A line separating the meandering and braided streams is described by the equation:

$$S = 0.06\ Q^{-0.44} \quad \ldots\ldots\ldots\ldots\ldots\ldots\ldots\ldots\ldots\ldots \quad (4)$$

where
S = slope in ft./ft.
Q = discharge in c.f.s.
This curve is plotted on Fig. 1.

Streams classified as meandering by Leopold and Wolman are those whose sinuosity is greater than 1.5. Braided streams are those which have relatively stable alluvial islands and, therefore, two or more channels. The authors note that sediment size is related to slope and channel pattern but they do not try to account for the effect of sediment size on the morphology of the streams. They further note that braided and meandering streams can be differentiated based on combinations of slope, discharge, and width/depth ratio, but regard the width as a variable dependent on mainly discharge.

The authors recognize that their analysis treats only two of the many variables affecting morphology, therefore do not expect this method to apply in every condition. However, because the data were all taken from natural streams, and because the analysis obviously does indicate a significant relation between slope and discharge, the analysis should give a reasonably effective prediction of channel pattern if slope and discharge are known.

It is interesting that Leopold and Wolman do not recognize a lower threshold combination of slope and discharge separating meandering and straight patterns. They state that such a threshold doesn't exist. This

is in contrast to the observations of Schumm (3), Lane (10), Edgar (6), Quraishy (14), and Ackers and Charlton (11). (See Fig. 1.) In addition to recognizing a low threshold between straight and meandering channels, these later investigators seem to indicate that river channels exhibit a straight pattern for two different reasons: (1) extremely low energy or slope, in which the tendency to meander is so weak that meandering cannot occur and (2) high energy or slope, in which the meandering tendencies are overcome by the gravitational forces due to high slope. Because this paper deals with the criteria between meandering and braided channels only, Leopold and Wolman's position on criteria separating straight and meandering streams is considered irrelevant. However, it should be noted that recent investigators have reached conclusions significantly different from Leopold and Wolman.

METHOD BY PARKER

Parker (12) refined a theoretical two-dimensional river model originated by others to differentiate between meandering and braided regimes. The stability model uses expansion techniques to also obtain a relation for meander wavelength in meandering streams and number of braids in a braided stream.

Parker developed mathematical equations by examining submerged bedforms in a shallow, rectangular channel of constant slope with a constant discharge. The two-dimensional approach ignores the effects of the helicoidal or secondary flow.

Solutions of the equations developed by Parker require reliance on observed phenomena for accuracy, and are, thus, partly empirically based.

The salient issue of criteria for braiding or meandering is presented as approximately:

$$E^* = \frac{SB}{\pi F d_o} \quad \ldots\ldots\ldots\ldots\ldots\ldots\ldots\ldots\ldots\ldots \quad (5)$$

where

$E^* \gg 1$ corresponds to extreme braiding
$E^* \ll 1$ corresponds to extreme meandering
$E^* = 1$ corresponds to a transition pattern
S = channel slope
B = width of channel
π = 3.14
F = Froude number $(V/\sqrt{gd_o})$
d_o = depth of channel
V^o = average velocity of channel

This equation indicates that meandering occurs for

$$S/F \ll d_o/B \quad \ldots\ldots\ldots\ldots\ldots\ldots\ldots\ldots\ldots\ldots \quad (6)$$

and that braided channel patterns occur for

$$S/F \gg d_o/B \quad \ldots\ldots\ldots\ldots\ldots\ldots\ldots\ldots\ldots\ldots \quad (7)$$

A transition between the two is indicated when

$$S/F \sim d_o/B \quad \ldots\ldots\ldots\ldots\ldots\ldots\ldots\ldots\ldots\ldots \quad (8)$$

These relations corroborate the observations, as noted by Friedkin (2) and many others, that meandering streams generally have gentle slopes and narrower channels, while braided streams generally have steeper slopes and wider channels. Thus, the same river may be braided in its mountain reaches and meandering in its lower reaches.

The theory does not indicate any conditions under which channels which transport sediment can remain straight. It has been experimentally determined that for large values of d_o/B, neither meandering nor braiding occur. The critical d_o/B value appears to be approximately 10^{-1}. Such large values of d_o/B are rarely attained in nature and are, therefore, not dealt with extensively by Parker.

PARAMETERS AND DATA USED IN ANALYSIS

Michael Church and Kenneth Rood (13) in 1983 published an extensive data set because of what they perceived to be a lack of consistency among hydraulic data used in riverine analysis. The data cover ten different morphological types of rivers and consist of about 500 sets of data. The data were obtained from an extensive search of available literature and include only data which was obtained by reasonable measurement. Ninety percent of the data is taken from rivers found in the western part of the North American continent and ten percent from British rivers.

Different type of data were used in the morphological analyses by Lane, Leopold and Wolman, and Parker. The data used in the present analysis will all be taken from Church (13), however, each parameter was carefully selected to avoid using data sets where one or all of the methods would not be applicable. The parameters and data sets used for this evaluation are discussed below.

SLOPE.—There were no inconsistencies observed as to slope measurement and use since each method includes this parameter and there is general agreement about slope determination.

DISCHARGE.—Lane used mean discharge for his analysis. Parker used bankfull discharge as much as possible, but also included mean discharge data. He observed that the results using mean discharge were acceptable. Leopold and Wolman used bankfull discharge.

For this analysis, data sets using either mean discharge or bankfull flow were considered acceptable.

WIDTH, VELOCITY, AND DEPTH.—Only Parker used these parameters, therefore no discrepancy can arise because of variations in the use of these parameters by different investigators.

SINUOSITY.—Since the analysis deals only with braided and meandering criteria, data sets describing straight channels were rejected.

SEDIMENT SIZE.—Lane restricted his analysis to predominantly sand channels. Leopold and Woman used predominantly gravel bed rivers. Parker did not specify any restrictions to a specific grain size and it is assumed that he used sand and gravel rivers. Sand and gravel rivers were therefore included in this analysis. This includes all data sets with a D_{50} of less than 64 mm. Data sets describing channel beds as predominatly cobble or boulder channels were excluded. Also rejected were sets describing streams as bedrock controlled.

CHANNEL MORPHOLOGY.—Lane made no effort to distinguish a sharp boundary between straight, meandering and braid patterns. He simply plotted a curve

for obviously meandering streams and one for highly braided streams. Those in between he termed transitional.

Leopold and Wolman distinguish between straight and meandering channels by using a value of sinuosity equal to 1.5 as the criteria. They class as braided any stable stream which has two or more channels.

Parker does not describe the criteria used for his pattern evaluation, but simply accepts the judgment of the investigators from the laboratory and field observations as to morphology.

Church separated river morphology into 7 patterns. By a careful reading of his description, these patterns may be regrouped into three categories: straight, meandering and braided. The data used in the analysis are presented in Appendix III.

METHOD OF COMPARISON

By far, the simplest method of comparison is to follow the methods of Leopold and Wolman and Parker. Following this approach, only one assumption is required to present Lane's results in a similar format. In addition, Church's morphology categories may easily be adjusted to facilitate this method of analysis.

The assumption required for Lane's method involves deciding on a boundary between meandering and braided streams. Two curves were tried. The first curve represents a position directly halfway between and parallel to those established by Lane for braided and meandering streams. The equation of this first curve is:

$$S = \frac{0.004}{\sqrt[4]{Q}} \quad \ldots\ldots\ldots\ldots\ldots\ldots\ldots\ldots \quad (9)$$

where

S = slope in ft./ft.

Q = mean discharge in c.f.s.

The curve is shown on Fig 2.

A second curve was drawn because such poor results were obtained with the first curve when all data sets were used. This second curve was fit by eye to separate Lane's data points which are not shown in this paper. Since both curves were somewhat arbitrarily drawn and better results were obtained with the second curve, it was decided to use the second curve for purposes of comparison with the other methods. The equation of the second curve is:

$$S = \frac{0.0075}{\sqrt[4]{Q}} \quad \ldots\ldots\ldots\ldots\ldots\ldots\ldots\ldots \quad (10)$$

where terms are defined as above. This curve is shown on Fig. 2. Eq. 9 was retained and is presented because it gives excellent results when greater restrictions are imposed on the sediment size of the data sets evaluated.

The effectiveness of Lane's method was evaluated by substituting the discharge from a given data set into Eq. 10 and computing the slope. If the computed slope was smaller than the observed slope, the predicted channel morphology would be braided. The results are compared to the observed morphology and are shown in Table 1. The observed data points are actually plotted on Fig. 2. In this figure, data points above the line should, according to Eq. 10, exhibit a braided channel morphology.

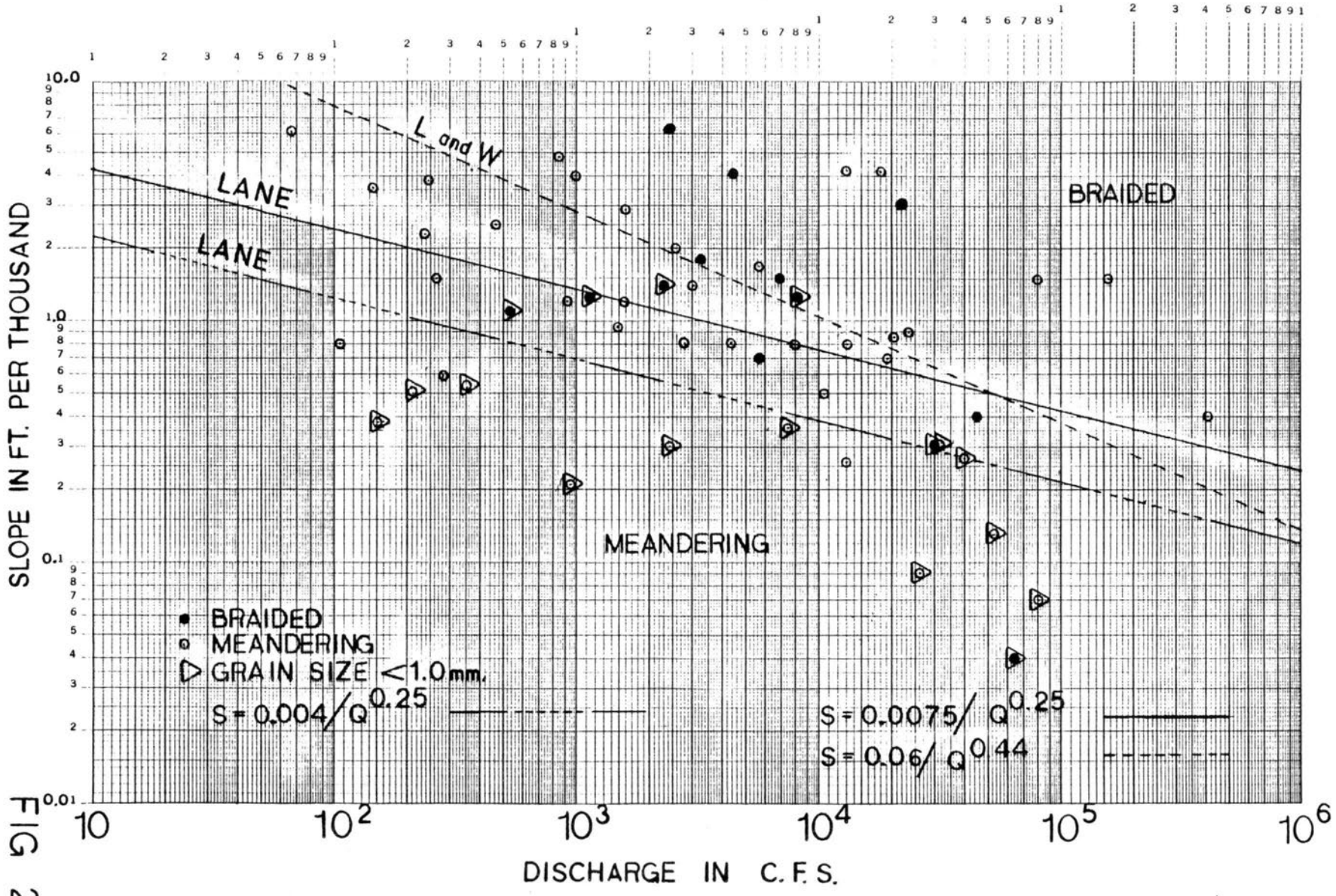
SLOPE IN FT. PER THOUSAND
DISCHARGE IN C.F.S.
L and W
LANE
LANE
BRAIDED
MEANDERING
BRAIDED
MEANDERING
GRAIN SIZE <1.0mm.
S = 0.004/ Q^0.25
S = 0.0075/ Q^0.25
S = 0.06/ Q^0.44
10.0
1.0
0.1
0.01
10
10^2
10^3
10^4
10^5
10^6

FIG 2

Leopold and Wolman's approach was evaluated using Eq. 4 and the observed morphology. The results are tabulated in Table 1. Eq. 4 is also plotted on Fig. 2. This facilitates comparison with Lane's method.

Table 1

Patterns Correctly Predicted

Observed		Lane		Parker		Leopold & Wolman	
Pattern	Number Observed	Number Accurately Predicted	Per Cent Accuracy	Number Accurately Predicted	Per Cent Accuracy	Number Accurately Predicted	Per Cent Accuracy
Braided	13	8	62	3	23	6	46
Meandering	45	22	49	43	96	31	69
Total	58						
Total Accur. Predicted		30		46		37	
Overall Accuracy (%)		52		79		64	

Parker's approach was evaluated by comparing the observed morphology to that predicted using the parameters shown in the data. The results are shown in Table 1. The S/F vs. D/B data points were computed and are shown along with the channel morphology on Fig. 3. Points above the curve should have a braided channel morphology according to Parker.

Because the results obtained in the above analysis so poorly matched the observed data, the evaluation was repeated based on a re-classification of the morphological patterns in Church's data. The accuracy of each method decreased confirming the propriety of the original classification scheme.

In a further effort to achieve more consistent results, another analysis was made by combining the predictions of each method and comparing the result to the observed pattern. The results are shown in Table 2. This procedure is the only one that results in accuracy greater than 50% for both meandering and braided patterns.

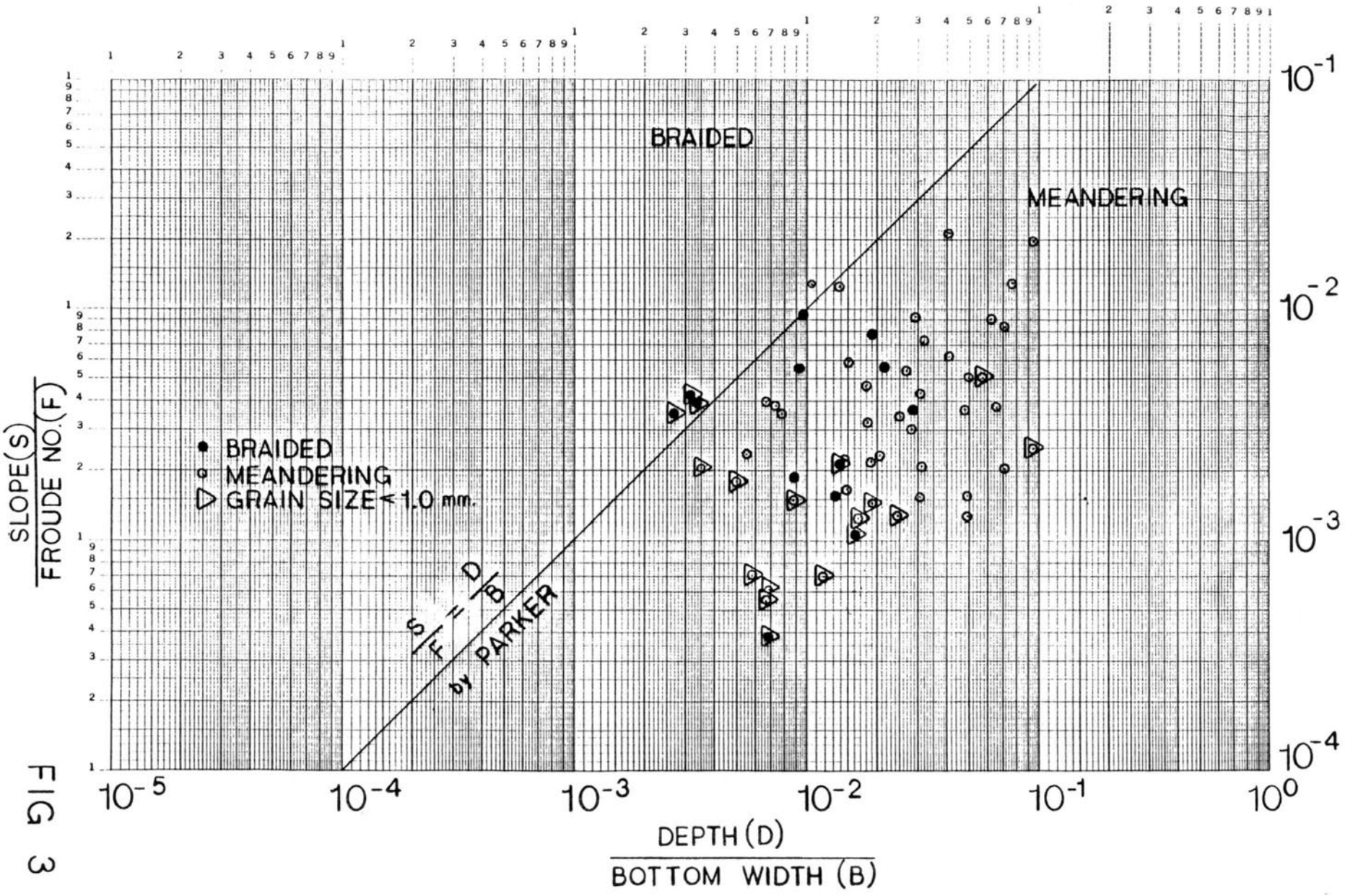
BRAIDED
MEANDERING
BRAIDED
MEANDERING
GRAIN SIZE < 1.0 mm.
S/F = D/B
by PARKER
SLOPE(S) / FROUDE NO.(F)
DEPTH (D) / BOTTOM WIDTH (B)
10^-5
10^-4
10^-3
10^-2
10^-1
10^0
10^-1
10^-2
10^-3
10^-4

FIG 3

Table 2

Patterns Correctly Predicted Using Combined Methods

Observed		Combined Methods	
Pattern	Number Observed	Number Accurately Predicted	Per Cent Accuracy
Braided	13	7	54
Meandering	45	31	69
Total	58		
Total Accur. Predicted		38	
Overall Accuracy (%)		66	

Finally, because the slope-discharge-sediment-size relation has been documented by Lane, Neill, Kellerhalls, Henderson and others, the data sets with a D_{50} less than 1 mm were plotted. This number was selected because Lane's analysis is based on similar grain sizes and because this represents a relatively large subset of the data. These data are shown on Figs. 2 and 3. Trends and relationships were noted and evaluated. Results are tabulated in Table 3.

Table 3

Patterns Correctly Predicted by Lane Using Data Sets with Sand Size D_{50}

Observed		Combined Methods	
Pattern	Number Observed	Number Accurately Predicted	Per Cent Accuracy
Braided	5	4	80
Meandering	12	11	92
Total	17		
Total Accur. Predicted		15	
Overall Accuracy (%)		88	

RESULTS OF COMPARISON

Results of the analysis using all the data are shown in Tables 1 and 2 and on Figs. 2 and 3. The observed data consists of 58 data sets; 13 of them are classed as braided, 45 are classed meandering.

Using Lane's method, the observed channel morphology was correctly predicted 30 times for an accuracy overall of 52%. Braided patterns were correctly predicted in 8 of 13 occurrences for 62% accuracy. Meandering patterns were correctly predicted in 22 of 45 occurrences for 49% accuracy.

Using Parker's method, the channel pattern was correctly predicted 46 of 58 times for an overall accuracy of 79%. However, braided patterns were predicted accurately 3 of 13 times for 23% accuracy and meandering patterns predicted accurately 43 of 45 times for 96% accuracy.

Using Leopold and Wolman's approach, the channel morphology was accurately predicted 37 of 58 times for an overall accuracy of 64%. Braided patterns were accurately predicted 46% of the time and meandering 69% of the time.

Using the method of combining all three of the above methods to predict morphology, the overall accuracy was 66%. Braided patterns were predicted correctly 54% of the time and meandering channels 69% of the time. This is the only procedure that resulted in accurate prediction of morphology greater than 50% of the time for both braided and meandering streams. Even though the total accuracy is not as high as that obtained by Parker's method, the high number of meandering stream data sets and low accuracy of Parker's method for predicting braided patterns indicate that using all 3 methods would probably result in the most reliable approach.

It is obvious from looking at all the data plotted in Figs. 2 and 3 that the scatter is so great that there is no curve that could be drawn to separate the braided and meandering patterns in a statistically significant manner. The data is trendy in the sense that the braided patterns are generally of higher slope than the meandering patterns, but not by much.

However, if the grain size is limited to a narrow range, the results are striking. A subset of the data used in the analysis was plotted to illustrate the point. The subset consists of only data in which the D_{50} was less than 1.0 mm. This data is so indicated on Figs. 2 and 3.

By plotting Eq. 9, one of the 2 average curves obtained from Lane's method on Fig. 2, an obvious pattern emerges. The results are tabulated in Table 3. Of the 17 points plotted, only 2 errors are obtained for an overall accuracy of 88% and 1 of those 2 errors is very close. Only 1 of 17 data is seriously out of order. Of the 5 braided streams, 4 are accurately predicted for 80% accuracy. Of the 12 meandering streams, 11 are accurately predicted for 92% accuracy. The results obviously confirm the proposition that the slope-discharge relation is much improved if the sediment size is considered.

The same approach was used to determine if the method by Parker results in greater accuracy if the sediment sizes of the data sets are restricted. The restricted subset of data is shown plotted on Fig. 3. A visual analysis of the data does not indicate an improved predictive capability therefore numerical evaluation was not pursued.

CONCLUSIONS

The analysis using all the data sets with D_{50} sizes ranging from small to 64 mm indicates that none of the methods should be relied on heavily to give an accurate prediction of channel morphology. Although it is true that Parker's method gave 79% overall accuracy, that statistic alone is misleading. It is significant that of the 13 braided streams, Parker predicts only 23% accurately.

Given no information about the sediment size of the stream, the best method to predict morphology is obtained from combining the results of all three of the above methods. It should be realized, however, that the results are not to be relied upon heavily. The best results by far are obtained when the sediment size is included in the prediction.

The scatter of the data as observed in Figs. 2 and 3 indicate that there is no curve which can effectively predict morphology by any of the methods evaluated unless sediment size is used to limit the range of applicability. It should not be surprising that the curve obtained from Lane's method (Eq. 9) should be so successful if grain sizes are limited to sand sizes, because this is the range of sediment to which Lane limited his analysis originally.

For sand size particles, Eq. 9 from Lane's method should be considered the method of choice for predicting morphology. Stream beds with a D_{50} in the sand range which are observed to have one morphological pattern but plot strongly on Lane's diagram in an opposite region should be considered incipiently unstable and on the verge of a major morphological metamorphosis. Those streams plotting on the curve for Eq. 9 should be considered in a transitional state capable of becoming braided or meandering. In either of these cases, a slight modification by the river engineer could result in major changes in the river morphology.

APPENDIX I.—REFERENCES

1. Brice, J.C., "Planform Properties of Meandering Rivers," River Meandering, Proceedings of the Conference Rivers '83, ASCE, 1983.
2. Friedkin, J.F., "A Laboratory STudy of Meandering of Alluvial Rivers," U.S. Army Corps of Engineers, May 1945.
3. Schumm, S.A., "The Fluvial System," John Wiley & Sons, 1977.
4. Davis, W.M., "The Geographical Cycle," Geogr. J., Vol. 14, pp. 481-504.
5. Thornbury, W.D., "Principles of Geomorphology," Wiley, 1969.
6. Edgar, D.E., "The Role of Geomorphic Thresholds in Determining Alluvial Channel Geomorphology," River Meandering, Proceedings of the Conference Rivers '83, ASCE, 1983.
7. Schumm, S.A., "Evolution and Response of the Fluvial System, Sedimentologic Implications," Special Publication No. 31, Society of Economic Paleontologists and Minerologists, pp. 19-29, August 1981.
8. Leopold, L.B. and Wolman, M.G. "River Channel Patterns: Braided, Meandering and Straight," USGS Professional Paper 282-B, 1957.
9. Schumm, S.A. and Khan, H.R., "Experimental Study of Channel Patterns," Geol. Soc. Am. Bull., Vol. 83, pp. 1755-1770, 1972.

10. Lane, E.W., "A Study of the Shape of Channels Formed by Natural Streams Flowing in Erodible Material," M.R.D. Sediment Series No. 9, U.S. Army Corps of Engineer Division Missouri River Corps of Engineers, Omaha, Nebraska, 1957.
11. Ackers, P. and Charlton, F.G., "The Slope and Resistance of Small Meandering Channels," Inst. Civil Eng. Proc., Suppl. SV, Paper 7362S, 1970.
12. Parker, G., "On the Cause and Characteristic Scales of Meandering and Braiding in Rivers," Journal of Fluid Mechanics, Vol. 76, Part 3, pp. 457-480, 1976.
13. Church, M. and Rood, K., "Catalogue of Alluvial River Channel Regime Data," Department of Geography, University of British Columbia, Vancouver, British Columbia, Canada, 1983.
14. Quraishy, M., "The Meandering of Alluvial Rivers," Sind Univ. Res. J. (Sci. Ser.), 7, pp. 35-152, 1973.

APPENDIX II.—NOTATION

The following symbols are used in this paper:

- B = width of channel (meters)
- Br = braided channel
- d_o = depth of channel (meters)
- E* = ratio indicating morphology
- F = Froude number ($V/\sqrt{gd}$)
- g = acceleration of gravity
- K = constant used by Lane
- Me = meandering channel
- Q = channel discharge
- S = longitudinal channel slope
- V = average channel velocity
- π = constant (3.1416)

APPENDIX III.—SELECTED DATA SET FROM CHURCH AND ROOD

Accession Number	Description	Pattern (Br=Braided; Me=Meandering)	Discharge (m^3/sec)	Slope	Width (Area/Depth, m)	Depth (m)	Velocity (m/sec)	Grain Size (D_{50} mm)
00001	Towanda Cr. Nr Monroeton, PA	Me	368	.00420	47	2.41	3.25	45
00004	Green R. at Munfordville, KY	Me	581	.00085	99	7.01	0.84	21
00005	Elk R. Nr Prospect, TN	Me	668	.00080	69	5.95	1.64	14
00020	Blacks Fork Nr Little America, WY	Me	226	.00080	58	1.78	2.19	18
00023	White R. Nr Soldier Summit, UT	Me	12.2	.00250	14	0.70	1.30	2.7
00024	Sweetwater R. Nr Alcova, WY	Me	79.3	.00080	29	1.43	1.91	1.0
00033	Cocolamus Ck. Nr Millerstown, PA	Me	45.3	.00290	29	1.71	0.92	35
00035	Rio Grande at Cochiti, NM	Br	229	.00127	90	1.25	2.04	0.4
00041	Valley Cr., Idaho, Nr mouth	Me	28.3	.00400	24	0.76	1.50	30
00075	N. Platte R. Nr Douglas, WY	Me	42.3	.00095	95	0.52	0.91	48.8
00092	N. Platte R., N. Platte, NE	Br	65.1	.00140	165	0.52	0.73	0.2
00093	N. Platte R. Nr Sutherland, NE	Br	15.2	.00110	104	0.28	0.52	0.2
00094	N. Platte R. Nr Lisco, NE	Br	32.2	.00125	122	0.41	0.64	0.5
00098	Peace R. at Ft. Vermillion, Alberta, Can.	Br	2130	.00004	616	4.81	0.73	0.3
00099	Peace R. at Peace Pt., Alberta, Can.	Me	2278	.00007	643	4.32	0.82	0.2
00101	Beaver R. at Gold Lk. Reserve, Alberta, Can.	Me	27	.00021	46	1.12	0.54	0.6
00102	Red Deer R. Nr Empress & Nr Blindloss, Alberta, Can.	Me	69	.00030	171	0.85	0.48	0.3
00103	S. Saskatchewan R. at Hwy 41, Alberta, Can.	Me	213	.00036	201	1.76	0.60	0.3
00105	E. Prairie R. Nr Enilda, Alberta, Can.	Me	6	.00050	22	0.42	0.70	0.3
00107	Medicine R. Nr Eckville, Alberta, Can.	Me	6	.00051	17	0.60	0.60	0.3
00108	Atabasca R. at Embarras Airport, Alberta, Can.	Me	767	.00009	384	2.65	0.76	0.2
00116	Red Deer R. Nr Sundre, Alberta, Can.	Me	24	.00490	51	0.54	0.88	28
00119	Sheep R. at Otocks & Nr Aldersyde, Alberta, Can.	Me	7	.00380	28	0.39	0.60	31
00124	Bow R. at Calgary, Alberta, Can.	Br	93	.00180	101	0.94	0.98	40
00126	Bow R. below Bassano Dam, Alberta, Can.	Me	124	.00081	143	1.12	0.76	32
00140	Clearwater R. Nr Rocky Mtn. House, Alberta, Can.	Me	26	.00120	54	0.82	0.57	27
00141	Prairie Ck. Nr Rocky Mtn. House, Alberta, Can.	Me	4	.00360	22	0.39	0.54	43
00152	Willow Ck. Nr Claresholm, Alberta, Can.	Me	3	.00080	19	0.51	0.33	23
00161	Milk R. at Milk River, Alberta, Can.	Me	8	.00059	27	0.51	0.60	19
00171	Oldman R. Nr Monarch, Alberta, Can.	Me	45	.00120	88	0.64	0.79	30

Appendix III (cont'd)

Accession Number	Description	Pattern (Br=Braided; Me=Meandering)	Discharge (m^3/sec)	Slope	Width (Area/ Depth, m)	Depth (m)	Velocity (m/sec)	Grain Size (D_{50} mm)
00172	Gakona R. at Gakona, AK	Br	127	.00410	61	1.17	1.77	21
00173	Gulkana R. at Gulkana, AK	Me	510	.00420	152	1.01	3.35	21
00174	Tazlina R. Nr Glenallen, AK	Br	630	.00310	108	2.30	2.60	40
00177	Squirrel Ck. Nr Tonsina, AK	Me	8.5	.01560	12	0.49	1.58	18
00178	McLaren Ck. Nr Paxson, AK	Br	161	.00070	90	1.19	1.55	8.5
00180	Yukon R. at Rampart, AK	Me	11553	.00040	594	8.84	2.23	13.4
00181	Salcha R. Nr Salchaset, AK	Me	368	.00080	99	2.79	1.37	18.8
00182	Chena R. Nr Two Rivers, AK	Me	163	.00170	68	1.23	1.83	19
00183	Little Chena R. at Fairbanks, AK	Me	73	.00200	37	3.51	0.59	13.5
00185	Copper R. Nr Chitina, AK	Me	4474	.00150	229	7.01	2.87	--
00187	Tanana R. at Harding Lake, AK	Br	1954	.00150	161	4.57	2.71	--
00188-00201 are tributaries of the Yukon River within the Yukon Territory of Canada								
00188	Wheaton R. Nr Carcross	Me	7.5	.00150	25	0.73	0.43	27
00189	Yukon R. above Frank Ck.	Me	296	.00050	88	2.74	1.24	14
00193	Yukon R. above White R.	Br	1272	.00040	351	3.10	1.17	13
00196	Stewart R. at Mayo	Me	368	.00026	202	2.89	0.63	22
00199	Lubbock R. Nr Atlin, B.C.	Me	4.3	.00038	10	0.94	0.46	0.4
00201	McClintock R. Nr Whitehorse	Me	10	.00053	22	1.25	0.37	0.4
00227	Wye R. Bredwardine Bridge, So. Britain	Me	550	.00070	59	4.19	2.20	28
00237	Dean R. at Adlington Hall	Me	0.7	.01150	8	0.20	0.47	23.8
00239	N. Saskatchewan R. at Drayton Valley, Alberta, Can.	Me	2270	.00150	244	4.36	2.10	30
00250	Niger R. at Jebba, Nigeria	Me	1500	.00013	515	3.00	1.00	0.5
00253	Red Deer R. Nr Duchess Bridge, Alberta	Me	1133	.00027	226	3.76	1.33	0.3
00254	Red Deer R. Nr Jenner Ferry, Alberta	Br	850	.00030	186	2.97	1.54	0.4
00255	Red Deer R. Nr Buffalo Bridge, Alberta	Me	850	.00031	187	2.20	2.06	0.3
00258	Chilliwack R., Ryder Ck. to Vedder Crossing, B.C., Can.	Br	69	.00690	66	0.64	1.65	32
00261	Little Grizzly Ck. above Hebron, CO	Me	6.7	.00230	10	0.48	1.35	23
00263	N. Platte R. Nr North Gate, CO	Me	0.7	.02600	2	0.20	1.50	49
00269	Little Muddy Ck. Nr Parshall, CO	Me	1.9	.00610	5	0.31	1.18	24

DESIGN OF CHANNELS WITH COHESIVE BOUNDARIES

by Terry S. Smith

Introduction

The design of stable channels has always been one of the most important and complex hydraulic engineering problems. Lane (1953) defined a stable channel as follows: "A stable channel is an unlined channel for carrying water, the banks and bed of which are not scoured by the moving water, and in which objectionable deposits of sediments do not occur."

Sediment is typically divided into two categories: (1) cohesionless, or coarse material consisting primarily of sand and gravel; and (2) cohesive, or fine material composed of mixtures of silts and clays which exhibit various degrees of cohesion. These two classes of sediment differ substantially in their interaction with flow-induced hydrodynamic forces. The primary resistance to erosion for cohesionless sediments is provided by gravitational forces. Many empirical and semi-theoretical relations have been determined for quantitative analysis for cohesionless sediments. None of these relations are applicable to cohesive sediments. For cohesive materials the hydrodynamic forces are greatly exceeded by the physico-chemical forces between the clay particles.

There has been vast research in the area of cohesive sediments; however, due to the variations in approach by the researchers, little correlation exists. The intent of this paper is to give a generalized discussion of the properties of cohesive soils and to make a comparison of design methods used today for channel design. This paper is not intended to be a basis for design; laboratory and field erosion investigations are still required at present to quantitatively evaluate a channel with cohesive bed and banks.

Background

Early studies of the resistance to erosion of cohesive soils were directed toward the development of design criteria for stable channels. Empirical correlations of bed shear stresses or critical velocity were formulated in terms of the mechanical properties of cohesive materials such as porosity, bulk density, vane shear strength, particle size, and compaction.

It was not until the early 1960's that researchers dealt with the effect of electro-chemical factors of cohesive sediments. From this research it was clear that the properties of the sediment that determine its resistance to erosion are not completely defined. Shear strength, plasticity index, and perhaps clay content have an important bearing on the phenomenon; but they apparently do not describe it completely. The chemical and environmental factors outlined by the numerous researchers (1, 2, 11, 15, 16, 18, 19, and

20) must also be considered. The effect of these has not been studied systematically in the laboratory investigations.

Continued developments on sediment fabric analysis, physico-chemical analysis, and mechanistic models for rates of erosion and deposition of cohesive sediments have continued to develop. The state-of-the-art has shown continued improvement, but methods for predicting the rates of erosion and deposition of cohesive sediments still require the laboratory evaluation of various constants and parameters for both empirical and mechanistic models.

Behavior of Cohesive Materials

A flowing fluid exerts hydrodynamic forces on its boundaries. The particles which comprise these boundaries are subjected to these hydrodynamic forces of drag and lift, in addition to the gravitational force on these particles. These forces apply to both cohesive and noncohesive materials. In addition to the above mechanical forces, cohesive material is subjected to physico-chemical forces which act in all directions.

Before a cohesive material can be eroded, its interparticle bond must be overcome by excessive shear stresses. This is different from noncohesive material where gravity is the only resistance to erosion. Due to this difference in the erodability of materials, the relations used for noncohesive materials are not applicable to cohesive materials. For this reason, the following factors in this section should be considered in the design of channels with cohesive boundaries.

Cohesive material. Cohesive material typically consists of variable amounts of clay-sized (colloidal) and silt-sized particles. Fine grained sand-sized particles sometimes comprise a smaller fraction of the cohesive mixture. A medium size clay of $2\,\mu$ or less in diameter must be present in sufficient quantities to produce the physico-chemical interparticle bond; therefore, fine-grained material does not necessarily produce cohesive properties.

There are numerous groups of clay minerals such as kaolinites, montmorillonites, etc., but each group possesses a common factor. This factor is the plate like structure of an individual discrete particle of the clay. The physico-chemical forces that produce the cohesive nature of a material is due in part to this physical shape. A residual electric charge is developed on the individual clay particles which attract neighboring particles, thus producing the cohesive value of a material.

Erodability. Before cohesive soils can be eroded, the interparticle bond must be broken. Thus, a critical shear stress has to be exceeded before erosion of a cohesive soil can occur (1). This is different from the case of cohesionless material where resistance to erosion is a result of gravity only. A bond is broken when a certain minimum or threshold internal bond energy is exceeded. This is caused as flow-induced shear deforms the aggregate at the bed surface, and if due to this process all inter-particle bonds connecting an aggregate to its neighbors are ruptured, the aggregate will be entrained.

The shear stress required to erode a cohesive sediment is significantly affected by such things as the amount and type of clay mineral, microscopic and macroscopic clay properties, water content, pH, and temperature of the eroding water as well as the pore water of the clay, the thixotropy and consolidation of the clay, and the resulting clay fabric (13).

Most of the work involved in the determination of the critical shear stress of cohesive soils has included the plasticity index. The plasticity index is the difference between the liquid limit and the plastic limit of the sediment. The liquid limit is the water content in percentage by weight of the dry sediment at which the sediment exhibits a small shearing strength. The plastic limit is the water content in percentage by weight of dry sediment at which the sediment begins to crumble when rolled into thin cylinders. This plasticity index can generally serve as an indicator of whether one class of soils is likely to be more erodable than another.

The general case is that a sediment with high plasticity is probably more resistant to erosion than a sediment with a low plasticity index; however, other variables are involved so that the plasticity index combined with vane shear strength and void ratio are not the primary means of soil classification. These variables tend to serve as a secondary type of classification only. Figure 1 shows the relationship between vane shear strength and void ratio to critical tractive force. A variation of critical shear stress with plasticity index is shown in Figure 2. Also, this figure demonstrates that the shear stress required to initiate erosion is increased as the consolidation pressure of the soil increases (13).

The clay material within a sample is responsible for the cohesive nature. As the percentage of clay increases, the net effect is a corresponding increase in the cohesiveness of the soil. Tests performed by Kamphies and Hall (13) on illite and montmorillonite clays have shown this relationship.

Raudkivi and Hutchinson (1974) studied the effects of salinity and temperature on the erosion resistance of clay. They concluded that at low salinities temperature is important, while at high salinity there is little effect of temperature on erosion rates. Generally, erosion rates increase with increasing temperature (14). Further research on salinity concentration (16) has determined that the influence of salinity decreases beyond 10 ppt. Figure 3 shows the effects of salinity on bed shear stresses.

The element of time has been proven to be essential in the evaluation of cohesive soils by numerous researchers. Time is of primary importance in determination of the resistance to erosion. This is particularly true in the laboratory testing of cohesive soils. Clays (depending on type) tend to take up to 10 days to develop the full resistance to erosion after compaction. This time is necessary for the clay particles to hydrate the free water content which increases their interparticle bonding strength. This process of time to increase interparticle strength is known as thixotropy. Without the consideration of the time in testing a soil sample, it may be underrated as to its resistance to erosion. Figure 4 shows the variation of shear strength in relation to time (16).

Ariathurai and Arulanandan (1) studied erosion rates as a function of physical and chemical interactions. Their research included evaluation of the sodium absorption ratio, cation exchange capacity, and pore fluid ion concentrations. Further evaluation of these chemical parameters is beyond the intended scope of this report. They were included only to indicate the evaluation of cohesive soils is beyond merely physical determination.

The permissible velocities as related to cohesionless sediment decrease with decreasing sediment size. This relation holds true until a sediment size of approximately 0.1 mm is reached. As sediment size continues to decrease from 0.1 mm, the sediment begins to exhibit cohesive properties and the permissible velocity increases. This opposite relation is due to the inter-particle bonding of cohesive soils. Figures 5 shows this relation as presented by Hjulstrom (1935).

Deposition. The deposition of a cohesive sediment should be considered in a channel design. As in many circumstances, the deposited sediment may tend to be more tolerant to shear stresses than that of the natural channel boundaries. This is significant in that the weaker (least erosion resistance) area may shift, as from bed to banks. Therefore, the changes cohesive sediment undergoes during deposition must be understood.

The suspended clay particles, for flocculation to occur, must be brought close enough together for their surface forces to interact. This is accomplished by (1) Brownian motion, (2) differential setting velocities, and (3) velocity gradients within the fluid mass. For particles less than 1 in diameter, the Brownian motion is predominant. For particles greater than 3μ the velocity gradients tend to outweigh the effects of Brownian motion. Therefore, once flocs of the order of 3μ begin to form in open channels, the velocity gradient can be considered as the governing factor (17).

From the above description of flocculation, it is indicated that deposition of cohesive soils is dependent more on amount of turbulent and thermal energy than on a minimum velocity. A velocity decrease, however, has a double effect on deposition. It reduces the turbulence intensity and the maximum floc-size the flow can carry in suspension. It also increases the floc size itself so that eventually flocs will be combined in floc aggregates and possibly into aggregate networks, at which time deposition will occur (17).

The freshly deposited bed has a highly honeycombed structure with a large void ratio. The basic unit of this structure is the floc were small clusters of clay particles are packed relatively densely with respect to the overall clay density. The flocs are grouped into floc aggregates which also join together to form the aggregate network. The network-like flocculated structures are crushed due to overburden after they deposit. Crushing increases the bed shear strength because aggregates of a given density and shear strength break up into constituent aggregated units which are more dense and possess a higher shear strength. Successive breakdowns of aggregates with increasing overburden results in increasing shear stress with depth (16). Beyond a certain overburden, however, the aggregates are difficult to crush further without applying an internal compressive force; therefore, the shear

stress approaches a maximum with depth of material. This overburden causes an increase in the consolidation pressure which results in a decrease in interparticle spacing. This, in turn, increases the cohesive strength of the mass by increasing the interparticle bonding forces, which results in an increase in the resistance to erosion.

Design Methods

The design methods presented in this section represent the more prominent relations used for channel design where cohesive materials are present. These methods are not recent, but do provide reasonable results. Research in the area of cohesive materials has increased in the past several years; however it tends to be centered on specific cohesive relations such as salinity, temperature, chemical interactions, etc. Thus, recently published procedures for a comprehensive cohesive channel design do not exist.

Simons method. The following method was predominantly developed by Simons (23) with additional research by Albertson. Simons' approach derived all relations from actual field observations. The channel design method that was developed allows for complete graphical design of a channel with cohesive bed and banks.

The method consists of the following calculations:

1. The required cross-sectional area of water

$$A = 1.076\ Q^{0.873}$$

2. The average velocity

$$\overline{V} = Q/A$$

3. The hydraulic radius

$$R = 0.285\ Q^{0.42}$$

4. Depth determined from Figure 6 with bottom and top widths

$$W_B = A/D$$

$$W_T = \frac{W_B + 2.0}{0.92}$$

Henderson method. Henderson (13) used the data presented by Simons and Albertson to develop numerical relations. The equations provide a reasonable correlation to that of Simons (22) in the previous section. These equations are as follows:

$$\text{Wetted Perimeter:} \quad P = 3.98\ Q^{0.33}$$

Bottom Width: $B = 0.9\ P$

Surface Width: $B_S = (B+0.61)/0.92$

Hydraulic Radius: $R = 0.407\ Q^{0.36}$

Depth: for $R<2.1$ $\quad Y = 1.21\ R$

for $R \geq 2.1 < 7$ $\quad Y = 0.61 + 0.93\ R$

for $R \geq 7$ $\quad Y = 0.93\ R$

Mean Velocity: $V = \frac{\nu}{B} \left(\frac{C^2}{0.87\ g}\right)^{1/0.37}$

where ν = kinematic viscosity
Q = flow, cfs
Y = depth, in feet
C = Chezy constant

Farraday and Charlton method. Farraday and Charlton (7) recognized that cohesive material behavior is more complex than that of noncohesive material. Their approach centered on the physico-chemical characteristics and the density of the cohesive material rather than just the gravitational effects as of noncohesive material.

Table 1 presents a summary of the physical properties of a clay material. These properties are to aid in the utilization of the equation

$$Y = 51(4N^{0.86})\ q^{0.86}\ \tau_c^{-0.43}$$

where

Y = mean depth of flow, m
N = Manning's coefficient of roughness
q = discharge per unit width, m^2/sec
τ_c = critical tractive stress, N/m^2

Mirtskhulava method. The method of channel design in cohesive material as presented by Mirtskhulava (24) is dependent on a single equation for permissible velocities.

$$U_{per} = \log\left(\frac{8.8}{D}\right)\left[\frac{2gm}{2.6\ \gamma_N}(\gamma_s-\gamma)D + 1.25\ C_f k\right]^{\frac{1}{2}}$$

where:

m = coefficient of the aggregates, typically equal to unity
n = 1 + D/(0.00005 + 0.3D)
C_f = 0.035 c

c = factor of cohesion
k = homogeneity factor of the soil
D = diameter, mm
d = depth of flow
U_{per} = permissible velocity in mps.

The above equation is a modified version of Mirtskulava's equation for noncohesive materials greater than 2 mm in diameter.

The above approach by Mirtshulava is somewhat novel in the evaluation of the resistance to cohesive soils. His approach considers erosion of aggregates from the bed rather than individual soil particles. The size of the aggregate was reported to indicate the influence of velocity, friction, and turbulence on the bed.

U.S.S.R. method. The method presented by the U.S.S.R. (24) is shown in Figure 7. This method of design estimates the permissible velocity as a function of gradation and void ratio. Little background information is available concerning this method, therefore, the sources underlying much of the development and the basis for selecting values of parameters cannot be determined.

Ven Te Chow (1959) has interpreted this method on permissible velocities and expressed them in terms of permissible tractive force which he stated depends on the clay content of the soil and the void ratio and covers a substantive range of values from 0.02 to 0.8 lb/ft^2.

Comparison of Methods

As emphasized previously, the properties of cohesive material are not fully understood even though considerable research has been performed over the past three decades. In an effort to evaluate and compare the methods, various assumptions were necessary. These assumptions pertained to the variations in the methods and included such items as sediment size, void ratio, compaction, moisture content, etc.

The Simons method was considered first since it was derived from actual field data. The associated data was collected from canals with cohesive bed and banks in Wyoming, Nebraska, and Colorado. It was, therefore, assumed that results of this empirical relation would be representative of natural channels with consideration to the cohesive properties associated with the test channels.

Discharge values of 500, 1000, 5000, and 10000 cubic feet per second were used for comparison. This flow range was selected to enable the evaluation of the methods over a range of channel sizes. Value of Manning's n was assumed to remain constant at 0.030 in this comparison. Results of this method for the assumed conditions are presented graphically in Figures 8 and 9.

As stated above, these results should be representative of cohesive bed and banks channels with the same cohesive properties from which the Simons method was derived.

The method presented by Henderson provides numerical functions based on Simons approach. Results of his equations are fairly close to those obtained graphically using Simons and therefore are not further covered in this report.

The method presented by Farraday and Charlton was evaluated based on the results of Simons. This was done for comparative purposes. The discharge and channel width remained fixed while the mean depth of flow was allowed to vary in relation to the critical tractive stresses of the cohesive boundaries. This critical tractive stress is related to soil moisture content and void ratio (Table 1). Results of this method are presented in Figures 8 and 9. It appears from Figure 8 that the method by Farraday and Charlton brackets the Simons approach. With fixed channel widths and constant discharge, one may determine the mean permissible channel velocities using these methods. It is apparent that with consideration given to the critical tractive stress of the cohesive material, channel geometry can change considerably. This relation to tractive stresses has been substantiated by numerous researchers.

The method by Mirtskhulava was also evaluated using the results of Simons; however, the diameter of the cohesive material was allowed to vary in this evaluation. Mean sediment size values of 0.2, 0.04, 0.01,. and 0.004 mm were arbitrarily selected to represent a comparable range of clay sizes for evaluation. The results of this method are presented in Figures 9 and 10. They substantiate the relationship presented by Hjulstrom (1935). Figure 5 shows Hjulstrom's relation where decreases in the mean sediment size below approximately 0.1 mm result in increases in the permissible velocity due to a factor of cohesiveness. It should further be noted that the velocities obtained by Mirtskhulava appear to be somewhat conservative compared to Hjulstrom for sediment sizes smaller than 0.01 mm. Also, permissible velocities are only slightly affected by depth in the Mirtskhulava approach.

The method presented by U.S.S.R. researchers was evaluated assuming a loosely compacted soil and a compacted soil. This method allows for complete graphical evaluation to determine maximum permissible velocities. These velocities were further corrected for the depths determined by Simons method, so as to allow comparison. Results are shown in Figure 9. As indicated, these results are closely related to those of Simons.

The variation in approaches by the different researchers makes a comparison difficult. These different approaches, however, do provide some good points for further consideration. In an effort to "take the best from each," the following relation was derived.

$$U_{per} = \frac{\rho_s}{2.65} d_c \, (0.2818 \, \overline{d}^{-0.73})$$

where:

U_{per} = permissible velocity in feet per second

ρ_s = density of soil

d_c = degree of compaction for loose, medium, and compacted soils (0.85, 1.00, and 1.15, respectively)

$\overline{d}$ = mean sediment size in millimeters.

This equation may be used to determine permissible channel velocities for a particular channel. Combining this relation with the relation by Simons for hydraulic radius allows a preliminary channel design to be obtained.

$$\text{Hydraulic Radius, } R = 0.407\ Q^{0.36}$$

A comparison of this method with that of Mirtskulava is shown in Figure 10.

Results

The methods for design of cohesive boundary open channels were evaluated to determine their applicability. From this evaluation, the following results were derived.

1. The Simons method appears to provide a good preliminary design; however, in a major channel design, the critical tractive stresses should be evaluated. These stresses, at present, can only be determined by laboratory analysis.

2. The equations by Henderson provide a close approximation to those of Simons.

3. The method by Mirtskhulava appears to be slightly conservative.

4. The method presented by Farraday and Charlton appears to provide a good representation of actual conditions and warrants further consideration; however, some consideration to mean diameter and chemical properties should be evaluated, especially in the higher compacted range.

5. The method presented by the author can be used for a preliminary design of a cohesive boundary channel and requires a minimum of data.

Conclusion

The evaluation of open channels with cohesive boundaries is very complex and not completely understood. Numerous researchers have evaluated cohesive material with only varying levels of success. The following conclusions were derived from the evaluation of research pertaining to cohesive soils as applied to channel design.

1. Physical and chemical properties (as well as time) are involved in the evaluation of cohesive soils.

2. Empirical relations are, at present, the best method for evaluation.

3. Generally, the cross-sectional area of a cohesive channel is less than that of a non-cohesive channel.

Recommendations

The analysis of channels with cohesive bed and/or banks is very complex and difficult. As a means of gaining a more comprehensive insight than this brief report provides, the following studies are proposed:

1. Determine the method of erosion (by single discrete particles or by an aggregate).
2. Determine variations in bed roughness as erosion is taking place.
3. Determine the effects of secondary circulation on erosion.
4. Determine the critical tractive stress as related to the various types of clay minerals.
5. Determine the erosional resistance of flocculated clay particles.

References

1. Ariathurai, R. and Arulanandan, K., "Erosion Rates of Cohesive Soils," Journal of the Hydraulics Division, Vol. 104, No. HY2, February, 1978, pp. 279-283.
2. Arulananda, K., "Fundamental Aspects of Erosion of Cohesive Soils," Journal of the Hydraulics Division, ASCE, Vol. 101, No. HY5, 1975, pp. 635-639.
3. Bogardi, J., "Sediment Transport in Alluvial Streams," Akademiai Kiado, Budapest, 1978.
4. Brice, J.C., "Factors in Stability of Relocated Channels," Journal of Hydraulic Engineering, Vol. 109, No. 10, October, 1983, pp. 1298-1313.
5. Chang, H.H., "Stable Alluvial Canal Design," Journal of the Hydraulics Division, Vol. 106, No. HY5, May, 1980, pp. 873-891.
6. Chitale, S.V., "Shape and Size of Alluvial Canals," Journal of the Hydraulics Division, Vol. 102, No. HY7, July, 1976, pp. 1003-1011.
7. Farraday, R.V. and Charlton, F.G., Hydraulic Factors in Bridge Design, 1983.
8. Flaxman, E.M., "Channel Stability in Undisturbed Cohesive Soils," Journal of the Hydraulics Division, Vol. 89, No. HY2, March, 1963, pp. 87-96.
9. Fortier, S. and Scoby, F.G., "Permissible Channel Velocities," Transactions, ASCE, Paper 1588, 1926.
10. Graf, W.H., Hydraulics of Sediment Transport, McGraw Hill Book Company, 1971.

11. Grissinger, E.H., "Resistance of Selected Clay Systems to Erosion by Water," Water Resources Research, Vol. 2, No. 1, 1966, pp. 131-138.

12. Haynie, R.M. and Simons, D.B., "Design of Stable Channels in Alluvial Material," Journal of the Hydraulics Division, ASCE, Vol. 94, No. HY6, November, 1968, pp. 1399-1419.

13. Henderson, F.M., "Stability of Alluvial Channels," Proceedings, ASCE, VOl. 87, No. HY6, November, 1961.

14. Izbicki, R.J., "Limit Plasticity Approach to Slope Stability Problems," Journal of the Geotechnical Engineering Division, ASCE, Vol. 107, No. GT2, February, 1981, pp. 228-234.

15. Kamphus, J.W. and Hall, K.R., "Cohesive Material Erosion by Unidirectional Current," Journal of Hydraulic Engineering, ASCE, Vol. 109, No. 1, January, 1983, pp. 49-61.

16. Kelly, W.E. and Gularte, R.C., "Erosion Resistance of Cohesive Soils," Journal of the Hydraulics Division, ASCE, Vol. 107, No. HY10, October, 1981, pp. 1211-1223.

17. Kuti, E.O., "Scouring of Cohesive Soils," Journal of Hydraulic Research, 1976, pp. 195-206.

18. Parchure, T.M. and Mehta, A.J., "Erosion of Soft Cohesive Sediment Deposits," Journal of Hydraulic Engineering, Vol. 111, No. 10, October, 1985, pp. 1308-1326.

19. Partheniades, E., "Erosion and Deposition of Cohesive Soils," Journal of the Hydraulics Division, Vol. 91, No. HY1, January, 1964, pp. 105-137.

20. Partheniades, E. and Paaswell, R.E., "Erodibility of Channels with Cohesive Boundary," Journal of the Hydraulics Division, Vol. 96, No. HY3, March, 1970, pp. 755-771.

21. Raudkivi, A.J., Loose Boundary Hydraulics, Pergammon Press, Oxford, 1976.

22. Sedimentation Engineering Manual No. 34, ASCE, 1975.

23. Simons, D.B., "Theory and Design of Stable Channels in Alluvial Materials," Master's Thesis, Colorado State University, Fort Collins, Colorado, 1957.

24. Simons, D.B. and Senturk, F., Sediment Transport Technology, Water Resources Publications, Fort Collins, Colorado, 1977.

25. Trout, T.J., "Channel Design to Minimize Lining Material Costs," Journal of the Irrigation and Drainage Division, ASCE, Vol. 108, No. IR4, December, 1982, pp. 242-250.

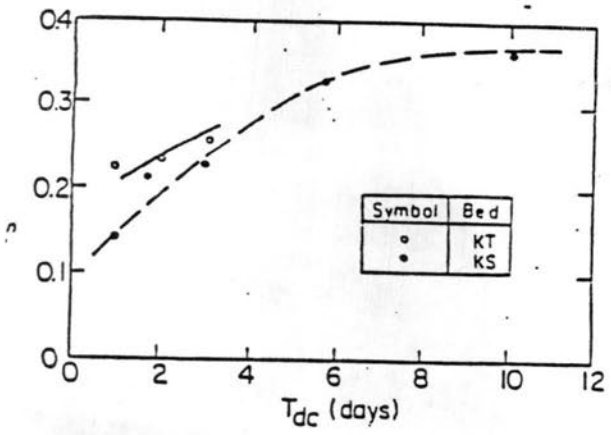

4. Shear strength versus time of consolidation.

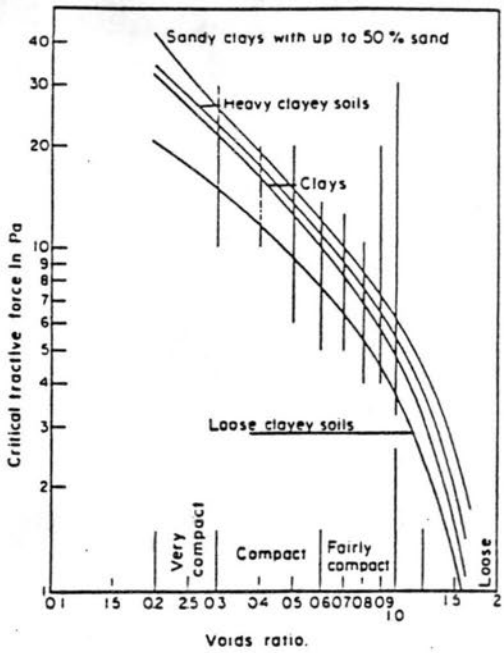

Figure 1. Void ratio versus critical shear stress.

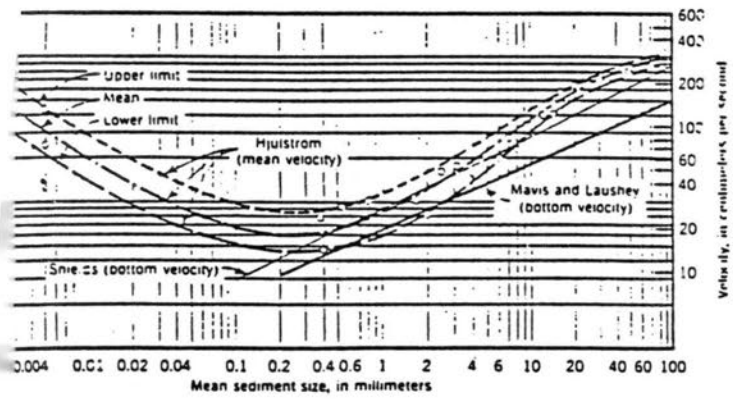

Permissible velocities as a function of sediment size.

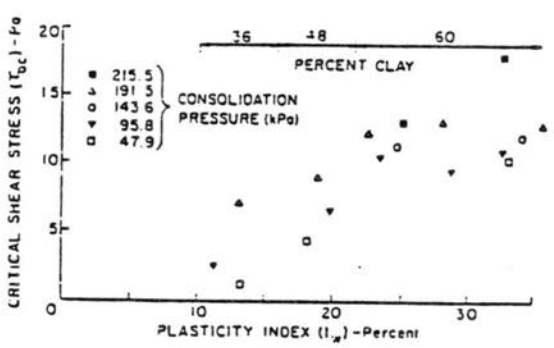

FIG. 2 —Critical Shear Stress as a Function of Plasticity Index

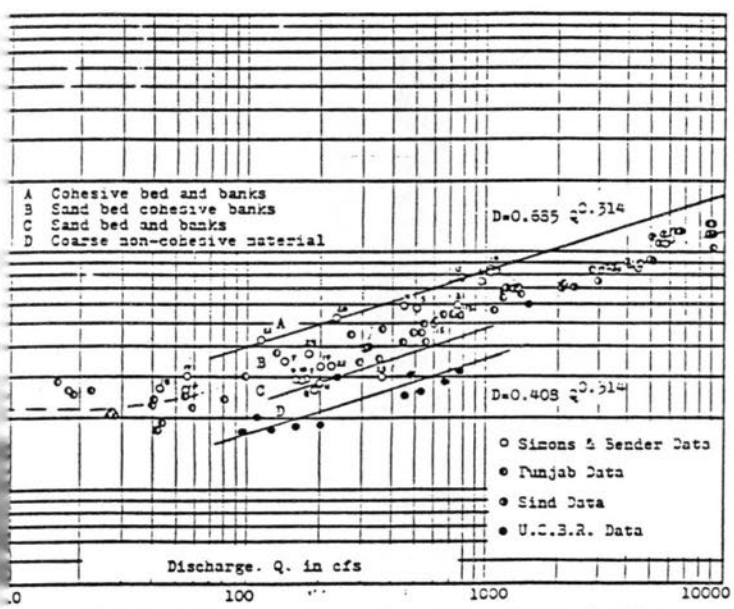

...ation of bed depth D with discharge Q and type of channel, all data

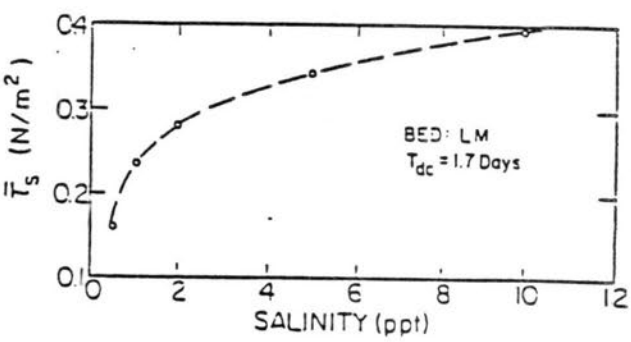

Figure 3. Shear strength versus salinity concentration.

gure 8. Depth versus Discharge.

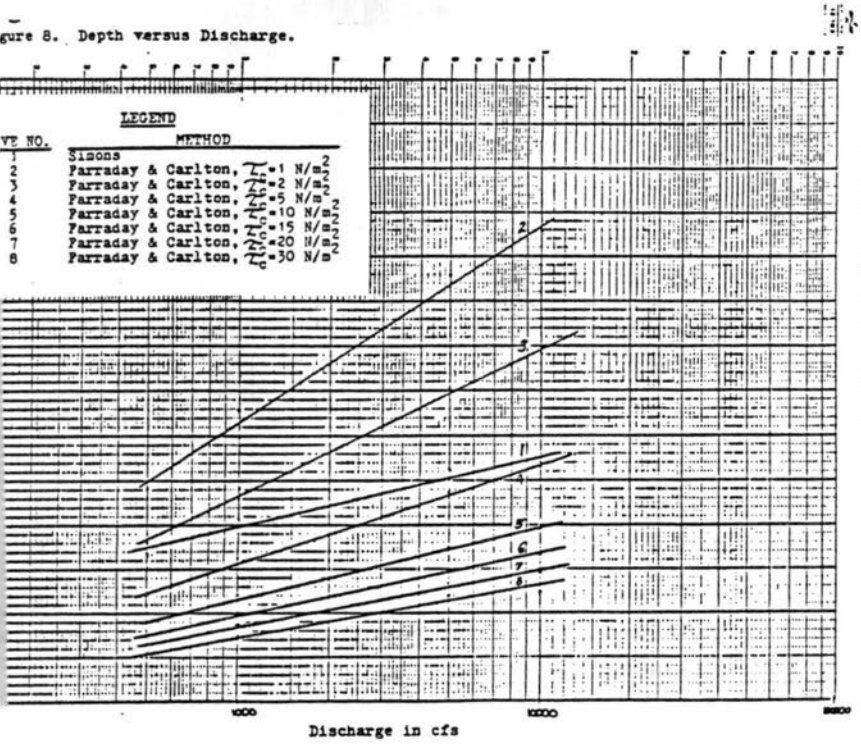

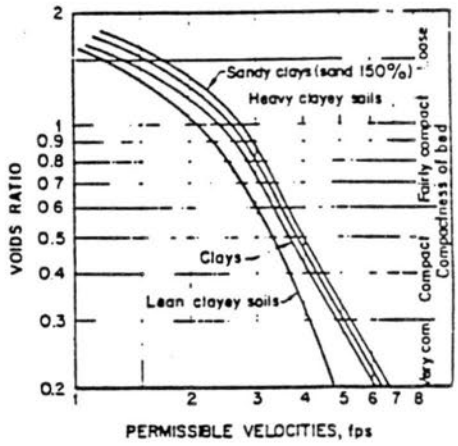

Figure 7. Permissible velocities for cohesive soils.

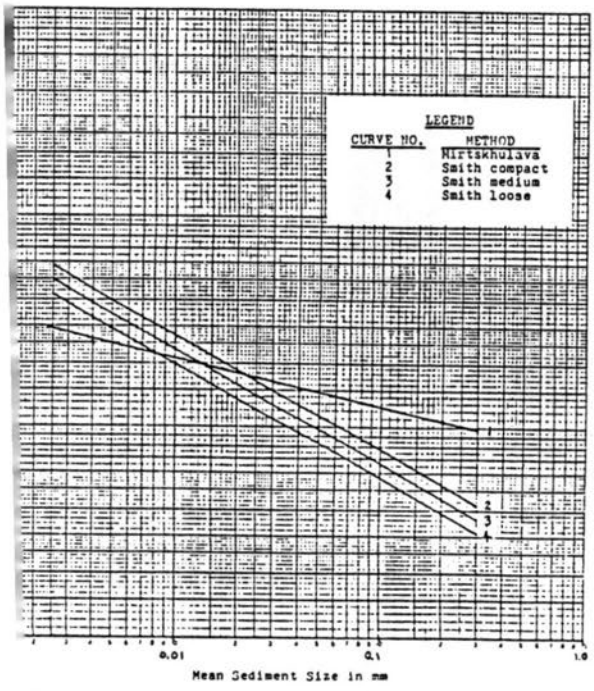

0. Permissible velocity versus mean sediment size.

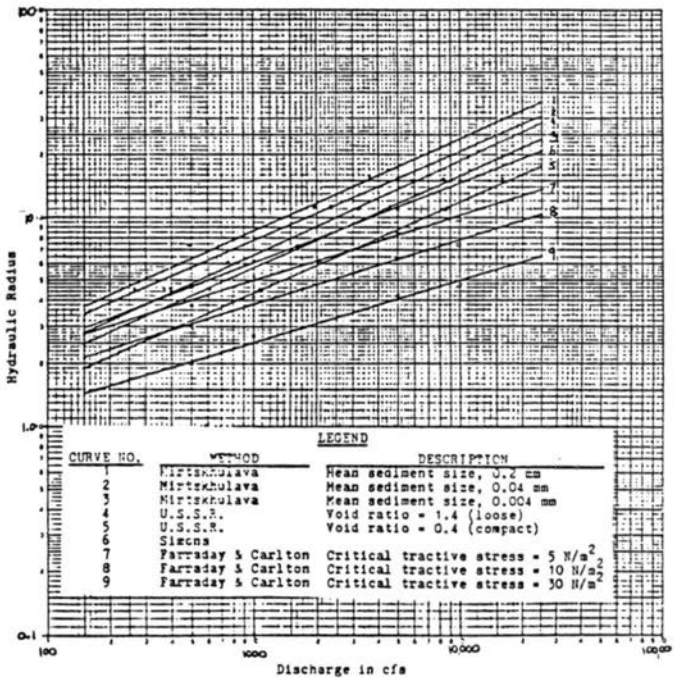

Figure 9. Hydraulic radius versus discharge for cohesive soils.

Table 1. Physical properties of clay

Voids ratio	2·0–1·2	1·2–0·6	0·6–0·3	0·3–0·2
Dry bulk density, kg/m³	880–1200	1200–1650	1650–2030	2030–2210
Saturated bulk density, kg/m³	1550–1740	1740–2030	2030–2270	2270–2370
Type of soil	Critical tractive stress, N/m²			
Sandy clay	1·9	7·5	15·7	30·2
Heavy clay	1·5	6·7	14·6	27·0
Clay	1·2	5·9	13·5	25·4
Lean clay	1·0	4·6	10·2	16·8

Table 2. Summary of Methods for Design of Channels with Cohesive Boundaries

Method	Equation	Consideration of Variables							
		Velocity	Discharge	Void Ratio	Depth	% Compaction	Moisture Content	% Clay Content	Soil Diameter
Simons	Graphical	X	X		X				
Henderson	$\overline{V}=\frac{v}{B}\left(\frac{C^2}{0.87g}\right)^{1/0.37}$	X	X		X				
Farraday & Charlton	$y=51(4N^{0.86}q^{0.86}t_c^{-0.93})$	X	X	X	X	X	X	X	X
Kirtskhulava	$U_{per}=\log\left(\frac{8.8d}{D}\right)\left[\frac{2gm}{2.6\gamma_N}(\gamma_s-\gamma D)+1.25\,C_f K\right]^{\frac{1}{2}}$	X		X	X	X	X	X	X
U.S.S.R.	Graphical	X		X	X	X		X	X
Smith	$U_{per}=\frac{\rho_s}{2.65}\,d_c\;0.2818\,d^{-.73}$	X				X			X

ON THE FALL VELOCITY OF PARTICLE IN NEWTONIAN AND NON-NEWTONIAN FLUID

Yongqiang Lan

ABSTRACT: The report is mainly concerned with the fall velocities of particles in sediment-water mixture of Newtonian or non-Newtonian fluids. A detail comparison and discussion of the several formulae developed in the past to predict the fall velocities of sediment particles in the mixture is presented. It's pointed out that Chu's formula is the best in dealing with the problem, although it's developed semi-emperically.

Meanwhile, the report also discuss the formulae predicting the fall velocities of free-settling particles in Newtonian fluid. It's concluded that Dou's formula is a very good improvement on Rubey's formula although it's too complicated to be used in practice.

I. INTRODUCTION

Most sediment transport processes need for their calculation of the fall velocities of the particles concerned therein. Normally there are different grain sizes and therefore different settling fall velocities. In natural, the fall velocity of the particle is affected by the following factors: 1) particle size; 2) particle shape; 3) mineral composition of the particles; 4) particle concentration; 5) size distribution of particles in suspension; 6) concentration of fine particles; 7) concentration of coarse particles; 8) tubulence; 9) particle rotation; 10) boundary conditions; 12) flocculation; 13) temperature of the fluids, and so on. In this report, only the effects of particle size and of concentration (including that of fine particles and of coarse particles) are discussed.

The settling fall velocities of particles in fluid has been investigated by many researchers since Stokes introduced his drag force law in 1851. As of instances there are Oseen's law, Goldstein's law, Rubey's formula,Dou's formula, etc, in quiescent distilled fluid; Steinour's formula, Richardson and Zaki's formula, Chu's formula, etc, in clay suspension or hyperconcentraed flow [Ref. 1,2,3,4,5,6]. In this paper, we can't list out all formulae developed in the past in order to make comparison, only those considered to be the representatives in this field are discussed.

II. FALL VELOCITY OF FREE SETTLING PARTICLE IN NEWTONIAN FLUID

When a spherical particle falls in a static Newtonian fluid, the drag force acting upon the particle is considered to be mainly related to the viscous force and the inertia force. Viscous force is dominated when the fall velocity is low, while inertia force becomes overwhelming as long as the particle Reynolds number exceeds 1,000. Considering only the viscous force led to Stokes' law, while Newton's law was derived by only considering the inertia force. Generally, both viscous force and inertia force are important to predict the fall velocities of sediment particles, so only Stokes' law or Newton's law is not enough. Although there is no theoretical solution to the problem involving both viscous force and inertia force up to now, many semi-empirical or empirical solutions are obtained by combining Stokes' law and Newtonian Law. Table (1) summarizes the representative analytical, semi-empirical or empirical formulae developed in the past to predict the fall velocity of sphere settling in quiescent Newtonian fluid. Meanwhile, the applicability of each formula is given.

From Fig.(1), it's easy to find that Dou's formula (for derivation,see appendex) provides the best approximation of drag coefficient to that given from the standard curve, compared with Stokes' law, Oseen's formula and the Rubey's formula. Although Dou's basic assumptions need to be corrected, his argument that the drag force is not a simply linear combination of Stokes' law and Newtonian law should be considered to be more reasonable than that of Rubey's formula. However, Dou's formula is to complicated due to the introduction of separarion angle θ . To apply Dou's formula, trial and error must be used, which is not convenient in practice although it can be applied to any size of sphere in Newtonian fluid. Instead, Rubey's equation is generally accepted when applied to the settling of natural particles although it has a big discrepancy from the standard curve. Besides, the author recommended the use of equation (6) when the particle Reynolds number is less than 300 (D=2.5 mm, for T=20^{o}c).

Besides those formulae mentioned above, there still are a number of empirical formulae developed in the past several decades, such as Swanson's ,

TABLE I REPRESENTATIVE FORMULAE PREDICTING THE FALL VELOCITY OF SPHERE

Athor	Drag coefficient	Eq.	Applicability	Ref.
Stokes	$C_D = 24/Re$	1	Accurate for $Re < 0.2$	
Oseen	$C_D = \frac{24}{Re}(1 + \frac{3}{16}Re)$	2	Accurate for $Re < 1.0$	1
Rubey	$C_D = \frac{24}{Re} + 2.0$	3	Accurate for $Re < 2.0$. Good for the prediction of fall velocity of Natural particles.	2
Dou	$C_D = 0.45\sin^2\frac{\theta}{2} + \frac{24}{Re}(1+\frac{3}{16}Re)\frac{1+\cos\frac{\theta}{2}}{2}$ $\theta = 1.78 \log(4Re)$ $\sin^2\frac{\theta}{2} = 1$ when $Re > 850$	4	Accurate for $Re < 6.0$. Applicable for the whole range of $Re < 10{,}000$; and the error will be less than 10%. Good for natural particles.	3
Kaskas	$C_D = \frac{24}{Re} + \frac{4}{Re^{1/2}} + 0.4$	5	$Re > 1.0$	12
Others	$C_D = \sqrt{\frac{24}{Re}\left(\frac{24}{Re} + 4.5\right)}$	17	$Re < 300$	13
	$C_D = \frac{18.5}{Re^{0.6}}$	18	$3 < Re < 200$	13

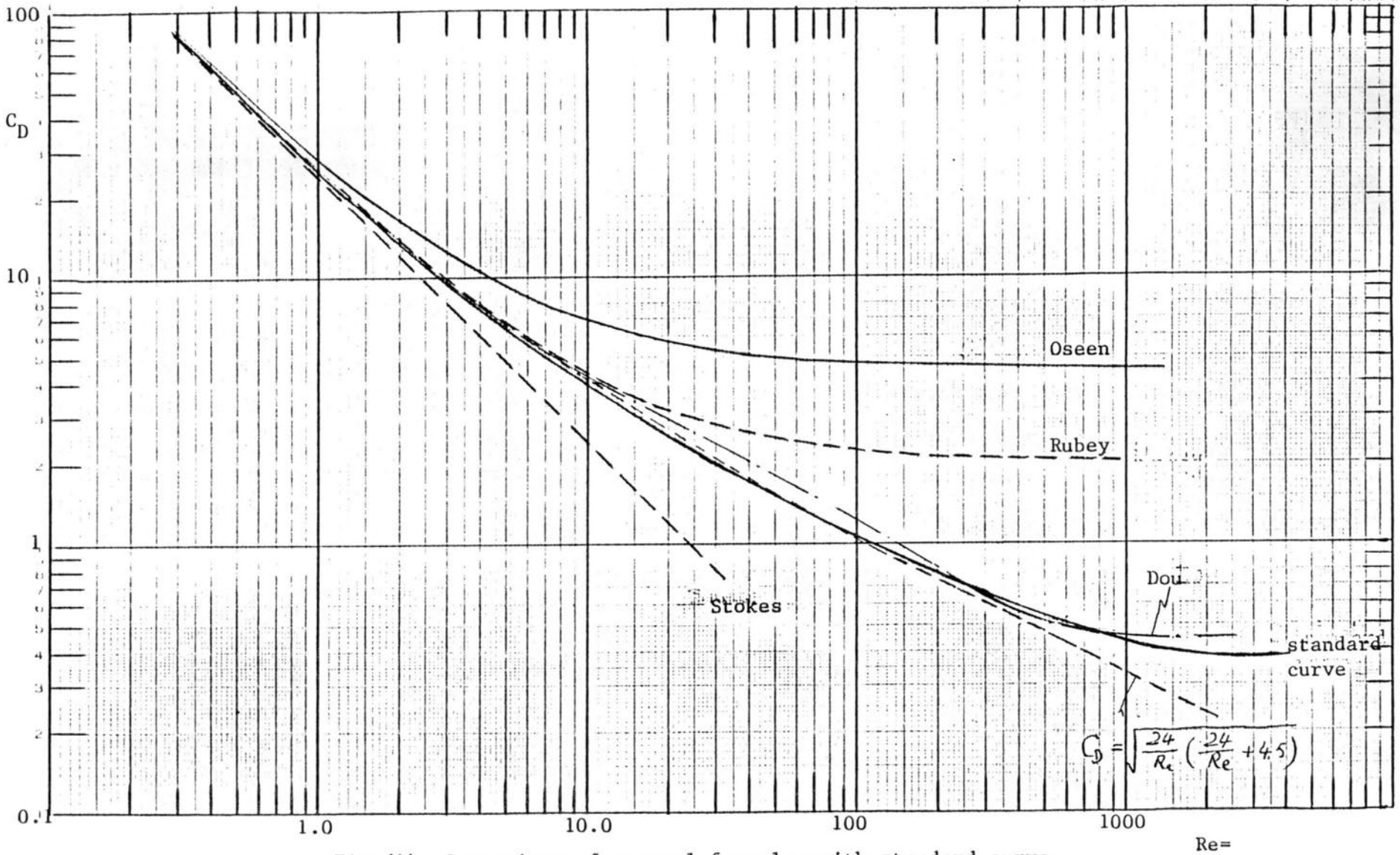

Fig.(1) Comparison of several formulae with standard curve.

Watson's formula and Gibb's formula, etc. However, those formulae are not widely used because of their complexity or lack of theoretical standing or both.

III. FALL VELOCITIES OF PARTICLES IN NON-NEWTONIAN FLUID.

With the increase of a certain number of sediment particles in the fluid the settling properties of any single particle in the fluid will be affected in the following ways;

(1) The existence of the large amount of sediment particles retards the movement of fluid around the particles, in equivalent, the viscosity will increase and the fall velocity of the particle will be decreased. Meanwhile if the extent of fine sediment in the fluid reaches a certain value to creat flocculation or loose structure, the viscosity of the sediment-water mixture will change remarkably. In sequence, the settling velocity of the particle will be changed dramatically.

(2) As the sediment concentration increases, the specific weight of the sediment-water mixture increases. Then the increasing of buoyance upon any particle will slow down the particle.

So the settling phenomena of sediment particle in sediment-water mixture is much more complicated than that in clear water. Especially when the sediment concentration is high , the fluid may change from Newtonian fluid to Non-Newtonian fluid, making the description of this phenomenon more difficult.

1. Uniform Settling in Fluid With Low Concentration.

Conventionally, there are two methods leading to the determination of fall velocities of sediment spheres in Stokes' range when sediment concentration is relative small: 1) The settling of all particles are considered to be the same as that one single particle settles in a small cylinder, the size of which is in equivalent to the center-distance between two particles. Cunningham's, MacNown's and Uchida's methods [7,8,9] are considered to this group; 2) The settling of any particle is affected by all the other particles in the fluid. The flow around any particle is the results induced by all the

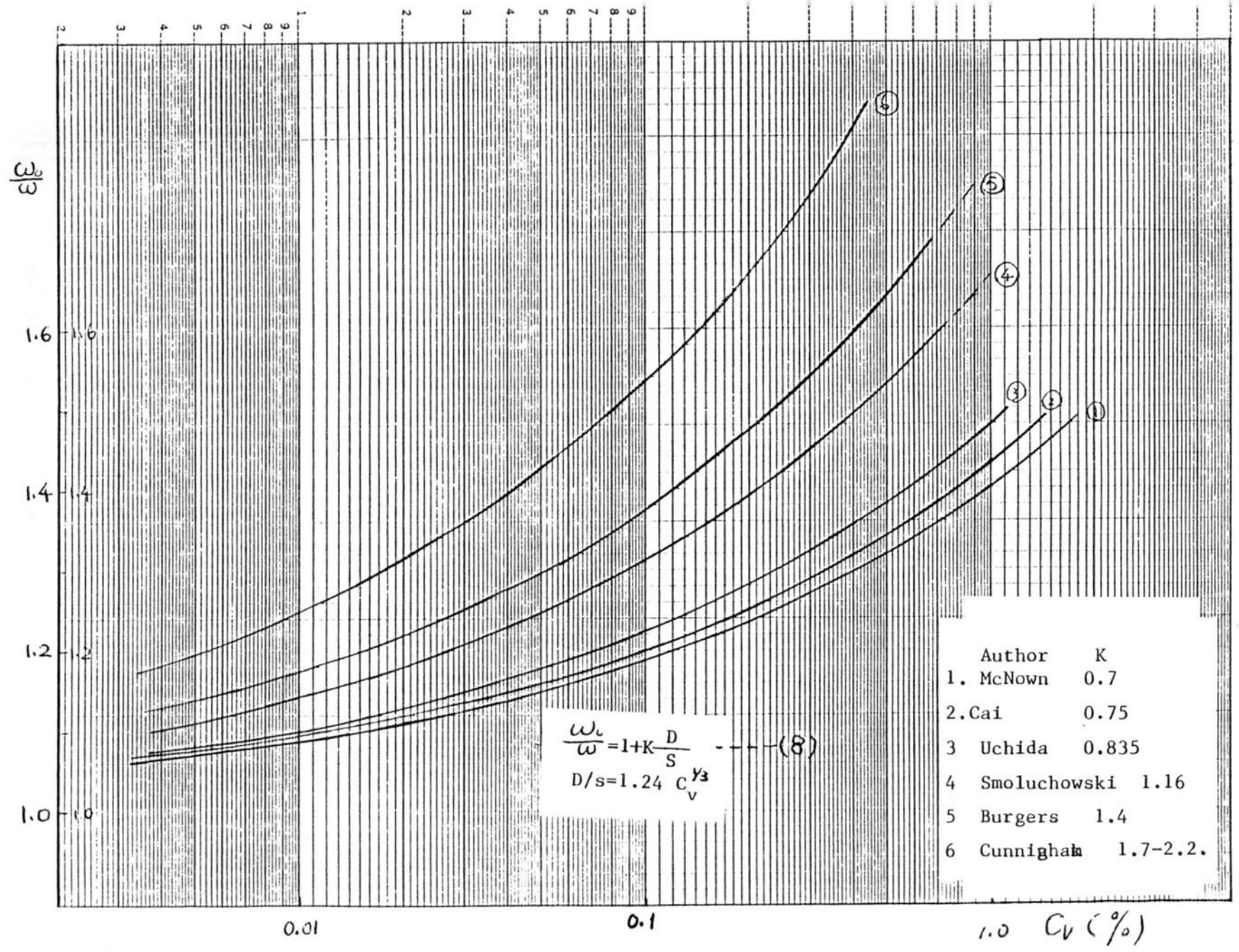
ω_c/ω
1.6
1.4
1.2
1.0
0.01
0.1
1.0
C_V (%)
$\frac{\omega_c}{\omega} = 1 + K\frac{D}{S}$ ----(8)
$D/s = 1.24\ C_v^{1/3}$
Author K
1. McNown 0.7
2. Cai 0.75
3 Uchida 0.835
4 Smoluchowski 1.16
5 Burgers 1.4
6 Cunnigham 1.7-2.2.

other particles in suspension. This theory was represented by Smoluchowski and Burgers (10,11).

Fig.(2) summarized the results given by the above mentioned researchers. It's interesting to find that those researchers gave their formula in the same form except that the coefficient in their formulae were different. It's observed that Cunningham's formula gave the largest value of $\frac{\omega_0}{\omega}$ and obviously it's questionable. Generally, Uchida's, Cai's and Smoluchowski's formulae can provide satisfactory results in Stokes' range. Beyond Stokes' range, Eq.(8) needs to be corrected, but the effect of sediment concentration will become smaller and smaller as the particle Re increases.[14] When Re exceeds 10, $\frac{\omega_0}{\omega}$ will be less than 1.1 for Cv$<$ 3%.

2. Uniform Settling in Fluid with High Concentration

Table II gives a list of several representative formulae developed previously to predict the fall velocities of non-flocculated particles uniformly settling in suspension. Steinour's, Hawksley's, Wan's formulae were based on the assumption that the effects of concentration could be taken into account by using the density and viscosity of the suspension, while Richardson and Zaki's method was based on the argument that the effect of concentration on the resistance force encounted by the particle is attributable to the increase in the velocity gradient rather than to the change in viscosity or density of the suspension.

From Fig.(3), we can see that those several formulae introduced in this section are in good agreement with each other within the Stokes' range, especially Wan's, Richardson & Zaki's and Qian's formulae almost coincide for Cv$<$0.3. Besides, Hawksley's formula gives somewhat larger value than any other formula gives. Nevertheless, all methods in the table are well defined and can be used within the Stokes range. Beyond the Stokes range, no satisfactory methods has been developed up to now. According to Richardson and Zaki, the coefficient n in their formula is a very complicated function of particle Reynolds number Re, and n approaches a constant (n=2.39) when Re exceeds 500. On the other hand, Qian's empirical formula from his experiments indicated that $\frac{\omega}{\omega_0}$ is affected not only

TABLE II[illegible].

Author	Formula	Explanation	Ref.
Richardson & Zaki	$\frac{\omega}{\omega_0} = (1-C_V)^n$ (9)	n is a function of Reynolds number; n=4.65 for laminar, n=2.39 for turbulent and N=f(Re) in intermediate region	5
Steinour	$\frac{\omega}{\omega_0} = \left[1-(1+K)C_V\right]^2 10^{-1.82(1+K)C_V}$ ----------(10)	K is a correcting coefficient due to the irregularity of the particles. For glass sphere with no-flocculation K=0,	4
Hawksley	$\frac{\omega}{\omega_0} = \beta(1-C_V)^2 \exp\left(\frac{-k_1 C_V}{1-k_2 C_V}\right)$ ----------(11)	β =1 for non-flocculated settling. K =5/2 for sphere and $\frac{5}{2}\Lambda$ for non-spherical particles. K =39/64 for spherical particles.	15
Wang	$\frac{\omega}{\omega_0} = (1-\beta C_V)^m$ ---------(12)	m=2.5. $\beta = \begin{cases} 1.77 & \text{for sphere sediment} \\ 3.92 & \text{for} \\ 5.0 & \text{sludge} \end{cases}$	16
Qian	$\frac{\omega}{\omega_0} = \frac{r_s-r_0}{r_s-r_m}\cdot e^{4.57 C_V}$ $= \left(\frac{r_m}{r_0}\cdot\frac{r_s-r_0}{r_s-r_m}\right)^{1/3} e^{4.57(C_V-0.36)+0.9}$ $= \left(\frac{r_m}{r_0}\cdot\frac{r_s-r_0}{r_s-r_m}\right)^{1/3}\left[e^{4.75(C_V-m)}+m\right]$ -----(13)	Suitable for Stokes settling for Newton's range for intermediate range, m=0.455logRe-0.27 n=0.21logRe -0.01	23 17
Wan	$\frac{\omega}{\omega_0} = \frac{(1-C_V)^2}{1+\frac{3}{\frac{1}{C_V}-\frac{1}{6.52}}}$ ------(14)		14

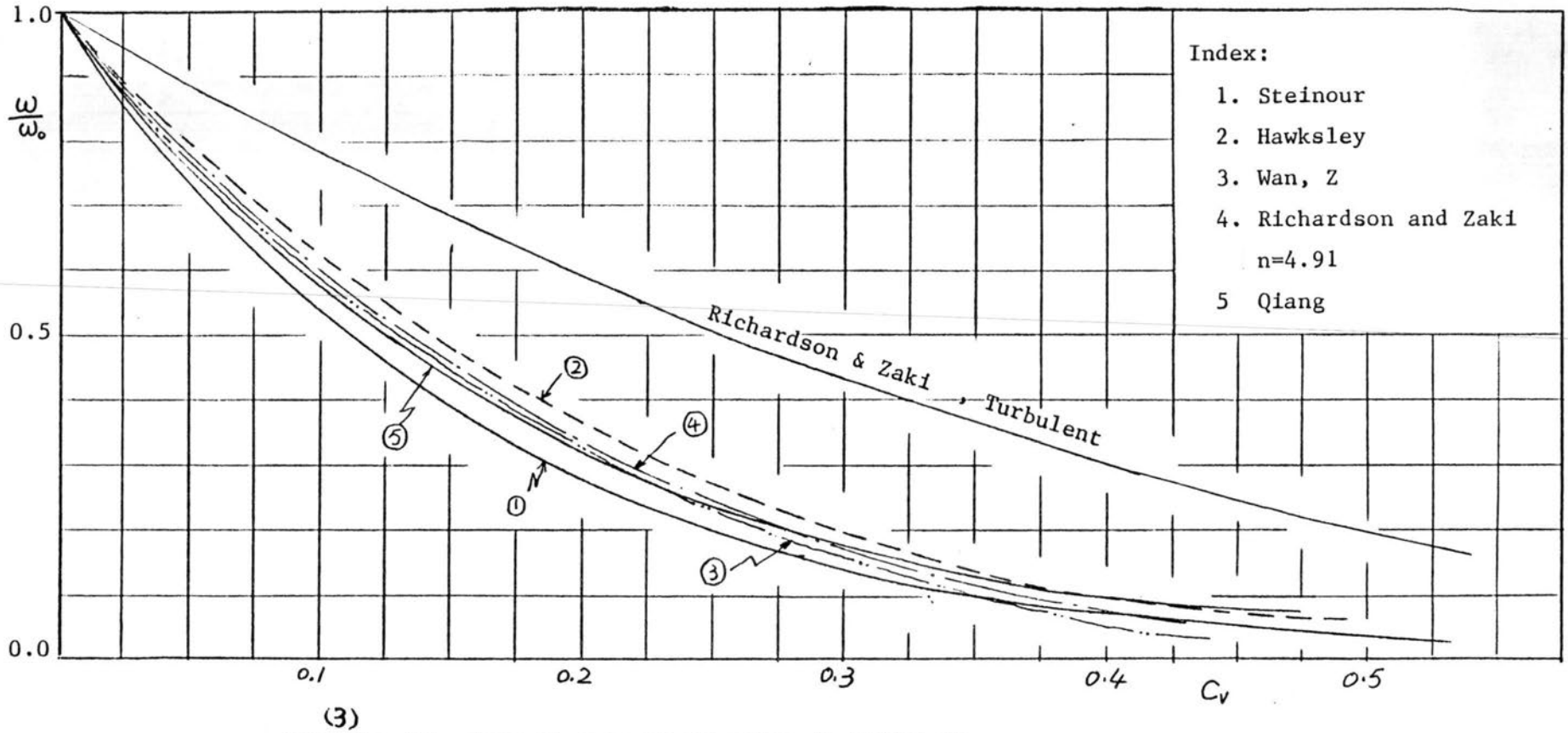

(3)

Fig. Graphic show of several formulae in Table II.

by the Reynolds number and the sediment concentration, but also by the density of the particles. [17] If we plot Richardson & Zaki's formula and Qian's formula in Fig.(4), we can see that there is a remarkable difference between these two curves. Obviously, Qian's formula is not reasonable when Cv approaches zero. But for high concentration (for instance, $Cv < 5\%$), which formula is more reliable needs futher researches. In fact, Richardson & Zaki's experiment was conducted only in the range that $Re < 500$, at which they assumed that n approached a constant 2.39. But if we look at the curve in Fig.(19) in their report [or Fig.(5) in this report], we can see that it's not sure to tell if n is independent of Re or not when Re is larger than 500. According to Wang and Chien's analysis [18], based on several researchers' experimental results, that the coefficient n in Eq.(19) does not have its maxomum below 5.0 (n=4.6 for $Re < 1.0$ according to Richardson and Zaki's formula), see Fig.(6).

It's also demonstrated by Yue's experiment [19] that the exponent in Richardson and Zaki's formula is not only a function of the Reynolds number, but also of sediment concentration. An empirical relation was given,

$$n = 2 + A(\log tg^{-1} Cv)^B \qquad (15)$$

where A and B are the coefficients to be determined by experiment. And it is pointed out that n is greater than 2.0 when $Cv < 0.4$, and less than 2.0 when $Cv > 0.4$. n decreases with the increase of Reynolds number.

IV. RATE OF SEDIMENTATION IN SUSPENSION WITH BOTH FINE AND COARSE PARTICLES

With fine and coarse particles in suspension at the same time, the settling properties of particles become much complicated. Collision, flocculation might happen after the sediment concentration reaches a certain value, and the change of fluid properties also affects the hydrodynamic interaction between particles. That is why there is no satisfactory schematical solution to the problem up to now.

For the most simple case that a single particle falls in clay suspension, most of the researches were based on Fidleris and Whitemore's assum-

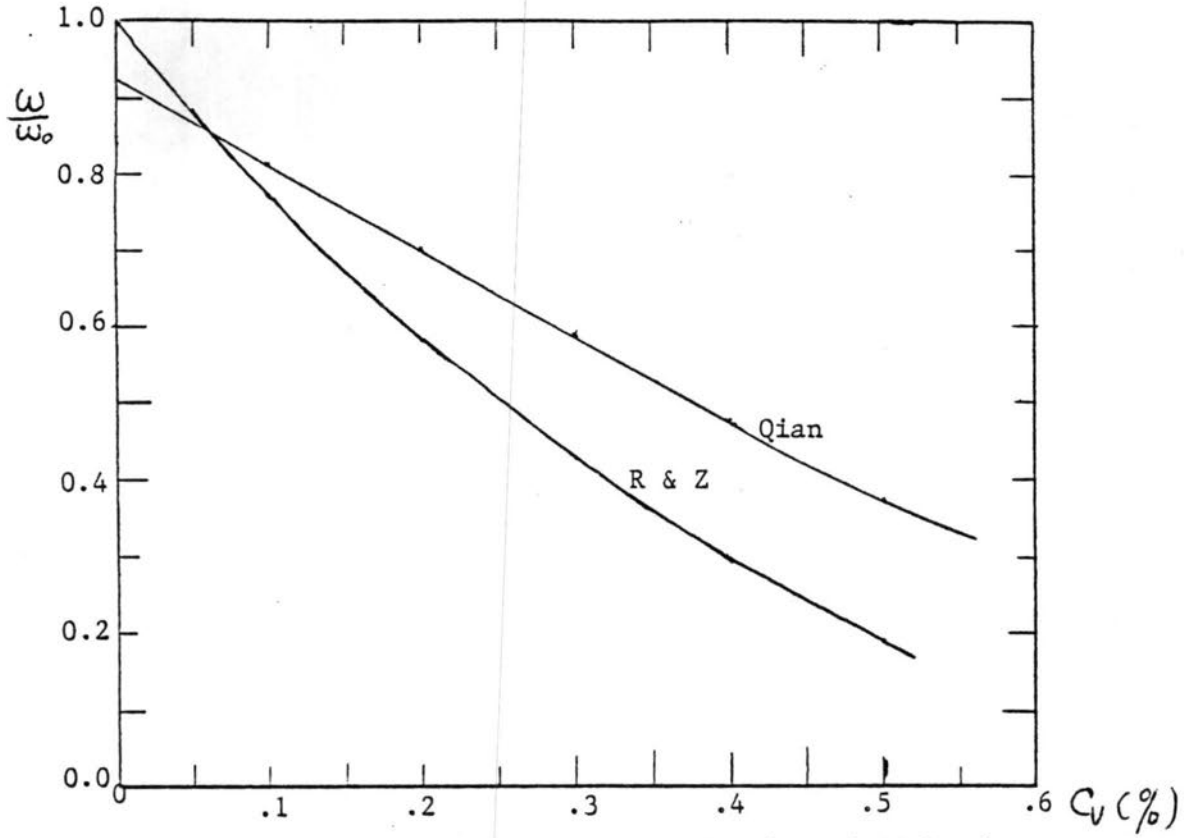

Fig.(4) Comparison between Qian's and Richardson and Zaki's Formula

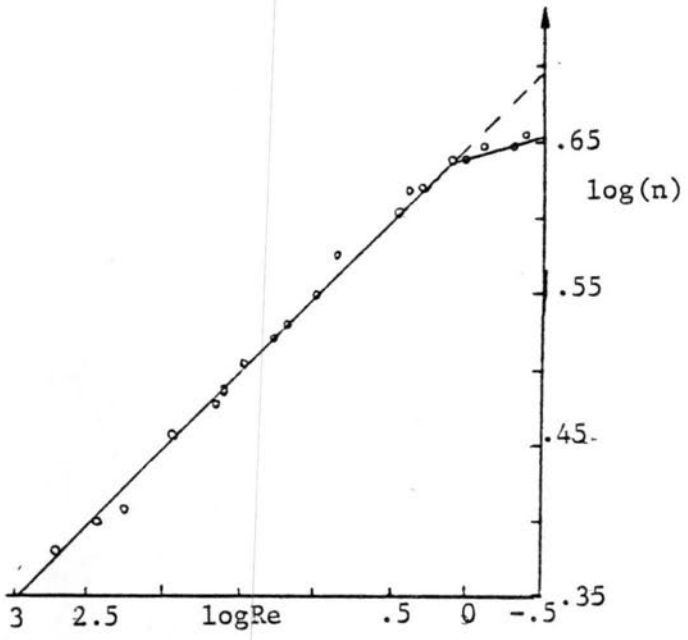

Fig.(5) Experimental relationship between n and Re in Richardson & Zaki's formula

tion that the settling of coarse particles in dilute suspension with fine particles can be considered to that as those settling of particles in a homogeneous fluid which has the density and viscosity of the suspension. In dealing with this problem, Plessis and Smith's method and Ansley and Smith's method are generally considered to be the most effective. In terms of drag coefficient, these methods were given in the following equations;

$$C_D = f(Re_B, He) \tag{16}$$

where $Re_B = \rho\omega D/\eta$ and $He = \frac{\rho\tau_y D^2}{\eta^2}$ are called Bingham Reynolds number and Hedstrom number, respectively. More specifically, Plessis and Smith defined

$$C_D = f\left(\frac{He+Re_B}{Re_B^2}\right) = f(P) = KP^{0.5} \tag{17}$$

while Ansley and Smith defined

$$C_D = f(Q) = f\left(\frac{Re_B^2}{Re_B + \frac{\pi}{24}He}\right) \tag{18}$$

in which Q was called dynamic parameter.[22].

As a matter of fact, Eqs. (17) and (18) are essentially the same. It's discussed by Woo [20] that these two methods could provide results in good agreement with experimantal data within a certain range of accuracy. But Woo's analysis also indicated that the scattering of data in C_D —P (or Q) diagram was remarkable when other than themselves' data was used. So it's hard to say that if Eqs. (17)and (18) are good description of particles settling in clay suspension or not, at least more accurate experimental data are needs.

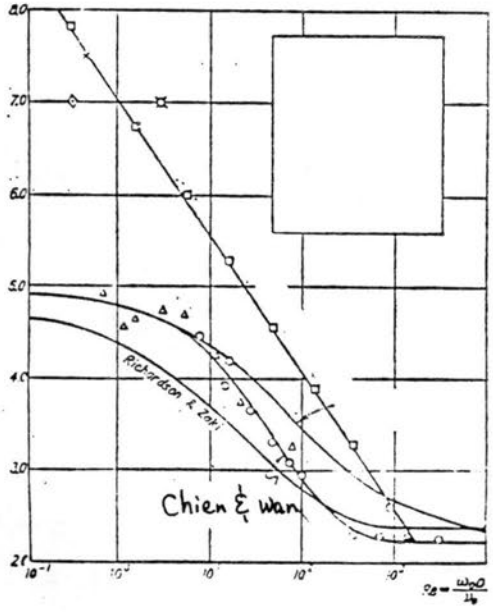

Fig.(6) n versus R_e

2. The Fall Velocity of Sand Particles in Hyperconcentrated Flow

The settling of mixed particles in hyperconcentrated flow can be devided into three stages: 1) Hindered settling when the initial concentration in a fluid is low and there is no mixing interface occurring when experiment of sedimentation is done; 2) Selective settling when the settling of coarse particles and fine particles is selective. At this stage, a mixing interface is turn out in sedimentation test; 3) sediment concentration continues to increase,those coarse particles which didn't flocculate in the stage of selective settling begins to join the floc. When the concentration reaches a certain critical value, all sediments together form a uniform suspension. To the end, there is no selective settling between fine and coarse particles. Settling velocity at this stage is extremely low. In different stages, the governing equations of settling velocity of particles are not the same [21].

Fine sediment in the suspension plays an important role in the determination of the properties of the sediment-water mixture. It's reported by Wang and Chien [18] that no yield stress τ_y can be measured if the sediment concentration is high, which means that the change of Newtonian to non-Newtonian fluid strongly depends on the extent of fine materials in the suspension. When Cv is small, the extent of the fine materials is the main factor affecting the rigidity (or plastic viscosity) of the suspension. However, when the sediment concentration Cv is high, the influence of fine materials on the rigidity diminishes, and then the yield stress is originally important. The influence of fine particles is described by

$$\frac{\omega'}{\omega_0} = (1-C_v)^n(1-KC_{vf})^{2.5} \qquad (19)$$

$$C_{vf} = \frac{rC_v}{1-(1-r)C_v}$$

where ω' is the fall velocity in the mixture, C_{vf} the concentration of fine materials in the suspension which has concentration C_v, r is the volumetric ratio of fine particles to all the particles in the suspension.

Chu, [6] also adopted Fidleris and Whitemore's assumption stated previously and put the effect of bounded water into consideration, gave the settling velocity of a swarm of non-flocculated particles for high concentration

as

$$\frac{\omega}{\omega_o} = [1-\theta KC_v]^{3.5} \qquad (19)$$

where K is the ratio of the volume of bounded particles to that of unbounded particles, and θ is the coefficient of the pores caused by collision particles. θ was taken to be 1.4 and K was expressed as

$$K = 1 + 6\int_0^1 \left(\frac{\delta}{d}\right) dp \qquad (20)$$

in which δ is the thichness of the bounded water on the sphere, δ =1 mm according to Woodruff's experiments, and dp is the percentage of the volume of a certain particle diameter to the total particle volume. Then Eq.(19) becomes

$$\frac{\omega}{\omega_o} = \left\{1-1.4\left[1+6\int_0^1 \left(\frac{\delta}{d}\right) dp\right]C_v\right\}^{3.5} \qquad (21)$$

or for convenience of application,

$$\frac{\omega}{\omega_o} = \left\{1-1.4\left[1+6\sum_{i=1}^{n} \left(\frac{\delta}{d_i}\right)\Delta p_i\right] C_v\right\}^{3.5} \qquad (22)$$

After compared with many data obtained by various researchers, Chu claimed that Eq.(22) is not only in very good agreement with the experimental data [Fig.(8)], but also more reasonable than Richardson and Zaki's formula.

From Eq.(22), we can see the influence of fine particles on the settling velocity of the swarm of non-flocculated particles by evaluating the term $\sum_{i=1}^{n} \left(\frac{\delta}{d_i}\right)\Delta p_i$. When there is no fine particles in the suspension, the term $\sum_{i=1}^{n} \left(\frac{\delta}{d_i}\right)\Delta p_i \longrightarrow 0$. Chu's Equation was certified in Fig.(8).

One merit of Chu's formela to Richardson and Zaki's formula is that Chu's formula reflects the effects of the fine particles in the suspension. It's applicable not only to uniform settling but also to settling of mixture with fine and coarse particles simutaneously. From Eq.(22), we can see that C_v=1 is not the necessity to make $\frac{\omega}{\omega_o}$ =0; while in Richardson & Zaki's formula, C_v must be 1 when $\frac{\omega}{\omega_o}$ =0, which is not true in natural case. Obviously, as long as the sediment concentration reaches a certain value, the fall velocities of the particles are zero, at which the bounded particles in the suspension attach each other and the particles can not move.

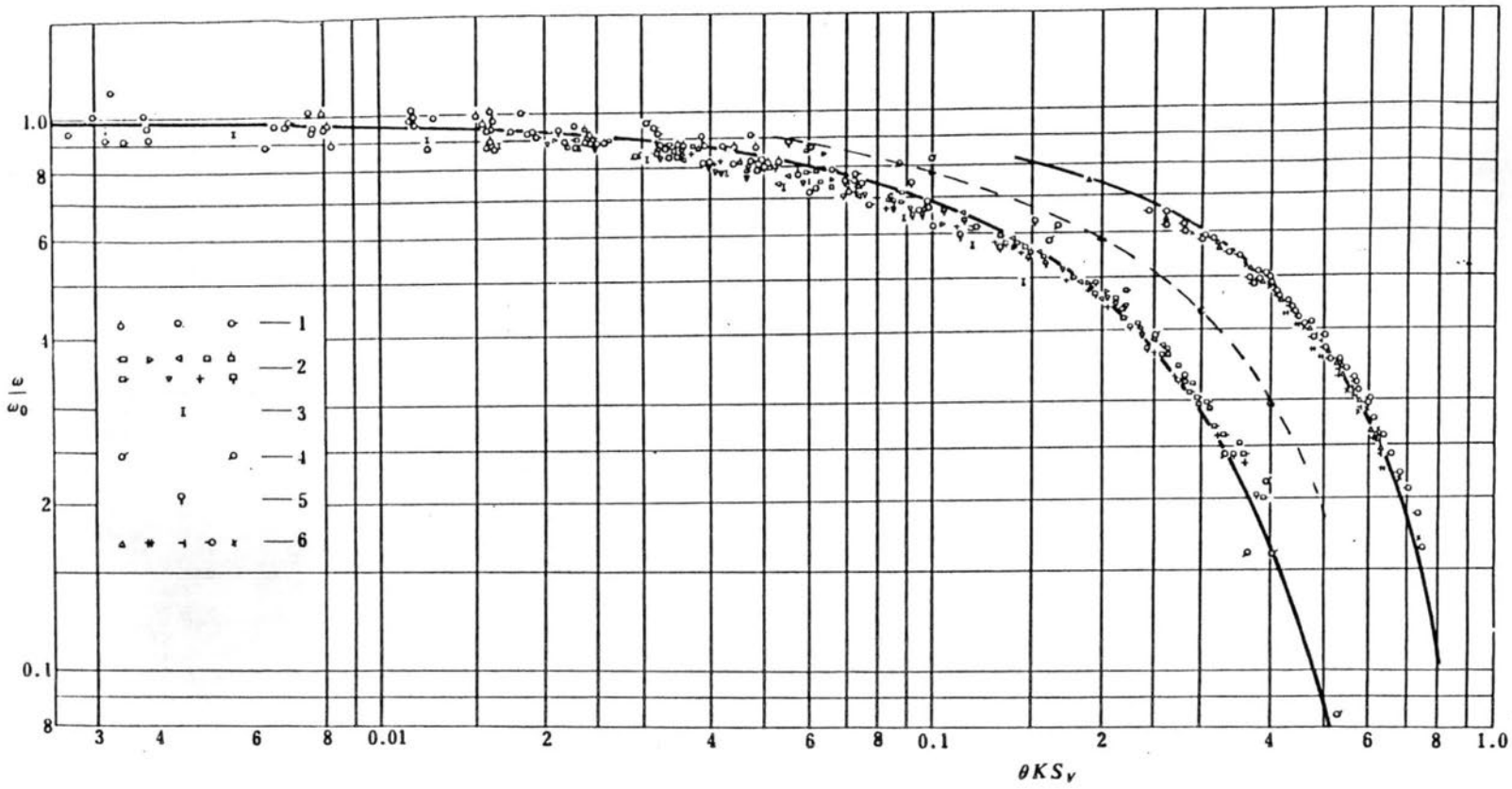

Fig.(8) Comparison of Eq.(22) with experimental data.

The curve on the right of the above figure is for the case that no fine materials in the suspension.

REFERENCES

1. Oseen, C., Hydrodynamik. Ch.10, Akademische Verlagsgesellschaft, Leipzig,1927.

2. Rubey,W.W., "Settling velocity of gravel, sand and silt particles", American J of Science, 5th series, Vol.25,NO.148, 1933,

3 Dou, G. Theory of sediment Movement. China Industrial Press, 1961. (in Chinese)

4. Steinour, H.H., "Rate of sedimentation 1)Non-flocculated suspensions of uniform sphere" Industrial and Engineering Chem., Vol.36,No. 7,1944, pp618-624.

5. Richardson & Zaki, " Sedimentation and Fluidisation", PartI, Trans. Instn, Chem. Engrs, Vol.32,No.1,1954,pp35-53.

6. Chu, J., "Basic characteristics of sediment-water mixture with hyper-concentration", Procs., 2nd Int'n Symposium on River Sedimentation, Nanjing, China, October,1983,pp265-271.

7. Cunningham, E, "On the fall velocity of steady fall of spherical particles through fluid medium", Procs., Royal Soc., London, Series A Vol.83, 1910,pp357-365.

8 MacNown, J.S. and P.N., Lin, "Sediment concentration and fall velocity", Procs, 2nd Midwestern Conference on Fluid Mechanics, Ohio State University, Columbus, Ohio, 1952, pp401-411.

9. Uchida,S. "Slow viscous flow past closely spaced spherical particles" Japaneous Inst. Sci. Tech, Vol.3,1949, pp97-104.

10. Smoluchowski, M.S, "On the pratical applicability of Stokes' law of resistance; and the modification of its reqired in certain cases", Proc., 5th Int'n Cong. Mwth., Cambrige press,1913.

11. Burgers,J.M., "On the influence of concentration of a suspension upon the sedimentation velocity"; Proc. Neb. Akad.Wet., Amsterdam, Vol.45,1942,pp126.

12. Bechleter, W., Farber, K and W. Schripf, "Settling velocity measurements in quiescent and tubulent water", Proc., 2nd Int'n Symposium on River Sedimentation, Nanjing, China, October,1983,pp1025-1037.

13. Bird, R.B et al. Transport Phenomenon, John Wiley & Sons, Inc. New York. London.Sydney,1960,chapter 16.

14 Chien, N and Z., Wan, Mechanics of Sediment Movement (in Chinese) Scientific Press, China, 1983.

15 Hawksley, P.G.W., "The effect of concentration on the settling of suspension and flow through porous media", In same aspects of Fluid Flow, Edward Arnold and Co., London,1951,pp114-135.

16. Wang, S. "Settling of fine particles in quiescent water", J. of Hydraulic Engineering (in Chinese), No.5,1964.

17. Qian, Y., "Basic characteristics of hyperconcentrated flow", Procs., 1st Int'n Symposium on River Sedimentation, Beijing,China,1980.

18. Wang, J. and Ning Chien, "Laboratory Research on physical properties of hyperconcentration", J. of Hydraulic Engineering(in Chinese) no.4, 1984, pp1-9.

19 Yue, P. "A preliminary research on sediemnt settling velocity in quiescent sediment-water mixture". J of Sediment Research (in Chinese), No.4, December, 1983.

20 Woo, H. "Sediment transport in Hyperconcentrated flow", Ph.D thesis, Colorado State University. 1985,pp203-216.

21. Song, G. "Experimental studies on settling of sediment mixtures", J of Sediment Research (in Chinese), No.2, June, 1985,pp40-50.

22. Plessis, M.P. and R.W. Ansley ,"Settling parameters in solid piplining", J Pipeline Division, ASCE, Vol.93,No.PL2, July,1967.

APPENDEX

The total drag force is expressed as that given by Rubey

$$F_{Total} = K1(1+3Re/16)(3\pi\mu D\omega_0)+K_2\left(\frac{\pi D^2}{4}\rho\omega_0^2\right) \qquad (A1)$$

where K1 and K_2 are considered to vary with particle Reynolds number. Dou assumed that the separation region behind the sphere is enlarged as the Reynolds number increases, in consequence, the form drag (second part on the right side in Eq.(A1)). He assumed further,

$$\frac{d\theta}{dRe} = \frac{a_1}{Re} \qquad (A2)$$

in which θ is the separation angle as seen in Fig.(A1). Take the boundary conditions that $\theta = 0$ when Re=0.25 and $\theta = 2\pi$ when Re=850. Eq.(a2) comes

out,

$$\theta = 1.78 \log(4Re) \qquad (A3)$$

Since the drag force is form drag behind the separation and viscous force in front of separation. Then

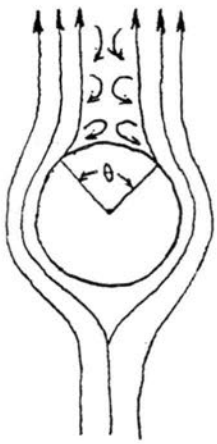

Fig.(A1) Flow patter around a sphere.
$\theta = 0$,when $Re < 0.35$
$\theta = 2\pi$ when $Re \geq 850$

$$F_{form} = \begin{cases} C_{D1}\left(\frac{\pi D^2}{4}\sin^2\frac{\theta}{2}\right) & \text{if } \theta < \pi \\ C_{D1}\cdot\frac{\pi D^2}{4}\cdot\frac{\rho\omega_0^2}{2} & \text{if } \theta \geq \pi \end{cases}$$

$$F_{vis} = [3\pi\mu D\omega_0(1+3Re/16)]\frac{1+\cos\frac{\theta}{2}}{2}$$

where $\frac{\pi D^2}{4}\sin^2\frac{\theta}{2}$ is the projected area of separation in the direction of settling and $\frac{1+\cos\frac{\theta}{2}}{2}$ is the raio of surface area in front of the separaion to that of the separation region. Then the total drag force is expressed as

$$F_{total} = F_{form} + F_{vis}$$

or
$$C_D\cdot\frac{\pi D^2}{4}\frac{\rho\omega_0^2}{2} = C_{D1}\left(\frac{\pi D^2}{4}\sin^2\frac{\theta}{2}\right)\frac{\rho\omega_0^2}{2} + 3\pi\mu_D\omega_0\left(1+\frac{3}{16}Re\right)\frac{1+\cos\frac{\theta}{2}}{2} \qquad (15)$$

Since the second part on the right of Eq.(A4) vanishes and $C_D = 0.45$ when $Re = 850$, then $C_{D1} = 0.45$. Then Eq.(A4) comes out

$$C_D = \begin{cases} 0.45\sin^2\frac{\theta}{2} + \frac{24}{Re}(1+3Re/16)\frac{1+\cos\frac{\theta}{2}}{2} ; & \text{if } \theta < \pi \\ 0.45 + \frac{24}{Re}(1+3Re/16)\frac{1+\cos\frac{\theta}{2}}{2} ; & \text{if } \theta \geq \pi \end{cases}$$

where θ is a function of the Renolds number Re expressed in Eq.(A3).

LOCAL SCOUR AT BRIDGE PIERS BASED ON FIELD MEASUREMENTS

By David C. Froehlich[1], A. M. ASCE

ABSTRACT: Seventy (70) field measurements of local scour at bridge piers were used to develop local-scour prediction equations. Variables used to predict local-scour depth include pier shape, pier width, pier width projected normal to the approach flow, approach flow depth, approach-flow velocity, and mean sediment size. These variables cover a wide range and provide a good data base for analysis. Several regression equations were developed to predict the dimensionless variable scour-depth/pier--width. Although the regression equations are based on only those observations considered to be live-bed scour, they are shown to closely predict the few clear-water scour depths as well. A factor to be added to the expected depth of scour obtained from the regression equations to provide a safe design scour depth is suggested.

INTRODUCTION

Exposure or undermining of bridge pier foundations due to the erosive action of flowing water can result in structural failure of the bridge requiring a major expenditure for repair or replacement (see Ref. 5, for case histories of scour problems at bridges). The design of bridge pier foundations must, therefore, include consideration of the maximum depth of scour that is likely to occur. Spread footings, drilled pier foundations, and caisson foundations in alluvial material obviously should be placed well below the estimated depth of scour while piles supporting piers need to be of sufficient length to support the structure after the estimated scour has occurred.

The term "scour" is used here to mean a lowering by erosion of the stream channel bed below an assumed natural level or other appropriate datum. "Depth of scour" refers to the depth of material removed below the stated datum. Scour is a natural phenomenon that is of concern primarily in alluvial streams but exists in nearly all waterways. Scour that occurs at a bridge waterway can be separated into three components:

1. General scour caused by progressive aggradation or degradation of the stream channel due to changes in channel controls (such as the construction of a dam or gravel mining), changes in sediment supply, or changes in stream form (such as from a meandering to a braided stream). General scour would occur whether or not a bridge was present.

---

[1] Hyrologist, US Geological Survey, Lakewood, CO 80255

2. Constriction scour caused by reduction of the waterway area by bridge approach embankments, piers, and other obstructions that increase flow velocities within and near the stream channel for a generally short distance up- and downstream of the bridge crossing.

3. Local scour caused by flow disturbances due to piers and abutments resulting in an abrupt decrease in the streambed elevation in the immediate vicinity of these structures.

Although the components of scour are not completely independent, separating them is helpful in understanding the underlying causes and in design. The design engineer must consider each component of scour separately and combine the results to estimate the total scour depth that may occur at the bridge site.

The subject of local scour around bridge piers has been extensively studied and numerous local scour prediction equations have been developed; however, most are based entirely on experimental laboratory data. When applied to particular bridge sites, these equations provide widely varying scour depths (4,6,7,10,12). The Highway Research Board (6) states:

> Because satisfactory quantity and quality of field measurements of scour are not available for comparison, it is not possible to recommend a specific method for predicting scour. Judgement must be exercised in selection of a method and in interpreting the resulting predictions.

Since 1970 a number of field measurements of local scour have been made and reported. The present study develops local scour prediction equations based only on these field measurements since they are of sufficient quantity and quality. A brief discussion of the mechanism of local scour precedes presentation of the collected field measurements and data analysis.

MECHANISM OF LOCAL SCOUR

Local scour around a pier is the result of the large-scale eddy structure, or the system of vortices, that develops as the flow is deflected about the pier (11,12,22). The vortex system can be composed of any, all, or none of the following three basic vortex systems: the horseshoe-vortex system, the wake-vortex system, and the trailing-vortex system. The most important of these are the horseshoe-vortex system and the wake-vortex system (12).

Piers are classified as either blunt-nosed or sharp-nosed. Blunt-nosed piers are typically those with square or rounded noses including cylindrical piers. All other piers are referred to as sharp-nosed although lenticular and wedge-shaped piers may act as blunt-nosed piers depending on the nose angle and the alignment of the pier with the approach flow.

Scour around a blunt-nosed pier is initiated by a downflow at the upstream face of the pier due to a vertical pressure gradient. The approach flow velocity decreases from the water surface downward and is zero at the bed. Since the approach velocity vanishes at the upstream side of the pier, the stagnation pressure also decreases from the surface downward. The resulting vertical pressure gradient drives the downflow.

Velocities around the base of a blunt-nosed pier increase from zero at the nose to a maximum at some point downstream, similar to a two-dimensional potential flow. High local velocities along the base of the pier initiate scour before general sediment motion begins in the approach flow. Scouring starts along the base of a cylindrical pier at the point where the local velocity is maximum when the mean approach-flow velocity, V, reaches about one-half of the threshold value for the beginning of sediment transport, V_c (19). The scour then propagates upstream around each side of the base of the pier until it meets at the front. The eroded bed material is transported downstream by the flow and a shallow scour hole around much of the pier is formed.

The horseshoe vortex is initially small in cross section and comparatively weak but with the formation of the scour hole, the vortex rapidly grows in size and strength as the strength of the downward flow increases. The eroded material is carried around the perimeter of the pier under a combination of the high local velocities due to the flow acceleration and the action of the horseshoe vortex. The scour hole rapidly develops in the shape of a frustrum of an inverted cone at a slope equal to the dynamic angle of repose of the bed material and the horseshoe vortex moves down into the developing scour hole and expands as the hole enlarges.

As the scour hole enlarges, the circulation associated with the horseshoe vortex increases, due to its expanding cross-sectional area, but at a decreasing rate. The rate of increase is controlled by the strength of the downflow ahead of the pier which in turn is determined by the discharge of the approach flow; or, for a particular flow depth and width, by the magnitude of the velocity of the approach flow. The magnitude of the downflow near the bottom of the scour hole decreases as the depth of the hole increases. Hence the rate of erosion decreases as the scour hole deepens.

A wake-vortex system is created by flow separation along the surfaces of the pier. The strength of the vortices in the wake system vary greatly depending on the pier shape and approach flow velocity. A sharp-nosed pier will create a relatively weak wake while a blunt-nosed pier will produce a very strong one. For pier Reynolds numbers of practical interest the wake-vortex system is unstable and the vortices are shed alternately from the sides of the pier and convected downstream (22). Wake vortices are initially shed with their axes vertical but are progressively bent by the mean flow as they are transported downstream (12). They also interact with the horseshoe vortex at the streambed

causing the horseshoe vortex to oscillate both laterally and vertically (19).

Wake-vortex systems help to remove bed material from in and around scour holes as the vortices shed from the sides of the pier lift sediment from the bed, much like tornados, and carry it downstream. When a horseshoe-vortex system does not form or is completely controlled, large scour holes may form downstream from a pier due to a wake-vortex system. The experiments of Shen and others (23) on sharp-nosed piers clearly show this possibility.

A trailing-vortex system is composed of one or more discrete vortices attached to the top of the pier and extending downstream. These vortices form when finite pressure differences exist along two surfaces meeting at a corner, such as at the top of a completely submerged pier. The effect of trailing vortices on scour has not been studied in detail but it is generally thought to be of secondary importance.

Another important feature of the flow past a pier that affects local scour is a bow wave that develops on the water surface at the upstream side of a pier. The rotation of flow within the bow wave is in a direction opposite to that in the horseshoe vortex. The bow wave becomes important in relatively shallow flows where it interferes with the approach flow and causes a reduction in the strength of the downflow at the front of the pier.

Scour Classification.--The scour hole that develops around a pier will increase in size until an equilibrium depth is reached. At the equilibrium depth, the capacity of the flow to remove bed material from the scour hole just equals the rate at which replacement material is supplied to the scour hole by the approach flow. Local scour is classified as either clear-water scour or live-bed scour based on the ability of the approach flow to transport sediment.

Clear-water scour occurs when the approach flow is unable to transport bed material to the scour hole. Thus sediment removed from the scour hole is not replenished by the approach flow and the maximum (equilibrium) scour depth is reached when the capacity for transport out of the scour hole is reduced to zero. At the equilibrium condition, the boundary shear stress within the scour hole just equals the shear stress required to set the scour hole sediment in motion (critical shear stress) and transport it downstream. Under clear-water scour conditions, the depth of scour approaches the equilibrium depth very slowly. Raudkivi and Ettema (20) report that in scale-model tests where the bed material was not in general motion about 50 hours was required before the maximum scour depth was reached.

Live-bed scour exists when the scour hole is continuously supplied with sediment by the approach flow. An equilibrium scour depth is reached when, over a period of time, the average rate of sediment transport from the scour hole is equal to the average rate of sediment transport into the scour hole by the approach flow. The minimum elevation of the local scour hole under live-bed conditions will fluctuate about a mean value as

bed forms pass by the pier. The range of fluctuations depends on the height of the bed forms which is a function of the flow conditions in the stream channel and is not affected by the pier. Many laboratory experiments have shown that the fluctuation in live-bed scour depth about the mean value is approximately 0.5 times the height of the passing dunes (19,24). The time required to reach equilibrium scour depth is less for live-bed conditions than for clear-water conditions.

The relation between local-scour depth at cylindrical piers in cohesionless bed material and mean approach-flow velocity for live-bed conditions is investigated by Melville (13). Experimental data are collected in which pier size, sediment size, and mean approach-flow velocity are systematically varied. These data show that the relation between local scour depth and approach-flow velocity with approach-flow depth held constant depends on whether or not the sediment is ripple-forming. In the case of ripple-forming sands, the maximum scour depth is shown to occur at the transition from flat-bed to ripples. For coarser sediments in which ripples do not form, the maximum scour depth is shown to occur at the threshold condition for general sediment motion (that is, at the transition from clear-water to live-bed scour).

FIELD MEASUREMENTS

The need for field measurements of local scour at bridge piers has long been recognized. In discussing research needs and priorities related to scour at bridge waterways, the Highway Research Board (6) states the following:

> The first priority in research on scour problems should be given to filed measurements. No relationship for predicting scour can be used with confidence until proof has been shown that it does predict what happens with reasonable accuracy and reliability.

Since this statement was made, a number of field measurements of local scour have been reported by various investigators. As many as possible of these measurements have been collected for this study and are listed in Table 1. The completeness of this list is not claimed but it does cover a wide range of flow, sediment, and pier conditions and provides a data base that can be analyzed to develop a local-scour prediction method. Bed material at all the measurement sites can be classified as noncohesive. Some measurements in this list are clearly more reliable than others as noted in the following discussions of the field measurement sources.

Neill (14).--Scour data measured at two bridges on the Beaver River in Alberta, Canada are presented. Sufficient data for use in this study is given only for one site. Depth measurements were made using an acoustic fathometer with the transducer mounted on the side of a boat. Velocity measurement techniques

are not discussed. Neill estimates the median diameter of Beaver River bed material to be 0.5 mm and notes that the presence of an underlying soil stratum containing gravel may have limited scour.

Melville (12).--Several case histories of local scour at bridge piers in New Zealand are presented. Sufficient data for use in this analysis is given for only one site. Data consisting of a channel cross-section at the bridge and the total river discharge at the time of the cross-section measurement are presented. A bed material sample was also obtained, however, when this sample was taken is not stated. Field data collection methods are not discussed.

Norman (18).--Measurements of local scour around piers were made at seven bridge crossings of streams in Alaska from 1965 to 1972 at or near peak flood discharges. Soundings to the streambed to determine channel cross-sections, longitudinal channel profiles, and scour hole depths were generally made using a recording acoustic fathometer with the transducer mounted on the side of a boat hull. Transducers were permanently mounted at the nose, tail, and on both sides of pier no. 5 of the Knik River bridge near Palmer to continuously monitor the change in depth of the scour hole around the pier. Another transducer was permanently mounted on the nose of pier no. 4 of the Knik River bridge near Eklutna. Velocities at all bridge crossings were measured using a Price Type AA current meter. Bed material samples were obtained using: (1) a US-BM 54 sampler for streambeds composed of sand and small gravel, (2) a locally constructed drag sampler for gravel- and cobble-bed streams, and (3) photographs of exposed bed material during low-flow conditions in gravel- and cobble-bed streams where use of the drag sampler was not possible.

The transducers permanently mounted on piers at the two Knik River bridges provided good records of the fluctuations of the scour hole bed elevations about their mean values. Where dunes were present, the minimum elevation of the scour hole fluctuated about its average value by one-half the dune height. It is observed that as the alignment angle of a long pier with the approach flow increases from zero the depth of local scour increases and the point of maximum scour moves downstream from the pier nose.

Chang (4).--Field measurements of local scour at bridge piers are obtained from files of the Louisiana Department of Transportation which had routinely conducted surveys as part of a bridge inspection program. Data are presented for seven bridge crossings where the channel approaches were fairly straight and uniform for about one km. Six of these sites have enough data given for them to be included in this study.

An acoustic fathometer with the transducer mounted on the side of a boat was used to make continuous records of bed elevations at several cross sections up to 60 m upstream and downstream from each bridge. The surveys were generally conducted after a flood peak when the water level had receded. Contour maps of the streambed elevation are prepared from the recorded

cross sections. Total stream discharge at each site at the time of the survey is estimated from stage and discharge records of nearby gaging stations. The mean velocity of flow approaching a pier is estimated as

$$V = V(y/\bar{y})^{2/3} \quad \text{.....(1)}$$

in which V is the mean velocity in the approach cross-section 60 m upstream of the bridge, $\bar{y}$ is the mean depth in the approach cross-section, and y is the approach-flow depth at a point less than or equal to 30 m directly upstream of the pier. The angle at which the upstream flow approached the piers is estimated from the streambed elevation contour lines in the scour hole.

Bed-material samples were taken at the time of the study (that is, long after the original stream surveys). Three or more bed material samples were taken with a core sampler to a depth of 15 cm at each of six locations at each bridge crossing during low-flow conditions. Sampling points were located at the water edge on both sides of the stream directly under the bridge and 60 m upstream and downstream from the bridge.

Hopkins and others (7).--The results of a field study to gather local scour data at bridge piers are presented. An automatic instrumentation system based on an acoustic fathometer was used to measure streambed elevations at three points around a bridge pier as well as the stream stage. Data for four bridge crossings are included; however, the data for only one of the sites is considered to be sufficient and appropriate for use in this analysis.

Two depth transducers, one stage transducer, and three velocity meters were attached to pier no. 6 of the Texas Street Bridge over the Red River in Shreveport, Louisiana. Core borings in the vicinity of the instrumented pier provide a measurement of the median size of the bed material. Enough data for use in this study were collected for only one event.

Breusers (1), **Breusers and others** (2).--A comparison is made between field measurements of local scour at a bridge pier and scour observed in a scale-model simulation of the same pier. It should be noted that the full sediment size distribution curve was reproduced in the model tests and that the scale of mean velocity and critical velocity for all sediment fractions was the same. Simulated scour depth closely matched field measurements. Detailed contour maps of streambed elevations for both the prototype and the scale model are presented by Breusers and others (2, Fig. 15). Methods of field data collection are not discussed.

Jarrett and Boyle (9) **and Jarrett** (written communication, 4 March 1986).--Local pier scour was measured at four bridge crossings in Colorado during 1984. Cross sections were obtained along the upstream and downstream sides of each of the bridges using a suspended sounding weight during high flows and a wading rod during low flows. Soundings were made as close as possible to the upstream and downstream ends of piers in order to define

to local scour depths. This procedure might not provide the maximum scour depth at sharp-nosed piers or at piers not aligned with the approach flow since the location of the minimum streambed elevation along such piers has been found to move from the nose towards the tail. However, the measurements are considered to be the reasonably accurate estimates of local scour depth and are used as reported.

Velocity was measured along both the upstream and downstream sides of the bridges using a Price Type AA current meter. bed material samples were collected using a US-BM 54 sampler during high flows and a hand-held drag sampler where flows were low enough to permit its use.

ANALYSIS OF SCOUR VARIABLES

The set of variables characterizing local scour at bridge piers is the sum of those describing the following components of this phenomenon: 1) bridge pier, 2) flow, 3) bed material, and 4) fluid. It follows that the depth of local scour at a bridge pier can be characterized by the following set of variables:

$$\phi,\ b,\ b',\ y,\ V,\ \rho_s,\ d_{50},\ \sigma_g,\ V_c,\ g,\ \rho,\ \nu.$$

in which ϕ = a pier shape factor, b = pier width or diameter, b' = pier width projected normal to the approach flow, y = approach flow depth, V = mean velocity of approach flow, ρ_s = density of bed material, d_{50} = mean size of bed material, σ_g = geometric standard deviation of bed material size distribution, V_c = critical mean velocity for beginning of sediment movement, g = gravitational acceleration, ρ = density of water, and ν = kinematic viscosity of water. The completeness of this set is not claimed, however, it does contain those variables that have been found to have the greatest effect on local scour at bridge piers.

A functional relation between the local scour depth, d_s, and the set of characteristic variables is written as

$$d_s = F(\phi,\ b,\ b',\ y,\ V,\ \rho_s,\ d_{50},\ \sigma_g,\ V_c,\ g,\ \rho,\ \nu) \quad \ldots\ldots\ldots\ldots (2)$$

Selecting ρ, V, and b as repeating variables leads to the dimensionless functional relation

$$\frac{d_s}{b} = f\left(\phi,\ \frac{b'}{b},\ \frac{y}{b},\ S_s,\ \frac{b}{d_{50}},\ \sigma_g,\ \frac{V}{V_c},\ F_a,\ Rp\right) \quad \ldots\ldots\ldots\ldots\ldots\ldots (3)$$

in which S_s = specific gravity of the bed material ρ_s/ρ, F_a = approach-flow Froude number, $V/\sqrt{gy}$, and Rp = Reynolds number based on approach-flow velocity and pier width, Vb/ν.

Specific gravity of bed material is rarely reported but is assumed to be nearly constant and can therefore be eliminated from the relation. Geometric standard deviation of the bed

material is reported for only a few of the field measurements and is reluctantly neglected in the analysis. The functional relation given in Eq. 3 is then reduced to

$$\frac{d_s}{b} = f\left(\phi, \frac{b'}{b}, \frac{y}{b}, \frac{b}{d_{50}}, \frac{V}{V_c}, F_a, Rp\right) \quad \ldots\ldots\ldots\ldots\ldots\ldots\ldots\ldots (4)$$

REGRESSION ANALYSIS

Multiple regression analysis was used to develop prediction equations for local live-bed scour based on the functional relation given in Eq. 4. The scour classification (clear-water or live-bed) was made using the critical mean-velocity given by Neill (15)

$$V_c = \{2.50\,[(\rho_s - \rho)/\rho]\,(y/d_{50})^{0.20}\,g d_{50}\}^{0.5} \quad \ldots\ldots\ldots\ldots\ldots (5)$$

This relation is based on experimental data on incipient motion of uniform bed material ranging in size from 6 to 30 mm in diameter with y/d_{50} ranging from 2 to 100. It was used outside these ranges in determining critical velocity for the field measurements but seems to provide a good value. Only those observations classified as live-bed scour were used in the regression analysis.

The effect of pier shape was determined by classifying piers based on their nose shape as either: (1) square-nosed, (2) round-nosed (which includes cylindrical piers), or (3) sharp-nosed (which includes wedge-shaped and lenticular piers). Thus two indicator variables were added to the set of independent variables to account for the qualitative pier-shape classification. Logarithmic transformations of all variables is found to provide the best results. The following regression equations provided the best prediction of local-scour depth:

$$\frac{d_s}{b} = 0.472\,\phi\,\left(\frac{b'}{b}\right)^{0.742};$$

$$\phi = \{1.525,\ 1,\ 0.894\},\ r_a^2 = 0.646 \quad \ldots\ldots\ldots\ldots\ldots\ldots (6)$$

$$\frac{d_s}{b} = 0.470\,\phi\,\left(\frac{b'}{b}\right)^{0.626}\left(\frac{y}{b}\right)^{0.256};$$

$$\phi = \{1.405,\ 1,\ 0.779\},\ r_a^2 = 0.695 \quad \ldots\ldots\ldots\ldots\ldots\ldots (7)$$

$$\frac{d_s}{b} = 0.326\,\phi\,\left(\frac{b'}{b}\right)^{0.607}\left(\frac{y}{b}\right)^{0.397}\left(\frac{b}{d_{50}}\right)^{0.045};$$

$$\phi = \{1.395,\ 1,\ 0.724\},\ r_a^2 = 0.727 \quad \ldots\ldots\ldots\ldots\ldots\ldots (8)$$

$$\frac{d_s}{b} = 0.167\,\phi\,\left(\frac{b'}{b}\right)^{0.620}\left(\frac{y}{b}\right)^{0.391}\left(\frac{b}{d_{50}}\right)^{0.037} Rp^{0.049};$$

$$\phi = \{1.467,\ 1,\ 0.704\},\ r_a^2 = 0.726 \quad \ldots\ldots\ldots\ldots\ldots\ldots (9)$$

$$d_s/b = 0.329\ \phi\ (b'/b)^{0.615}\ (y/b)^{0.402}\ (b/d_{50})^{0.066}\ F_a^{0.120};$$

$$\phi = \{1.362,\ 1,\ 0.720\},\ r_a^2 = 0.725 \quad \ldots\ldots\ldots\ldots\ldots\ldots (10)$$

in which ϕ = {square-nosed pier factor, round-nosed pier factor, sharp-nosed pier factor} and r_a^2 is the coefficient of determination adjusted for degrees-of-freedom. The inclusion of both Rp and F_a in the regression model did not increase its predictive ability.

Eqs. 6 through 10 provide a good explanation of the variation in d_s/b for live-bed scour conditions. As presented, however, they are unnecessarily complicated for design purposes. In order to simplify these equations, the pier shape factor, ϕ, was considered to be constant with ϕ = 1.4 for square-nosed piers, 1.0 for round-nosed piers, and 0.75 for sharp-nosed piers. These values were chosen based on those found from the regression analysis leading to Eqs. 6 through 10 and are in close agreement with shape factors based on nose forms given by Breusers and others (2). In addition, the adjustment factor for pier alignment with the approach flow was assumed to be

$$\zeta = (b'/b)^{0.6} = [\cos\alpha + (l/b)\sin\alpha]^{0.6} \quad \ldots\ldots\ldots\ldots\ldots\ldots (11)$$

in which the exponent was obtained from the b'/b term exponent in Eqs. 6 through 10. The pier alignment factor, ζ, is within 10 percent of the factor given by Laursen and Toch (11) for l/b up to 16 and α less than or equal to 45 degrees.

Defining as a new dependent variable $d_s/\phi\zeta b$, the following regression equations were obtained:

$$d_s/\phi\zeta b = 0.53\ ,\ r_a^2 = 0 \quad \ldots\ldots\ldots\ldots\ldots\ldots (12)$$

$$d_s/\phi\zeta b = 0.48\ (y/b)^{0.27}\ ,\ r_a^2 = 0.210 \quad \ldots\ldots\ldots\ldots\ldots\ldots (13)$$

$$d_s/\phi\zeta b = 0.33\ (y/b)^{0.39}\ (b/d_{50})^{0.044}\ ,\ r_a^2 = 0.294 \quad \ldots\ldots\ldots (14)$$

$$d_s/\phi\zeta b = 0.24\ (y/b)^{0.39}\ (b/d_{50})^{0.039}\ Rp^{0.025}\ ,\ r_a^2 = 0.286 \quad \ldots (15)$$

$$d_s/\phi\zeta b = 0.33\ (y/b)^{0.39}\ (b/d_{50})^{0.064}\ F_a^{0.113}\ ,\ r_a^2 = 0.289 \quad \ldots (16)$$

The coefficients of determination for these equations are small because of the large amount of variation already explained by the pier shape and alignment factors contained in the dependent variable.

Discussion of Equations.--A comparison of observed values of d_s/b and values computed using Eqs. 12 through 16 is shown in Figs. 1 through 5. Field observations for all scour types (live-bed, clear-water, and unknown) are included in these figures except for those with missing velocity measurements which are necessarily not plotted in Figs. 4 and 5. These figures show that d_s/b is accurately predicted for the few clear-water scour observations even though the regression equations are based

on only live-bed scour measurements. While this evidence is certainly not conclusive, Eqs. 12 through 16 can be applied to cases of clear-water scour with some degree of confidence.

There are a number of reasons why differences between clear-water and live-bed scour might not be apparent, not the least of which is the critical velocity criterion used to distinguish between clear-water and live-bed scour. Shen and others (24) suggest that the maximum equilibrium scour depth reached under clear-water conditions is only about 10 percent larger than for live-bed scour conditions. Such a small difference would be hard to observe with the limited number of field observations. In addition, Melville (13) finds that, for a constant flow depth, the maximum depth of live-bed scour for ripple-forming sand is greater than the maximum clear-water scour depth. For coarser sediment in which ripples do not form the maximum clear water scour depth is found to be greater than the maximum live-bed scour depth. There are just not enough field measurements for both types of scour conditions to allow prediction of such a difference in scour depth.

Most existing scour prediction equations can be written with relative scour depth, d_s/b, as a function of the relative flow depth, y/b (4,7,8) thus indicating the importance of this term in computing local scour depth. It is by far the most important independent variable after the pier alignment factor. Eq. 14 is similar to the equation given by Neill (16) to approximate the design curve presented by Laursen and Toch (11) for a square-nosed pier aligned with the flow. The design curve was drawn "somewhat conservatively" and represents the predicted equilibrium live-bed scour depth.

The effect of relative sediment size given by the parameter b/d_{50} in Eqs. 12 through 16 is in general agreement with experimental results presented by Raudkivi (19) except that the influence does not seem to vanish for values of b/d_{50} greater than 100. The influence of sediment size may appear to be insignificant because of the small exponent on the b/d_{50} term, but this is not true because of the wide variation in bed material sizes that occur. For the field measurements listed in Table 1, 0.008 mm $< d_{50} <$ 90 mm and $22 < b/d_{50} < 1{,}225{,}000$. An extremely accurate estimate of d_{50} is not essential, however, since a factor of 10 error in d_{50} results in only about a 10 percent difference in the computed scour depth. A qualitative description of the bed material (for example, coarse silt, medium sand, fine gravel) can provide a reasonable estimate of d_{50} for use in the scour prediction equations.

Neither the pier Reynolds number, Rp, nor the approach Froude number, F_a, improves the accuracy of the regression model already containing the parameters y/b and b/d_{50}. It should be noted that the parameters y/b and F_a can be combined to form a Froude number based on pier width rather than approach-flow depth.

DESIGN EQUATIONS

A rational means of dealing with the uncertainties contained in Eqs. 12 through 16 must be found in order for them to be used in designing bridge piers. While a rigorous determination of a confidence region for the entire regression surface associated with a particular equation is certainly possible (17, p. 232), it is much too cumbersome for practical design purposes. A simple method, employed in virtually all engineering designs, is to use a factor of safety .

A factor of safety provides a margin of error that allows for a considerable variation from an expected scour depth without threatening the stability of a pier. An excessive margin of error is uneconomical, therefore, a decision must be made as to just how much to add to the expected local scour depth in order to design a safe yet economical bridge pier.

Local scour depth predicted by Eqs. 12 through 16 are the best estimates of the value of d_s/b (actually the logarithm of d_s/b) to be expected given the values of the independent variables (actually their logarithms). For all of these equations, the observed value of d_s/b is always less than the computed value of d_s/b plus 1.0 . For design purposes, therefore, the following relation is proposed:

$$(d_s/b)_{design} = (d_s/b)_{expected} + 1.0 \quad \text{.....(17)}$$

in which the pier shape factor, ϕ, is defined as

$$\phi = \begin{cases} 1.4 \text{ for square-nosed piers} \\ 1.0 \text{ for round-nosed piers} \\ 0.75 \text{ for sharp-nosed piers} \end{cases}$$

and the pier alignment factor, ζ, is given by Eq. 11. Based on field measurements of local scour as shown in Figs. 1 through 5, these design equations can be used for both live-bed and clear-water scour conditions.

SUMMARY AND CONCLUSIONS

Seventy (70) field measurements of local scour at bridge piers located in cohesionless bed material were collected from published references. These measurements provided a data base that was sufficient to allow development of local scour prediction equations based only on field data.

Several regression equations for predicting d_s/b were presented. Pier shape and pier alignment factors are very similar to those obtained by others based on experimental laboratory data. The effect of relative flow depth, y/b, is also in general agreement with the findings of others. Relative sediment size, b/d_{50}, does not explicitly appear in many existing prediction methods but its influence is also in general agreement with results of laboratory experiments. Although only live-bed scour

depths were used in the regression analysis, the equations are shown to closely predict clear-water scour depths as well; however, this may be due to the limited number of observations classified as clear-water scour.

The best prediction equation for d_s/b is one involving the pier shape factor, the pier alignment factor, relative flow depth, and relative sediment size. A factor of 1.0 is added to the expected value of d_s/b computed from all the regression equations to provide a sufficient margin of error and insure a safe bridge-pier design.

ACKNOWLEDGMENT

The assistance of Robert D. Jarrett, Hydrologist, U. S. Geological Survey, who supplied field notes related to local scour measurements in Ref. 9, is gratefully acknowledged.

APPENDIX I.--REFERENCES

1. Breusers, H. N. C., Discussion of "Local Scour Around Bridge Piers" by Shen, H. W., Schneider, V. R., and Karaki, S. (in Journal of the Hydraulics Division, ASCE, v. 95, no, HY6, p. 1919-1940): Journal of the Hydraulics Division, ASCE, v. 96, no. HY7, 1970, p. 1638-1639.
2. Breusers, H. N. C., Nicollet, G., and Shen, H. W.,"Local Scour Around Cylindrical Piers," Journal of Hydraulic Research, v. 39, no. 3, 1977, p. 211-252.
3. Chabert, J. and Engeldinger, P.,"Etude des affouillements autour des piles de ponts", Laboratoire National d'Hydraulique 6, Quai Watier, Chatou, France, 1956.
4. Chang, F. M., "Scour at bridge piers - field data from Louisiana files", Report No. FHWA-RD-79-105, Federal Highway Administration, 1980, 32 p.
5. Davis, S. R., "Case histories of scour problems at bridges", Transportation Research Record 950, Second Bridge Engineering Conference, v. 2, 1984, p. 149-155.
6. Highway Research Board, "Scour at bridge waterways", Synthesis of Highway Practice 5, National Cooperative Highway Research Program, 1970, 37 p.
7. Hopkins, G. R., Vance, R. W., and Kasraie, B., "Scour Around Bridge piers", Report No. FHWA-RD-79-103, Federal Highway Administration, 1980, 131 p.
8. Jain S. C., "Maximum Clear-water Scour Around Circular Piers," Journal of the Hydraulics Division, ASCE, v. 107, no. HY5, 1981, p. 611-628.
9. Jarrett, R. D., and Boyle, J. M., "Pilot study for collection of bridge-scour data," U.S. Geological Survey Water-Resources Investigations Report, 1986, 89 p.
10. Jones, J. S., "Comparison of prediction equations for bridge pier and abutment scour," Transportation Research Record 950, Second Bridge Engineering Conference, v. 2, 1984, p. 202-208.

11. Laursen, E. M., and Toch, A., "Scour around bridge piers and abutments," Bulletin No. 4, Iowa Highway Research Board,1956, 60 p.
12. Melville, B. W., "Local scour at bridge sites," Report No. 117, University of Auckland, School of Engineering, Auckland, New Zealand, 1975.
13. Melville, B. W., "Live-bed scour at bridge piers," Journal of Hydraulic Engineering, ASCE, v. 110, no. 9, 1984, p. 1234-1247.
14. Neill, C. R., "Measurements of bridge scour and bed changes in a flooding sand-bed river," Proceedings, Inst. Civil Engineers, London, v. 30, 1965, p. 415-435
15. Neill, C. R., "Mean-velocity criterion for scour of coarse uniform bed material," Proceedings, 12th Congress of the International Association for Hydraulic Research, September 11-14, 1967, Fort Collins, CO, v. 3, 1967, p. 46-54.
16. Neill, C. R., "River-bed scour, a review for bridge engineers," Technical Publication No. 23, Canadian Good Roads Association, 1970, 37 p.
17. Neter, J., and Wasserman, W., "Applied linear statistical models: Homewood, IL, Richard D. Irwin, Inc., 1974, 842 p.
18. Norman, V. W., "Scour at selected bridge sites in Alaska," U.S. Geological Survey Water-Resources Investigations Report 32-75, 1975, 160 p.
19. Raudkivi, A. J., "Functional trends of scour at bridge piers," Journal of Hydraulic Engineering, ASCE, v. 112, no. 1, 1986, p. 1-13.
20. Raudkivi, A. J., and Ettema, R., "Effect of sediment gradation on clear-water scour," Journal of the Hydraulics Division, ASCE, v. 103, no. HY10, 1977, p. 1209-1213.
21. Raudkivi, A. J., and Ettema, R., "Clear-water scour at cylindrical piers," Journal of Hydraulic Engineering, ASCE, v. 109, no. 3, 1983, p. 338-350.
22. Roper, A. T., Schneider, V. R., and Shen, H. W., "Analytical approach to local scour," Proceedings, 12th Congress of the International Association for Hydraulic Research, September 11-14, 1967, Fort Collins, CO, v. 3, 1967, p. 151-161.
23. Shen, H. W., Schneider, V. R., and Karaki, S., "Mechanics of local scour," Report No. CER66HWS22, Colorado State University, Engineering Research Center, 1966, 57 p.
24. Shen, H. W., Schneider, V. R., and Karaki, S., "Local scour around bridge piers," Journal of the Hydraulics Division, ASCE, v. 20, no. HY6, 1969, p. 1919-1940.

APPENDIX II.--NOTATION

The following symbols are used in this paper:

b = width or diameter of pier,
b' = width of pier projected normal to the approach flow, $b \cos\alpha + l \sin\alpha$,
d_s = depth of local scour below ambient bed level,

d_{50} = bed material size of which 50% by weight are smaller,
F_a = Froude number of the approach flow, V/ gy,
g = gravitational acceleration,
ℓ = length of pier from nose to tail,
R_p = Reynolds number based on pier width, Vb/ ,
r^2_a = coefficient of determination adjusted for degrees-of-freedom,
S_s = specific gravity of bed material,
V = mean velocity of approach flow,
V_c = critical mean velocity for beginning of sediment movement,
y = depth of approach flow,
$\bar{y}$ = mean depth in approach cross-section,
α = angle at which flow approaches the pier,
ν = kinematic viscosity of water,
ζ = pier alignment factor, $(b'/b)^{0.6}$,
ρ = density of water,
ρ_s = density of bed material,
σ_g = geometric standard deviation of bed-material size distribution, $(d_{84}/d_{16})^{1/2}$,
ϕ = pier shape factor.

Table 1. -- Field Measurments of Local Scour at Bridge Piers

Reference(s) and Location of Measurement	Obs. No.	Date of Observation	Scour Depth in meters	Pier Type	Pier Width in meters	Pier Length in meters	Approach Flow Depth in meters	Approach Flow Velocity in meters per second	Approach Flow Angle in degrees	Sediment Mean diameter in millimeters	Sediment Geometric standard deviation	Comments
Neill (1965):												
Beaver River La Corey bridge, Alberta, Canada	1	06/19/62	1.74	2	1.92	17.37	5.39	1.8	5	0.5	---	center pier
Melville (1975):												
Waikato River Tuakau bridge	2	08/15/58	2.75	1	2.40	8.85	3.45	0.96	10	0.78	2.3	
Norman (1975):												
Susitna River Anchorage-Fairbanks Hwy. bridge near Sunshine, AK	3	07/02/71	0.76	3	1.52	6.10	5.8	1.98	0	70	---	pier no. 1
	4	"	0.76	3	1.52	6.10	4.1	2.59	0	70	---	pier no. 2
	5	"	0.61	3	1.52	6.10	3.4	2.13	0	70	---	pier no. 3
	6	08/11/71	0.61	3	1.52	6.10	5.3	3.05	0	70	---	pier no. 1
	7	"	0.61	3	1.52	6.10	6.6	2.90	0	70	---	pier no. 2
	8	"	0.61	3	1.52	6.10	5.2	3.51	0	70	---	pier no. 3
Knik River Glenn Hwy. bridge near Palmer, AK	9	07/11/65	0.82	3	1.80	9.60	5.5	3.67	0	1.5	---	pier no. 5
Knik River bridge near Eklutna, AK	10	06/17/66	0.30	2	1.52	11.58	1.2	0.49	0	0.5	---	pier no. 3
	11	"	0.30	2	1.52	11.58	1.5	0.76	0	0.5	---	pier no. 4
	12	"	0.30	2	1.52	11.58	1.2	0.88	0	0.5	---	pier no. 5
	13	"	0.76	2	1.52	11.58	0.5	0.27	0	0.5	---	pier no. 6
	14	"	1.22	2	1.52	11.58	0.6	0.15	0	0.5	---	pier no. 7
	15	06/24/66	0.61	2	1.52	11.58	2.1	1.52	0	1.6	---	pier no. 1
	16	"	0.61	2	1.52	11.58	2.0	1.55	0	1.6	---	pier no. 2
	17	"	0.91	2	1.52	11.58	3.0	1.58	0	1.6	---	pier no. 3
	18	"	1.22	2	1.52	11.58	3.2	1.98	0	1.6	---	pier no. 4 exposed foundation
	19	"	1.37	2	1.52	11.58	3.0	1.80	0	1.6	---	pier no. 5
	20	"	1.07	2	1.52	11.58	2.6	2.07	0	1.6	---	pier no. 6
	21	"	1.83	2	1.52	11.58	3.0	1.83	0	1.6	---	pier no. 7
	22	06/28/66	0.46	2	1.52	11.58	0.9	0.94	0	1.6	---	pier no. 1
	23	"	0.61	2	1.52	11.58	0.9	0.98	0	1.6	---	pier no. 2
	24	"	0.46	2	1.52	11.58	1.8	1.10	0	1.6	---	pier no. 3
	25	"	0.61	2	1.52	11.58	2.4	1.16	0	1.6	---	pier no. 4 exposed foundation
	26	"	0.76	2	1.52	11.58	2.3	1.13	0	1.6	---	pier no. 5
	27	"	0.46	2	1.52	11.58	1.5	1.13	0	1.6	---	pier no. 6
	28	"	0.76	2	1.52	11.58	2.0	0.98	0	1.6	---	pier no. 7
Tazlina River Richardson Hwy. bridge near Glennallen, AK	29	04/22/69	0.6	3	4.60	---	0.6	---	0	90	---	
	30	09/02/71	1.5	3	4.60	---	3.7	2.90	0	90	---	
	31	09/04/71	1.7	3	4.60	---	4.6	3.51	0	90	---	
	32	10/01/71	0.9	3	4.60	---	1.5	0.61	0	90	---	
Tanana River Richardson Hwy. bridge at Big Delta, AK	33	07/16/71	1.8	2	1.52	10.36	3.7	2.16	35	14	---	pier no. 1
	34	"	2.1	2	1.52	10.36	3.7	2.22	35	14	---	pier no. 2
	35	"	1.8	2	1.52	10.36	4.6	2.07	35	14	---	pier no. 3
	36	"	2.4	2	1.52	13.56	4.3	1.74	35	14	---	pier no. 4
Tanana River Anchorage-Fairbanks Hwy. bridge at Nenana, AK	37	07/30/67	1.8	2	3.05	17.60	6.7	2.59	0	15	---	
Snow River Seward Hwy. bridge near Seward, AK	38	09/22/70	0.9	2	0.98	0.98	1.7	1.61	0	8	---	
Chang (1980):												
Red River LA-6 bridge near Grand Encore, LA	39	12/27/77	4.0	2	4.9	12.8	1.8	---	0	0.053	8.8	
	40	06/16/78	4.6	2	4.9	12.8	4.6	---	0	0.053	8.8	

Table 1. -- continued

Reference(s) and Location of Measurement	Obs. No.	Date of Observation	Scour Depth in meters	Pier Type	Pier Width in meters	Pier Length in meters	Approach Flow Depth in meters	Approach Flow Velocity in meters per second	Approach Flow Angle in degrees	Sediment Mean diameter in millimeters	Sediment Geometric standard deviation	Comments
Red River LA-8 bridge near Boyce, LA	41	06/28/77	3.7	2	8.2	8.2	4.9	0.46	0	0.060	11.5	
	42	06/06/78	4.3	2	8.2	8.2	4.3	0.61	0	0.060	11.5	
Red River LA-3026 bridge near Alexandria, LA	43	06/06/77	7.3	2	13.0	38.0	4.1	0.55	5	0.027	8.3	
	44	11/21/77	6.8	2	13.0	38.0	3.4	0.66	15	0.027	8.3	
	45	06/19/78	8.5	2	13.0	13.0	5.4	1.16	20	0.027	8.3	
Atchafalaya River Hwy. 190 bridge near Krotz Springs, LA	46	07/14/77	4.3	3	9.8	12.5	11.0	0.73	5	0.008	18.7	
	47	"	8.2	3	9.8	12.5	12.8	0.81	30	0.008	18.7	
	48	2/29/77	4.6	3	9.8	12.5	13.6	1.08	15	0.008	18.7	
	49	"	7.9	3	9.8	12.5	16.3	1.22	25	0.008	18.7	
	50	07/12/78	4.0	3	9.8	12.5	11.6	0.82	15	0.008	18.7	
	51	"	7.6	3	9.8	12.5	13.4	0.91	25	0.008	18.7	
Mississippi River Hwy. 65 bridge at Natchez, MS	52	09/07/77	6.1	1	9.4	19.5	19.5	1.80	0	0.036	6.1	
Mississippi River Hwy. 190 bridge at Baton Rouge, LA	53	06/14/77	10.4	2	19.5	38.0	11.3	0.66	15	0.036	6.3	
Hopkins and others (1980):												
Red River Texas St. bridge at Shreveport, LA	54	12/18/72	2.8	2	3.66	17.30	3.60	0.64	0	0.1	---	
Breusers (1970) and Breusers and others (1977):												
Niger River Onitsha bridge	55	--/--/--	7.8	2	8.5	8.5	9.0	0.65	12	0.67	---	
Jarrett and Boyle (1986):												
South Platte River County Road 87 bridge at Masters, CO	56	10/02/84	0.61	1	0.29	3.66	0.76	1.04	15	1.5	---	pier no. 5
	57	"	0.61	1	0.29	3.66	0.61	1.36	15	1.5	---	pier no. 6
	58	"	0.52	1	0.29	3.66	0.73	1.17	15	1.5	---	pier no. 7
	59	06/25/84	0.58	1	0.29	3.66	0.43	1.13	10	2.3	---	pier no. 5
	60	"	0.46	1	0.29	3.66	0.58	1.02	10	2.3	---	pier no. 6
	61	"	0.49	1	0.29	3.66	0.70	1.12	10	2.3	---	pier no. 7
	62	05/18/84	0.66	1	0.29	3.66	1.81	1.22	15	2.3	---	pier no. 5
Arkansas River County Road 613 bridge near Nepasta, CO	63	05/23/84	0.64	2	1.22	6.40	2.13	1.17	0	0.6	---	pier no. 1
	64	"	0.40	2	1.22	6.40	0.55	0.69	0	0.6	---	pier no. 3
	65	06/05/84	1.22	2	1.22	6.40	2.32	1.70	0	0.6	---	pier no. 1
	66	09/27/84	0.61	2	1.22	6.40	0.70	0.66	0	0.6	---	pier no. 1
Rio Grande Hwy. 285 br. at Monte Vista, CO	67	05/22/84	0.37	3	0.94	27.43	1.40	1.54	0	7.9	---	
	68	06/01/84	0.15	3	0.94	27.43	1.22	1.35	0	4.3	---	
South Platte River Hwy. 37 bridge near Kersey, CO	69	05/21/84	0.98	3	0.52	8.29	3.21	1.68	10	1.2	---	pier no. 1
	70	06/26/84	0.65	3	0.52	8.29	2.14	1.17	10	1.8	---	pier no. 1

Note - Pier type defined as: 1 = square-nosed, 2 = round-nosed, 3 = sharp-nosed

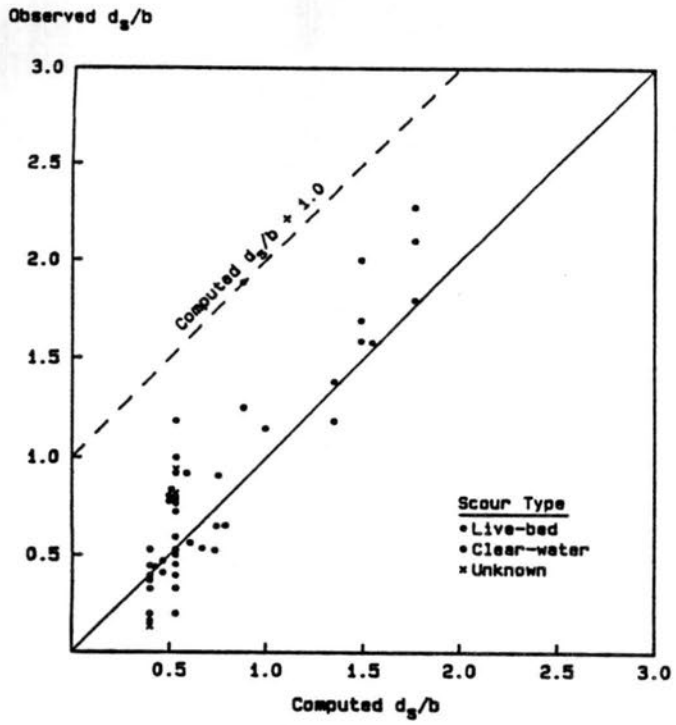

Fig. 1.-- Observed value of d_s/b plotted against d_s/b computed by Eq. 12.

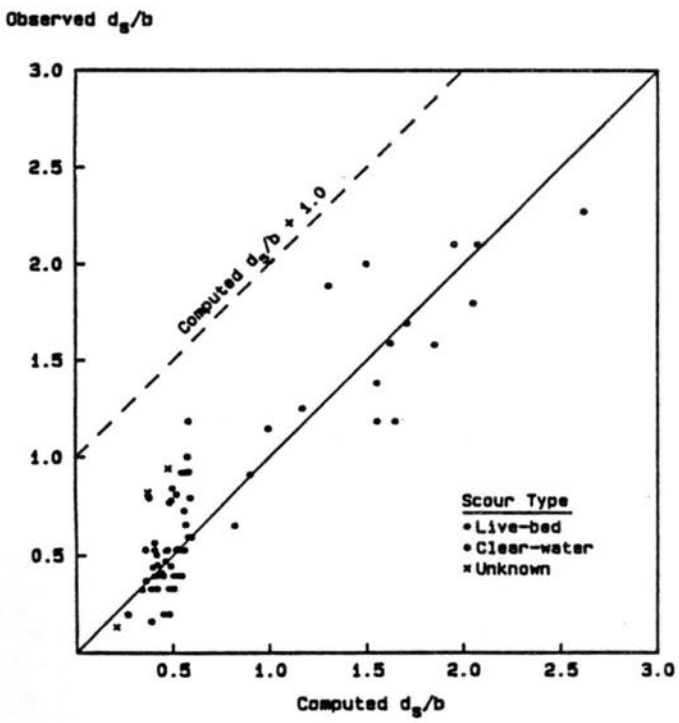

Fig. 2.-- Observed value of d_s/b plotted against d_s/b computed by Eq. 13.

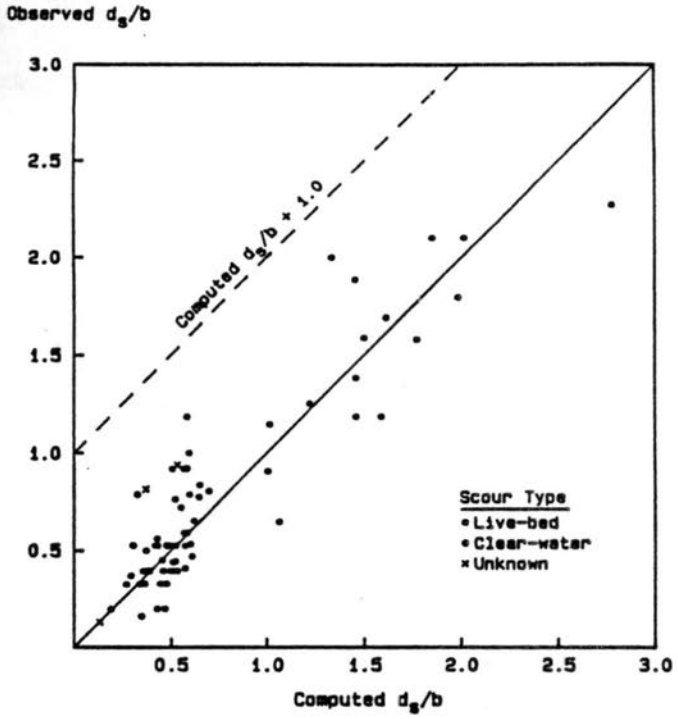

Fig. 3.-- Observed value of d_s/b plotted against d_s/b computed by Eq. 14.

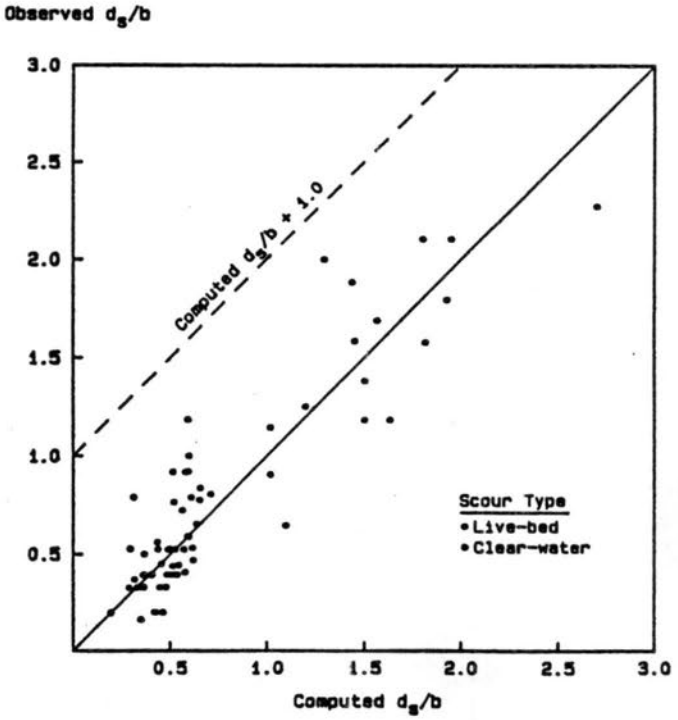

Fig. 4.-- Observed value of d_s/b plotted against d_s/b computed by Eq. 15.

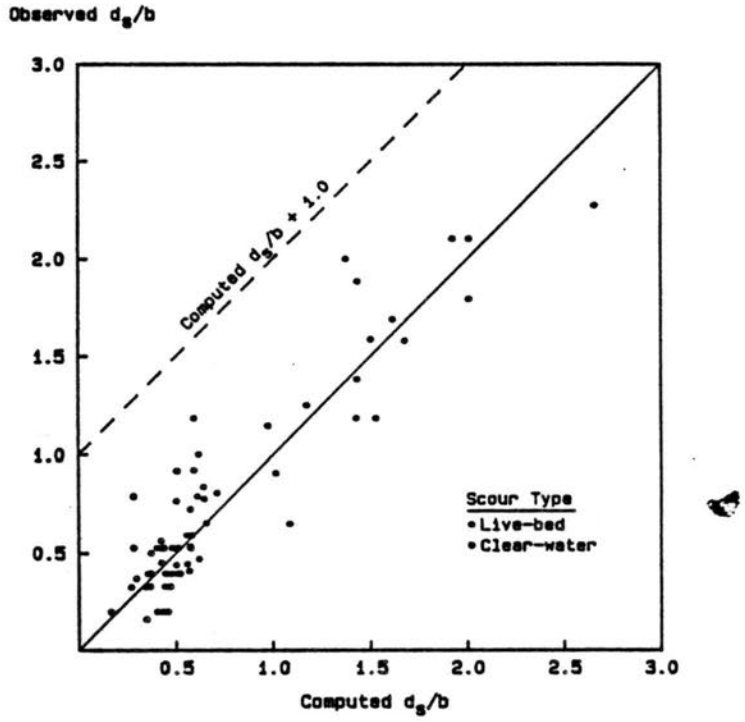

Fig. 5.-- Observed value of d_s/b plotted against d_s/b computed by Eq. 16.

LOCAL SCOUR DOWNSTREAM OF RIGID GRADE-CONTROL STRUCTURES

By Noel Bormann[1]

Abstract: To properly design grade-control structures in alluvial channels the local scour caused by flow over the structure must be predicted. Prior to this study empirical equations frequently used to predict this local scour were based on investigations of free overfall jets. In most situations grade-control structures in alluvial channels do not experience free overfall conditions and predictions of scour based on free overfall equations have been found to overpredict scour for flows which are well submerged. This paper presents the results of a large scale ratio hydraulic model for channel conditions in the Pima County, Arizona, region with submerged flow conditions. Model test discharges varied between 3 and 25 cfs/ft, drop heights varied between 0.17 and 1.0 feet and the face slope of the structure varied between vertical and 3:1. The scale ratios of the model were 1:4 and 1:6. Based on observed model results empirical equations are developed for use in prediction of local scour for practical design purposes.

INTRODUCTION

Grade-control structures are used to limit excessive or unacceptable channel bed degradation in specific channel reaches. A grade-control structure typically causes a local scour on the downstream side of the structure. The foundation elevation (i.e. the burial depth) of the grade-control structure must be sufficient to prevent failure of the structure due to foundation undermining due to scour. The structure design of these structures can thus be considered to be a function of the fluvial system (e.g. runoff characteristics, sediment discharge, sediment size, etc.), spacing between grade-control structures, drop height and depth of local scour (Simons, Li & Associates, Inc., 1983).

In the Pima County, Arizona, region, surrounding Tucson, extensive use is made of grade-control structures constructed of soil cement. An important factor in the total construction cost of these structures is the burial depth of the structure foundation. Prediction of the required burial depth of these structures has in the past been made using empirical equations developed for flow phenomena involving the presence of free overfall jets. However, in the majority of installations, the flow over grade-control structures is not a free overfall jet (i.e. submerged conditions exist). To improve local scour predictions in submerged conditions, a large scale ratio hydraulic model study has been performed. By using the empirical equation developed in this study, more cost-effective designs can be made for grade-control structures in these conditions.

---

[1]Consulting Hydraulic Engineer, 1021 North Taft Hill Road, Fort Collins, Colo.

HYDRAULIC CONDITIONS

The physical characteristics and processes which govern the formation of local scour holes downstream of grade-control structures are numerous and complex. The complexity is increased by the interrelationship between the flow phenomena and the geometry of the movable bed. The difficult nature of this phenomenon has thus far forced investigations to concentrate on empirical equations based on ultimate scour depths observed in hydraulic models or in prototype installations (Mason and Arumugam, 1985). Therefore, in developing an empirical equation for flow over grade-control structures with submerged conditions, it is desirable to use variables which concisely and completely characterize the hydraulics of submerged flow. Dimensional analysis and comparison to previously developed scour equations (15, 1, 2, 3, 5, 7, 9, 11, 12, 13, 14, 16, 17, 19, 20, 21) led to the consideration of H, Hd, Twd, q, dp, Sub, Y_1 and Y_2. The combinations of variables which are not well known is illustrated in Figure 1. It must be emphasized that due to budgetary constraints, only one prototype bed material distribution was tested in this study, and reflected stream bed material in the Pima County region. Therefore, the effect of changes in bed material is not shown.

In approximately 25 previously developed empirical equations (Mason and Arumugam, 1985) the form of equation most widely used is represented by (Mason and Arumugam, 1985):

$$Dsc + Twd = \frac{3.27\ q^{0.60}\ H^{0.05}\ Twd^{0.15}}{g^{0.30}\ d_{50}^{0.10}} \qquad (1)$$

The units for equation 1 are metric and are as explained in Appendix II. Mason and Arumugam (1985) propose equation 1 for use in both free overfall jet and for outlet spillway scour situations if the headloss in the outlet works is subtracted from the overall head available. They also acknowledge the difficulty in developing a physically based equation and after analyzing many data sets simply added the constant g exp(0.30) to make the equation dimensionally consistent with Froude number scaling criteria.

None of the previously available equations (15, 1, 2, 3, 5, 7, 9, 11, 12, 13, 14, 16, 17, 19, 20, 21) have the ability to incorporate the effects of submergence or the effect of the face slope of the structure on the local scour processes. Therefore, the hydraulic testing was concentrated upon the submerged flow conditions.

HYDRAULIC MODEL

The modeling facility utilized in this study is located at the Engineering Research Center (ERC) at the Foothills Campus of Colorado State University in Fort Collins, Colorado.

The model facilities consist of a steel walled flume with a headbox and tailbox, having a total length of 90 feet. The steel flume has a total inside width of three feet, with an overall height of 11.5 feet. The model grade-control structure has a crest which is seven feet above the flume floor. The tailbox of the model contains the gates used to control the water level in the

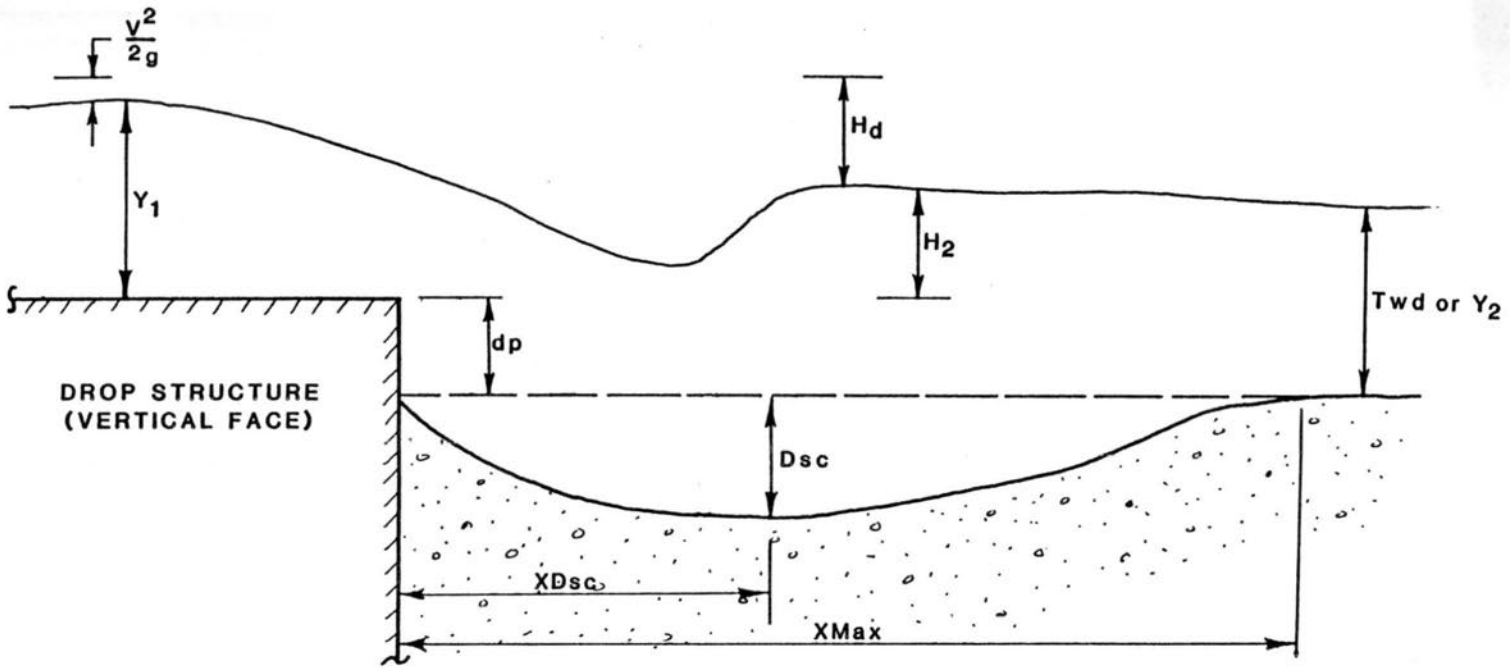

$$Sub = \frac{Y_2 - dp}{Y_1} \times 100 = \frac{H_2}{Y_1} \times 100 \qquad HdT = \frac{(Y_1 + \frac{V^2}{2g} - Y_2 + dp)}{Y_2} \times 100 = \frac{H_d}{Twd} \times 100$$

FIG.1.--Relationship of variables

flume. The gates consist of a vertical series of four hinged flap gates controlled with winch cables. A 36-inch diameter inlet pipe conveys water into the model headbox. The diagrammatic representation of the flume is shown in Figure 2. Water was provided to the flume through an Aurora 30LM36 vertical mixed flow pump powered by a Detroit Diesel 8V-92T engine. This pump engine system is capable of providing approximately 75 cfs to the flume, providing a model unit discharge of 25 cfs/ft.

The single bed material gradation selected for this study was a characteristic gradation representing the majority of stream beds in the Pima County, Arizona, region. Table 1 shows the bed material gradation used in this study. Many previous equations have ignored the effect of bed material sizes on scour hole development and show scour to be independent of sediment size (15, 5, 6). Although this was not confirmed by this study, it is not felt that scour can be independent of sediment size.

TABLE 1.--Bed-Material Gradation

Percent of Material Finer Than (1)	Prototype Size (2)	1:4 Model Scale (3)	1:6 Model Scale (4)
90	9 mm	2.3 mm	1.5 mm
50	1.8 mm	0.43 mm	0.3 mm
16	0.5 mm	0.16 mm	0.12 mm

Three types of similarity are important in hydraulic modeling: geometric similarity, dynamic similarity, and kinematic similarity. Complete dynamic similarity, however, is not possible if the model and prototype fluids are the same. However, by establishing which forces are the most important for the phenomenon under investigation, partial dynamic similarity can be achieved. Partial dynamic similarity is in many cases adequate (Farhoudi and Smith, 1985). For phenomena involving flow with a free water surface at high Reynolds numbers (Rn), hydraulic modeling using Froude number (Fr) modeling criteria is acceptable.

Using the Froude number scaling criteria requires that the model Froude number is equal to the prototype Froude number. This requirement must be reflected in empirical equations based on models to insure that when model results are used to predict prototype behavior the calculated Froude number for the prototype situation has the same value as the representative model situation.

MODEL DATA

A total of 99 test data sets was collected. Table 2 shows a summary of the data collected in the testing program. Runs with a decimal value other than zero (e.g. Run 1.1) are runs for which scour data were taken at different time intervals.

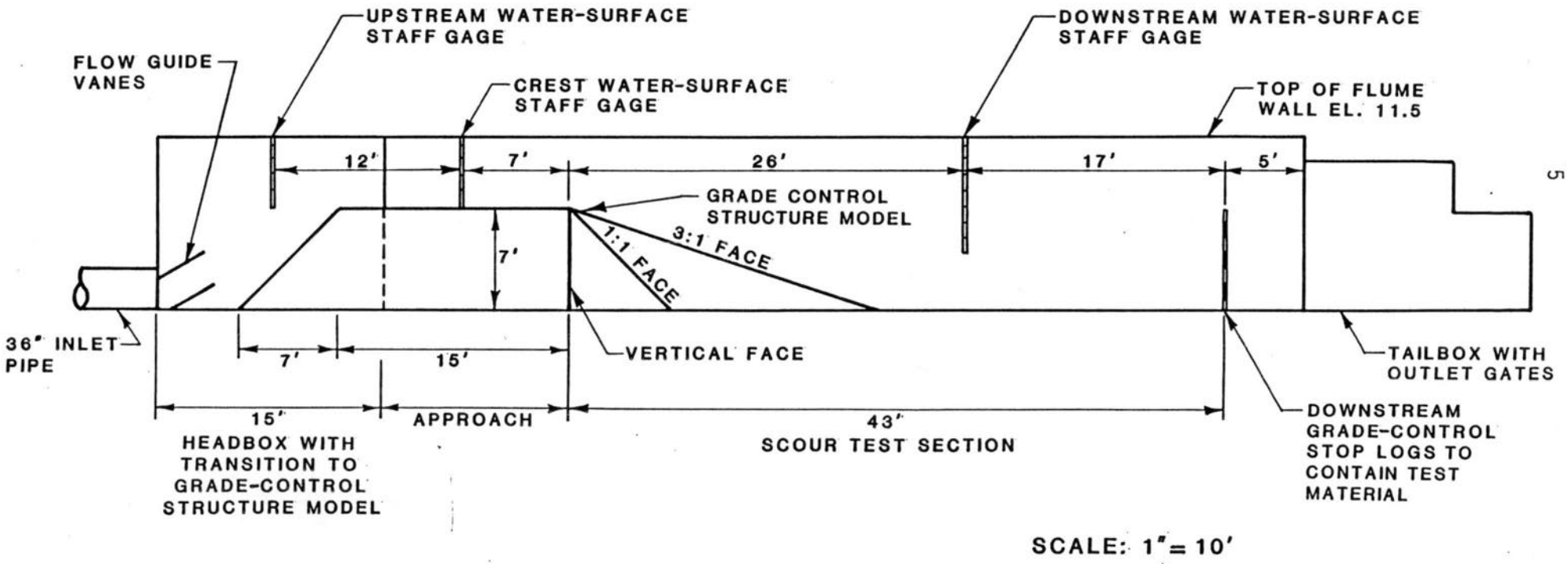

FIG. 2.--Cross section of experimental flume

TABLE 2.--Hydraulic Model Test Data

Run (1)	Date (2)	Scale (3)	Model Drop (4)	Face (5)	Prototype q (6)	Model q (7)	* WS_1 (8)	WS_2 (9)	Submerge (10)	Prototype Max Scour Depth (11)
1.1	09/06/85	6.	0.50	1:1	355.37	24.18	11.00	10.60	90.	22.86
1.2	09/06/85	6.	0.50	1:1	355.37	24.18	11.00	10.60	90.	20.04
1.3	09/06/85	6.	0.50	1:1	355.37	24.18	11.00	10.60	90.	20.94
2.0	09/09/85	6.	0.50	1:1	351.55	23.92	10.80	9.70	71.	28.80
3.0	09/09/85	6.	0.50	1:1	351.55	23.92	10.80	9.40	63.	30.00
4.0	09/10/85	6.	0.50	1:1	271.60	18.48	11.20	10.95	94.	20.76
5.1	09/11/85	6.	0.50	1:1	272.78	18.56	10.50	10.00	86.	21.12
5.2	09/11/85	6.	0.50	1:1	272.78	18.56	10.50	10.00	86.	21.66
5.3	09/11/85	6.	0.50	1:1	272.78	18.56	10.50	10.00	86.	21.30
6.1	09/11/85	6.	0.50	1:1	270.42	18.40	10.30	9.20	67.	23.34
6.2	09/12/85	6.	0.50	1:1	273.54	18.61	10.32	9.20	66.	21.90
6.3	09/12/85	6.	0.50	1:1	273.54	18.61	10.32	9.20	66.	23.10
6.4	09/12/85	6.	0.50	1:1	273.54	18.61	10.32	9.20	66.	25.20
7.0	09/12/85	6.	0.83	1:1	286.59	19.50	11.40	11.10	93.	14.10
8.0	09/13/85	6.	0.83	1:1	280.86	19.11	10.95	9.75	70.	19.62
9.0	09/13/85	6.	0.83	1:1	280.86	19.11	10.95	9.20	56.	25.92
10.0	09/16/85	6.	0.83	1:1	379.77	25.84	11.30	10.90	91.	15.72
11.0	09/16/85	6.	0.83	1:1	362.13	24.64	11.05	9.80	69.	17.22
12.0	09/18/85	6.	0.83	1:1	367.42	25.00	11.15	9.15	52.	25.92
13.0	09/20/85	6.	0.17	1:1	305.55	20.79	11.35	11.03	93.	13.38
14.0	09/20/85	6.	0.17	1:1	359.19	24.44	11.15	9.90	70.	21.18
15.0	09/20/85	6.	0.17	1:1	367.28	24.99	11.18	9.15	51.	26.28
16.0	09/23/85	6.	0.17	1:1	298.76	20.33	11.20	10.95	94.	8.88
17.0	09/23/85	6.	0.17	1:1	307.61	20.93	10.73	9.65	71.	19.08
18.0	09/23/85	6.	0.17	1:1	314.15	21.38	10.65	9.25	62.	25.14
19.0	09/24/85	4.	0.75	1:1	213.12	26.64	11.42	11.05	92.	12.80
20.0	09/24/85	4.	0.75	1:1	200.00	25.00	11.02	9.80	70.	13.96
21.0	09/24/85	4.	0.75	1:1	200.00	25.00	11.02	9.15	53.	18.28
22.0	09/25/85	4.	0.75	1:1	122.40	15.30	10.70	10.40	92.	9.96
23.0	09/25/85	4.	0.75	1:1	125.80	15.73	10.02	9.10	70.	11.64
24.0	09/25/85	4.	0.75	1:1	126.00	15.75	9.95	8.40	47.	14.60
25.0	09/26/85	4.	0.75	1:1	52.20	6.53	9.38	9.29	96.	3.48
26.0	09/26/85	4.	0.75	1:1	49.92	6.24	8.62	8.17	72.	5.16
27.0	09/26/85	4.	0.75	1:1	51.52	6.44	8.55	7.71	46.	7.32
28.0	09/26/85	4.	0.75	1:1	51.04	6.38	8.63	7.54	33.	8.20
29.1	09/27/85	4.	0.75	1:1	28.86	3.61	8.56	8.50	96.	-0.68
29.2	09/27/85	4.	0.75	1:1	28.86	3.61	8.56	8.50	96.	3.40
30.0	09/27/85	4.	0.75	1:1	28.86	3.61	8.12	7.81	72.	1.28
31.0	09/27/85	4.	0.75	1:1	28.86	3.61	8.08	7.52	48.	1.96
32.0	09/27/85	4.	0.75	1:1	28.51	3.56	8.09	7.22	20.	5.16
33.0	09/27/85	4.	0.75	1:1	28.51	3.56	8.08	7.16	15.	12.16
34.0	10/01/85	4.	1.25	VERT	203.28	25.41	11.42	11.17	94.	7.56
35.0	10/01/85	4.	1.25	VERT	199.92	24.99	10.95	9.75	70.	12.36
36.0	10/01/85	4.	1.25	VERT	199.92	24.99	10.87	9.45	63.	20.48
37.0	10/02/85	4.	1.25	VERT	125.44	15.68	10.20	10.02	94.	3.72

TABLE 2.--Hydraulic Model Test Data (continued)

Run (1)	Date (2)	Scale (3)	Model Drop (4)	Face (5)	Prototype q (6)	Model q (7)	* WS_1 (8)	WS_2 (9)	Submerge (10)	Prototype Max Scour Depth (11)
38.0	10/02/85	4.	1.25	VERT	126.00	15.75	9.93	9.13	73.	7.72
39.0	10/02/85	4.	1.25	VERT	126.00	15.75	9.92	8.31	45.	13.72
40.0	10/02/85	4.	1.25	VERT	127.40	15.93	9.92	7.71	24.	18.92
41.0	10/03/85	4.	1.25	VERT	50.16	6.27	10.08	9.90	94.	0.80
42.0	10/03/85	4.	1.25	VERT	53.76	6.72	8.98	8.35	68.	4.04
43.0	10/03/85	4.	1.25	VERT	50.50	6.31	8.57	7.66	42.	6.40
44.0	10/03/85	4.	1.25	VERT	49.56	6.19	8.61	7.32	20.	8.48
45.0	10/03/85	4.	1.25	VERT	52.00	6.50	8.60	7.02	0.0	11.60
46.0	10/04/85	4.	1.25	VERT	24.72	3.09	8.18	8.07	91.	3.72
47.0	10/04/85	4.	1.25	VERT	25.70	3.21	8.01	7.71	70.	2.20
48.0	10/04/85	4.	1.25	VERT	26.28	3.28	8.01	7.42	42.	3.48
49.0	10/04/85	4.	1.25	VERT	24.64	3.08	8.00	7.20	20.	9.32
50.0	10/04/85	4.	1.25	VERT	25.70	3.21	8.00	6.70	0.0	18.24
51.0	10/07/85	4.	0.25	VERT	25.16	3.15	8.27	8.21	95.	3.00
52.0	10/07/85	4.	0.25	VERT	24.96	3.12	8.01	7.71	70.	4.92
53.0	10/09/85	4.	0.25	VERT	25.75	3.22	8.06	7.53	50.	6.00
54.0	10/09/85	4.	0.25	VERT	53.00	6.63	9.45	9.31	94.	1.40
55.0	10/09/85	4.	0.25	VERT	54.00	6.75	8.85	8.30	70.	5.32
56.0	10/10/85	4.	0.25	VERT	51.04	6.38	8.71	7.96	56.	7.00
57.0	10/10/85	4.	0.25	VERT	126.72	15.84	10.85	10.62	94.	3.76
58.0	10/10/85	4.	0.25	VERT	124.80	15.60	9.90	9.03	70.	10.12
59.0	10/11/85	4.	0.75	VERT	26.24	3.28	8.52	8.41	93.	-0.72
60.0	10/11/85	4.	0.75	VERT	29.22	3.65	8.15	7.82	71.	1.72
61.0	10/11/85	4.	0.75	VERT	29.22	3.65	8.14	7.50	44.	2.76
62.0	10/14/85	4.	0.75	VERT	27.86	3.48	8.13	7.21	19.	5.56
63.0	10/14/85	4.	0.75	VERT	50.84	6.35	9.20	9.10	95.	2.28
64.0	10/14/85	4.	0.75	VERT	49.68	6.21	8.64	8.14	70.	5.24
65.0	10/14/85	4.	0.75	VERT	51.04	6.38	8.62	7.73	45.	6.84
66.0	10/14/85	4.	0.75	VERT	51.04	6.38	8.62	7.54	33.	8.24
67.0	10/15/85	4.	0.75	VERT	126.72	15.84	10.91	10.63	93.	4.84
68.0	10/15/85	4.	0.75	VERT	131.60	16.45	9.96	9.18	74.	9.16
69.0	10/15/85	4.	0.75	VERT	123.76	15.47	9.93	8.45	49.	13.68
70.0	10/16/85	4.	0.00	VERT	124.64	15.58	11.01	10.76	94.	3.68
71.0	10/16/85	4.	0.00	VERT	124.64	15.58	10.00	9.10	70.	9.20
72.0	10/17/85	4.	0.00	VERT	51.04	6.38	9.43	9.29	94.	2.00
73.0	10/17/85	4.	0.00	VERT	51.84	6.48	8.74	8.07	61.	6.80
74.0	10/23/85	4.	0.00	VERT	176.00	22.00	11.40	10.90	89.	7.84
75.0	10/23/85	4.	0.00	VERT	176.00	22.00	11.20	9.60	62.	11.68
76.0	10/25/85	4.	0.25	VERT	191.95	23.99	11.41	11.00	91.	6.12
77.0	10/25/85	4.	0.25	VERT	187.68	23.46	10.85	9.70	70.	15.36
78.0	10/25/85	4.	0.75	VERT	198.64	24.83	11.24	10.87	91.	7.80

DEVELOPMENT OF EMPIRICAL RELATIONSHIP FOR SUBMERGED FLOW CONDITIONS

The observed maximum scour depth for each test was regressed against various combinations of the observed hydraulic and geometric data. The regression algorithm used was a nonlinear regression program named BMDPAR. A nonlinear regression was used instead of a linearized model using logarithms so that the statistical properties of the regression (e.g., standard deviation of parameter estimates, Cook's distance, etc.) would have an untransformed mathematical interpretation when analyzing the regression results. It has been shown that statistical models which are linearized by using a logarithmic transformation may not accurately reflect the nontransformed nonlinear equation performance (Ferguson, 1986). Using the BMDPAR routine, the observed maximum scour depth in prototype scale was regressed against the observed geometric and hydraulic variables in prototype scale. Combinations of the variables were regressed to find the variables and/or combination of variables which would best predict the observed scour depth. An initial group of regressions indicated some data sets had inexplicable inconsistencies. These data sets, which had been identified by having very large residuals or very large Cook's distances, were examined for input and observational errors. Only in cases where errors were apparent in the observation of input was the data set deleted. No observations were treated as "outliers" without evidence of observational errors.

This approach was taken to insure that predictions were based on the information available, inherent scatter of the scour process was not artificially reduced to give a false impression of artificially high accuracy or precision. A total of 24 test data sets was deleted in the analysis, leaving 75 test data sets for development of the empirical equation. A total of 23 regression equations for each face slope was developed and the performance of each was compared to select the best predictive equation. The general form of the regression equation examined was:

$$Dsc = P_1 Q^{P_2} H^{P_3} dp^{P_4} Twd^{P_5} \left(\frac{dp}{Twd}\right)^{P_6} \left(\frac{Hd}{Twd}\right)^{P_7} \left(\frac{Hd}{dp}\right)^{P_8} Sub^{P_9} \qquad (2)$$

with the various values of the regression parameters set to zero in various analysis and combinations of variables for each separate face angle (e.g., vertical, 1:1 and 3:1). The regression equation selected as a result of this analysis is:

$$Dsc = C\, q^{0.667}\, HdT^{P_1}\, Sub^{P_2} \qquad (3)$$

where the values of the constant (C) and parameters are given in Table 3 for the various face slopes. The unit discharge is taken as a measure of the erosive potential of the flow. The dimensionless ratio HdT is a measure of the erosive energy added to the flow by dropping over the grade-control structure in proportion to the reduction of erosive energy caused by the dissipative effects of the tailwater depth. The dimensionless ratio Sub is a method to quantify the dissipation of erosive energy by the submergence of the flow over the structure. These lumped variables are used to include physical considerations in the regression when the empirical equation is developed. Table 4 presents measures of the statistically derived performance of equation 2.

TABLE 3.--Values of Parameters for Use in Equation 2

Face Angle (1)	C (2)	P_1 (3)	P_2 (4)
Vertical	0.151	0.411	-0.118
1:1	0.483	0.158	-0.134
3:1	0.011	0.989	0.161

TABLE 4.--Performance of Equation 2

Statistical Parameter (1)	Vertical Face (2)	1:1 Face (3)	3:1 Face (4)
Standard deviation of P_1	0.047	0.041	0.181
Standard deviation of P_2	0.015	0.013	0.041
t-value of P_1	8.74	3.85	5.46
t-value of P_2	7.87	10.31	3.93
Correlation between P_1 and P_2	0.8516	0.8233	0.913
Maximum standard deviation of prediction	0.60	1.35	2.15

Note: $\text{t-value} = \frac{\text{Value of P}}{\text{Std. Dev. P}}$

Figures 3, 4 and 5 show the relationship of the measured scour depth to the scour depth predicted by equation 2 for the vertical, 1:1 and 3:1 face slopes, respectively.

COMPARISON WITH EXISTING EQUATIONS

Equation 3 was compared with the predictive ability of nine equations as presented in Mason and Arumugam (1985). The scour data collected were compared to predictions of all ten scour equations in prototype scale. The results of the comparison are given in Table 5. The values of sum of squared residuals (ssr) and mean square error (mse) have been rounded to the nearest foot. The results shown in Table 5 show an extraordinary variation in predictions for the hydraulic conditions tested in this study, with equation 3 showing predictive ability significantly better than existing equations.

PRACTICAL APPLICATIONS

This study was undertaken to provide designers in the Pima County, Arizona, region with a predictive equation to estimate local scour more accurately than existing equations which were typically based on free overfall conditions. Equation 3 is used below in a hypothetical example. For this

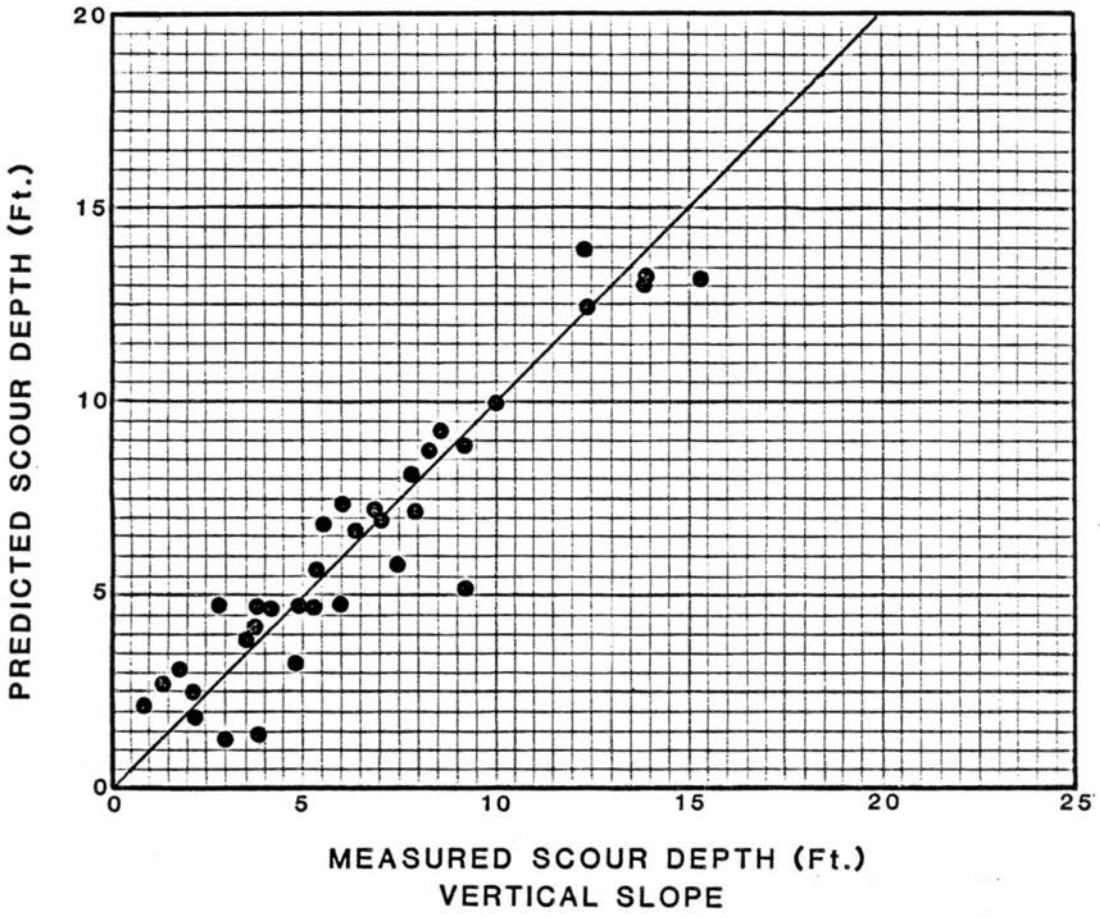

FIG. 3.--Predicted scour depth using Equation 3 versus measured scour depth for vertical face slope

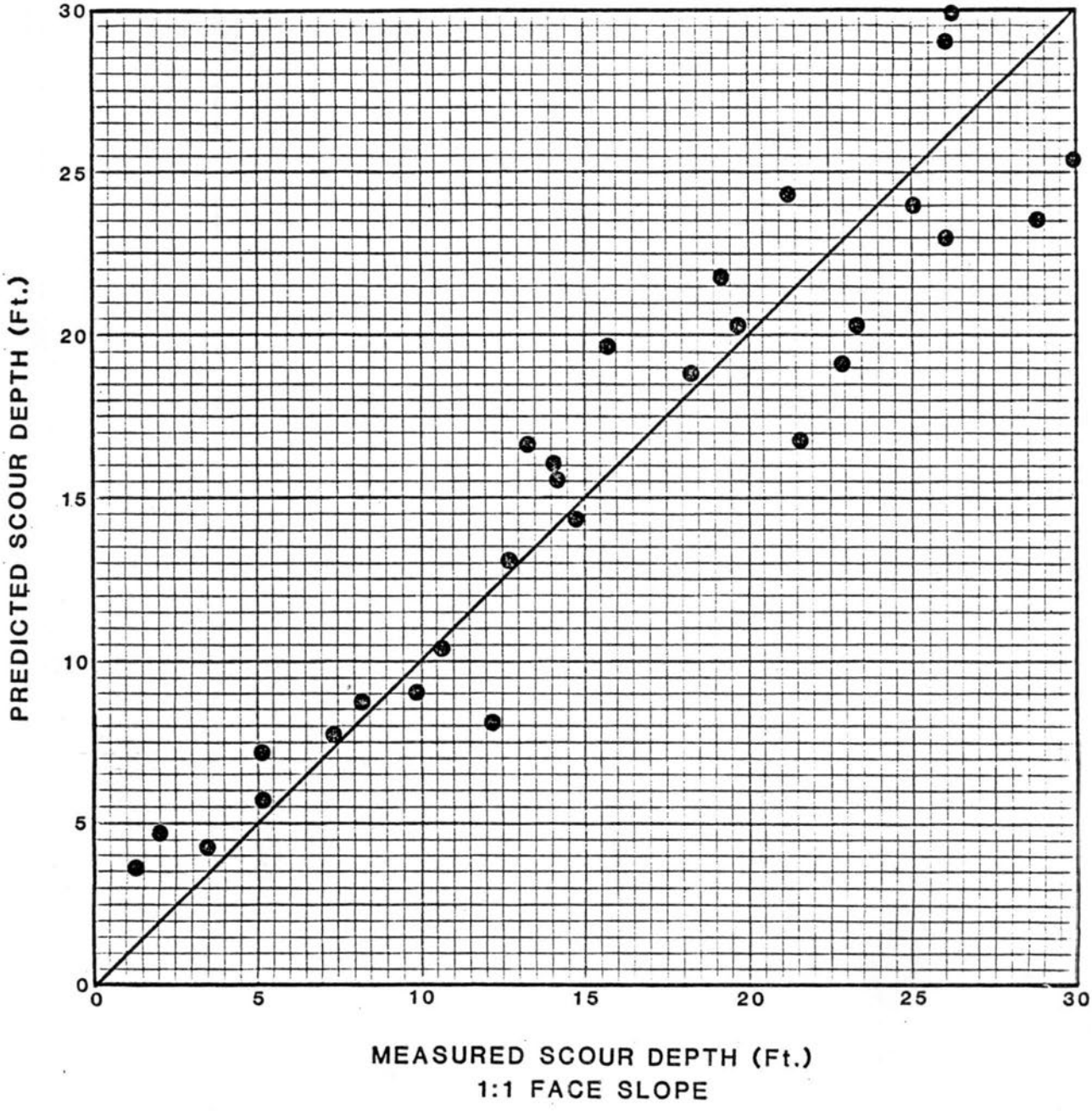

FIG. 4.--Predicted scour depth using Equation 3 versus measured scour depth for 1:1 face slope

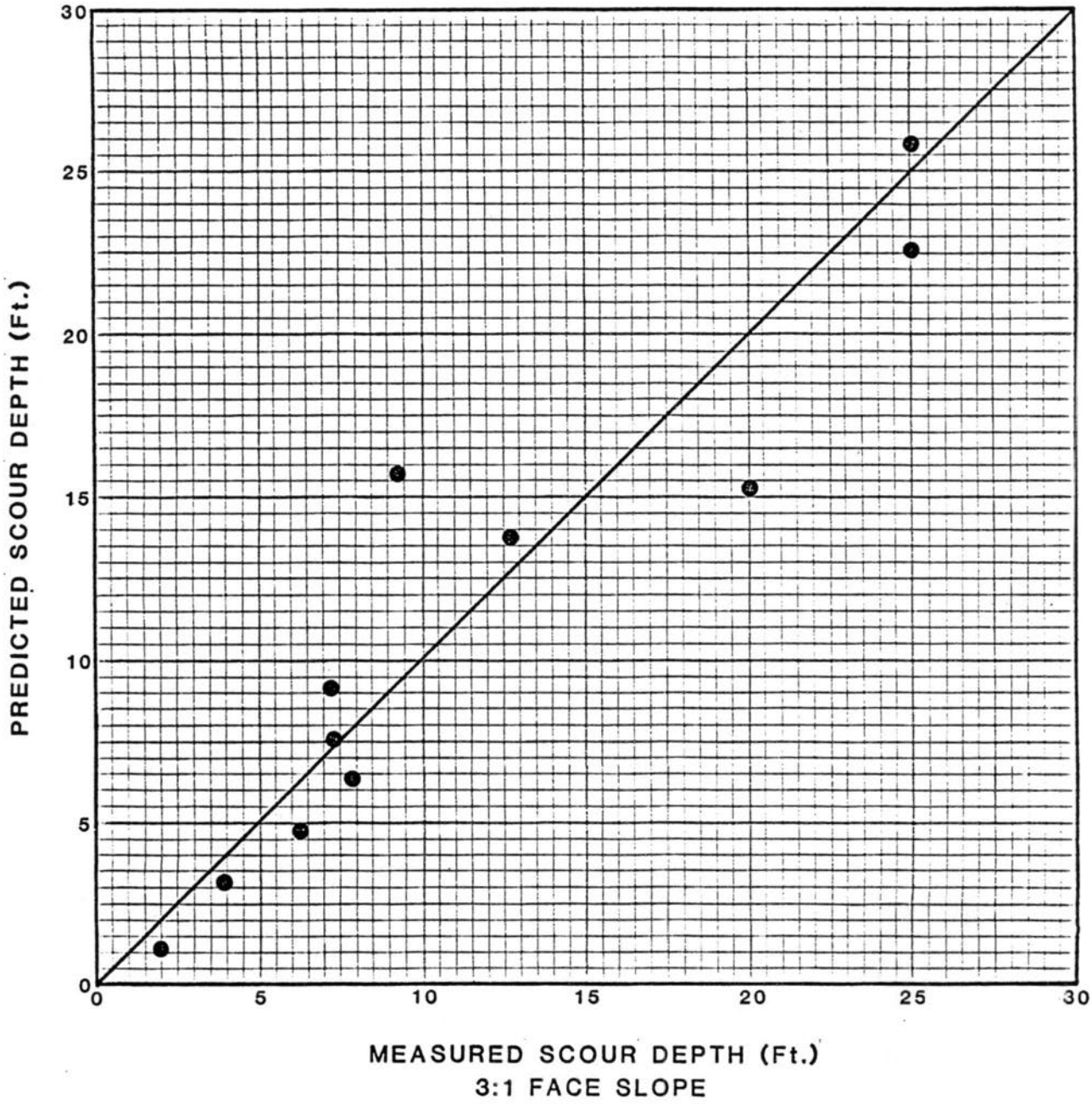

FIG. 5.--Predicted scour depth using Equation 3 versus measured scour depth for 3:1 face slope

TABLE 5.--Comparison of Scour Prediction Equations

Equation (1)	Vertical Face ssr (2)	Vertical Face mse (3)	1:1 Face ssr (4)	1:1 Face mse (5)	3:1 Face ssr (6)	3:1 Face mse (7)
Veronese (A)	4,158	134	12,983	519	557	83
Veronese (B)	437	14	1,270	51	382	55
Schoklitsh	2,146	69	6,934	277	308	44
Martins (A)	1,014	33	512	21	568	81
Martins (B)	249	8	618	25	572	82
Chee and Kung	11,397	368	39,666	1,587	2,284	326
Jaeger	83,879	2,705	344,533	13,781	23,835	3,405
Damle	7,668	247	21,120	844	4,482	640
Mason and Arumugam	24,826	800	69,483	2,779	6,445	920
Equation 3	58	2	217	9	79	11

Note: All results are in feet.

example the drop height will be four feet, and the face slope will be vertical. Selecting six values from a hydrograph shown in Table 6a, we will use:

TABLE 6a.--Example Data for Scour Calculation

Time (1)	Stream Discharge (cfs) (2)	Channel Width (ft) (3)	Unit Discharge (cfs/ft) (4)
1 hour	11,250	450	25
2 hours	15,750	450	35
3 hours	39,100	460	85
5 hours	60,450	465	130
7 hours	92,000	460	200
9 hours	138,000	460	300

For the hydraulics assume the following, and calculating the depth of scour using equation 3, we obtain the values in Table 6b.

SUMMARY

Prior to this study, no prediction equation existed which had been developed for predicting the maximum scour depth downstream of submerged grade-control structures. Using scaled, physical, hydraulic model data, a new equation has been developed to predict scour at grade-control structures. The developed equation significantly improves the prediction of scour at submerged

TABLE 6b.--Example Data with Calculated Scour

Unit Discharge (cfs/ft) (1)	Flow Depth Upstream (ft) (2)	$Y_1 + \frac{v^2}{2g}$ (ft) (3)	Flow Depth Downstream (Y_2) (ft) (4)	Dsc (ft) (5)
25	3.25	4.17	4.30	6.51
35	3.97	5.18	5.00	6.83
85	6.76	9.23	7.66	10.65
130	8.73	12.19	9.88	13.06
200	13.33	16.84	15.20	13.53
300	20.00	23.51	22.20	14.70

grade-control structures when compared to nine other previously developed scour equations.

The developed equation predicts the scour resulting from a constant flow acting until the quasi-equilibrium scour depth is achieved. The equation must be used to examine the scour of a range of flows (i.e., a hydrograph), since the peak discharge may not cause the maximum scour. This study indicates that for a given flow condition, scour increases as the face slopes of grade-control structures flatten. The use of face slopes flatter than 1:1 for grade-control structures is not recommended.

These equations are developed for use with flow situations which have submergence levels greater than 15 percent. Submergences of flow greater than zero, but less than 15 percent, should be analyzed with caution. Prototype discharges of between 25 and 400 cfs/ft were modeled with HdT values of between 3 and 96 percent. Predictions for 3:1 face slope structures are not recommended.

In order that the results or data developed in this study be understood and used properly, the conditions of this study which may impact or limit its application are explicitly stated below.

1. Model behavior is assumed to accurately reflect prototype behavior by using Froude number scaling criteria and scale ratios of 1:6 and 1:4.

2. This model was tested with only one prototype bed material. Therefore, the influence of bed-material size on scour depth was not evaluated.

3. The water input to the test section did not carry any sediment load into the test section, causing essentially clear-water scour conditions. Therefore, the effect of sediment load on scour depth was not evaluated.

4. The flow conditions tested were of a constant discharge, not for a hydrograph condition. It will be the responsibility of the user to determine the flow conditions which will cause maximum scour for the given structure, design hydrograph and associated hydraulic characteristics under consideration.

5. The influence of time on the scour depth was not investigated. If a peak discharge has a small duration, the scour process may not have completed its expected response. This effect was not evaluated.

6. The flow conditions which existed in the model had no exact prototype analogy but are intended to represent, as accurately as possible, the possible flow conditions in a river system, considering the model test section had a length of approximately 40 feet from crest to downstream grade-control structure.

APPENDIX I - REFERENCES

1. Altinbilek, H. D., Basmaci, Y., "Localized Scour at the Downstream of Outlet Structures," International Congress on Large Dams, Question 41, Reply 7, Madrid, Spain, June 1973.

2. Breusers, H. N. C., "Time Scale of Two Dimensional Local Scour," Proc. 12th Congress of the International Association for Hydraulic Research, Colorado State University, Fort Collins, Vol. 3, Paper C32, pg. 275-282, September 1967.

3. Chee, S. P., and Padiyar, P. V., "Erosion at the Base of Flip Buckets," Engineering Journal, Canada, Vol. 52, No. 11, pg. 22-24, November 1969.

4. Dixon, W. J., editor, BMDP Statistical Software, University of California Press, Berkeley, 1983.

5. Doddiah, D., "Comparison of Scour Caused by Hollow and Solid Jets of Water," Masters Thesis, Colorado State University, December 1949.

6. Doddiah, D., Albertson, M. L., and Thomas., R., "Scour from Jets," 5th Congress of the International Association for Hydraulic Research, Minneapolis, Minnesota, pg. 161-169, 1953.

7. Fanti, K., and Zbikowski, A., "Local Scour Downstream from Weirs," International Congress on Large Dams, Question 41, Reply 23, Madrid, Spain, June 1973.

8. Farhoudi, J., and Smith, K. V. H., "Local Scour Profiles Downstream of Hydraulic Jump," Journal of Hydraulic Research, Vol. 23, No. 4, Pg. 343-358, December 1985.

9. Farhoudi, J., and Smith, K. V. H., "Time Scale for Scour Downstream of Hydraulic Jump," Journal of Hydraulics Division, Proceedings of the American Society of Civil Engineers, Vol. 108, No. HY10, pg. 1147-1162, October 1982.

10. Ferguson, R. I., "River Loads Underestimated by Rating Curves," Water Resources Research, Vol. 22, N1, p. 74-76, January 1986.

11. Hartung, F., and Hausler, E., "Scours, Stilling Basins and Downstream Protection Under Free Overfall Jets at Dams," Transactions of the 11th International Congress on Large Dams, Vol. II, Question 41, Reply 3, Madrid, Spain, June 1973.

12. Hartung, F., and Csalner, K., "The Scouring Energy of the Macroturbulent Flow Downstream of a Hydraulic Jump," Proc. 12th Congress of the International Association for Hydraulic Research, Colorado State University, Fort Collins, Vol. 3, Paper C27, pg. 227-237, September 1967.

13. Martins, R., "Contribution to the Knowledge on the Scour Action of Free Jets on Rocky River Beds," Transactions on the 11th International Congress on Large Dams, Vol. II, Question 41, Reply 44, Madrid, Spain, pg. 799-814, June 1973.

14. Martins, R. B. F., "Scouring of Rocky Riverbeds by Free-jet Spillways," International Water Power and Dam Construction, Vol. 27, NO. 5, England, pg. 152-153, April 1975.

15. Mason, P. J., and Arumugam, K., "Free Jet Scour Below Dams and Flip Buckets," Journal of Hydraulic Engineering, ASCE, Vol. 111, No. 2, pg. 220-235, February 1985.

16. Mason, P. J., "Erosion of Plunge Pools Downstream of Dams Due to the Action of Free-Trajectory Jets," Proceedings of Institution of Civil Engineers Part 1, Vol. 76, pg. 523-537, May 1984.

17. Neill, C. R., "Mean-Velocity Criterion for Scour of Coarse Uniform Bed Material," Proc. 12th Congress of the International Association for Hydraulic Research, Colorado State University, Fort Collins, Vol. 3, Paper C6, pg. 46-54, September 1967.

18. Simons, Li & Associates, Inc., Engineering Analysis of Fluvial Systems, Simons, Li & Associates, Inc., Fort Collins, Colorado, 1983.

19. Thomas, R. K., "Scour in a Gravel Bed at the Base of a Free Overfall," Masters Thesis, Colorado State University, May 1953.

20. Vanoni, V. A., editor, "Sedimentation Engineering," ASCE, Manual and Report of Engineering Practice, No. 54, ASCE Task Committee for the Preparation of the Manual on Sedimentation of the Sedimentation Committee of the Hydraulics Division.

21. Volkart, P., Tschoop, J., and Bisaz, E., "The Effect of Sills on River Bed," Proc. of International Association for Hydraulic Research Symposium on River Mechanics, Vol. 4, Bangkok, Thailand, January 1973.

APPENDIX II - NOTATION

cfs - Cubic feet per second.

Depth of Scour (Dsc) - Distance from the original bed elevation downstream of a grade-control structure measured downward to the deepest point of the scour hole formed by the flow, in feet.

Drop Height (dp) - Vertical distance from the crest of a grade-control structure to the unscoured bed elevation downstream of the structure, in feet.

d_x - Grain size of bed material of which x percent of the material is finer, in millimeters.

Froude Number (Fr) - Ratio of inertial forces in fluid flow to gravitational forces.

g - Gravitational constant, equal to 32.2 ft/sec^2

γ - Unit weight of water in pounds per cubic foot.

H - Vertical distance from the upstream water-surface elevation, above a grade-control, structure to the downstream water-surface elevation in units as stated.

HdT - The vertical distance from the upstream energy grade line of the flow to the downstream water surface, in feet, divided by the downstream tailwater depth above the original bed surface, in feet, multiplied by 100 to express the ratio in percent.

Model Scale Ratio - Ratio of the prototype to model dimensions, usually given as the length dimension. For example, a ratio of 1:4 means a 4 foot distance in the prototype is 1 foot in the model.

ρ - Specific gravity of water in slugs per cubic foot.

q - Unit discharge of water given in cubic feet per second per foot of channel width, $ft^3/sec/ft$.

Submergence (Sub) - Downstream depth of water above the grade-control structure crest, divided by the depth of flow upstream of the crest, multiplied by 100 to express the ratio in percent.

Twd - Tailwater depth, measured as the depth of water flowing above the original bed surface downstream of the grade-control structure, in feet.

WSE - Water-surface elevation, in feet.

XDsc - The approximate location of the maximum depth of scour downstream from a grade-control structure, measured from the face of the grade-control structure at the original downstream bed surface, in feet.

XMax - The approximate downstream extent of the scour-hole, measured from the face of the grade-control structure at the original downstream bed surface, in feet.

Y_1 - The depth of flow of the water upstream of the grade-control structure, in feet.

Y_2 - The depth of flow of the water downstream of the grade-control structure above the original unscoured downstream bed surface, in feet. Identical to tailwater depth, Twd.

PREDICTION OF BEDFORMS*

By Magdy M. Saleh[1], and
Pierre Y. Julien[2], A.M. ASCE

ABSTRACT: Simons, and Richardson and Van Rijn's approaches for predicting the type of bedform in alluvial channels are discussed. Mathematical formulation of each approach is presented to help in solving alluvial channel problems. The variation of bedforms with the change of main flow parameters is also analyzed.

INTRODUCTION

The bedforms in alluvial channels affect the resistance to flow. Many investigators studied the prediction of bedforms in natural streams but till now there is no definite approach to define accurately the type of bedform and its size.

Simons and Richardson (3) introduced an approach to define the bedforms based on experimental work. This approach has been accepted for the last twenty years. Recently (1984), Van Rijn (6) presented a method to classify the bedforms, predict their dimensions, and estimate the hydraulic roughness (friction factor).

SIMONS AND RICHARDSON APPROACH

Simons and Richardson (2) divided the flow in sand bed channels into two regimes with a transition zone between them.

The first is the lower flow regime which develops with the beginning of motion. The resistance to flow is large and sediment transport is small. The bedform is either ripples, dunes or some combination of them. The resistance to flow is caused due to form roughness.

The second is the upper flow regime where the resistance to flow is relatively small and sediment transport is large. The usual bedforms are plane bed or antidune. The transition zone occurs during the passage from lower regime to upper regime.

---

* This paper is a summary for the term paper for CE717 Class; River Mechanics, Spring 1986.

1 Graduate student, Colorado State University, Fort Collins, Colorado.

2 Assist. Prof., Civil Engineering Department, Colorado State University, Fort Collins, Colorado.

The classification of bedforms by Simons and Richardson was based on experiments that were conducted in a tilting recirculating flume 150 ft. long, 8 ft. wide, and 2 ft. deep. In addition to the extensive flume data, others were collected from several rivers and canals including: 1) the Elkhorn in Nebraska, 2) the Rio Grande in Texas, 3) the Middle Loup River in Nebraska, 4) the Rio Grande in New Mexico, 5) large irrigation canals with fine-sand beds in India and Pakistan.

Using the flume and natural stream data, Simons and Richardson classified the bedforms as a function of the stream Power (γRSV), and the grain size (D_{50}) as shown in Fig. (1).

MATHEMATICAL REPRESENTATION OF SIMONS AND RICHARDSON'S APPROACH

It is useful to design a computer program to predict the type of bedforms according to Simons and Richardson's graph, Fig. (1). Therefore, the equations for curves (1), (2), (3) and (4), Fig. (1) must be determined. According to this figure, curve (1) separates flat bed from ripples, curve (2) separates ripples from dunes, curve (3) separates dunes from transition and antidunes, and curve (4) separates transition from antidunes. Using the least square method curves (1), (2), (3), and (4) can be defined as,

$$Pw1 = 0.0068 + 0.0722\, D_{50} - 0.154\, D_{50}^2 + 0.132\, D_{50}^3 \quad (D_{50} \geq 0.4) \qquad (1)$$

with correlation coefficient = 0.99968, for curve (2) is

$$Pw2 = 0.097 - 0.0454 D_{50} - 0.298 D_{50}^2 + 0.496 D_{50}^3 \quad (D_{50} \leq 0.4\text{mm}) \qquad (2)$$

and

$$Pw2 = 0.997 - 4.788 D_{50} + 7.86 D_{50}^2 - 4.375 D_{50}^3 \quad (D_{50} \geq 0.4\text{mm}) \qquad (3)$$

with correlation coefficient = 1 for both cases for curve (3) is

$$Pw3 = 0.0786 + 3.537\, D_{50} - 14 D_{50}^2 + 27 D_{50}^3 - 14.65 D_{50}^4 \quad (D_{50} \leq 0.3\text{mm}) \qquad (4)$$

and

$$PW3 = 0.36 + 0.36 D_{50} + 0.454 D_{50}^2 - 0.65 D_{50}^3 + 0.47 D_{50}^4 \quad (D_{50} \leq 0.3\text{mm}) \qquad (5)$$

with a correlation coefficient $\simeq 1$ for both cases and for curve (4) is

$$Pw4 = 0.36 + 0.36D_{50} + 0.454D_{50}^2 - 0.65D_{50}^3 + 0.47D_{50}^4 \quad (6)$$

with a correlation coefficient = 0.999

Equations (1) through (6) represent the four curves that classify the type of bedforms.

COMPUTER PROGRAM TO PREDICT THE TYPE OF BEDFORMS

In order to construct computer program representing Simons and Richardson's graph, Fig. (1), it is useful to divide this graph into four vertical sections. These sections are 1) Section (A) for $D_{50} < 0.3$mm, 2) Section (B) for $0.3\text{mm} \leq D_{50} \leq 0.4$mm, 3) Section (C) for $0.4\text{mm} < D_{50} \leq 0.6$mm, and 4) Section (D) for $D_{50} > 0.6$mm. For each section the equations of the four curves are known, as determined in Section 4. These sections occur due to discontinuity of the shape of any of the four curves. For example, section or strip (C) represents change in the shapes of curves (1) and curve curve (2) and so on.

For a given water discharge, (Q), bed width (B), water depth (Y), bed slope (S) side slope (Z) for trapezoidal section, and mean grain size of bed material (d50), the stream power can be determined as

$$\text{Stream Power (Pw)} = (\tau_0 U) = (\gamma YS)\, Q/A \quad (7)$$

where

$$A = \text{Trapezoidal cross-sectional area} = Y(B + ZY) \quad (8)$$

Then, the values of stream power PW1, PW2, PW3 and PW4 associated with curves (1), (2), (3) and (4) can be determined for the given D_{50}. When the actual stream power, calculated from Eq. (7) is compared with PW1, PW2, PW3 and PW4 the type of bedform can be defined. As an example if D_{50} lies in the first section, section (A) in Fig. (1), and the calculated stream power is larger than PW1 and less than PW2, then the bedform is ripple bed.

Thus, computer program has been developed to predict the type of bed form for the given Q, B, Y, S, Z, and D_{50} according to Simons and Richardson's approach. Fig. (2) shows a flow chart of that program.

ANALYSIS OF THE RESULTS

The type of bedform changes with the variation of Q , Z , B , Y , S , and D_{50}. The stream power (γRSV) represents the first five parameters. Each variable, Q , Z , B , Y and S , can be studied separately by changing the variable and let the other variables to be constant in order to evaluate the effect of each variable on type of bedforms. But it will be more

useful to study the change of bedform due to the change of stream power for different grain sizes, because any change in R , S , or V will be exactly the same for stream power.

Therefore the change of bedforms due to increasing stream power is studied for sections A , B , C , and D of Simons and Richardson's graph, Fig. (1).

For section (A) two grain sizes, D_{50} = 0.05mm, and 0.25mm, are chosen to predict type of bedform for increasing stream power from 0.002 lb/ft/sec. to 0.5 lb/ft/sec. The results show that for small values of stream power, between 0.008 and 0.07 lb/ft/sec., the ripple bed is not sensitive to stream power increase as we can increase the power six or seven times and still ripples are predicted. On the other hand, the dune formation is more sensitive than ripples because if the power increases 2.3 times for D_{50} = 0.05mm or 4.4 times for D_{50} = 0.25mm the bedform will be antidunes. No transition between the dunes and antidunes is predicted and the flat bed without sediment movement can be predicted for very small stream power values, less than 0.006 lb/ft/sec. Dune bed for greater grain size, 0.25mm, occupies large area than for smaller, 0.05mm, as shown in Fig. (3) which represents the bedform change due to increasing the stream power for both previous grain sizes.

Figure (4) represents the change of bedforms in section (B) for grain size = 0.35mm due to increase stream power. The same comments for section (A) can be mentioned for section (B) except that a short transition zone is formed between dunes and antidunes. Also the area of dunes is bigger, from power = 0.08 to 0.52 lb/ft/sec.

The change of bedforms due to increasing stream power for section (C) is given in Fig. (5) for D_{50} = 0.42mm and 0.58mm. Same comments on Section B can be mentioned for section C. The area of ripples decreases, as the grain size increases, while the transition zone increases.

Finally, for section (D) two grain sizes, 0.65mm and 0.90mm, are chosen to represent the change of bedforms due to change of stream power. The results are shown in Fig. (6) for D_{50} = 0.65 and 0.90mm respectively. Larger flat bed area without sediment motion is predicted. The ripples disappeared and the dunes and transition to antidunes are increased.

VAN RIJN APPROACH IN PREDICTING THE BEDFORM IN THE LOWER REGIME

Recently, Van Rijn (4), (5), (6) proposed a method to predict the type of bedforms and their dimensions in the lower region. This method is based on the analysis of flume and field data.

Van Rijn assumed that the bedforms and their dimensions are controlled mainly by the bed-load transport. He also suggested to describe the bed-load transport as function of a dimensionless particle parameter, D_* and a transport stage parameter T , as follows.

1) particle diameter, $D_* = D_{50} \{ (S_o - 1)g/\nu \}^{1/3}$ (9)

in which D_{50} = grain size, S_o = Specific density, and ν = Kinematic viscosity coefficient. And

2) transport stage parameter, $T = (U'_*)^2/(U_{*cr})^2 - (U_{*cr})^2/(U_{*cr})^2$ (10)

in which U'_* = bed-shear velocity related to grains, according to Vanoni-Brooks (3) and U_{*cr} = critical bed-shear velocity according to Shields (4).

Rijn's analysis was focused on the lower and transitional regimes. These regimes can be well-defined without the use of Froude number, since the sediment transport is not related to the Froude number in this regime. Literature (observations) indicated that the transitional stage with washed-out dunes is generated for Froude number about 0.6 in-flume conditions and, about 0.2-0.3 in field conditions. Only in the upper flow regime with antidunes the Froude number is important. Fig. (7) represents the change of bedfomrs in the lower and transition regime as function of particle diameter, D_* , and transport stage parameter, T , according to Rijn.

Each parameter in equations (9) and (10) must be defined in order to classify the bedform. The grain size, D_{50}, specific gravity for particles , S_o, gravity force, g , and kinematic viscosity, ν , can be determined easily. The critical shear velocity, U_{*cr}, is determined from Shields curve, Fig. (8), for known particle parameter, D_*. The bed shear velocity that related to grains, U'_*, is calculated (3) according to Vanoni and Brooks. Vanoni and Brooks simplified Einstein approach to solve the problem of resistance to flow by using two dimensionless Parameters, $U^3/g\nu S$, $U/\sqrt{GK_s S}$, where U = flow mean velocity, S = slope of energy grade line, ν = kinematic viscosity and Ks = equivalent roughness ($3.5\ D_{84}$). These two parameters were plotted as shown in Fig. (9) to define U/U'_* ratio.

In order to define the type of bedforms according to Van Rijn, the following steps can be followed,

1) Compute the average velocity U = Q/A.

2) Calculate the equivalent roughness

Ks = (3.5)(St)(D50)

where St = standard deviation of bed particles.

3) Compute particle parameter as
$D_* = D_{50} \{ (S_o - 1)g/\nu^2 \}^{1/3}$

4) Determine the critical shear velocity from, U_{*cr}, Shields diagram, Fig. (8).

5) Compute Vanoni and Brooks parameters $U^3/g\nu s$, and $U/\sqrt{gKsS}$ to define the U/U'_* ratio, Fig. (9), and then determine U'_*.

6) Calculate the transport stage parameter,

$$T = (U'_*)^2/U_{*cr})^2 - (U_{*cr})^2/(U_{*cr})^2$$

7) From Van Rijn chart, Fig. ( ), determine the type of bedform as

*Ripples if $D_* \leqslant 10$ and $T \leqslant 3$

*Dunes if $D_* > 10$ and $T < 10$ and if $3 < T \leqslant 15$

*Transition if $15 < T \leqslant 25$.

*Upper flow regime if $T > 25$.

If the critical bed shear stress U_{*cr} is larger than the bed shear stress that related to grains, U_* , then transport stage $T = (U'_*)^2/U_{*cr})^2 - (U_{*cr})^2/(U_{*cr})^2$ will be negative and no motion will be predicted. A computer program has been designed according to the previous steps. Fig. (10) shows a flow chart for that program which defines the type of bedforms according to Van Rijn.

ANALYSIS OF RESULTS

According to Rijn's approach the type of bedform is defined knowing the main variables Q , B , Y , slope, D_{50} and temperature. In the following sections the effect of changing each of the main variables will be discussed.

CHANGE OF BEDFORMS WITH WATER TEMPERATURE

If the water temperature is increased the kinematic viscosity ν , will decrease. This change will increase Rijn's particle parameter, D_*, as $D_* \alpha 1/\nu$. This change will also increase Vanoni $U^3/g\nu S$, and consequently the ratio of U/U'_*, will be affected. Therefore, Rijn's second parameter, transport stage parameter, $T = \phi (U'_*, U_{*cr})$, will change. Generally, increasing D_* or T may change the bedforms from ripples to dunes, and further increase in T dunes may be changed to be transition or antidunes. But Rijn approach is valid only for bedforms in the lower flow regime.

To study this change numerically, let the temperature change from 10°C to 100°C with constant Q, B, Y, S and D_{50} and predict the corresponding bedform. Fig. (11) shows this change for constant Q = 7.56m^3/sec, B = 21.49m, Y = 0.47m, S = 134.5 cm/km and D_{50} = 0.31mm. For temperatures from 10°C to 30°C the bed is ripples and for further increase in temperature the bed will change to dunes to 100°C. This indicates that the portion of dune bed is larger than ripples when increasing the temperature from 10°C to 100°C.

CHANGE OF BEDFORMS WITH GRAIN SIZE

The particle parameter (D_*) and transport stage parameter (T) depend on the grain size. Therefore changing the grain size will change D_* and T and consequently the type of bedform.

The particle parameter (D_*) is proportional to the grain size (D_{50}). the stage transport parameter (T) is based on (U'_*) and U_{*cr}. The shear velocity U'_* is function of the equivalent roughness (K_s) and thus depends on D_{50}, as well as U'_{*cr}.

To study the change in bedforms due to grain size change, let D_{50} to increase from 0.05mm to 1mm and all other variables are constant. Figure (12) describes the bedform change if D_{50} is increased from 0.05mm to 1mm with constant Q = 7.56m^3/sec, B = 21.49m, Y = 0.47m , S = 134.5, and temp = 24°C. For fine sands bedform changes from flat bed without sediment motion to ripples if the D_{50} increased from 0.05mm to 0.1mm. As the bed material becomes coarser the bed will change from ripples to dunes. Figure (12) also shows that the change in D_{50} affects the sediment parameter (D_*) more than the stage parameter (T). As the grain size (D_{50}) changes from 0.1 to 1, D_* changes from 2.65 to 26.5 and T changes from 0.26 to 0.65 with little increase in between. Thus, D_* is predominant factor in developing different bedforms when grain size changes and Q , B , Y , S , and temperature are constant.

CHANGE OF BEDFORMS WITH WATER DISCHARGE

Different bedforms are predicted when the water discharge (Q) changes in alluvial channels.

Increasing water discharge (Q) will increase the flow velocity when the cross-sectional area is constant. In Rijn's approach increasing Q will not affect the particle parameter (D_*) when the grain size and temperature are constant, $D_* = \phi$ (D_{50}, ν, g, and S). But the discharge increase will increase Vanoni parameters, $U/\sqrt{gK_s}S$, and $U^3/g\nu S$. As the second parameter will increase more rapidly than the first one, the ratio of U/U'_*, will increase. Because of the increase of U/U'_* the transport stage parameter (T) will increase. Figure (13) shows different bedforms due to increasing the water discharge and keeping B_1, Y, D_{50}, slope and temperature to be constant. It is apparent that the change in Q changes the transport stage parameter without changing the particle parameter (D_*). for this sample of calculations the bedform is sensitive to the discharge increase. The bedforms are ripples for $Q \leq 8m^3$/sec, dunes for $9 \leq Q \leq 19m^3$/sec transition for $20 \leq Q \leq 26$, and finally the upper flow regime for $Q \geq 27m^3$/sec.

CHANGE OF BEDFORMS WITH BEDSLOPE

The slope of bed is one of the parameters that affects the type of bedforms in alluvial channels.

In order to analyze the effect of increasing the Slope (S) on the type of bedforms, a sample. Q , B , Y , D_{so} and temperature are constant and equal to 7.56m^3/sec, 21.49m, 0.47m, and 24°C, respectively will be examined. Figure (14) represents the change of bedforms with bed slope (S), according to Van Rijn. The results of this prediction is unrealistic. As the slope increases from 10 cm/km to 20 cm/km the bedform changes from the upper regime to the transition zone and from 100 cm/km to 120cm/km the bedform changes from dunes to ripples. For further slope increase, the predicted bedform is flat bed. Generally, increasing the bed slope will increase the stream power, mean velocity, shear velocity, and Froude number. Therefore the bedforms begin to develop towards the upper regime zone, and successive process with slope increase is changing the bedform from ripples to dunes, dunes to transition and then to antidunes. To analyze the non-significant bedform prediction the main parameters that classify the bedforms according to Van Rijn must be studied if the bed slope changes. The first parameter (D_{so}) is independent of slope and it is constant with slope increase. The second parameter (T) depends on the shear velocity, U'_*, and U_{*cr}. Thus the U'_* will be the main parameter in this case. U'_* is obtained from Fig. (9). If the slope is increased, Vanoni parameters U^3/gv_s, and $U/\sqrt{gK_sS}$, as shown in Fig. (9) will decrease, and consequently, the ratio U/U'_*. As the discharge and the cross section are constant, the average velocity (U) will be constant, U'_* will decrease if the slope is increased and consequently the transport stage parameter (T), $T = (U'_*)^2/U_{*cr})^2 - (U_{*cr})^2/(U_{*cr})^2$. In summary, if the bed slope is increased the U/U'_* ratio will decrease as well as the transport stage parameter (T). The decrease in T with D_* constant will develop bedforms from the upper regime to the lower regime. So in this case, increasing the bed slope, the combination between Vanoni and Rijn's parameters gives unrealistic prediction of bedforms.

VERIFICATION OF SIMONS AND RICHARDSON AND VAN RIJN APPROACHES

Data (1) and (7) from stable alluvial channels in U.S.A., Pakistan and Egypt were used to verify Simons and Richardson and Rijn approaches.

The discharge of the whole data varies from 0.04m^3/sec to 335.7m^3/sec, slope varies from 0.646cm/km to 370 cm/km, the grain size varies from 0.084mm to 0.6mm and bedforms from flat bed to antidunes. A summary of these ranges is given in Table (1).

TABLE 1. DATA RANGE

	Discharge m^3/sec	Slope cm/km	Grain Size mm	Bedform
Min.	000.04	0.646	0.065	Flat-bed
Max.	335.70	370.000	0.600	Antidunes

Simons and Richardson approach correctly predicts 16 points out of 25, where Rijn's approaches predict point out of the same 25 points. Fig (15) shows the results of this prediction compared to the actual bedforms.

SUMMARY AND CONCLUSIONS

Simons and Richardson divided the flow in sand bed channels into two regimes with a transition zone between them.

The first is the lower flow regime which develops with the beginning of motion. The resistance to flow is large and sediment transport is small. The bedform is either ripples, dunes or some combination of them. The resistance to flow is caused mainly due to form roughness.

The second is the upper flow regime where the resistance to flow is relatively small and sediment transport is large. The usual bedforms are plane or antidune. The transition zone occurs during the passage from lower regime to upper regime.

Simons and Richardson predicted the type of bedforms using stream power ($\tau_o V$) and grain size parameter, as shown in Fig. (1). Computer program, is designed to predict the bedform according to Simons an Richardson's approach. Data from U.S.A., Pakistan, and Egypt are used to verify that approach, where 16 points out of 25 are correctly predicted.

For the data the discharge varies from $0.04 m^3/sec$ to $335.7 m^3/sec$, slope varies from 0.646 cm/km to 370 cm/km, the grain size varies from 0.065mm to 0.6mm and bedforms from flat bed to antidunes.

Van Rijn's approach that predicts the bedforms and their dimensions in the lower flow regime. The Rijn's classification of bedforms is based on the particle parameter (D_*), $D_* = D50 \left((S-1)g/\nu^2\right)^{-0.333}$, Stage parameter (T), $T = (U'_*)^2/U_{*cr})^2 - (U_{*cr})^2/(U_{*cr})^2$.

Computer program, is constructed to define the bedforms according to Van Rijn. Using the computer program data from U.S.A., Egypt and Pakistan are used in verifying this approach. Eleven points out of twenty five are correctly predicted. The bedforms will be developed towards the upper regime due to increasing water discharge, temperature, and grain size.

The results of bedforms prediction due to the increase of bed slope gives unrealistic results as the bedforms changes from upper regime to lower regime.

Fig. (15) is a comparison of predicting bedforms between Simons and Richardson and Van Rijn's approach. Finally, further effort is required to give a definite classification of bedforms in different flow regimes.

APPENDIX 1. - REFERENCES

1. Saleh, M.M., "Design of Stable Alluvial Channels," M. Sc., Cairo University 1984, pp. 33-36.

2. Simons, D. B., and Richardson, E. V., "Resistance to Flow in Alluvial Channels," U.S. Geological Survey Professional Paper 422-J.

3. Simons, D. B., and Senturk, K. F., "Sediment Transport Technology," 1976, Water Resources Publications, U.S.A., pp. 215-277.

4. Van Rijn, L.C., "Sediment Transport, Part I: Bed-load Transport," Journal of Hydraulic Engineering, ASCE, Vol. 110, No. 10, 1984, pp 1431-1456.

5. Van Rijn, L. C., "Sediment Transport Part II: Suspended Load Transport," Journal of Hydraulic Engineering, ASCE, Vol. 110, No. 11, 1984, pp 1613-1641.

6. Van Rijn, L. C., "Sediment Transport, Part III: Bedforms and Alluvial Roughness," Journal of Hydraulic Engineering, ASCE, Vol. 110, No. 12, 1984, pp 1733-1742.

7. William Brownlie, R., "Compilation of Alluvial Channel Data: Laboratory and Field," California Institute of Technology, Pasadena, California, November 1981, Report No. KH-R-43B, pp 47, 53, 84, 168 and 192.

APPENDIX II. - NOTATIONS

The following symbols are used in this paper:

D_{50} = particle diameter where 50% of the mixture is finer (L);

d = depth (L);

K_s = equivalent roughness (L);

S = energy gradient;

S_o = specific *density*

T = transport stage parameter;

U = mean flow velocity (LT^{-1});

U_{*cr} = critical bed-shear velocity for initiation of motion (LT^{-1});

Z = side slope in trapezoidal channels;

μ = dynamic viscosity coefficient ($ML^{-1}T^{-1}$); and

ν = kinematic viscosity coefficient (L^2T^{-1}).

APPENDIX III : figures

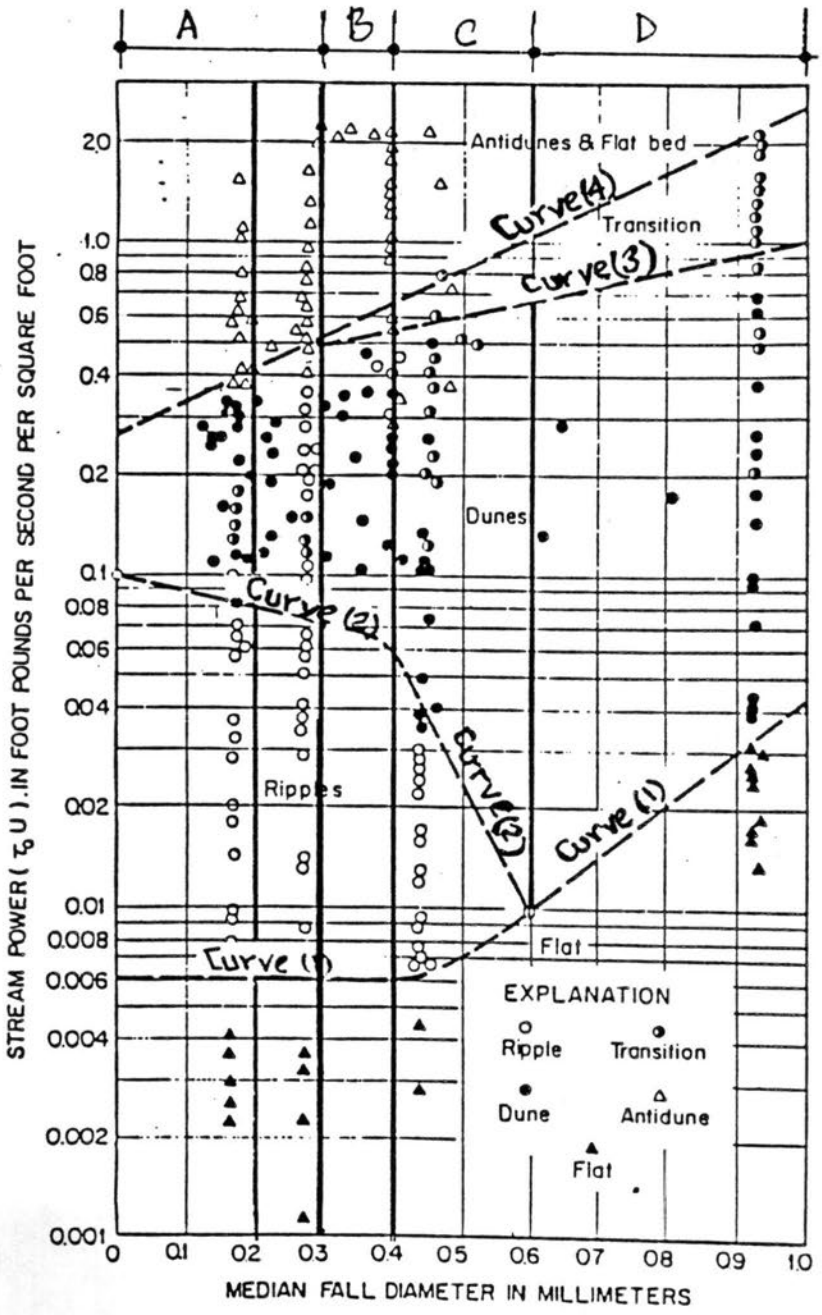

Figure (1) Relation of bedform to stream power and median fall diameter of bed sediment (after Simons and Richardson, 1966).

Fig.(2) Flow Chart to Predict Bedforms using Simons and Richardson Approach

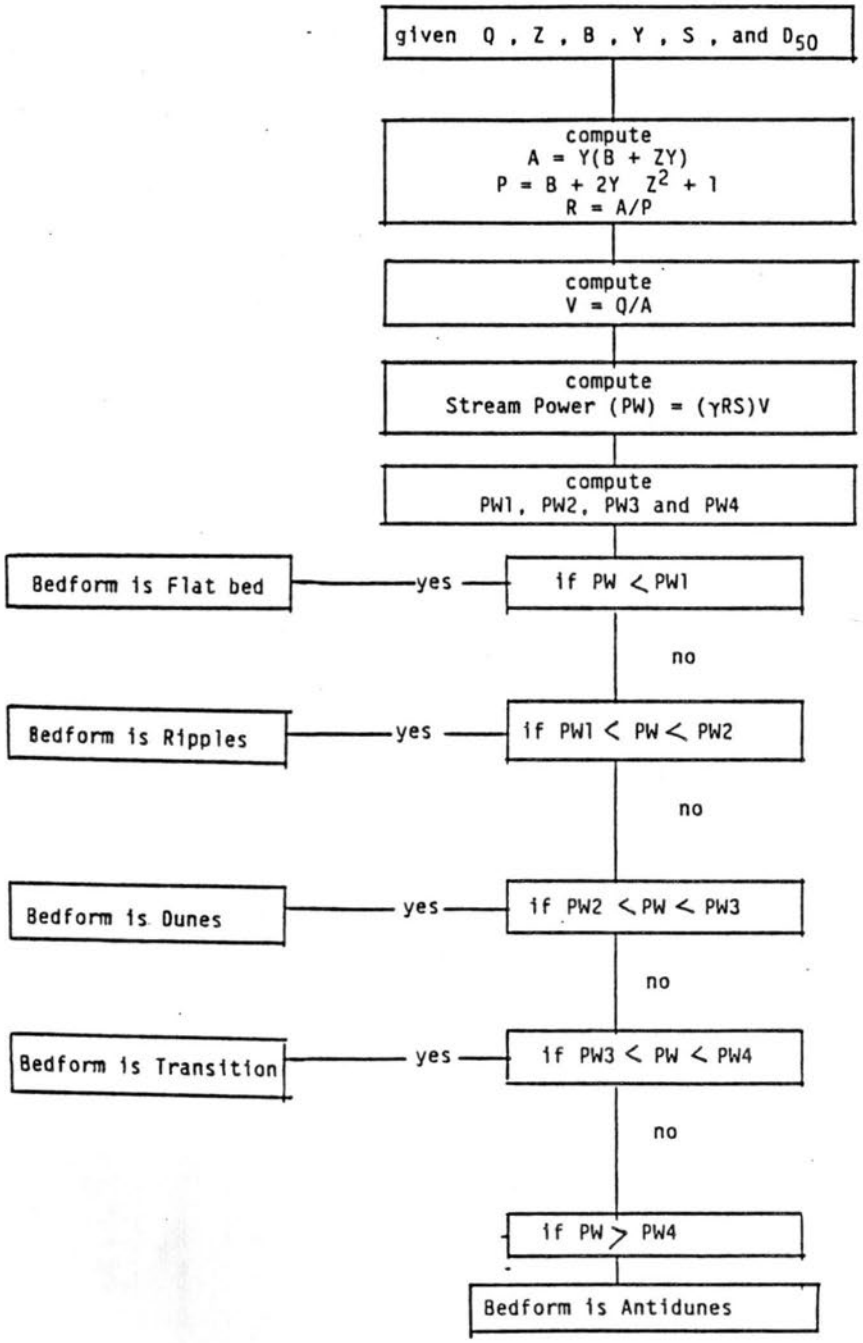

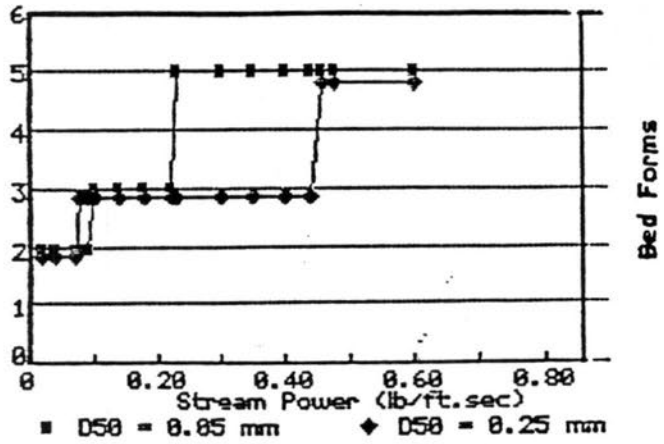

Fig(3) : Change of Bed Forms with Stream Power for D50 = 0.05 & 0.25 mm

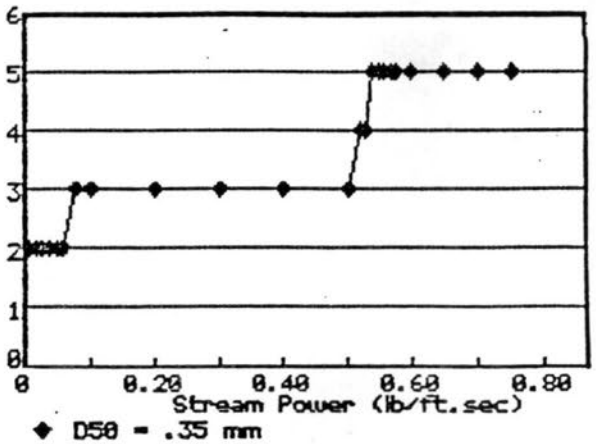

Fig(4) : Change of Bed Forms with Stream Power for D50 = 0.35 mm

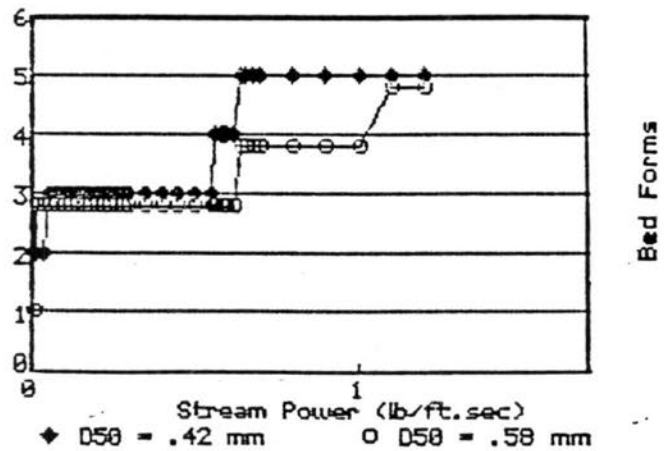

ig(5) : Change of Bed Forms with Stream. ower for D50 = 0.42 & 0.58 mm

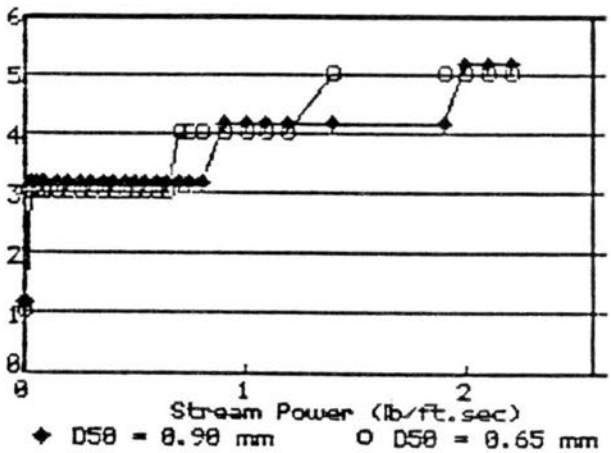

Fig(6) : Change of Bed Forms with Stream Power for D50 = 0.65 & 0.90 mm

Bed Forms

1 ..... Flat Bed
2 ..... Ripples
3 ..... Dunes
4 ..... Transition
5 ..... Antidunes

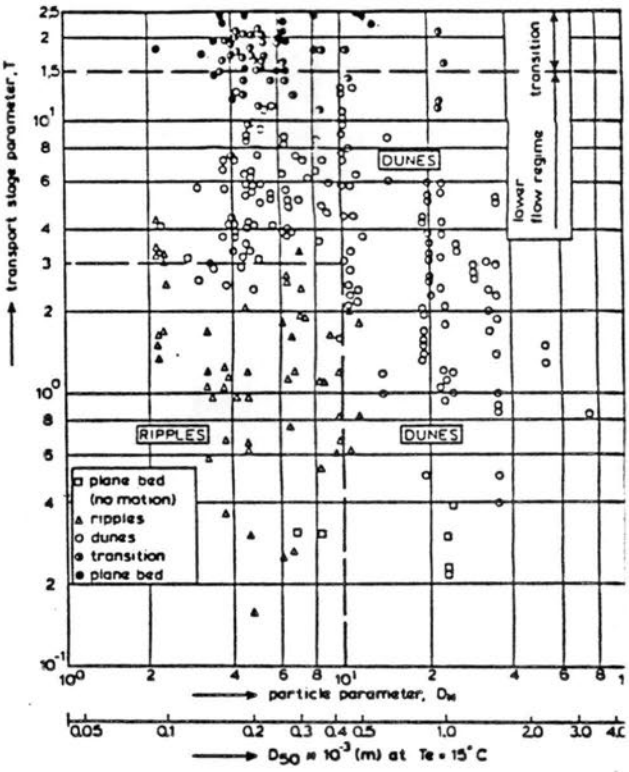

ure(7): Diagram for bed form classification in lower transitional flow regime (Van Rijn, 1984)

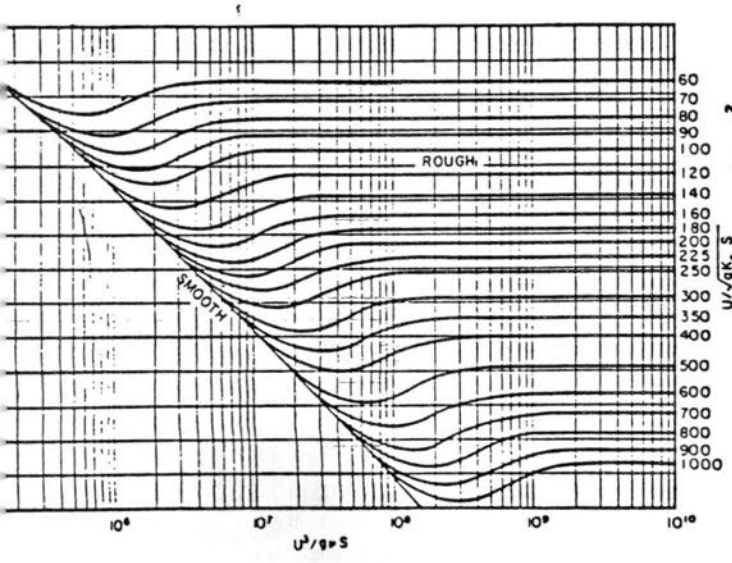

qure(9): Determination of bed shear ity (U'_*) according to Vanoni & Brooks

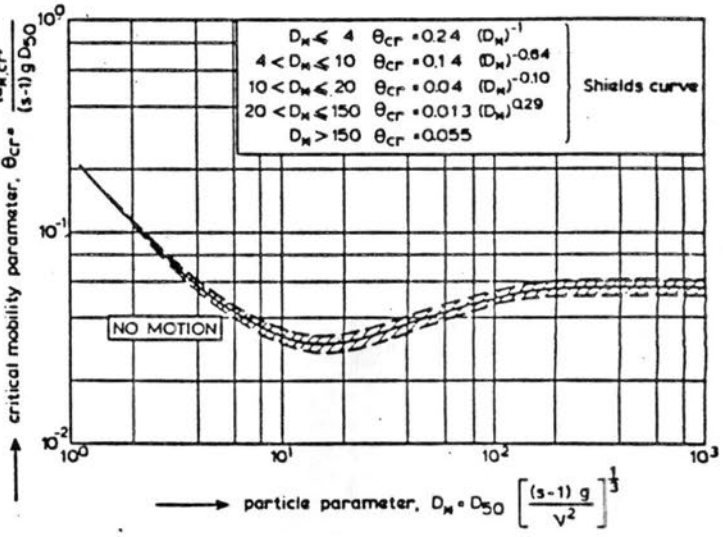

Figure(8): Initiation of motion according to Shie

121

Fig. (10) Flowchart for Van Rijn's Approach of Predicting Bedforms

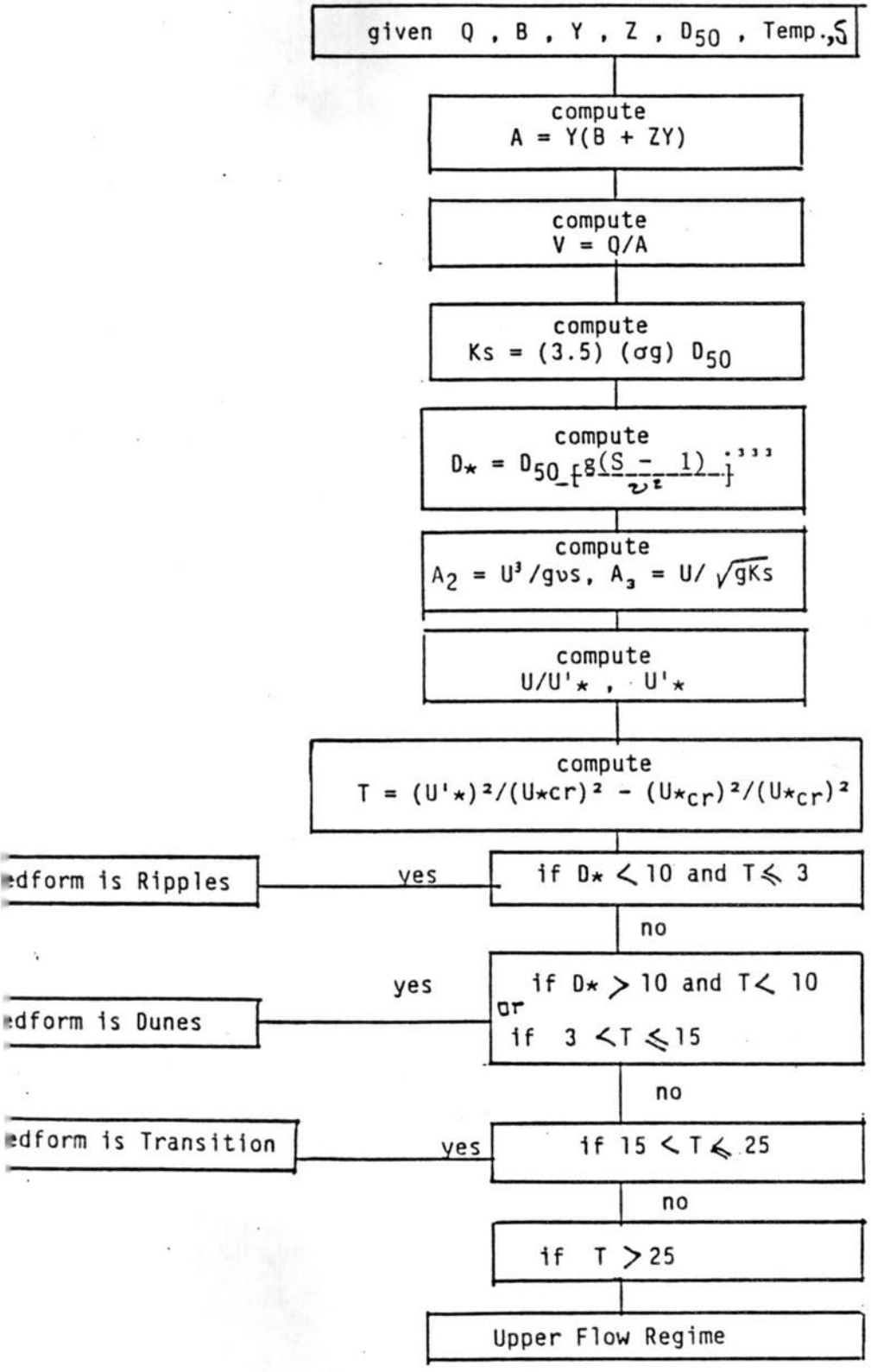

Fig(11): Change of Bed Forms&Temp.

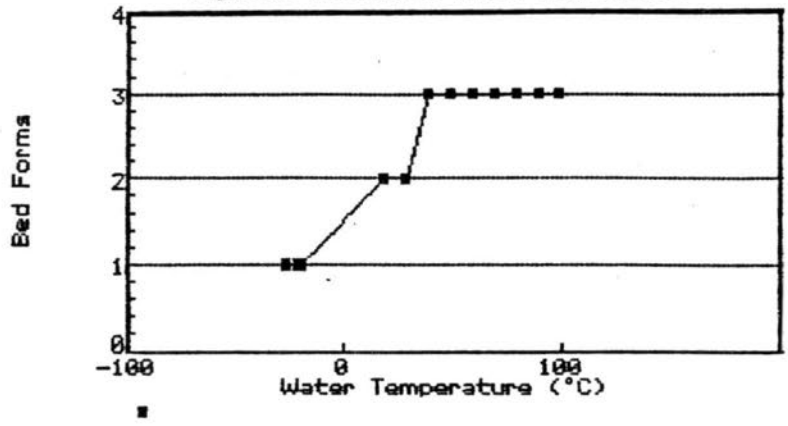

Bed Forms
---

1 ..... Flat Bed
2 ..... Ripples
3 ..... Dunes
4 ..... Transition
5 ..... Antidunes

Fig(12): Change of Bed Forms&D50

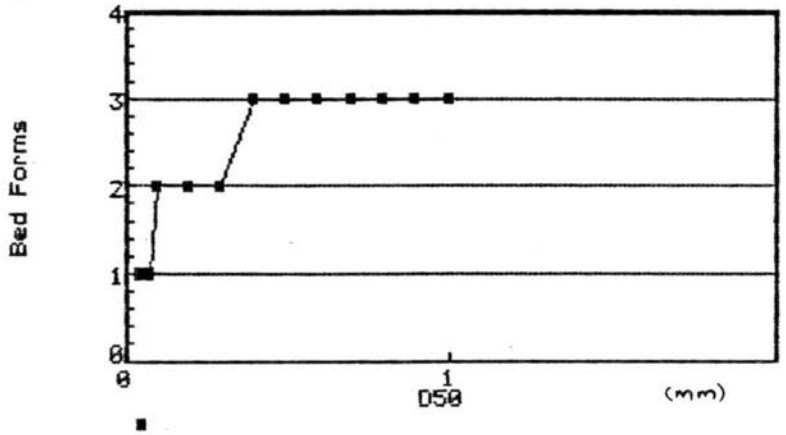

Bed Forms
---

1 ..... Flat Bed
2 ..... Ripples
3 ..... Dunes
4 ..... Transition
5 ..... Antidunes

Fig(13): Change of Bed Forms & Q

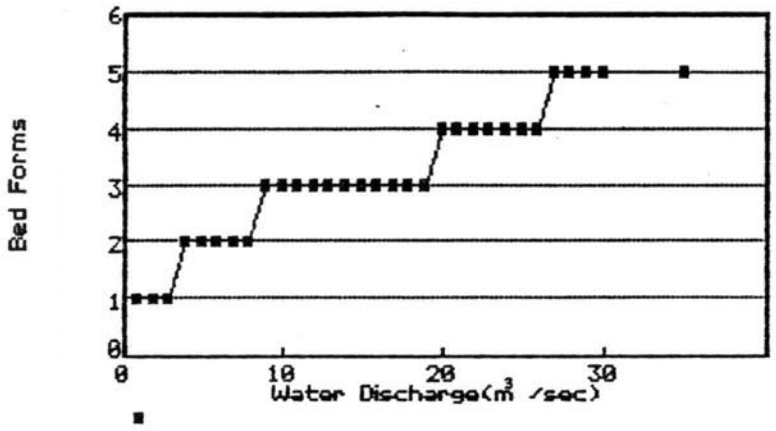

Bed Forms
---
1 ..... Flat Bed
2 ..... Ripples
3 ..... Dunes
4 ..... Transition
5 ..... Antidunes

Fig(14): Change of Bed Forms & Slope

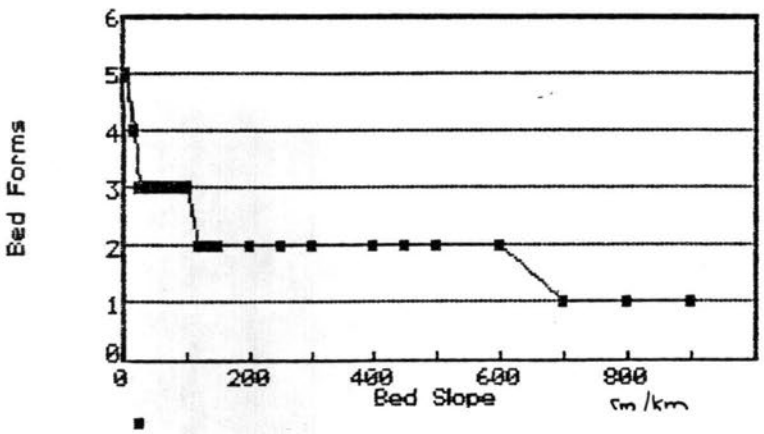

Bed Forms
---
1 ..... Flat Bed
2 ..... Ripples
3 ..... Dunes
4 ..... Transition
5 ..... Antidunes

Fig(15): Comparison between Simons&Rijns

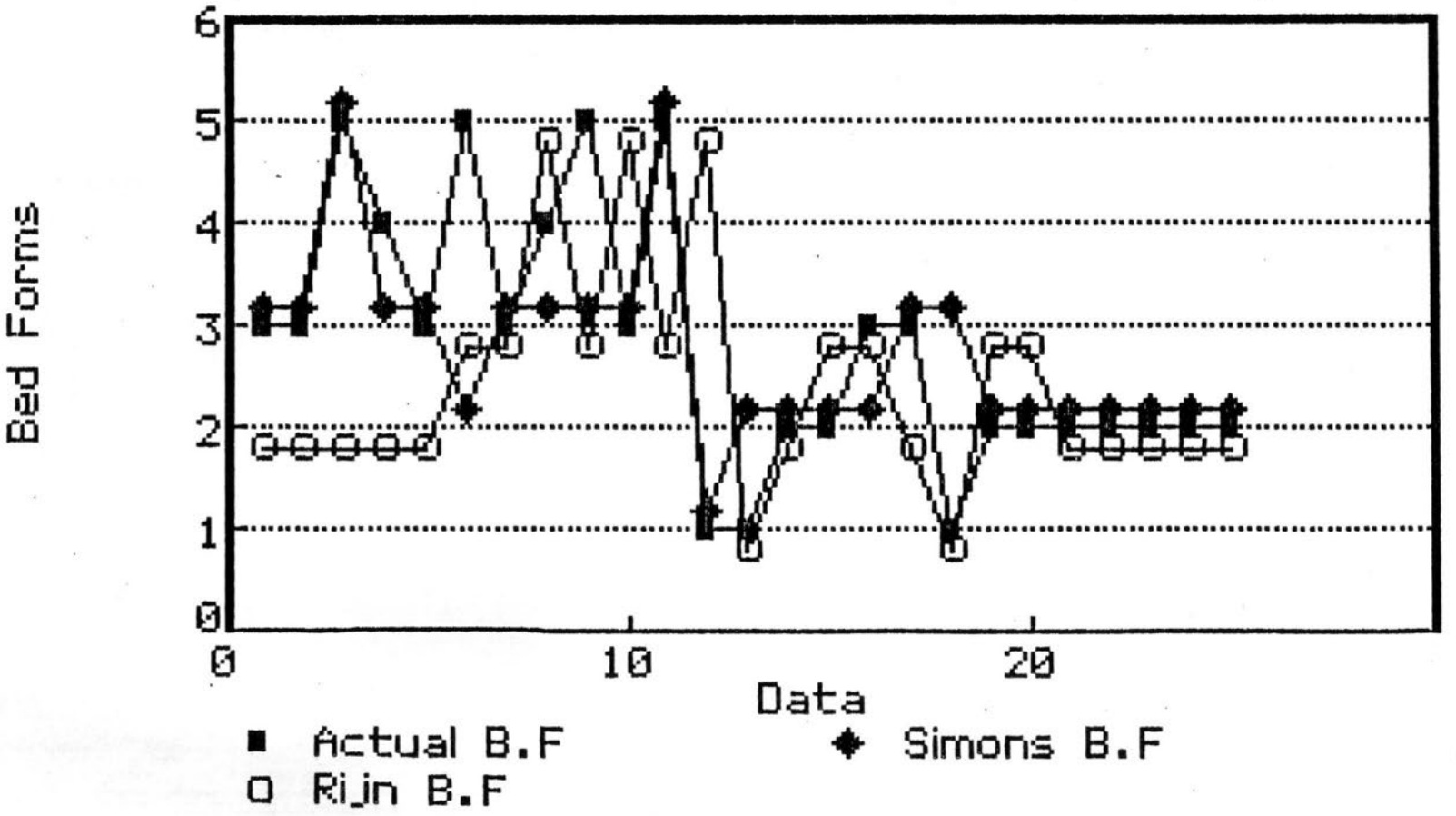

CONSIDERATIONS IN THE SELECTION OF TRANSPORT EQUATIONS IN SEDIMENT MODELING

By
David T. Williams[1], M. ASCE

ABSTRACT: The selection of an appropriate sediment transport relationship is very important in modeling a river's response to existing and project conditions. A sediment transport selection procedure based upon sediment and hydraulic characteristics of the system is presented. For hypothetical river conditions, four sediment transport methods, Ackers and White, Shen and Hung, Toffaleti, and Yang, is analyzed. Each method's data range used in its development is compared to the hypothetical conditions and areas of applicability are identified. The hypothetical river conditions had a flow depth ranging from 0.5 to 20 feet, a constant slope of 0.0005, and a Manning's "n" of 0.02 resulting in a unit water discharge ranging from 0.52 to 244.8 cfs/ft and flow velocities ranging from 1.05 to 12.24 ft/sec. The sediment sizes analyzed were from 0.0625 to 2.0mm. For these conditions, the Ackers and White method works well for medium sands and depths less than five feet, and Shen and Hung's method is satisfactory for medium sands also, but only for depths less than two feet. Toffaleti's method is useful for medium sands for a wide range of depths while Yang's method is applicable for medium sands at depths less than 10 feet.

INTRODUCTION

Presently, there are numerous sediment transport relationships developed under various river and flume conditions. In fact, Alonso (2) identified 14 bedload formulas and 17 total bed material load formulas that have been used to some extent. There are many more that have not attained prominence and more formulas will continue to be developed.

The sediment modeler is often confronted with the problem of which transport function to use for the river problem at hand. This paper presents a selection procedure and the analysis of four transport functions subjected to hypothetical hydraulic and sediment conditions. The analyses of the four total bed material transport functions are intended to be examples of the thought processes necessary to select the appropriate transport function for the river investigated. These thought processes can be applied to other transport functions as well.

SELECTION PROCEDURE

Sediment transport rates depend on such variables as particle size and gradation, stream dimensions and configuration, amount of washload, bedforms, turbulent intensity, and bed armoring. The macroscale variables such as differing hydrology, geology, and climate also affect the transport rate. Because of the large range and number of influencing variables, it is not possible to select a sediment transport function that satisfactorily encompasses all the stream conditions that the sediment engineer would encounter. However, a stream may be conducive to analysis using certain transport functions if the selection of these functions is performed under a systematic selection procedure and the limitations are fully understood.

---

1 Research Hydraulic Engineer, Hydraulics Laboratory, USAE Waterways Experiment Station, Vicksburg, Mississippi.

The following selection procedure is suggested by Shen (12).

If field data is available:

1. Use the modified Einstein's method (5) to estimate the unmeasured suspended load and bedload based on measured data. There is a question of whether Einstein's intensity of bedload transport should be arbitrarily divided by a factor of two.

2. Separate bed material load from washload and analyze them separately.

3. Decide which available sediment transport equations best agree with the measured data and use it to estimate the sediment transport load for the design flow, where actual measurement is not available.

When no measured data are available:

1. Use Einstein's (6) procedure if bedload is a significant portion of the total bed material load. Otherwise see 4 below.

2. Use Colby's (4) method for rivers with flow depth less than or about 10 feet: also see 4 below.

3. Use Toffaleti's (15) method for large rivers.

4. Use Shen and Hung (13) method for flume data and small rivers.

Yang (16) makes these further suggestions for no measurement data:

1. Use Meyer-Peter and Muller's (10) formula when the bed material is coarser than 5mm.

2. Use Yang's (18) sand formula for sand bed laboratory flumes and natural rivers with washload excluded. Use Yang's (17) gravel formula for gravel transportation when the bed material is between 2 and 10mm.

3. Use Ackers and White (1), or Engelund and Hansen's (7) equation for subcritical flow condition in the lower flow regime.

4. Use Laursen's (9) formula for laboratory flumes and shallow rivers with fine sand or coarse silt.

5. A regime or regression equation can be applied to a river only if the flow and sediment conditions are similar to that from which the equation was derived.

The above procedure and recommendations are useful but no guidance is given on what criteria must be satisfied to decide which transport equation best agrees with the data. Also, the range of conditions to be analyzed is

often larger than the transport equation's range of data conditions. This does not necessarily preclude the use of the function but no guidance is given to evaluate the confidence in these transport functions if applied beyond their data range with no field data for verification. The following analysis addresses these problems.

DESCRIPTION OF TOTAL BED MATERIAL TRANSPORT FUNCTIONS

Ackers and White (1) based their analysis on the concept of stream power as proposed by Bagnold (3). They applied dimensionless analysis techniques in terms of dimensionless groups: size, mobility, and transport. The hypothesis is that the efficiency of the transport process is dependent on the grain mobility. This mobility is a function of the grain size and hydraulic parameters and is

$$F_{gr} = \frac{U_*^n}{\sqrt{gd(s-1)}} \left[\frac{V}{\sqrt{32} \log \left(\frac{\alpha D}{d}\right)} \right]^{1-n}$$

in which U_* is the shear velocity, s is the specific gravity of the sediment particle, g is the gravitational acceleration, V is the average flow velocity, n is the transient exponent depending on sediment size (n = 1 for fine sediment, n = 0 for coarse sediment), α is the coefficient in the rough turbulent equation, D is the flow depth, and d is the sediment particle size. A dimensionless grain size is also introduced as

$$d_{gr} = d \left[\frac{g(s-1)}{\nu^2} \right]^{1/3}$$

where ν is the kinematic viscosity. Then the dimensionless sediment transport equation which is a function of d_{gr} and F_{gr} is

$$G_{gr} = \frac{XD}{sd} \left(\frac{U_*}{V} \right)^n$$

where X is the sediment transport rate expressed as a concentration by weight. The coefficients were determined using flume data having depths less than 0.4m and sediment particle size greater than 0.04mm.

Shen and Hung (13) recommended the use of a regression formula based upon 587 sets of laboratory and field data. This was done in lieu of determining a dominate parameter, such as stream power or shear stress, which dominates sediment transport. The assumption was that the total concentration, C_t, is related by

$$\log C_t = a_0 + a_1 X + a_2 X^2 + a_3 X^3$$

where

$$X = V^{a4} S^{a5} W^{a6} D^{a7}$$

The variables a_0 through a_7 are parameters determined by regression, S is the energy slope, and W is the bed material particle fall velocity. The final result was

$$\log C_t = -107404.45938164 + 324214.747734085X - 326309.58908739X^2 + 109503.87232539X^3$$

in which

$$X = \left(\frac{VS^{0.57}}{W^{0.32}} \right)^{0.00750189}$$

Because the water depth range of the data was from 0.07 to 2.8 feet, the depth term varied little in the regression and was dropped from the final equation. The d_{50} of the bed material varied from 0.13mm to 1.3mm. Note that the dominating variables of the X parameters are flow velocity and slope of which their product is a form of stream power.

Toffaleti (18) based his procedure for sediment transport determination on concepts developed by Einstein (6). The actual stream is approximated by a two-dimensional stream having a width, b, and hydraulic radius, r. The hydraulic radius is divided into four zones comprising of a bed zone and lower, middle, and upper zone. Using an empirical relationship, an equivalent form of Einstein's Φ_* versus Ψ_* relationship (6), the suspended load discharge at the lower bound of the lower zone is determined and its associated concentration is used as the concentration of the bed zone. The concentrations of the lower, middle, and upper zones are given by power relationships similar to that proposed by Rouse (11). The concentrations, in conjunction with a power relation velocity profile are integrated over each zone to obtain the total bed material discharge. Toffaleti based his formula on seven rivers and flume data. The rivers had depths ranging from 1 foot to over 50 feet and bed material ranging from fine to medium sand. The flume ranged in width from 10.5 inches to 8 feet, the flow depth from 2 inches to 2 feet, and bed material size from 0.3mm to 0.93mm.

Yang (18) suggested that the total sediment concentration is related to potential energy dissipation per unit weight of water, i.e., the unit stream power, which can be expressed as the product of the velocity and slope. Although this concept is expanded to gravels by Yang (17), only the expression for sands is presented here. The dimensionless unit stream power equation is

$$\log C_t = 5.435 - 0.286 \log \frac{Wd}{\nu} - 0.457 \log \frac{U_*}{W}$$

$$+ (1.799 - 0.409 \log \frac{Wd}{\nu} - 0.314 \log \frac{U_*}{W}) \log (\frac{VS}{W} - \frac{V_{cr}S}{W})$$

in which the dimensionless critical velocity, V_{cr}/W, at incipient motion, can be expressed as:

$$\frac{V_{cr}}{W} = \frac{2.5}{\left[\log\left(\frac{U_* d}{\nu}\right) - 0.06\right]} + 0.66; \qquad \text{for} \quad 1.2 < \frac{U_* d}{\nu} < 70$$

and

$$\frac{V_{cr}}{W} = 2.05; \qquad \text{for} \quad 70 \leq \frac{U_* d}{\nu}$$

C_t is the total sediment concentration in parts per million by weight, V_{cr} is the average flow velocity at incipient motion, VS is the unit stream power, and VS/W is the dimensionless unit stream power. Regression methods were used to obtain the coefficients and were based upon field and flume data. These data had ranges of 0.137 to 1.71mm for particle size, and 0.037 to 49.9 feet for water depth. The majority of the data was in the 0.25 to 0.8mm range and water depths less than 3 feet.

HYPOTHETICAL CONDITIONS

A hypothetical wide river was proposed having a water depth range of 0.5 to 20 feet, sediment sizes to be transport of 0.0625mm to 2mm, and with a 0.0005 slope. The water temperature was 70° F and the specific gravity of the sediment was 2.65. For simplicity, the Manning's roughness "n" was 0.02 and assumed to be constant for all conditions. The applications of the transport functions were performed assuming each size analyzed represented a uniform bed of that size. The friction slope was considered to be the same as the bed slope for all conditions. Sediment discharge is expressed as tons per day per unit width (q_s).

In order to evaluate the range of the above data, it is helpful to categorize them into three dimensionless parameters:

Dimensionless grain size $\qquad d_{gr} = d \left[\frac{g(s-1)}{\nu^2}\right]^{1/3}$

Mobility number $$F_{gr} = \frac{U_*^2}{gd(s-1)}$$

Dimensionless flow depth $$Z = \frac{D}{d}$$

In his analysis of transport functions, Alonso (2) used these parameters plus specific gravity of the particle. The hypothetical conditions produce a range of 1.6 to 51.3 for d_{gr}, 0.0447 to 57.3 for F_{gr}, and 76.2 to 97,536 for Z as shown in Figure 1 through 3. These ranges cover the range of most sand bed rivers with sediment being transported mostly as suspended load. Since Z is greater than 70, this assures that the flow depth dominates the particle roughness thereby giving confidence in the usage of Manning's equation in determining hydraulic parameters.

For each hydraulic depth, the unit water discharge and flow velocity were calculated using Manning's equation. These results are:

Hydraulic depth, ft.	0.50	2.00	5.00	10.00	20.00
Unit Discharge, cfs/ft.	0.52	5.28	24.30	77.10	244.80
Flow Velocity, ft/sec.	1.05	2.64	4.86	7.71	12.24

For each hydraulic condition, the sediment transport potential was calculated using the four transport relationships for uniform bed particle sizes of 0.0625, 0.125, 0.25, 0.5, 1.0 and 2.0mm. The results are shown in Figures 4 through 8.

METHOD OF ANALYSIS

The function should reproduce measured data over the entire range of sediment and hydraulic conditions that may occur. Such a range of reliable data is rarely collected. It must be remembered that these measurements are made under natural or pre-project conditions and may not be applicable under proposed or modified conditions. Also, frequently the analysis of the river include extreme hypothetical events of which no data could be collected even if the rare event occurred during the data collection period. The range of sediment and hydraulic conditions that the transport functions was developed as compared to the river being studied should be compatible but if the function development range is less than the sediment and/or hydraulic range, it does not necessarily mean the function is not applicable. These functions can be extended beyond the data if the equations adequately describe the important transport mechanisms for the extended range and the minor mechanisms absorbed in the regression coefficients continue to be small compared to the dominating transport parameters in the equations.

The results of the transport function must be reasonable. This is particularly important if no data is available for comparison. This requires judgement and is not "cut and dry." For example, a function may predict

270,000 tons per day sediment transport at 1000 cfs. This may not seem unusual but calculations would show that the concentration is 100,000 ppm; unusually high for natural rivers with a relatively undisturbed watershed.

It may be pointed out that under the proposed hydraulic conditions, say for a high shear stress, a bed as fine as that used in the analysis may not be realistic and could not exist. It could be realistic under certain conditions. For instance, the sediment engineer may be required to determine the equilibrium conditions for a proposed meander cutoff through fine material. The fine bed would be subject to a higher than usual shear velocity due to the increased friction slope created by the cutoff. The sediment and hydraulic conditions would not be in equilibrium, and for proper modeling, the transport potential must be determined under these conditions. Because of these possible conditions, the entire range and possible combinations of sediment and hydraulic conditions must be analyzed.

ANALYSIS OF RESULTS

For each method, the range of the three dimensionless parameters were computed. If a given sediment size--flow depth combination fell within the range of all of these parameters, that combination was considered to be highly applicable and designated as high (H). If only two, or one of the parameters were applicable to the sediment size--flow depth combination, then they were designated as having medium (M) or low (L) applicability, respectively.

The Ackers and White relationship (1) is based on a d_{gr} range of 1 to 60. Examination of their data reveals only one data point is at $d_{gr} = 1$ and 2 points at $d_{gr} \approx 2.6$, with the next $d_{gr} \approx 4$. This makes the effective range of d_{gr} down to only 4. An F_{gr} range of 0.2 to 5.7 is calculated with the 5.7 maximum being calculated using the largest U_* and smallest sediment size within the data range given in their paper. The actual maximum would be less than this. Looking at the example calculation nomograph from their paper, F_{gr} does not exceed 1.0 which further supports the F_{gr} being lower than the maximum of 5.7.

The Ackers and White relationship is not applicable for sediment sizes less than 0.125 because it is outside the range of d_{gr} and Z. This is supported by the overestimation of transport shown in Figures 5 - 8. Depths greater than 5 feet and sediment sizes greater than 0.5mm are outside the F_{gr} and Z range and causes underestimation of the transport as seen in Figure 7 and 8. The underestimation for sediment sizes greater than 0.25mm for a depth of 0.5 feet (Figure 4) is not of great concern because all the functions show a low transport rate and an error of an order of magnitudes does not appreciably affect bed morphology. In general, the Ackers and White relationship is not applicable for very coarse or very fine sediment sizes and rivers deeper than 5 feet. A summary of the analysis is in Table 1.

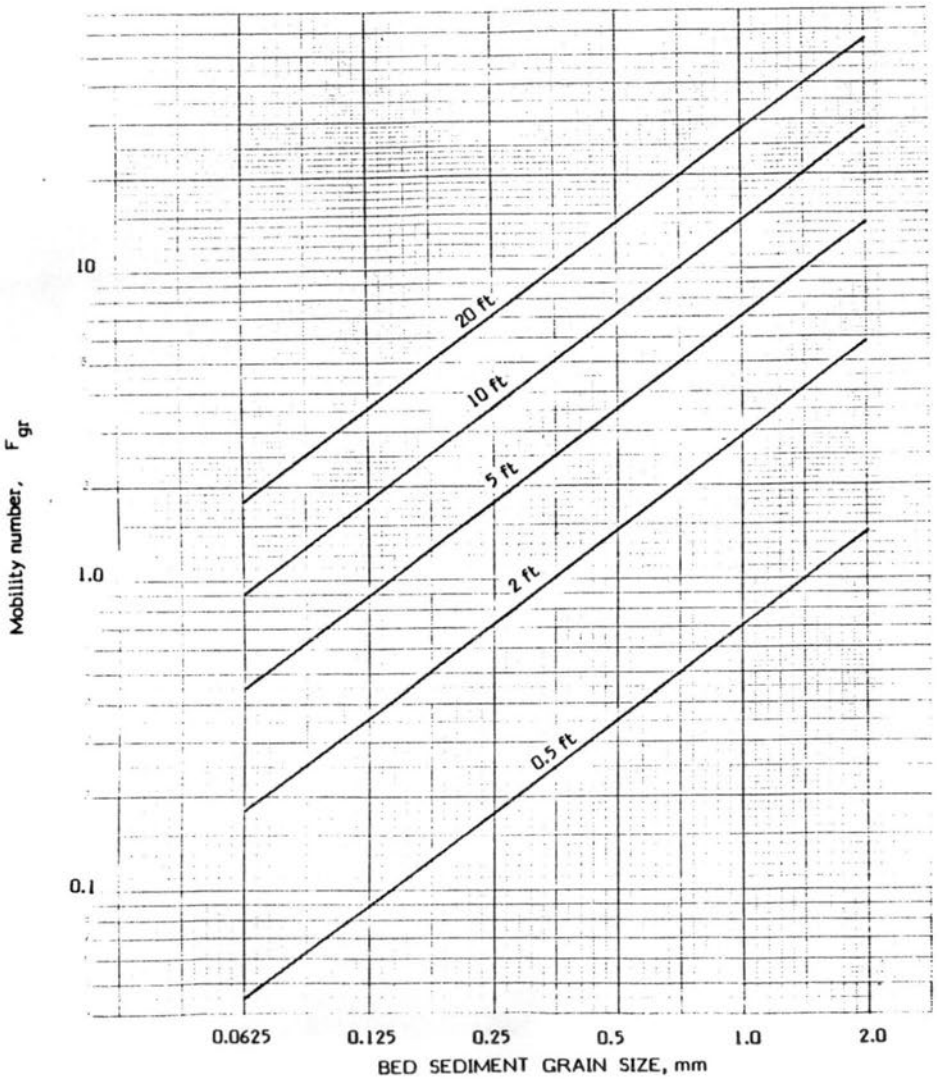

FIGURE 2. GRAIN MOBILITY NUMBER RANGE FOR HYPOTHETICAL CONDITIONS

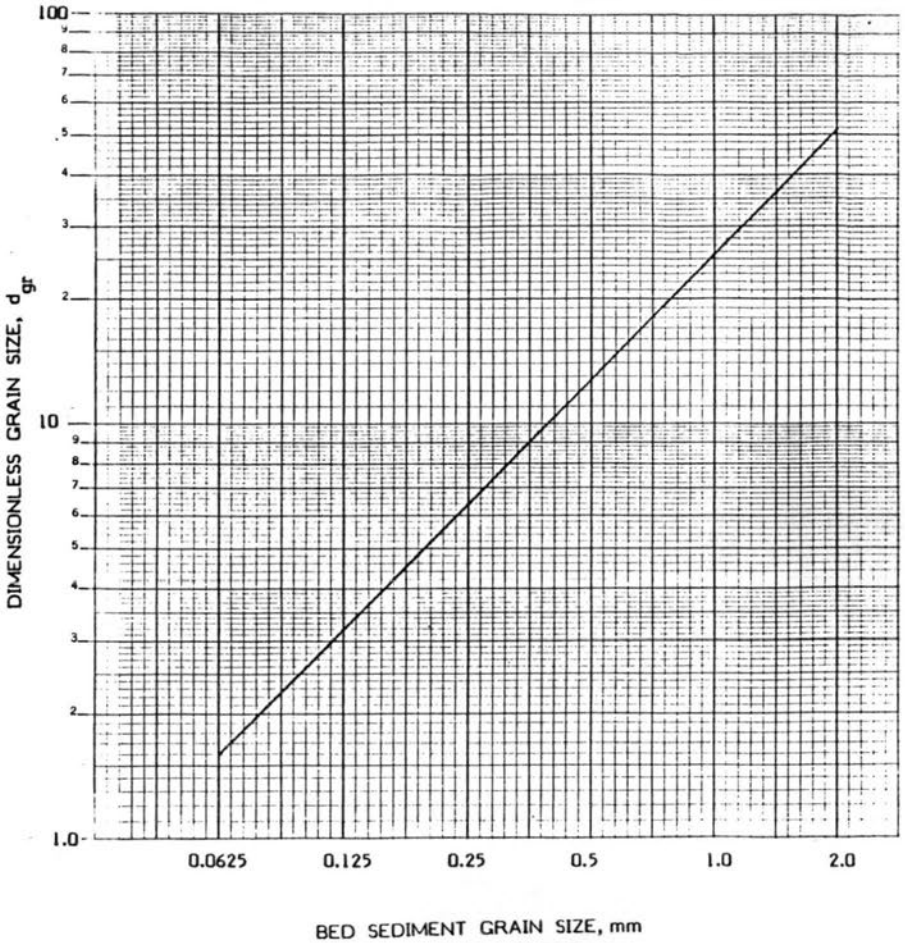

FIGURE 1. DIMENSIONLESS GRAIN SIZE RANGE FOR HYPOTHETICAL CONDITIONS.

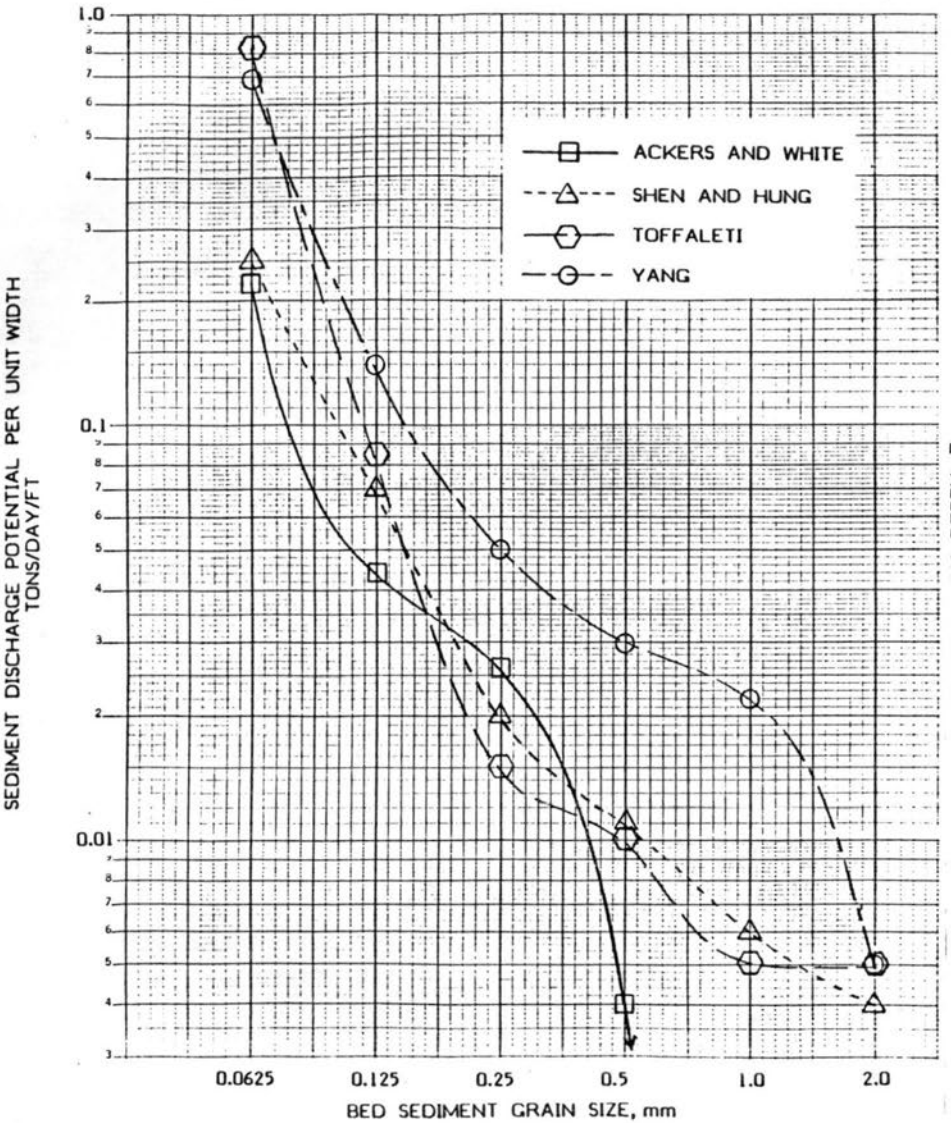

FIGURE 4. SEDIMENT TRANSPORT POTENTIAL VERSUS BED SEDIMENT GRAIN SIZE FOR 0.5 FEET HYDRAULIC DEPTH

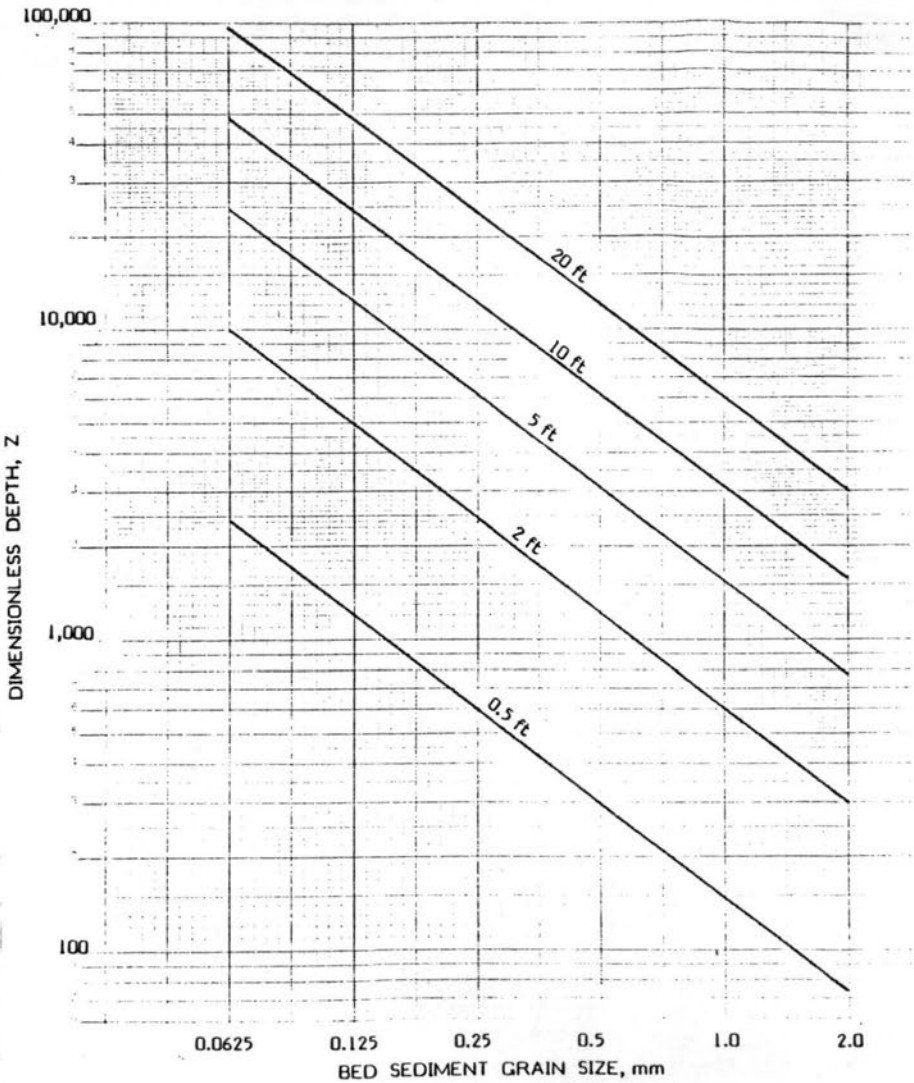

FIGURE 3. DIMENSIONLESS DEPTH RANGE FOR HYPOTHETICAL CONDITIONS

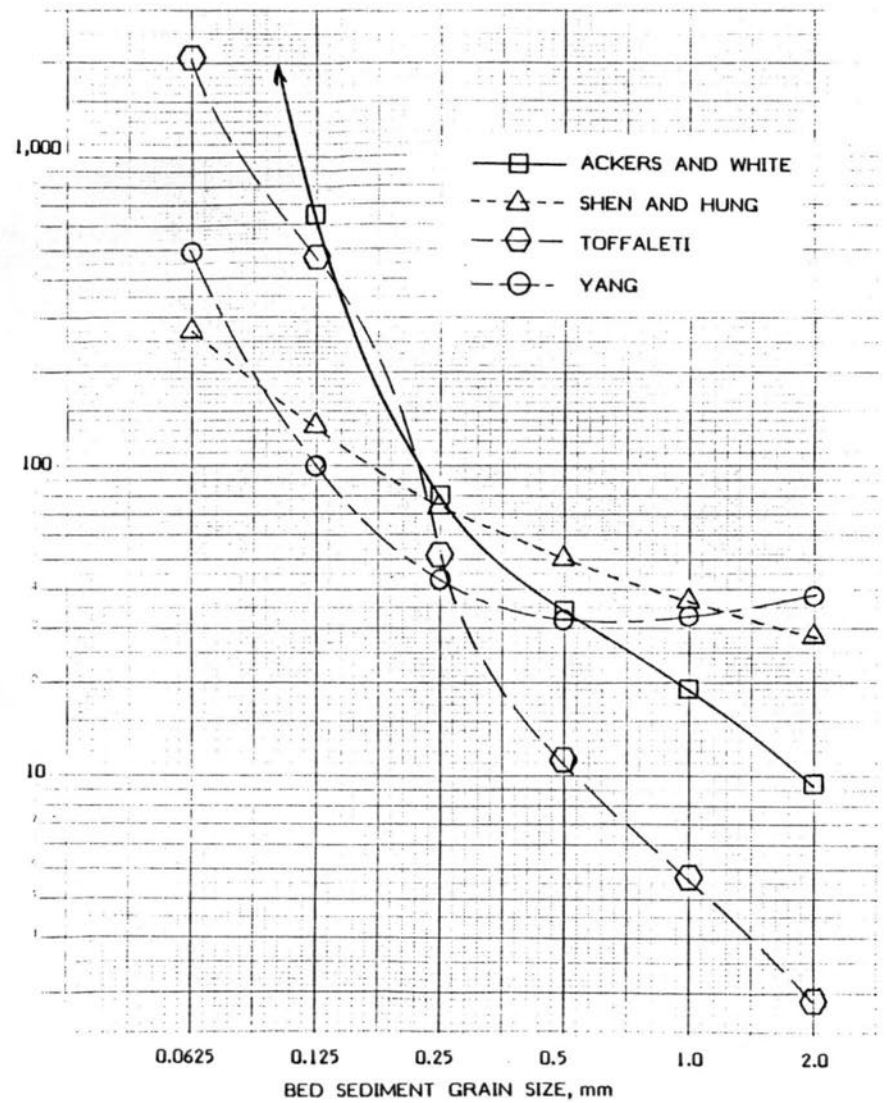

FIGURE 6. SEDIMENT TRANSPORT POTENTIAL VERSUS BED SEDIMENT GRAIN SIZE FOR 5.0 FEET HYDRAULIC DEPTH

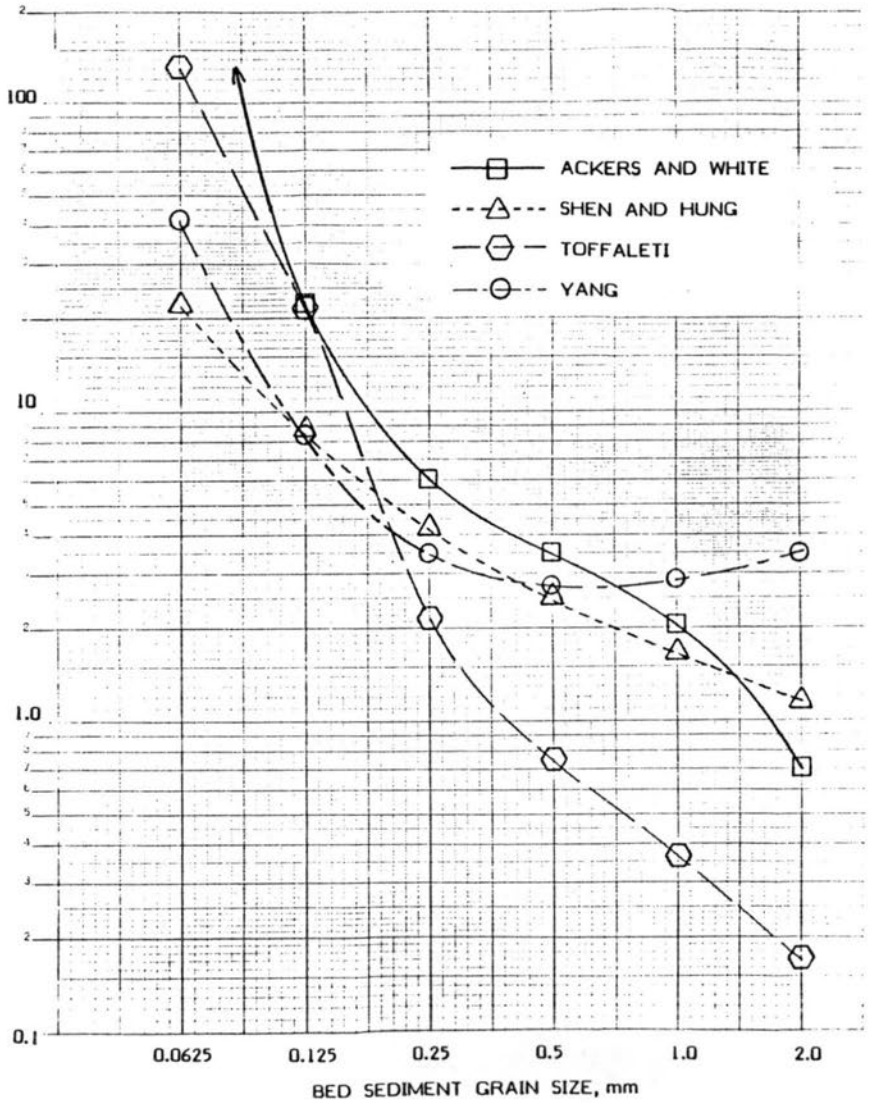

FIGURE 5. SEDIMENT TRANSPORT POTENTIAL VERSUS BED SEDIMENT GRAIN SIZE FOR 2.0 FEET HYDRAULIC DEPTH

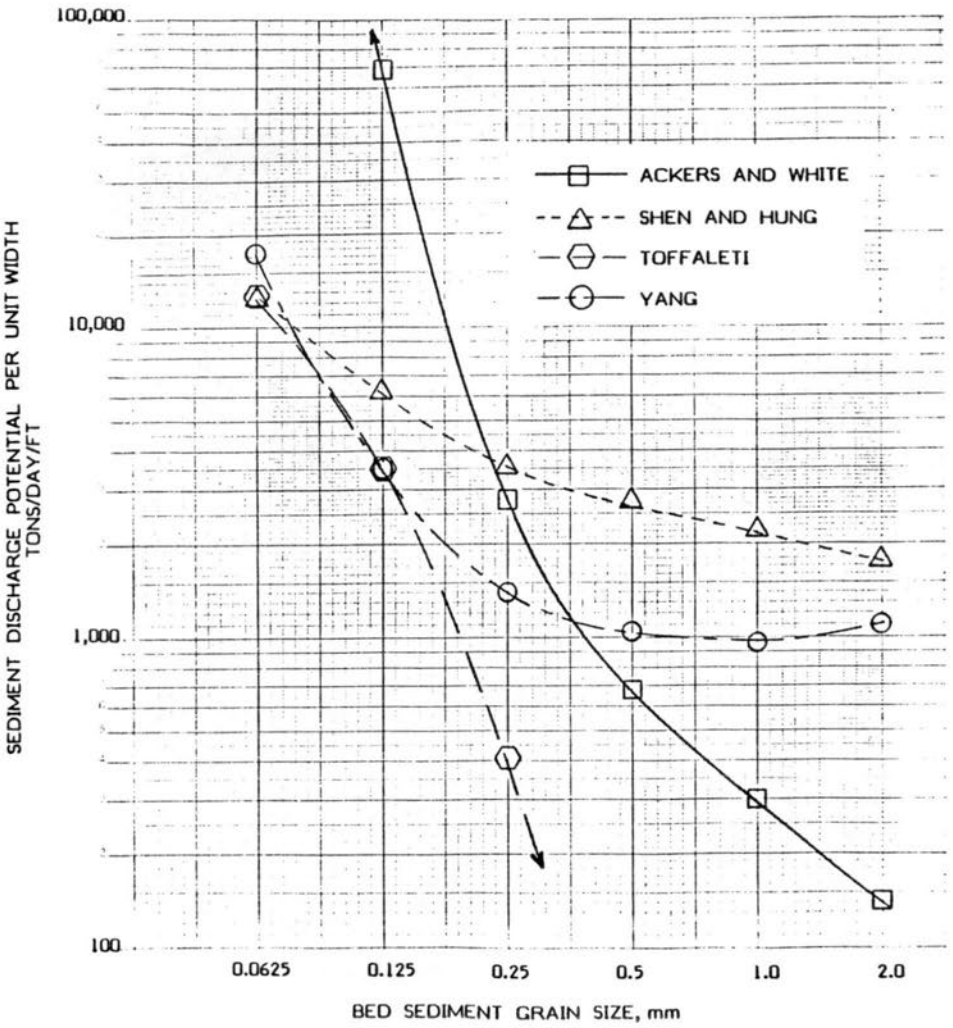

FIGURE 8. SEDIMENT TRANSPORT POTENTIAL VERSUS BED SEDIMENT GRAIN SIZE FOR 20.0 FEET HYDRAULIC DEPTH

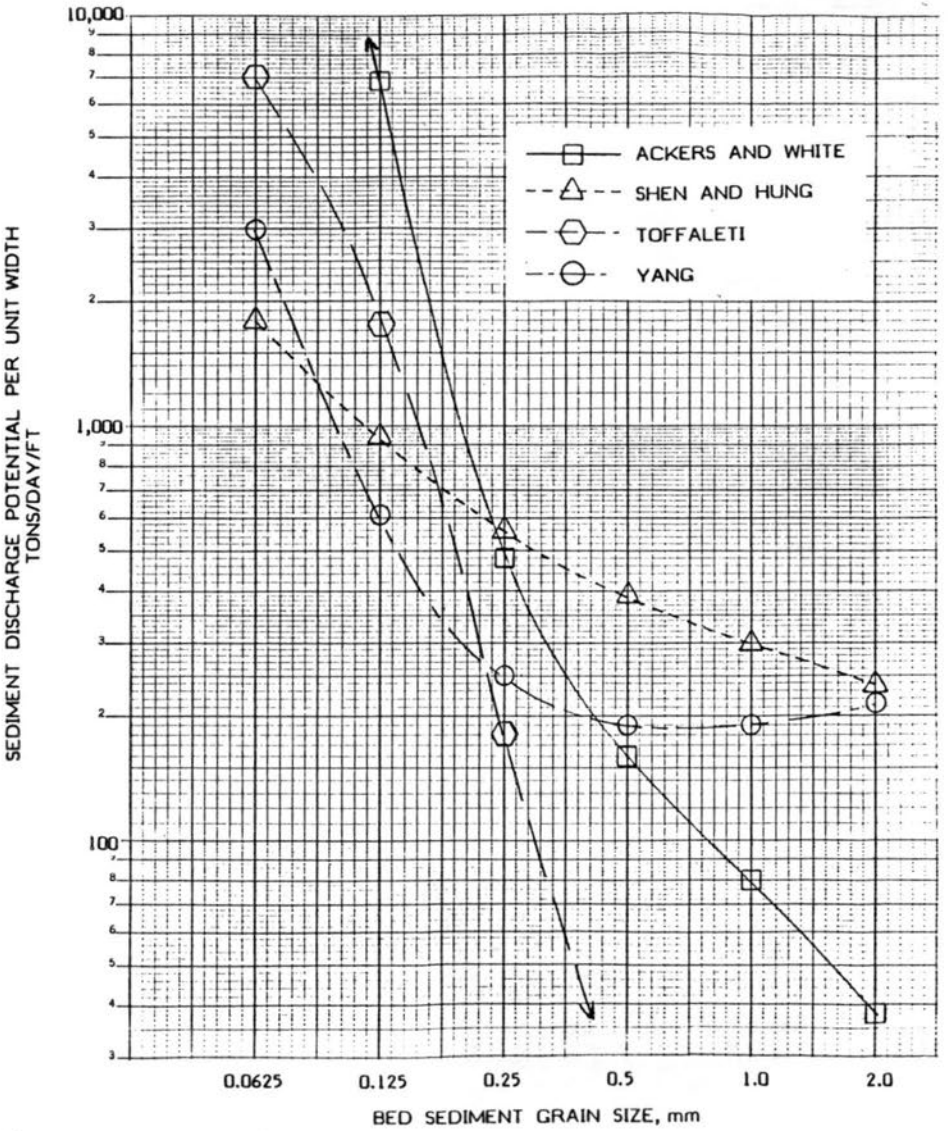

FIGURE 7. SEDIMENT TRANSPORT POTENTIAL VERSUS BED SEDIMENT GRAIN SIZE FOR 10.0 FEET HYDRAULIC DEPTH

David T. Williams

TABLE 1 - Areas of Applicability for Hypothetical Conditions, Ackers and White Method

Sediment Size (mm)	Depth, Feet				
	0.5	2.0	5.0	10.0	20.0
0.0625	L	L	L	L	L
0.125	M	M	L	L	L
0.25	H	H	H	M	L
0.5	L	H	M	L	L
1.0	L	H	M	L	L
2.0	L	M	M	M	L

L = Low, M = Medium, H = High

TABLE 2 - Areas of Applicability for Hypothetical Conditions, Shen and Hung Method

Sediment Size (mm)	Depth, Feet				
	0.5	2.0	5.0	10.0	20.0
0.0625	M	M	M	M	M
0.125	M	M	M	M	M
0.25	H	H	M	M	L
0.5	H	H	H	M	L
1.0	H	H	M	L	L
2.0	H	H	M	L	L

L = Low, M = Medium, H = High

Shen and Hung's data (13) had a range of up to 7.2 for F_{gr} and d_{gr} ranged from 3.33 to 3.33; however, Z ranged from 23 up to only 3,400. For depths greater than 5 feet and grain sizes greater than 0.5mm, F_{gr} and Z are out of the data range and results in overestimation of the transport as seen in Figures 7 and 8. Figures 4 - 8 show slight underestimation for sediment sizes less than 0.125mm because Z is extremely out of Shen and Hung's data range. In general, Shen and Hung's relationship is not applicable for rivers greater than 2 feet deep and very coarse or very fine sediment sizes. Table 2 summarizes the results.

Toffaleti's data had the widest range for Z at 41 to 92,500 and the largest F_{gr} at 11.8. The large Z is attributed to the Atchafalaya River data with the high F_{gr} coming from flume data. Unfortunately d_{gr} ranged only from 2.2 to 24. Because of the limited range of d_{gr}, the function is highly applicable only for grain sizes smaller than 1.0mm and if within the range of F_{gr}. This is evident by the underestimation of the transport for sediment sizes greater than 0.5mm as shown in Figure 5-8. Note that as the depth increases, the underestimation becomes worse. The function is generally applicable in deep rivers if the grain size is near 0.125mm. The function also overestimates the transport for small sediment sizes with shallow depths as shown in Figure 4-6 because d_{gr} is outside the data range. This shows that the transport is very sensitive to sediment size. In general, Toffaleti's relationship is applicable for medium sand sizes over a very wide range of depths. The applicability is summarized in Table 3.

TABLE 3 - Areas of Applicability for Hypothetical Conditions, Toffaleti Method

Sediment Size (mm)	Depth, Feet				
	0.5	2.0	5.0	10.0	20.0
0.0625	M	M	M	M	M
0.125	H	H	H	H	H
0.25	H	H	H	H	M
0.5	H	H	M	M	L
1.0	M	M	M	L	L
2.0	M	M	L	L	L

L = Low, M = Medium, H = High

Yang's data (18) had a range for d_{gr} of 2.6 to 43.8, F_{gr} of up to 5.8, and Z of 20 to 19,500. Since Yang's and Shen and Hung's methods have the velocity-slope product (stream power) as a dominate parameter, both show the same tendencies as shown in Figure 5-8. Again the differences in Figure 4 for large sediment sizes are not generally of concern because of the low transport. Figure 5-8 show increases in transport as sediment sizes increase for coarse sediment. This is due to the sediment size being near or past the data range. The function underestimates transport, though not as much as Shen and Hung's method, for sediment size of 0.0625mm and depths greater than 2 feet because d_{gr} and Z are beyond the function's range (see Figures 6-8). Coarse sediment at depths greater than 5 feet is outside the F_{gr} and Z range which results in an overestimation of the transport as seen in Figure 7 and 8. In general, Yang's method is applicable for a sediment range of 0.125mm to 0.5mm and depths less than 10 feet. The areas of applicability are summarized in Table 4.

DISCUSSION

The selection of the parameters d_{gr}, F_{gr} and Z as transport selection indicators should be done according to the important mechanisms of the system. For instance, a gravel bed river with shallow depth would have as an important parameter the relationship between size of the sediment and the laminar sublayer thickness. If bedforms significantly affect transport, the mobility index, U_*/W, and the particle Reynolds number, Wd/ν, could be important parameters. Other important parameters could be dimensionless stream power, VS/W, and shear velocity Reynolds number, U_*d/ν.

TABLE 4 - Areas of Applicability for Hypothetical Conditions, Yang Method

Sediment Size (mm)	Depth, Feet				
	0.5	2.0	5.0	10.0	20.0
0.0625	L	L	L	L	L
0.125	H	M	M	M	M
0.25	H	M	M	M	L
0.5	H	H	M	L	L
1.0	H	H	M	L	L
2.0	H	M	M	M	L

L = Low, M = Medium, H = High

Of particular interest is the range of hydraulic and sediment combinations that the four transport functions are generally applicable. To assess this, each L, M, and H in Tables 1 through 4 were assigned points of 1, 2, 3, respectively. The points were added up for the four tables for each sediment size-depth combination. The maximum number is 12 (3 pts x 4 transport functions) and the minimum is 4. High applicability is associated with 10-12 points, Medium with 7-9 points and Low with 4-6 points. The results are shown in Table 5. This table reflects the range of flume and river data used by all the developers of the transport function. As can be seen, there is very little data for sediment sizes less than 0.125mm and depths greater than 5 feet. Examination of Figure 4 - 8 show that the transport functions generally agree for depths less than 5 feet and sediment sizes between 0.125mm and 1.0mm. This is reflected in Table 5 by the areas of high applicability.

SUMMARY

The sediment modeler is often presented with the problem of selecting an appropriate sediment transport method to aid in evaluating a river's response to existing and project conditions. A selection procedure suggested by Shen (12) and furthered by Yang (16) is presented. To aid in the selection procedure, the applicability of four total bed material transport methods are presented. These methods are Ackers and White, Shen and Hung, Toffaleti, and Yang. The parameters used in determining applicability are dimensionless grain size, d_{gr}, mobility number, F_{gr}, and dimensionless flow depth, Z.

TABLE 5 - Areas of Applicability for Hypothetical Conditions with Weightings from all Methods.

Sediment Size (mm)	Depth, Feet				
	0.5	2.0	5.0	10.0	20.0
0.0625	I	I	I	L	L
0.125	H	M	M	M	M
0.25	H	H	H	M	L
0.5	H	H	M	L	L
1.0	M	H	M	L	L
2.0	M	M	M	L	L

L = 4-6 pts., M = 7-9 pts, H = 10-12 pts.

All methods were analyzed under hypothetical hydraulic and sediment conditions. The flow depth ranged from 0.5 to 20 feet at a constant slope of 0.0005 and Manning's "n" of 0.02. These conditions produce unit water discharges ranging from 0.52 to 244.8 cfs/ft and flow velocities ranging from 1.05 to 12.24 ft/sec. The sediment grain sizes analyzed ranged from 0.0625 to 2.0mm. The analyses involved the calculation of sediment transport potential by sediment size and flow depth. These results are shown in Figures 4 through 8. The areas of applicability for each transport method are displayed in Table 1 through 4 and were determined by comparing the dimensionless parameters for the hypothetical conditions to the range of data used in the development of each transport method.

The following generalized statements were made based upon the analyses of the hypothetical conditions. The Ackers and White method works well for medium sands at depths less than 5 feet. Shen and Hung's method is satisfactory for medium sands also, but for depths less than 2 feet. Toffaleti's method is useful for medium sands for a large range of depths. Yang's method is applicable for medium sands at depths less than 10 feet.

The selection parameters would change according to the type of sediment and river being studied. The range of applicability would also change from river to river and project modifications to the river. Though these parameters and conditions may change, the procedures and analyses is appropriate for all conditions.

APPENDIX I - REFERENCES

1. Ackers, P. and White, W. R., "Sediment Transport: New Approach and Analysis," Journal of the Hydraulics Division, ASCE, Vol. 99, No. Hy11, Nov. 1973, pp. 2041-2060.

2. Alonso, C. V., "Selecting a Formula to Estimate Sediment Transport Capacity in Nonvegetated Channels," Conservation Research Report No. 26, CREAMS (A Field Scale Model for Chemicals, Runoff, and Erosion from Agricultural Management System), Chapter 5, W. G. Knisel, ed., U. S. Department of Agriculture, May 1980, pp. 4265-439.

3. Bagnold, R. A., "An Approach to the Sediment Transport Problem from General Physics," U. S. Geological Survey, Professional paper 422-I, 1966, 37 pp.

4. Colby, B.R., "Practical Computation of Bed-Material Discharge," Journal of the Hydraulics Division, ASCE, Vol. 90, No. HY2, Proc. Paper 3843, March 1964, pp. 217-246.

5. Colby, B. R., and Hembree, C. H., "Computation of Total Sediment Discharge, Niobrara River near Cody, Nebraska," U. S. Geological Survey Water-Supply Paper 1357, 1955, 187 pp.

6. Einstein, H. A., "The Bed-Load Function for Sediment Transport in Open Channel Flows," Technical Bulletin No. 1026, U. S. Department of Agriculture, Soil Conservation Service, 1950.

7. Engelund, F., and Hansen, E., "A Monograph on Sediment Transport in Alluvial Streams," Teknisk Forlag, Technical Press, Copenhagan, Denmark, 1967.

8. Graf, W. H., Hydraulics of Sediment Transport, McGraw-Hill Book Co., New York, N. Y., 1971.

9. Laursen, E. M., "The Total Sediment Load of Stream," Journal of the Hydraulic Division, ASCE, Vol. 54, No. HY1, Proc. Paper 1530, Feb. 1958, pp. 1-36.

10. Meyer-Peter, E., and Muller, R., "Formulas for Bed-Load Transport," Proceedings of the 3rd Meeting of the International Association of Hydraulic Research, Stockholm, 1948, pp. 39-64.

11. Rouse, H., "Modern Concept of the Mechanics of Fluid Turbulence," Transactions, ASCE, Vol. 102, Paper No. 1965, 1937, pp. 463-543.

12. Shen, H. W., "Total Sediment Load," River Mechanics, Edited by H. W. Shen, Chapter 13, Fort Collins, Colorado, 1971.

13. Shen, H. W., and Hung, C. S., "An Engineering Approach to Total Bed Material Load by Regression Analysis," Proceedings of the Sedimentation Symposium, Chapter 14, Berkeley, Calif, 1971.

14. Simons, D. B., and Senturk, F., "Sediment Transport Technology," Water Resources Publications, lst Ed., Fort Collins, Colorado, 1977.

15. Toffaleti, F. B., "A Procedure for Computation of the Total River Sand Discharge and Detailed Distribution, Bed to Surface," Technical Report No.5, Committee on Channel Stabilization, Corps of Engineers, United State Army, Vicksburg, Miss., Nov. 1968.

16. Yang, C. T., "Sediment Transport and Unit Stream Power," Handbook of Civil Engineering, Technomic Publicating, 1986. (To be published).

17. Yang, C. T., "Unit Stream Power Equation for Gravel," Journal of Hydraulic Engineering, ASCE, Vol. 110, No. HY12, December 1984.

18. Yang, C. T., "Incipient Motion and Sediment Transport," Journal of the Hydraulics Division, ASCE, Vol. 99, No. HY10, Proc. Paper 10067, Oct. 1973, pp. 1679-1704.

19. Yang, C. T., "Unit Stream Power Equation and Sediment Transport," Journal of the Hydraulics Division, ASCE, Vol. 98, No. HY10, Proc. Paper 9195, Oct. 1972, pp. 1805-1826.

SALINITY INTRUSION IN ESTUARIES

In this paper I will first present a physical introduction to estuaries. Then,using the Prandle's method (1980),we shall get an analytical solution for partially to well mixed estuaries in a time averaged mode.This solution will allowe us to try a space dependent longitudinal dispersion coefficient. The results will be compared.

PART I : PHYSICAL INTRODUCTION.

Classification of estuaries

Pritchard (1955) has classified estuaries by their stratification and the charateristics of their salinity distributions.In this classification three estuarine types are defined : Highly stratified; partially mixed; homogeneous.

Higly stratified.salt wedge type.

This structure stems usually from an estuary emptying into a tideless sea,with a source of fresh water at the head (upper end).Fig 1 shows a typical salinity profile.

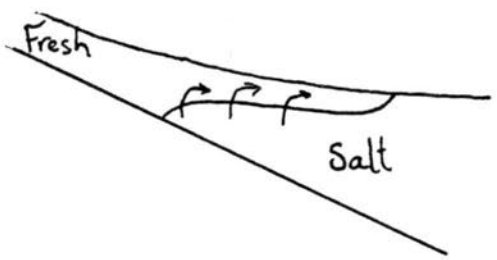

Figure 1 : Salinity profile in a salt wedge estuary.

Because of the viscosity, we have a velocity shear across the interface, and a thin layer at the top of the salt wedge will be swept seaward.When the shear is sufficiently intense, waves form and break on the interface and salty water is mixed into the surface fresh water.This is called entrainment.In order to preserve continuity a slight compensating landward flow is necessary in the salt wedge, to replace the salt water passing into the upper layer.Exemples: Mississippi,Vellar estuaries.

Higly stratified estuaries.Fjord type.

In many ways those estuaries are similar to the salt wedge type, but in this case the lower layer is very deep.River inflow must be

dominant over tidal flow, and entrainment is again the main process mixing fresh and salt water.

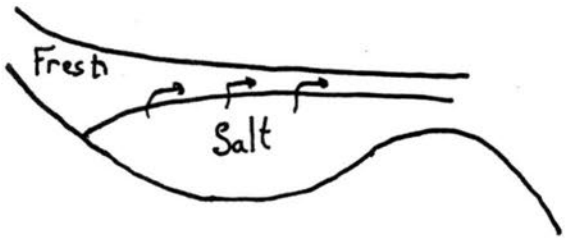

figure 2: Salinity profile in a fjord type estuary.

Partially mixed estuaries.

If we now introduce tides into the estuary, then the entire contents of the estuary will oscillate. It requires only a small tidal range to make this occur, though there is likely to be a particular range of tidal prism (total volume of water exchanged between the estuary and the sea during the tide) to estuary volume ratio over which it is effective in producing a partially mixed estuary.

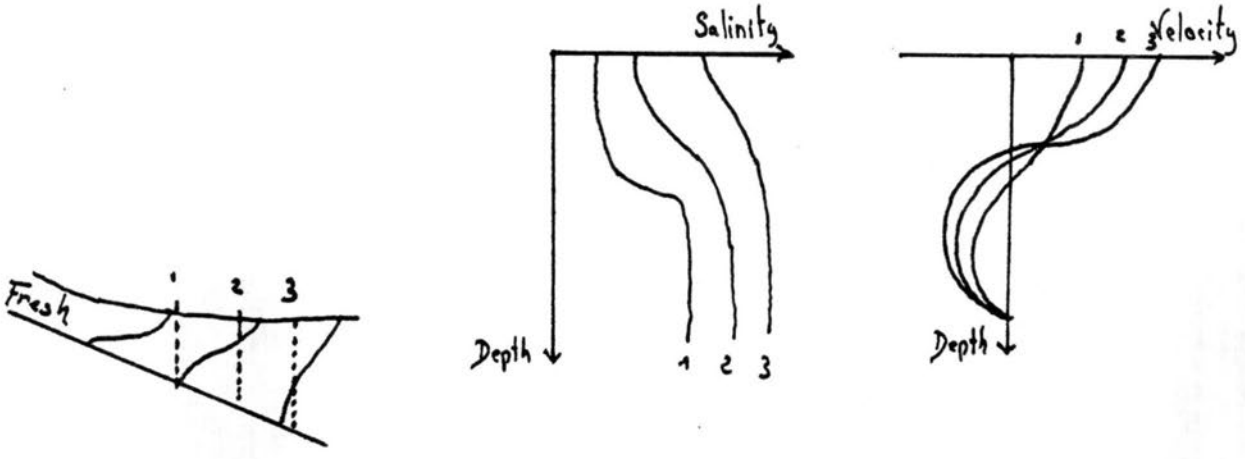

fig 3: Salinity and velocity profile in a partially mixed estuary

The entrainment process is still working, causing a distinctive two-layer flow system as in the case of the Higly stratified estuary,but in addition to that, we have now turbulent diffusion. Because of the efficient exchange of salt and fresh water, the salinity structure of the estuary is different from that of a salt wedge type.The surface salinity increases much more steadily down the estuary and undiluted fresh water only occurs very near the head of the estuary.Now there is also a longitudinal gradient of salinity on the bottom.Consequently there is a large section in the middle of this type of estuary in which the horizontal salinity gradients are almost linear.The form of the vertical salinity profile does not change much along the estuary either.There is normally a zone of high salinity gradient at about mid-depth and the surface and bottom layers are almost homogeneous.Exemples: James river;Mersey.

Vertically homogeneous estuaries.

When the estuary cross section is small the velocity shear on the bottom may be large enough to mix the water column completly and make the estuary vertically homogeneous.It is difficult to be sure, however, that vertically homogeneous estuaries really exist, as small vertical variation may be lost in the average process.When there is no vertical salinity gradient , there is no flux of salt and mixing occurs only in the horizontal direction.In this estuaries tidal flow must be much larger than river flow.If the estury is wide Coriolis forces will cause a horizontal separation of the flow.Thus the circulation will be in a horizontal plane rather than in the vertical sense as found in other estuaries.When the width is smaller,lateral shear may be sufficiently intense to create laterally homogeneous conditions.

Simmons' parameter.

Simmons (1955) notes that the physical ocanographic conditions, and particularly salinity intrusion, of an estuary can normally be related to the ratio of the river runoff over a tidal cycle to the tidal prism of the estuary.When this ratio is of the order of 10^{0}, an higly stratified estuary normally exists, when it is of the order of 10^{-1},partially conditions must exist, and when it is of the order of 10^{-2} a well-mixed estury normally exists.
An other, more theoretical classification has been presented by Hansey and Rattrey (1966).It is based on simple observable quantities plotted on a graph.It is commonly used and is usefull to quantify how an estuary is well mixed.

Characterization of the flow.

The Reynolds number compares the relative importance of inertial and viscous forces.
The Richardson number Ri is a comparaison of the stabilizing forces of the density stratification to the destabilizing influences of velocity shear.It can be defined by:

$$Ri = -\frac{g}{\rho}\frac{\partial \rho}{\partial z}\Big/\left(\frac{\partial u}{\partial z}\right)^{2}$$

145

For Ri>0 the stratification is stable, for Ri=0 it is neutral, (no stratification),and for Ri<0 it is unstable.When the stratification is above a certain level turbulance will be damped out and the flow will be essentially laminar. This transission from turbulent to laminar is generally taken at Ri=0.25 under conditions of uniform flow. In estuaries the flow is non-uniform so the transition will occur at higher Ri. Generally,the conditions are more or less neutral in the surface and bottom layers and stable at midepth.
In case of highly stratified estuaries, it is also possible to define a layer Richardson number:

$$Ri = \frac{(\Delta\rho/\rho)\, g D}{u^2}$$

D is the depth of the upper layer flowing with a velocity u relative to the lower layer and ρ is the density difference between the layers.The square root of the inverse layer Richardson number is the interfacial Froude number Fi:

$$Fi = \frac{u}{\sqrt{\Delta\rho/\rho\, g D}}$$

This Froude number is an alternative way of considering the influence of density stratification. As the usual Froude number it can be thought as comparing the velocity of the flow to the velocity of a propagation of a wave along a density interface.

Conclusion

The mixing of salt and fresh water in estuaries is carried out by two processes: Entrainment and turbulent diffusion .Entrainment is a one way process in which a less turbulent water mass becomes drawn into a more turbulent layer.The rate of entrainment will increase with increasing velocity differences between the layers (with Fi). We have seen that this process is responsible for a two layer current system: landward in the bottom, seaward in the upper layer. Diffusion is a two way process in which equal volume of water is exchanged between the two layers.This requires the presence of turbulence in the two layers.
In both processes we have energy dissipation.
The rate of mixing by the two different methods depends on the degree of turbulence in the two layers.Same turbulence gives no entrainment and only diffusion ;no turbulence in the upper layer gives only entrainment.

PART II : ANATICAL SOLUTION FOR WELL-MIXED ESTUARIES

Introduction

In 1980 Prandle and Rahaman calculated tidal response in estuaries described by the following geometry:

For depth: $H(X)=H_o(X/L)^m$ (1)
For width: $B(X)=B_o(X/L)^n$ (2)

X is the distance measured from the head, $L=(gH_o)^{0.5}P$, with g acceleration due to gravity and P the tidal period. H_o, L_o, m, n, are parameters which relate (1) and (2) to the geometry of the estuary. The tidal response was expressed by Bessel's functions in terms of the distance along the estuary and an 'estuarine shape number', $ns=(n+1)/(2-m)$.
In 1981 Pandle seeked to extend this approach to salinity intrusion in estuaries. He used the linearized equations of motion and mass conservation to get a one-dimensional solution. As we have seen in Part I, a one-dimmensional model is justified only for the well-mixed to homogeneous estuaries.
A major difficulty however is to find the good expression for the longitudinal-dispersion coefficient D which in fact must take in account for the dispersion in three dimmension. One may have doubt on the Physical meaning of such a coefficient since as we have seen in Part I the dominent process is vertical dispersion. Clearly then, the magnitude or the expression of this coefficient cannot easly be defined. Some studies have assumed constant values, others have related D to the gradient along the estuary or the Richardson number. Taylor found it proportional to the velocity and the depth which brings Ippen to propose a coefficient increasing with X, $D=D_oB/(B-X)$, for an estuary with uniform section.

Prandle integrated the equations averaged over a tidal cycle, for D=cte., $D=(dc/dx)$, $D=(dc/dx)^2$ and compared his results with observed data. In the following sections we will extend the integration for $D=D_oX^p$, and compare the results to those of Prandle

Equations of motion and continuity.

Tidal propagation in a narrow channel of rectangular cross section may be approximated by the following linearized equations (Ippen, 1966, Chap. 10):

Motion along X : $$\frac{\partial U}{\partial T} + g\frac{\partial Z}{\partial X} + SU = 0 \qquad (3)$$

Continuity : $$\frac{\partial Z}{\partial T} + \frac{1}{B}\frac{\partial}{\partial X}(BHU) = 0 \qquad (4)$$

Mass conservation (Ippen Chap14) : $$\frac{\partial c}{\partial T} + U\frac{\partial c}{\partial X} = \frac{1}{A}\frac{\partial}{\partial X}\left(AD\frac{\partial c}{\partial X}\right) \qquad (5)$$

where:

147

U velocity along the X axis
Z elevation above horizontal datum
g acceleration due to gravity
B channel breadth
H channel depth
A cross-sectinal area (=BH)
T time
c relative massique concentration of any consevative substance.
D longitudinal dispersion coefficient

In order to convert Eqs (1)-(5) to dimensionless form P is introduced as unit of time,L as unit of horizontal dimension and H_o, as unit of vertical dimension.Prandle relates those parameters by:

$$L=(gH_o)^{0.5}P.$$

Thus we obtain the dimensionless variables:

$x=X/L$; $t=T/P$; $z=Z/H_o$; $s=SP$; $b=B/L$; $h=H/H_o$; $u=U(P/L)$;
$d=D(P/L^2)$ (7)
Equations (1)-(5) may be rewritten as follow:

$$h(x)=x^m \qquad (8)$$

$$b(x)=x^n \qquad (9)$$

$$\frac{\partial u}{\partial t} + \frac{\partial z}{\partial x} + su = 0 \qquad (10)$$

$$\frac{\partial z}{\partial t} + \frac{1}{x^n}\frac{\partial}{\partial x}\left(ux^{m+n}\right) = 0 \qquad (11)$$

$$\frac{\partial c}{\partial t} + u\frac{\partial c}{\partial x} = \frac{1}{x^{m+n}}\frac{\partial}{\partial x}\left(dx^{m+n}\frac{\partial c}{\partial x}\right) \qquad (12)$$

In the case of an estury subject to tidal forcing at the frequency w we seek solutions of the form:

$$z(x,t)=zz(x)+z'(x)e^{iwt}, \qquad (13)$$

$$u(x,t)=uu(x)+u'(x)e^{iwt} \qquad (14)$$

$$c(x,t)=cc(x)+c'(x)e^{iwt} \qquad (15)$$

where the double letter indicates time-averaged value and the prime the complex amplitude.
Substituing (13),(14),(15) into (10),(11),(12) we get two set of three equations, a time-averaged set and the oscillatory part.solutions for u' and z'can be obtained (Prandle and Rahaman), but not for c'.Consequently,only the time averaged equations will be considered.

time-averaged equations

The time averaged equations are:

$$\frac{\partial \gamma}{\partial x} + s u = 0 \qquad (16)$$

$$\frac{\partial}{\partial x}\left(u x^{m+n}\right) = 0 \qquad (17)$$

$$u \frac{\partial c}{\partial x} = \frac{1}{x^{m+n}} \frac{\partial}{\partial x}\left(d x^{m+n} \frac{\partial c}{\partial x}\right) \qquad (18)$$

In using those time-averaged equations we assume that all the tides are the same, which is unfortunatly not true, there is an evolution between two sucessive tides. Here is one of the bigest limitations of this approach.Prandle proposes to take in account the variation of the range of the tide by doing some adjustments of Q so that for example, increased upstream storage during the time of increasing tidal ranges might be compensated by deacreasing Q.

we can integrate (17):

$$u x^{m+n} = q/b_o \qquad (19)$$

q is the dimensionless fresh water flow:

$$Q = UBH = (uL/P) B_o H_o x^{m+n} = q(L^2 H_o/P) \qquad (20)$$

Substituing (19) into (16) we get:

$$\frac{d\gamma}{dx} = \frac{-sq}{b_o x^{m+n}} \qquad (21)$$

This demonstrates that mean sea level rises toward the head (x=0) of an estuary when 1) the fresh water flow increases, 2) m+n increases, 3) x decreases.Substituing (19) into (18) gives:

$$\frac{q}{b_o} \frac{dc}{dx} = \frac{d}{dx}\left(d x^{m+n} \frac{dc}{dx}\right) \qquad (22)$$

Integrating (22):

$$\frac{q}{b_o} c = d x^{m+n} \frac{dc}{dx} + k \text{ (constant)} \qquad (23)$$

The boundary conditions are:
c(a)=0, the limit of the salt water intrusion is for x=a.
c(x1)=0, if x>x1, the influence of fresh water is negligible
It should be noted that those boundaries conditions,and particularly x1, are dependent on the range of the tide, and this relation, special for each estuary, may be not easy to find.

Analytical solutions

When Prandle in 1981 integrated (23), it turned out that the best results where for d=cte, and not $d=d_o dc/dx$, or $d=d_o(dc/dx)^2$. However,he did not always get a good fit between his data and the theory.Thus one of his conclusions was that we could improve the model by relating the dispersion coefficient to the velocity. Taylor found also experimentaly, for an idealized estuary, $D=7.1hu(f^{o\cdot5})$, h is the depth, u the velocity and $C=(8g/f)^{o\cdot5}$, where C is the Chezy coefficient. Thus using (19) d should have the form $d=d_o/x^n$. So it seems justified to try an expression for this coefficient as: $d=d_o x^p$, or $D=D_o(X/L)^p$ with $D_o=(L^2/P)d_o$.

The equation (23) can be integrated and, gives:

$$\frac{c}{c_1} = \frac{e^{V\left(\frac{x}{x_1}\right)^{1-r}} - e^{V\left(\frac{a}{x_1}\right)^{1-r}}}{e^{V} - e^{V\left(\frac{a}{x_1}\right)^{1-r}}} \qquad (24)$$

where $V=(q/b_o d_o)(x_1^{1-r}/(1-r))$

and $r=m+n+p$

It is convenient to note $V'=(1-r)V = (U_1 X_1)/D_o$

We now have three parameters in order to fit the theoretical curve with the experimental data: a;p;d_o.However,p should be negative.

Results

In this section, we will compare the new results with the results using a constant diffusion coefficient, and with experimental data of three estuaries: Thames, Potomac, and Bristol channel.All the parameters, B_1,H_1,m+n,Q,etc... are the same as those used by Prandle.The sources of those parameters are given in his article.While the observed data might reasonably be assumed to represent cross-sectionally averaged values, some doubt about the effectivness of the associated time-averaging must arise.
The first parameter 'a' has been taken to 0,because it was shown to have little effect on the solution.In addition, by adopting the value a=0,the change in salinity distribution under varying river discharges may be determined directly without the necessity of determining corresponding variations in the value of a. This will be used for the Bristol channel where two simulations are done, changing only Q.
The parameter p, was first taken equal to 0.Then we move p on the left or on the right, and recompute the parameter V, in order to keep approximativly the same inflection point for the data and the theoretical distribution.(this was the way Prandle fitted his curves).If we observed an improvment we keep moving p in the same direction until no significant improvment was observed.

Given data

	m+n	x1	L(KM)	B_1(KM)	H_1(m)
THAMES	3.0	0.078	1212	7	10
POTOMAC	1.4	0.370	495	18	10
BRISTOL	2.9	0.014	9815	20	25

Computed data with D=cte.(Prandle's results).

	Q (m^3/s)	V'(U_1X_1/D)	D (m^2/s)	D*(m^2/s)
THAMES	19	0.47	54	53-84
POTOMAC	112	1.30	87	
BRISTOL	80	0.08	270	54-174
BRISTOL	480	0.48	270	54-174

D*= Diffusion coeft. observed.

Computed data with $D=D_o(X/L)^p$

	Q m^3/s	V'	D_o m^2/s	p
THAMES	19	0.90	29	-1
POTOMAC	112	0.50	227	+2.6
BRISTOL	80	0.10	210	-0.4
BRISTOL	480	0.62	210	-0.4

151

Bristol channel Q = 480

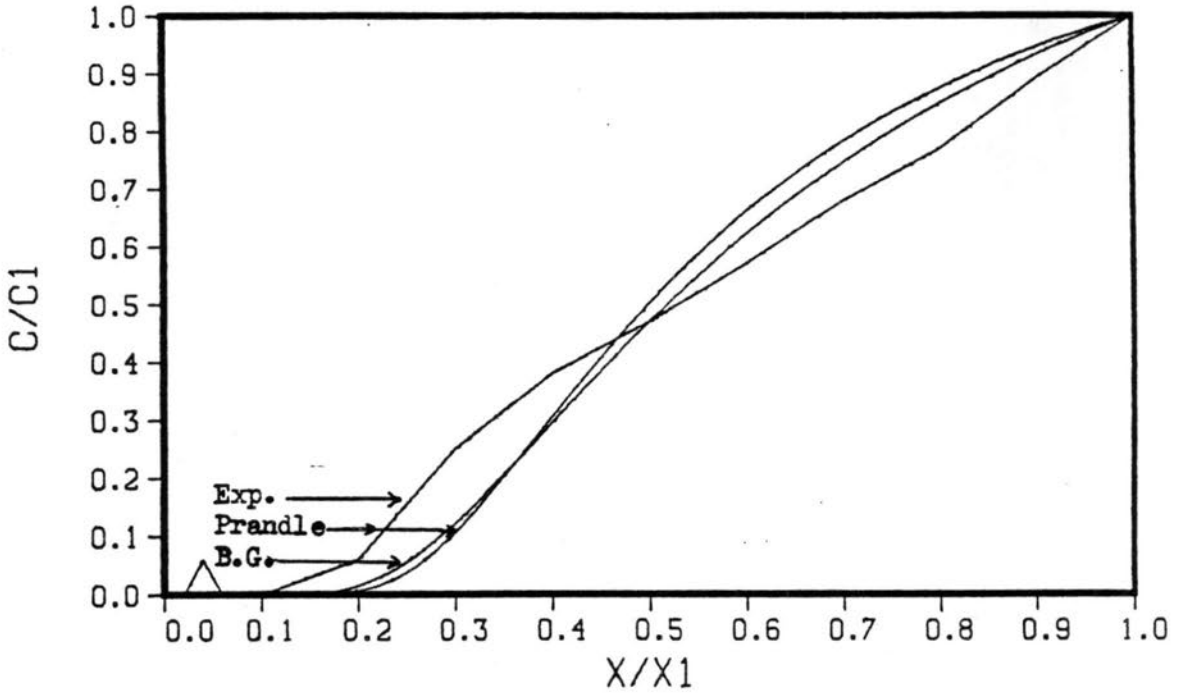

Q = 80

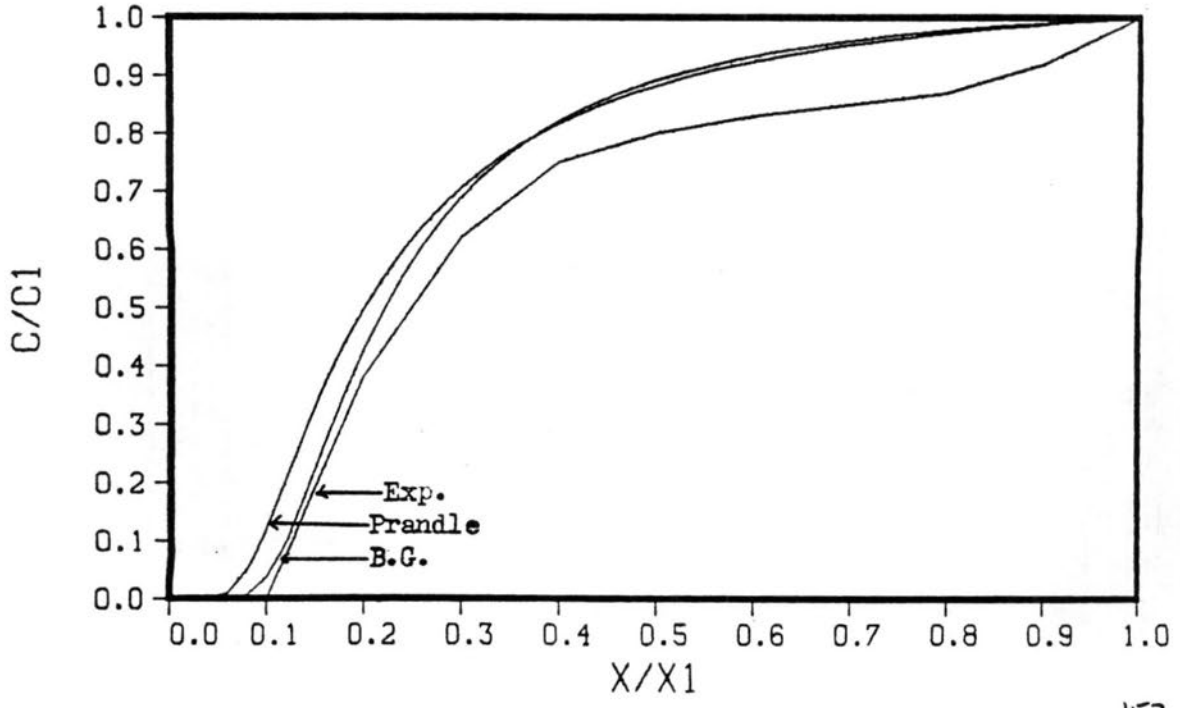

152

Thames

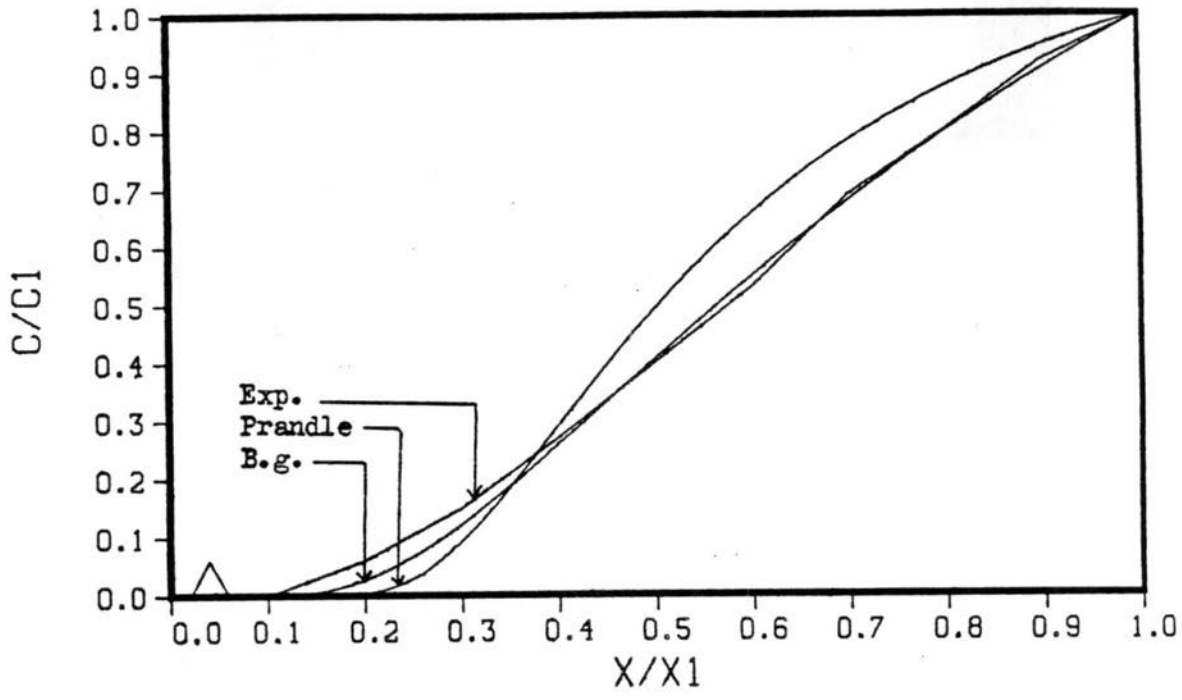

Potomac

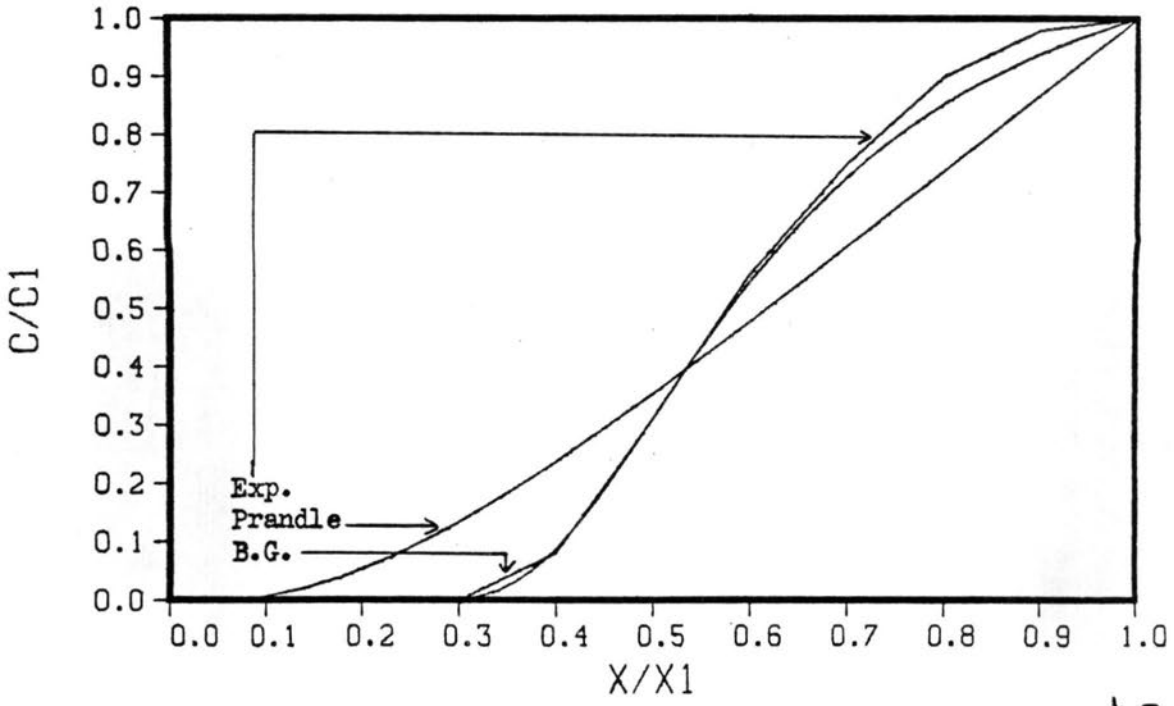

153

THAMES.....: $D=29(X/L)^{-1}$
BRISTOL CHANNEL.....: $D=210(X/L)^{-0.4}$ in m^2/s
POTOMAC.....: $D=227(X/L)^{2.6}$

On the graphs (pages 10-11),the new results seem much better than the previous one.However this not surprising since we have one more parameter that we can vary in order to fit the curve.Thus it is difficult without a deeper knowledge of the estuaries to determine if p as a physical meaning or not,particularly in the case of Potomac, where D increase with X, which is in contradiction with the theory.
Nevertheless,in the case of Bristol channel I have calibrated p for Q=480 m^3/s without looking at the curve corresponding to Q=80. but we can see that both curves have been improved.This seems to prove that p has a physical meaning,in this case it indicates that D must decrease with X.
However, the worst thing in those results is that X being small with respect to L, D varies in a very large range and its values are not realistic at all when compared with observed values.
An alternative would be to assume an other form for D as: $D=a+bX^p$

conclusion

An attempt has been made to use a space varied diffusion coefficient using only two parameters D_o and p.The results have been improved but one may have some doubt about the reliability of those results when looking at the values of the longitudinal-dispersion coefficient found.Thus others form should be tried, as suggested in the previous section.However, if one want to use such an approach, one must have a good knowledge and understanding of 'his' estuary and check if the space variations of the dispersion coefficient are realistic.
My goal was not to promote the use of one-dimensional models.The limitations of such models are obvious.However,they help to understand the influence of differents parameters such as the estuarine shape or the dispersion coefficient on salinity diffusion.

references:

Dyer K.R.,1974. Estuaries : A physical introduction.

Ippen A.T. 1966. Estuary and coastline Hydrodynamics.

Prandle D. and M. Raham 1980. Tidal response in estuaries.J .Phys. Oceangr.

159

Prandle D. 1981. Salinity intrusion in estuaries. J. Phys. Oceangr.

Pritchard D.W. 1955. Estuarine circulation Pattern.ASCE.

Taylor G.I. 1954. Dispersion of matter in turbulent flow through a pipe

West J.R 1984. An evaluation of a moving coordinate system model for salinity intrusion in the Mersey estuary.

Simmons H.B. 1955. Some effects of upland discharge on estuarine hydraulics.

The Finite Element Solution of the Shallow Water Equation on Overland Flow

submitted by

Khalid Behnam Marcus

CE 716, River Mechanics

spring, 1986

Summary

The shallow water equation has its different application in the flow field problems. In this paper, the finite element method (Galerkin method of weighted residual) will be used as a proper tool to solve the shallow-water equations and its reduced form (kinematic wave approach). Different aspects of the finite element method such as stability, convergence, using different approximation functions, and different element lengths will be examined in order to see the effect of these aspects on the output solution.

Governing Equation

The problem of overland flow in one dimension form as show in figure (1) can be represented by the following vertically integrated equations (shallow water equations)

The continuity equation

$$\frac{\partial h}{\partial t} + u\frac{\partial h}{\partial x} + h\frac{\partial u}{\partial x} = r \qquad \text{---------- (1)}$$

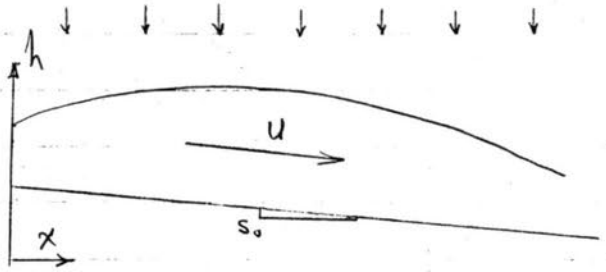

Figure (1) Overland Flow

The momentum equation

$$\frac{\partial u}{\partial t} + u\frac{\partial u}{\partial x} + g\frac{\partial h}{\partial x} = g(S_o - S_f) - \frac{u}{h}r \qquad \text{---------- (2)}$$

Equation (2) can be written in reduced form as:

1) $S_o = S_f$ ← Kinematic wave approximation

2) $\frac{dh}{dx} = S_o - S_f$ ← diffusive wave equation

where:

h = depth (L) , u = velocity (L, T) , t = time (T)
x = horizontal distance (L) , r = lateral inflow (L^3/TL^2)
g = acceleration of gravity (L/T^2) , S_o = the plane slope
S_f = friction slope

It is more useful to write the shallow-water equations in general dimensionless form. To obtain the dimensionless term, the concerned variable is divided by a normalizing quantity having the same dimension:

$$x^* = \frac{x}{L_o} \quad , \quad h^* = \frac{h}{H_o} \quad , \quad u^* = \frac{u}{V_o} \quad , \quad t^* = \frac{V_o t}{L_o} \quad , \quad r^* = \frac{r L_o}{V_o H_o} \quad , F = \frac{V_o}{\sqrt{g H_o}}$$

where H_o and V_o are the normal depth and velocity at $x = L_o$. The friction slope for the turbulent flow can be approximated by Chezy or Manning equation.

$$V_o = \frac{1.49}{n} H_o^{2/3} S_o^{1/2} \quad \leftarrow \text{Manning equation}$$

$$V_o = C H_o^{1/2} S_o^{1/2} \quad \leftarrow \text{Chezy equation}$$

where C and n are Chezy and Manning coefficients respectively.
For laminar flow $V_o = \frac{g S_o}{3\nu} H_o^2$
where ν is the kinematic viscosity of the water.
By using the above dimensionless parameters in equations (1) and (2) with Chezy's equation to represent the turbulent flow we will get:

$$\frac{\partial h^*}{\partial t^*} + u^* \frac{\partial h^*}{\partial x^*} + h^* \frac{\partial u^*}{\partial x^*} = r^* \qquad (3)$$

$$\frac{\partial u^*}{\partial t^*} + u^* \frac{\partial u^*}{\partial x^*} + \frac{1}{Fo^2} \frac{\partial h^*}{\partial x^*} = K\left(1 - \frac{u^{*2}}{h^*}\right) - \frac{u^* r^*}{h^*} \quad ----(4)$$

The quantity (K) is called the Kinematic flow number (5). It constitues of the following parameters: $K = \frac{So\, Lo}{Fo^2\, Ho}$

These parameters are significant in the solution of the shallow water equations. In their paper Woolhiser and Liggett (8) have shown that the dynamic solution approachs the kinematic solution when (K) becomes large, $K > 10$, i-e the outflow hydrograph compared favourably with the kinematic wave theory. They also have shown that for many overland flow the kinematic flow number exceeds (1000). As (K) approachs infinity equation (4) reduces to the kinematic flow equation or

$u^{*2} = h^*$, which is valid for turbulent flow.

By substituting equation (5) in equation (3), the dimensionless form of the kinematic wave equation can be obtained:

$$\frac{\partial h^*}{\partial t^*} + \frac{3}{2} h^{*\frac{1}{2}} \frac{\partial h^*}{\partial x^*} = r^* \quad ---- \quad ---- \quad ---- \quad (6)$$

Lighthill and whitham (6) show that the kinematic wave theory is a good approximation to the shallow water equation provided that the Froude number is less than 2. Eagleson (3) stated that two conditions should be provided in order to use the kinematic wave theory in predicting the direct runoff and those conditions are: $Fo < 2$ and $K > 10$. Al-mashidani and Taylor (1) proved that it is not necessary to have the condition $Fo < 2$ provided that the value of K is large.

The Finite Element Method

In the finite element method, the domain of interest is divided into elements. The value of the dependent variable with in each element is written in terms of the unknow value

at the nodal points,

$$h^*(x,t) = \sum_{i=1}^{n} N_i(x)\, h_i^*(t) = N_1 h_1^*(t) + N_2 h_2^*(t) \quad \text{---} \quad (7)$$

$$U^*(x,t) = \sum_{i=1}^{n} N_i(x)\, U_i^*(t) = N_1 U_1^*(t) + N_2 U_2^*(t) \quad \text{----} \quad (8)$$

where:

n = number of nodal points in an element, $n=2$ for one dimensional element.

$h_i^*(t)$ = depth as a function of time

$U_i^*(t)$ = velocity as a function of time

$N_i(x)$ = Interpolation function

The Galerkin method of weighted residual states that

$$\int_D N_i R \, dD = 0 \quad \text{----------} \quad (9)$$

where

D = domain of interest

R = residual obtained by substituting the approximation functions into the exact function.

The kinematic wave approach will be used in the finite element formulation. By inserting equation (6) as a residual, and substituting the shape function representation of equation (7) into equation (9) we will obtain the matrix form for one element. The astensik will be dropped in the following equation

$$l_e [K]\left\{\frac{\partial h}{\partial t}\right\} + \frac{3}{2}[L] h^{3/2} - r\, l_e [M] = 0 \quad \text{---} \quad (10)$$

The time derivative can be represented by the forward finite difference scheme

$$\frac{\partial h}{\partial t} = \frac{h(t+\Delta t) - h(t)}{dt} \quad \text{---(11)}$$

After introducing equation (11) into equation (10), the finite element equation for one element can be written in short matrix form as

$$\frac{l_e}{dt}[K]\{h\}_{t+\Delta t} - \frac{1}{dt}[K]\{h\}_t + \frac{3}{2}[L]\{h^{3/2}\}_t - r\,l_e[M] = 0 \quad \text{---(12)}$$

where each of the matrices [K], [L], and [M] is two by two. The contribution of other elements can be obtained by a method called the direct stiffness method. The resulting matrix can be solved by a suitable iterative technique.

The initial and boundary conditions should be specified. Zero initial condition of $h(x,0) = u(x,0) = 0$ can be specified. A value of $h(0,t) = u(0,t) = 0$ can be specified for the boundary conditions. The formulation of the dynamic equation can be done in the same way as has been done with the continuity equation. The use of the continuity and the diffusive wave equation is called the parabolic equation approach.

In his work, Ross(7) investigated his finite element model on overland flow and channel flow for both the kinematic equation and the complete full dynamic equation. He examined different aspects of the finite element method such as: convergence, stability, using different approximation functions, and different mesh sizes.

Application of the Model to overland Flow

Ross(7) used some data to evalute the applicability of the kinematic wave equation to overland flow on turf and concrete surfaces. The results for turf surface that were obtained for the kinematic wave equation and the complete momentum equation is shown in figure (2). The two approximations appear satisfactory and in close agreement with the measured hydrograph. The Manning (n) that varies with depth, if used would probably give a better fit. The close agreement between the computed hydrographs indicates that the conditions for application of the kinematic wave approach were met (i.e the frictional

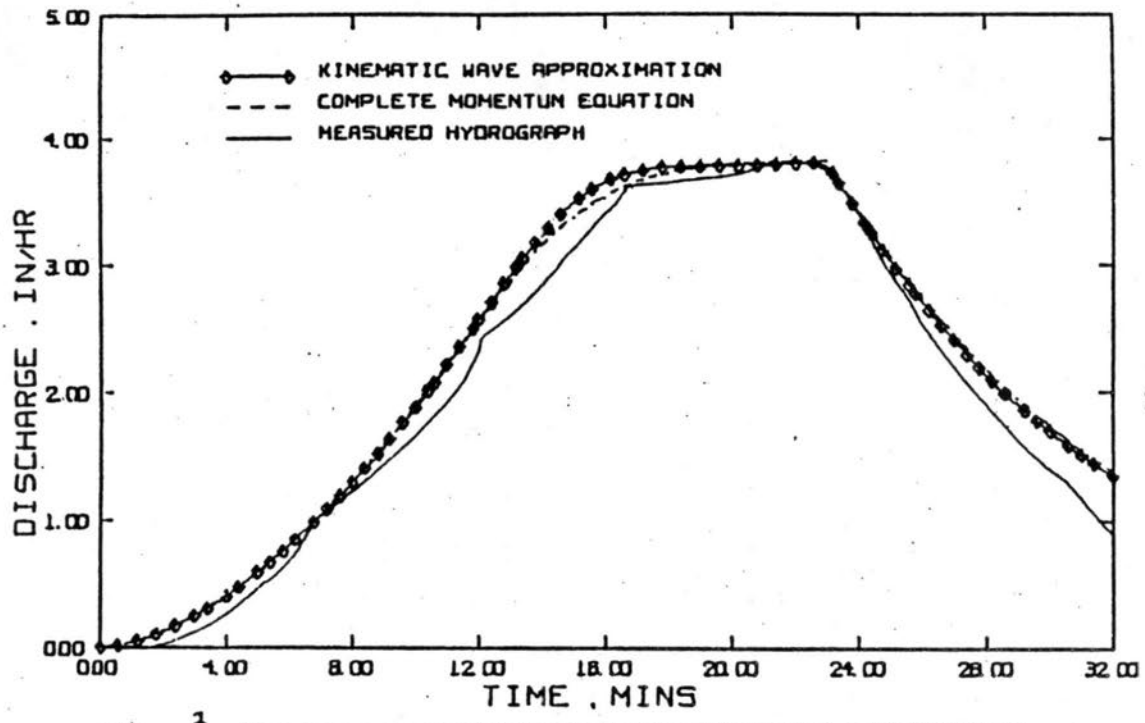

Figure 1. Comparison of simulated and measured flow over a turf surface (length = 72 feet, slope = 0.01, Manning n = 0.35 and rainfall = 3.81 inches/hour for 23 minutes). After Ross

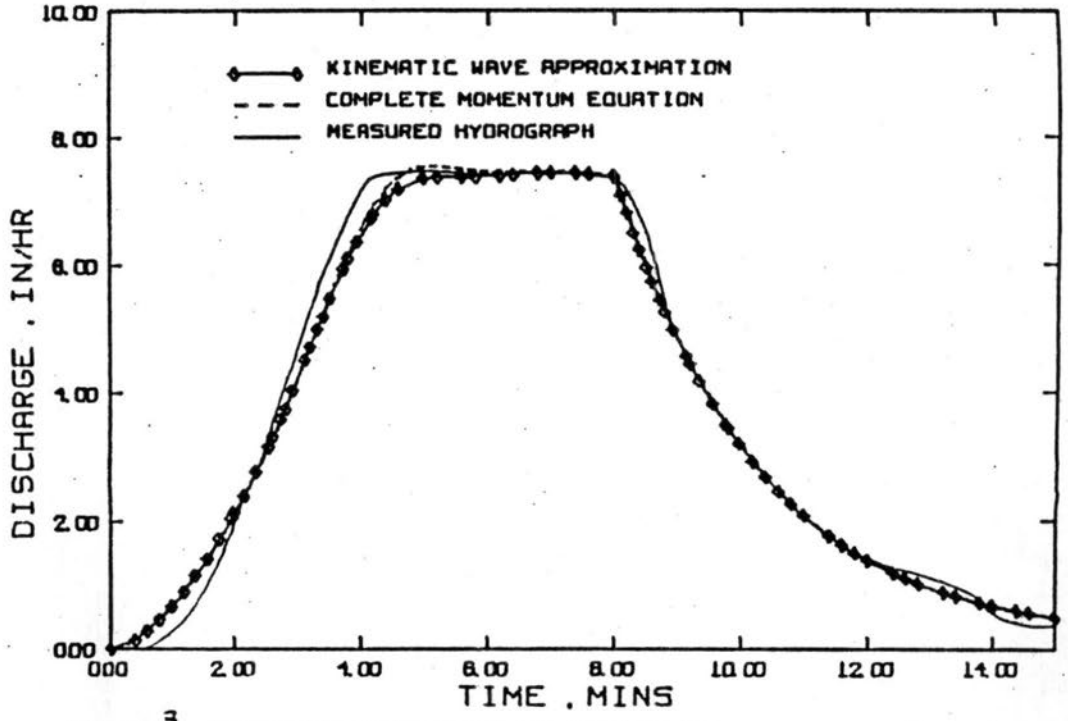

Figure 3. Comparison of simulated and measured flow over a concrete surface (length = 467 feet, slope = 0.02, Manning n = 0.014 and rainfall = 7.44 inches/hour for 8 minutes). After Ross

and gravitional forces are dominant compared to the acceleration and gradient terms. The Froude number (F) and the Kinematic wave number (K) at peak flow conditions were (0.05) and (3600) respectively. The results for concrete surface are shown in figure (3). Good agreement is shown between the results. The criteria that define the range of applicability of the Kinematic wave approach are $F = 1.4$ and $K = 87$, which indicate that, for extereme overland flow conditions (smooth surface and intense rainfall, these criteria were met.).

Application to River Flow

To test the applicability of the kinematic wave approach to river routing, Ross(7) used the data prepared by Viessman, et. al. (9). to model a river system. Figure (4) shows the results obtained by the finite element method compared with the explicit finite difference and characteristic method obtained by Viessman, et. al (9). Good agreement between the finite element solution and the explicit finite difference method. The method of characteristic is slightly different. In order to see that the kinematic wave approach is valid in this case, the data prepared by viessman, et. al (9) was used in the full dynamic equation and the parabolic equations and the results were compared with results obtained by using the kinematic wave approach (figure 5). In this figure, we can see that there is a large error in the kinematic wave approach. The other two approximations (i-e) the full dynamic equation and the parabolic equations improve the solution. The close agreement between the parabolic equations approach and the full dynamic approach indicates that the local and convective accelerations terms eliminated from the full dynamic equation to form the diffusive wave equation are unimportant. The values of (F) and (K) for the peak downstream discharge were (0.47) and (7) respectively. The error in kinematic wave approximation in due to low value of (K).

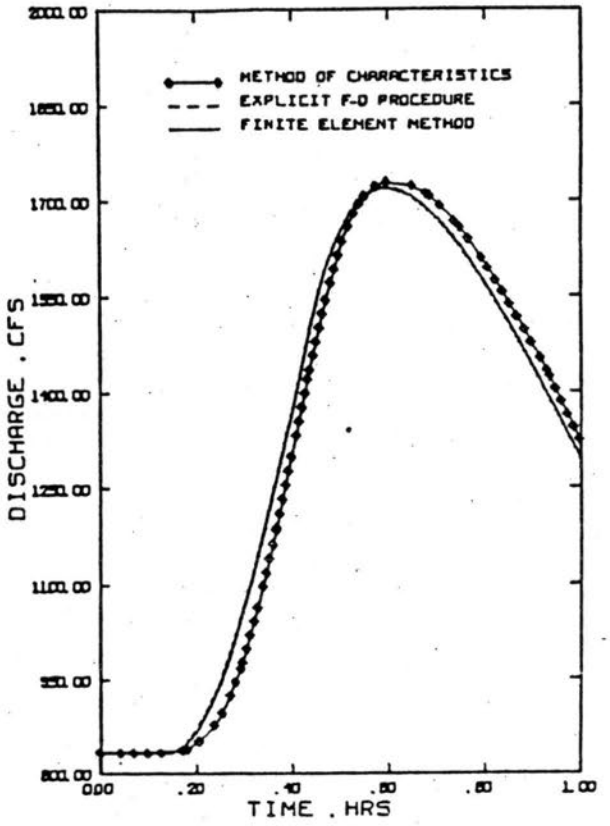

Figure #4. Comparison of hydrographs generated for a river flow example using three numerical solution techniques. After Ross

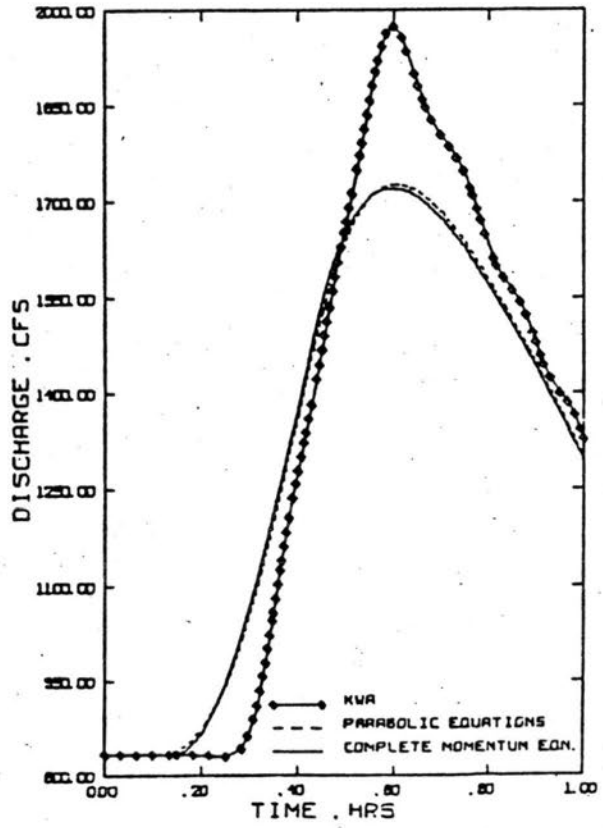

Figure #5. Comparison of hydrographs generated for the river flow example given in Figure #3 with the complete momentum solution, KWA and parabolic approximation. After Ross

Application to channel in small watersheds

Ross (7) applied his model to a channel in natural watershed. The steep slope in such channels allow the application of the kinematic wave approach which gives good results. Figures (6) and (7) show the application of both the full dynamic and the kinematic wave equations for two channels in a natural watershed area. Close agreement can be seen in the two figures by the two approaches. The value of (F) and (K) in the two channels are $F = 0.59$, $K = 374$ in figure (6) and $F = 0.56$, $K = 300$ in figure (7).

Solution Convergence due to Time increment

Two time integration schemes have been used; those are the explicit and the implicit procedures. The finite element numerical procedures may result in unconditionally stable solution, but the time dependent solutions obtained by the explicit procedure may result in an stable solution. In an unstable solution, the error growth with time; so it become necessary to choose the proper time increment to get an accurate solution.

The fully explicit scheme is conditionally stable because of the condition required to choose the time increment in order to meet certain criteria required for stability. This might result in decreasing the time step and therefore increasing the total time of computation which would result in unsuitable and inefficient way of solving the concerned problem.

The implicit scheme is unconditionally stable and may utilize a larger time step. Since the implicit method introduce terms evaluated at time $(t+dt)$, this method requires an additional boundary condition over the explicit method in the finite element equation. These values of the boundary conditions are obtained from a known downstream hydrograph. In ungauged watershed, the explicit method presents

a problem since no measurements are available for the downstream hydrograph.

The criterion that provides a guide for the selection of the time increment "dt" in case of using the explicit scheme is known as the Courant condition and can be written as

$$dt \leq \frac{dx}{c} \qquad \text{---------- (13)}$$

where

c = celerity of small wave

dt = time increment

dx = space increment

A similar relationship to the Courant condition for both the kinematic approach and the full dynamic approach can be obtained by the method of characteristics.

For the kinematic wave approach, the characteristic equation is

$$\frac{dx}{dt} = c_K \qquad \text{---------- (14)}$$

where c_K = kinematic wave speed

For the dynamic wave approach, the characteristic equation is

$$\frac{dx}{dt} = c_d = V \mp \sqrt{gh} \qquad \text{---------- (15)}$$

where c_d = dynamic wave speed

In the case of application of the kinematic wave equation, the kinematic wave speed (c_K) should be used. The value of the kinematic wave speed depends on the resistance formula being used. If the resistance formula is expressed in the following form

$$q = a h^m \qquad \text{---------- (16)}$$

where q = discharge/unit width, then from Manning formula

$$q = \frac{1.49}{n} h^{5/3} S^{1/2} \qquad \text{---------- (17)}$$

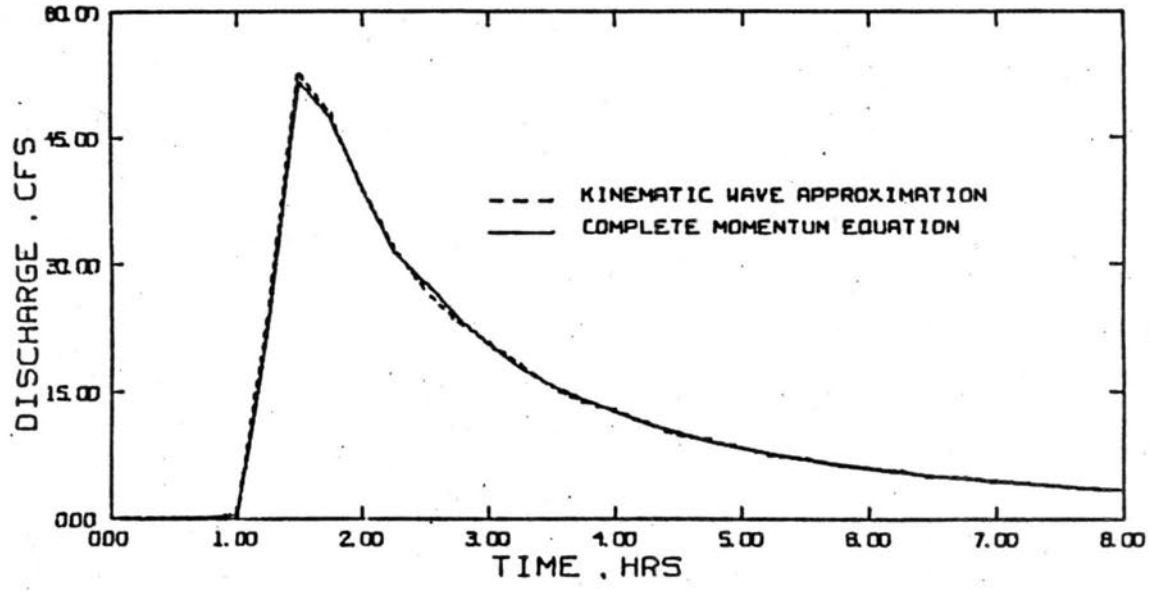

Figure 6. Comparison of channel hydrographs generated for subshed No. 1 of Crab Creek watershed (see Figure 54) using the full momentum solution and the KWA. After Ross.

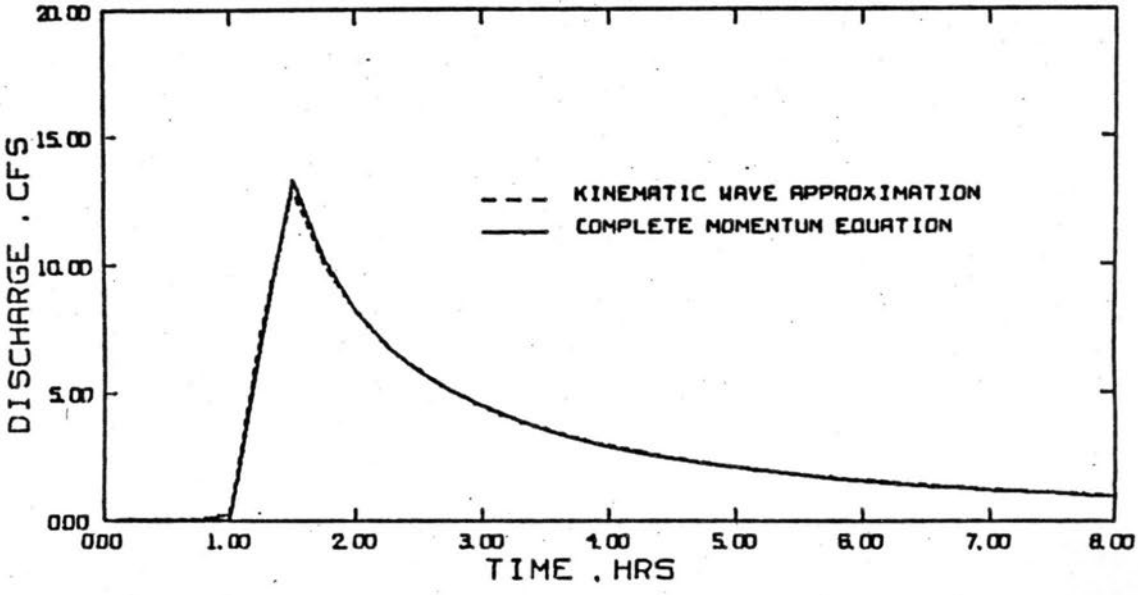

Figure 7. Comparison of channel hydrographs generated for subshed No. 2 of Crab Creek watershed (see Figure 54) using the full momentum solution and the KWA. After Ross.

$$a = \frac{1.49}{n} S^{\frac{1}{2}} \qquad m = \frac{5}{3}$$

Henderson (41) gives the kinematic wave speed as

$$C_K = \frac{dq}{dh} = m a h^{m-1} \qquad (18)$$

Since $$V = \frac{q}{h} = a h^{m-1} \qquad (19)$$

$$\therefore C_K = \frac{5}{3} V \qquad (20)$$

Ross (7) gives a mathematical example to illustrate the above concept. He considered a flow with a depth of (2) ft., velocity of 1.5 ft/sec, length of flow plane of 100 feet, and a slope of 5%. Solving for (F) and (K) gives (0.187) and (71.6), respectively. If we assume that the kinematic wave approach can be applied, then, from equation (20), $C_K = 2.5$ and from equationn (15) $C_d = 9.52$ and the corresponding maximum values of "dt" for the kinematic and the dynamic wave approximations were obtained from equation (13) as 40 and 10.5 seconds, respectively. The smaller time increment will obviously result in saving in time and money.

In case of using the complete momentum equation in routing the flows, another time increment criterion must be satisfied. This criterion is due to the effect of the friction term S_f. The following condition govern the stability of the explicit integration scheme which can be obtained from Manning relationship.

$$dt \leq \frac{2.22 R^{4/3}}{g n^2 V|V|} \qquad (21)$$

Satisfying the above condition on small watersheds may require small time increments because of the small magnitude of the hydraulic radius relative to the flow velocity. This condition exists because channel slopes are generally steeper on small watersheds. The lesser

value of "dt" obtained by the Courant condition in equation (13) and the friction criterion in equation (21) must be used in order to get stable solution when the complete momentum equation is adapted.

The above criterion illustrate an advantage for using the kinematic wave approach in small watersheds when applicable. In the kinematic wave application, the Courant condition is the only time criterion that must be satisfied.

Figure (8) shows the differences in computational efficiency where the solution is shown for a concrete surface by the complete momentum and kinematic wave approachs. In this figure, the complete momentum and the kinematic wave theory solutions are shown at $dt = 5$ second compared to the kinematic wave approach solution at $dt = 1$ second. There is a small divergence of the solution of the complete momentum equation at $dt = 5$ second. This situation occurs even though the Froude number for this flow example is approaching the kinematic wave theory criterion of Froude number = 2. In case of smaller values of Froude number, the divergence in the solution will be more.

The best choice for selecting "dt" at any point in time would be that value which is equal to, or slightly less than, the travel time of flow from one node to the next during that time step. Following the above idea is impractical since each element would require a unique "dt" because of the different flow properties in each which will result in different velocities. Moreover, the value of the unique "dt" would vary as the flow properties change during the computational process represented in the marching in time solution. During the marching in time process, if the value of the new computed "dt" is too large, then there will be errors which would result from sudden change in flow pattern. In this case the linear function representation during this large time increment will not be valid.

With the above consideration in mind, it is clear that small

lengths, such as those in small watersheds will require small value of "dt" in order to get a stable solution. So from time = $\frac{\text{length}}{\text{velocity}}$, a small value of velocity will determines a longer time of "dt" to be used. This case is exist on the overland flow phase where the depth and velocity are small relative to those in the channel. Therefore the selection of a larger time increment for overland flow in conjunction with smaller time increment selected for channel flow will improve the computational efficiency.

Ross (7) suggested that the best approach is to assume a probable maximum velocity of flow for any given element node in a strip and use that value with the lengths of the shortest overland flow and channel flow elements to assign a "dt" to the entire flow strip. This can be done for every strip in the entire flow domain. But since the flow properties will not vary greatly from one strip to another in a given watershed, the same value of "dt" can be used for the entire watershed. The value of "dt" selected above is small enough to satisfy the extreme case of overland flow.

Using the same principle as in the overland flow, a smaller time increment can be choosen for the channel routing flow.

A reliable method should be followed to determine these time increments before running the model. The selection of the probable maximum velocity for both overland flow and channel flow was done from prior experience with the model (7).

The maximum value of "dt" obtained from the Courant condition might not give an acceptable convergent solution. Viessman, et. al. (9) state that for the fully explicit scheme, the best results can be obtained with a time increment that in 20 % of the time obtained from the Courant condition. This criterion in found to be applicable to the finite element method since the procedures for using the integration were identical to the fully explicit finite difference methods.

Using the data for the concrete surface mentioned before, Courant Condition was used to define the value of "dt" before the model excusion. The data for the concrete surface are : Length = 467 ft., Slope = 0.02, Manning n = 0.014 and rainfall = 7.44 inch/hr for 8 minutes. The computed velocity at peak discharge for dt = 1 second was assumed to approach the convergent solution. Using equation (20), the value of the kinematic wave speed C_K can be found. By using Courant condition equation (13) and for dx = 93.4 ft., the maximum allowable value of "dt" is 30.35 seconds. Figures (9) gives the hydrographs for different values of "dt". Error can be seen for the solution at dt = 10 seconds and higher. The solution for dt = 5 seconds is an acceptable one because of the small error involved. The 20% criterion of the time found by the Courant Condition is 6.7 seconds which can give a solution for the hydrograph that is nearly the same as that given at dt = 5 seconds. Therefore, the 20% criterion is necessary for valid hydrograph simulation using the explicit time integration scheme. The change in time increment on the output hydrograph can be seen clearly from figure (9).

Solution Convergence Due to Finite Mesh Refinment

The convergence of a solution might be affected by the size of the mesh. Coarse mesh might result in a non-convergent solution which will not improved by using a smaller time increment.

The above problem is significant where there is only single element in the flow strip. The problem is to determine the minimum number of elements need in a flow strip inorder to get a convergent solution.

Figure (10) shows the solution for the turf surface which was analyzed with different numbers of elements in the flow plane. The value of $\frac{dx}{dt}$ was held constant for each case. The solution is converged when the number of the elements

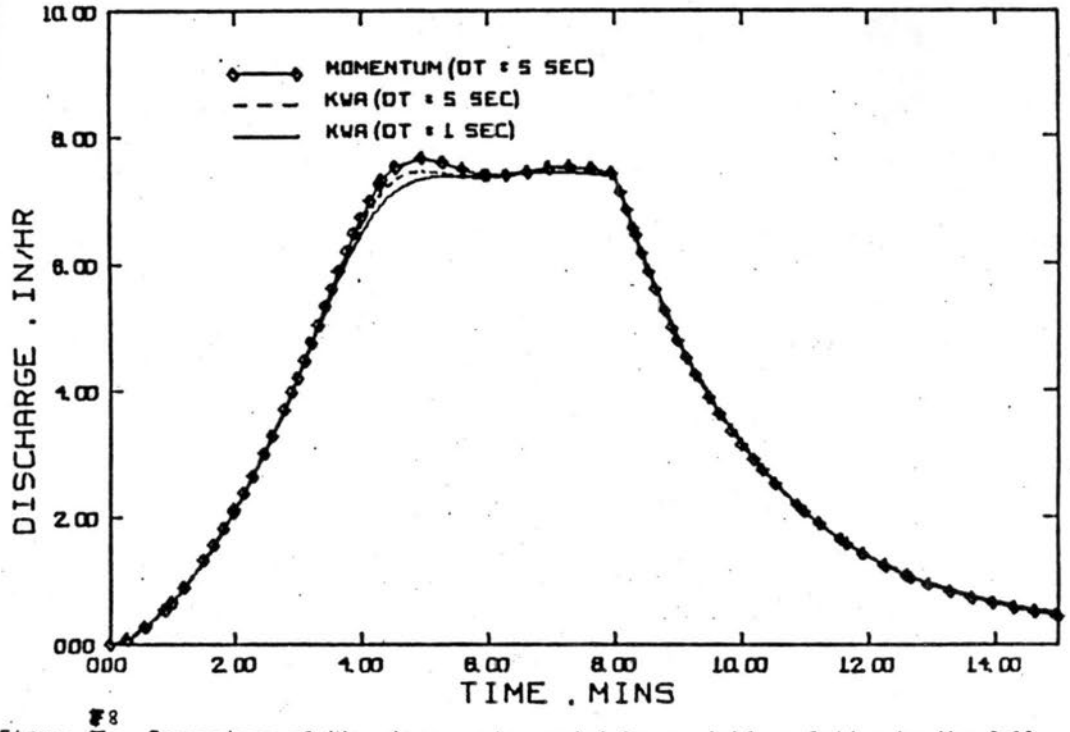

Figure 88. Comparison of time increments needed for a stable solution by the full momentum equation and KWA for a flow situation where the KWA is valid. After Ross.

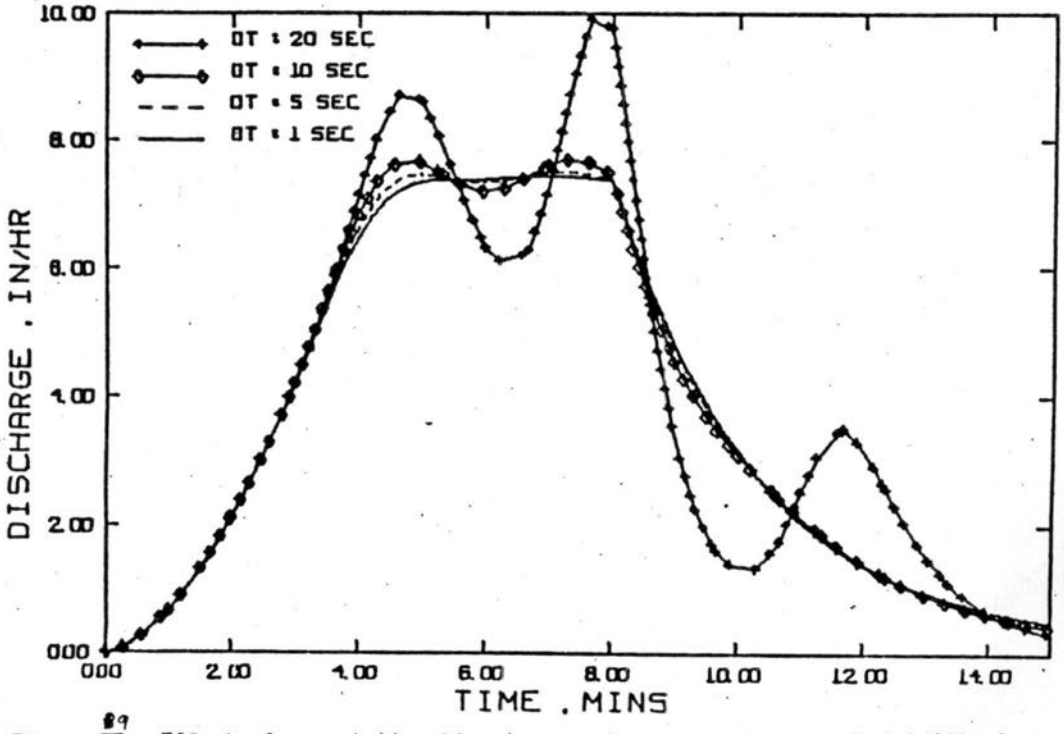

Figure 89. Effect of computation time increment on convergence and stability for a concrete surface. After Ross.

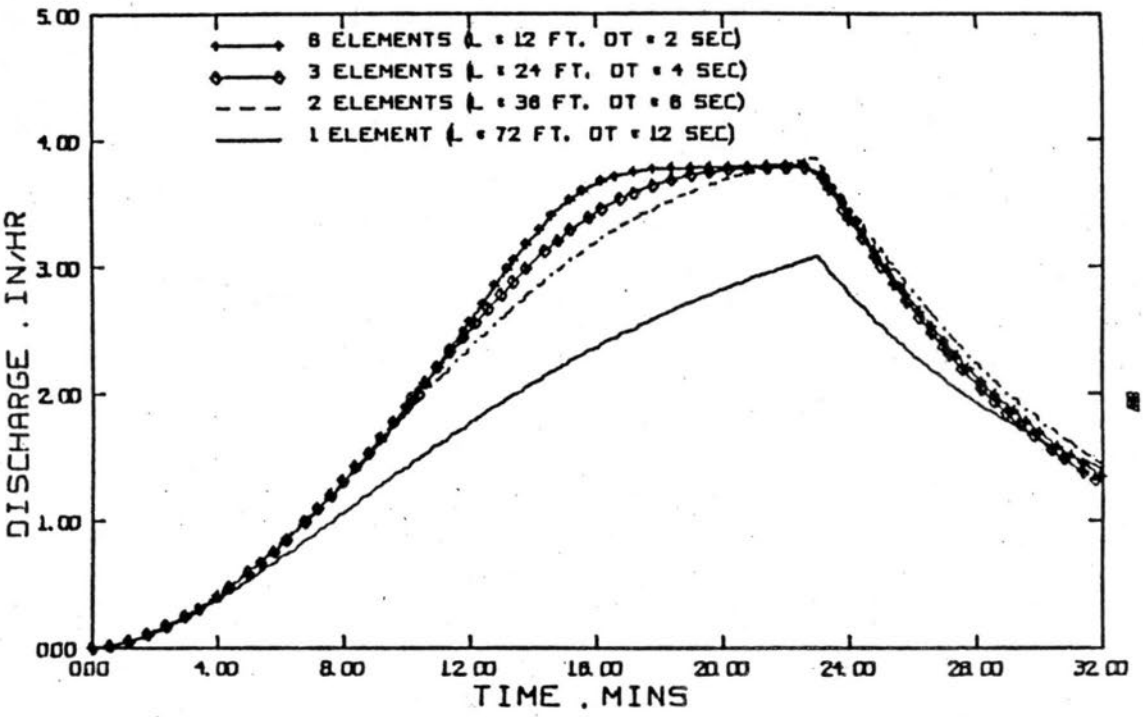

Figure 10. Effect of the finite element grid structure on convergence for a turf surface. After Ross.

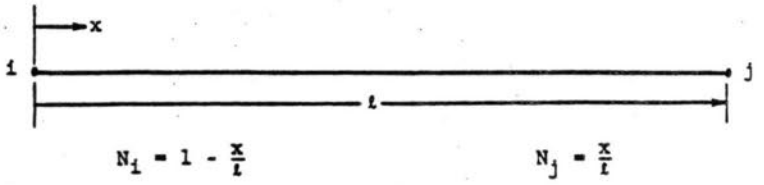

$N_i = 1 - \frac{x}{\ell}$ $\qquad$ $N_j = \frac{x}{\ell}$

(a) Linear interpolation functions

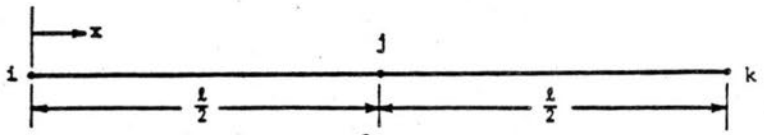

$N_i = (1 - \frac{2x}{\ell})(1 - \frac{x}{\ell})$

$N_j = \frac{4x}{\ell}(1 - \frac{x}{\ell})$

$N_k = \frac{x}{\ell}(1 - \frac{2x}{\ell})$

(b) Quadratic interpolation functions

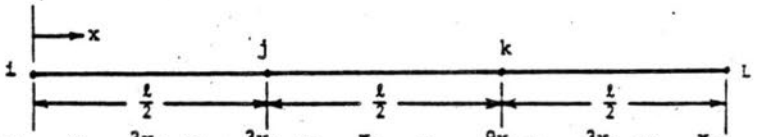

$N_i = (1 - \frac{3x}{\ell})(1 - \frac{3x}{2\ell})(1 - \frac{x}{\ell})$ $\qquad$ $N_j = \frac{9x}{\ell}(1 - \frac{3x}{2\ell})(1 - \frac{x}{\ell})$

$N_k = -\frac{9x}{2\ell}(1 - \frac{3x}{\ell})(1 - \frac{x}{\ell})$ $\qquad$ $N_L = \frac{x}{\ell}(1 - \frac{3x}{\ell})(1 - \frac{3x}{2\ell})$

(c) Cubic interpolation functions

Figure 11. Linear, quadratic and cubic interpolation functions for one-dimensional elements. After Ross.

increased. Assuming that a convergent solution can not be obtained with a minimum of one or two elements. There are two approaches which may be taken. One of these is to generate additional elements inside the existing ones. The problem with this approach is the requirement to reduce the time step in order to accomodate the reduced length of the elements. Also due to the insertion of new elements, data preparation for these elements is needed.

The alternative approach without increasing the computational steps involves using higher order approximation functions for the interpolation functions. Quadratic or cubic interpolation functions can be used.

Ross(7) stated that the latter approach is the most efficient one since the same number of equations results for the assembling matrix from both the discretization procedure. Or in other words, the same number of equations must be solved in a flow strip consisting of three elements approximated linearly or one element approximated by a cubic function. However, some efficiency was lost due to the using of the higher order approximation function which results in a larger band width. Figure (11) shows the linear, quadratic, and cubic approximation functions. Figure (12) shows the comparison of solutions obtained by linear, quadratic, and cubic approximation functions for the tan f surface. From figure (12) it can be seen that the cubic and quadratic solutions approximate the (3) and (2) linear element solutions.

Ross(7) examined the effect of using higher-order interpolation functions on the total response of a natural water shed. He used one element per overland flow strip. Figure (13) shows that the convergence is enhanced as the order of the approximation function increased.

Ross(7) also examined the effect of using higher-order approximation functions to channel routing flow in order to

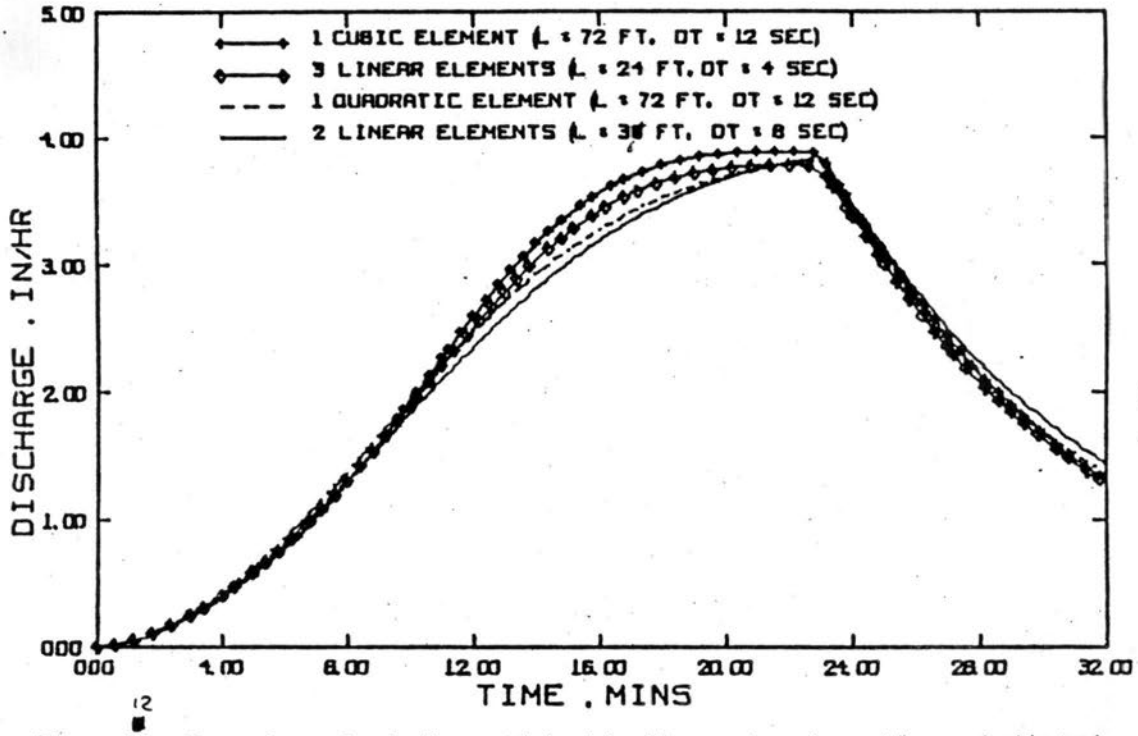

Figure 12. Comparison of solutions obtained by linear elements and by quadratic and cubic elements for a turf surface. After Ross.

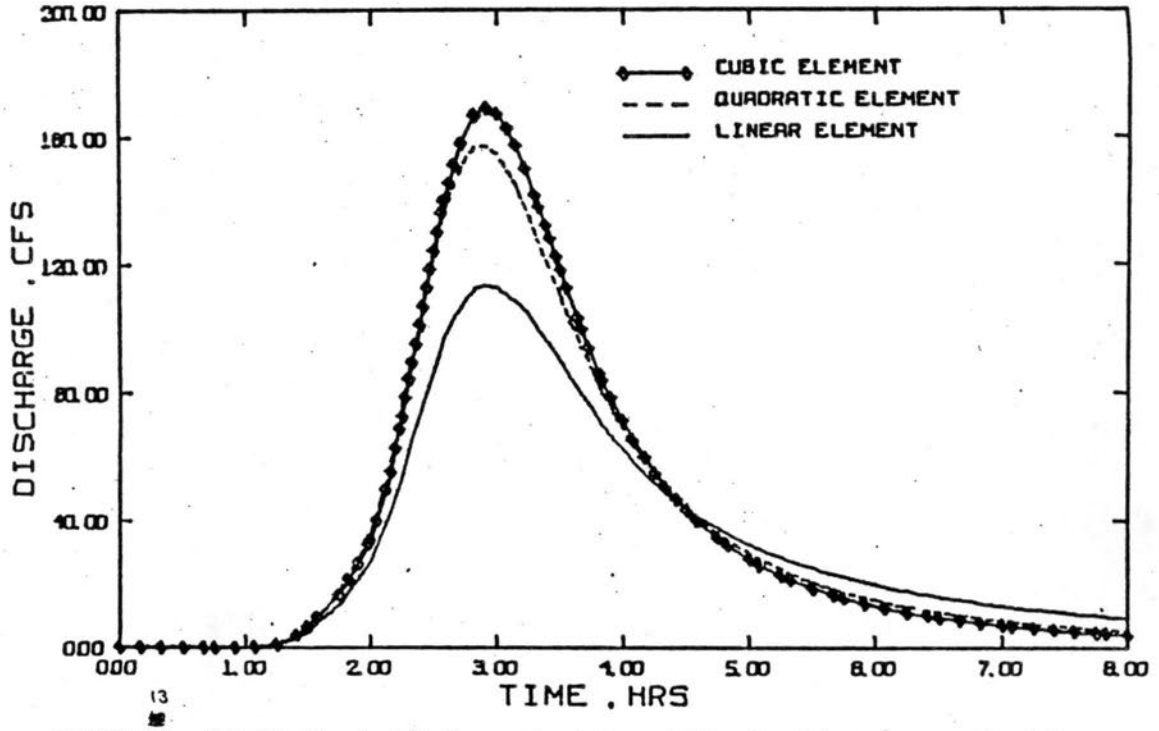

Figure 13. Effect of using higher-order interpolation functions for overland flow elements on convergence, Pony Mountain Branch watershed (Figure 47). After Ross.

see how these functions improve the solutions. Figure (14) shows the solutions for the channel flow in a subshed and in a total watershed. The improvement in the solution is very small.

These were a great improvement in the solution of overland flow phase by using higher-order approximation functions in contrast to little improvement in channel flow phase by using the same higher-order functions in spite of the identical mathematical formulation for the flow phases. Ross (7) claimed that the relative magnitude of the velocities is responsible for this inequality.

To examine the effect of velocity, the turf surface was used with the following data:

Length = 72 ft., slope = 0.01, Manning n = 0.35, and rainfall = 3.81 inch/hr for (23) minutes.

The flow velocities were changed to a higher values. This was done by changing the Manning coefficient to (0.175) and (0.035) from the original Manning value of (0.35). The original velocity was changed by a factor (2) and (10) for a given cross-section area of flow.

The results of these analyses show that as the velocity increases, the magnitude of the error between the linear and the higher order approximations decreases. Figure (15) shows that as the velocity increases, the error between the linear and the quadratic approximations decreases.

Ross (7) examined another aspect of the finite element method and that is the effect of using different element lengths verses using equal element lengths on the solution represented by the outflow hydrograph. Figure (16) shows the effect of using different line element lengths ratio. The turf surface as it was explained before is used in figure (16) as an example. The result shows that different line element length has small influence on the outflow hydrograph.

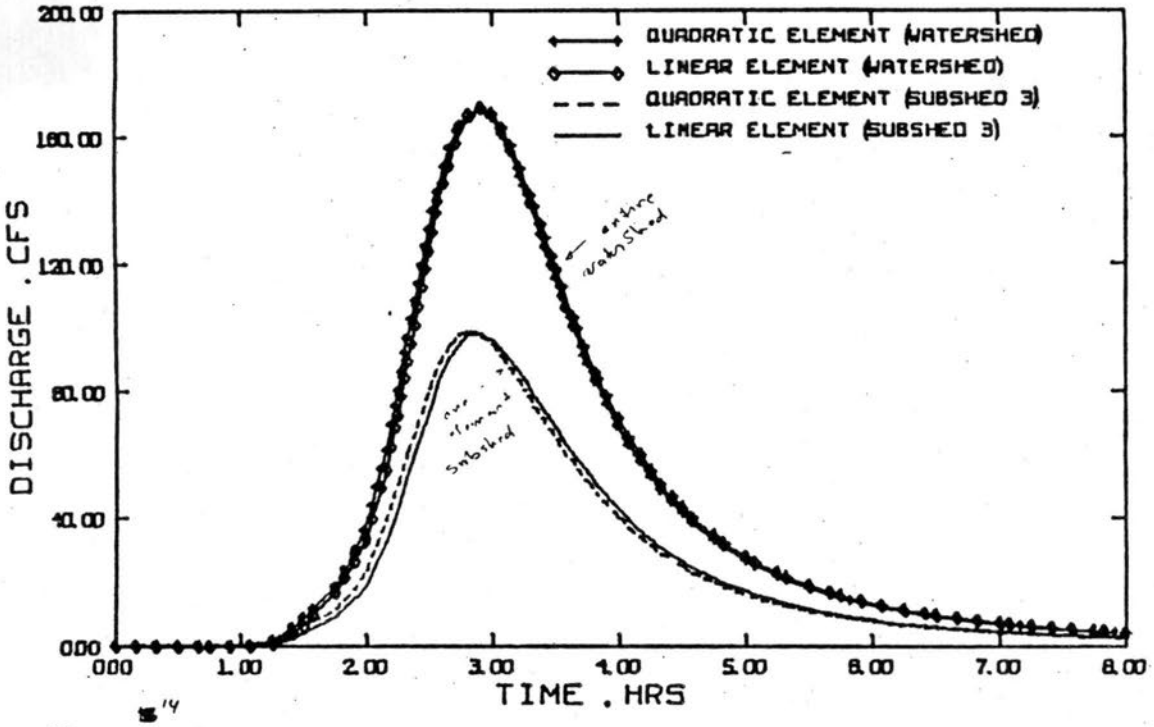

Figure 14. Effect of using a quadratic interpolation function for the channel flow element in subshed No. 3 of Pony Mountain Branch watershed (Figure 47). After Ross.

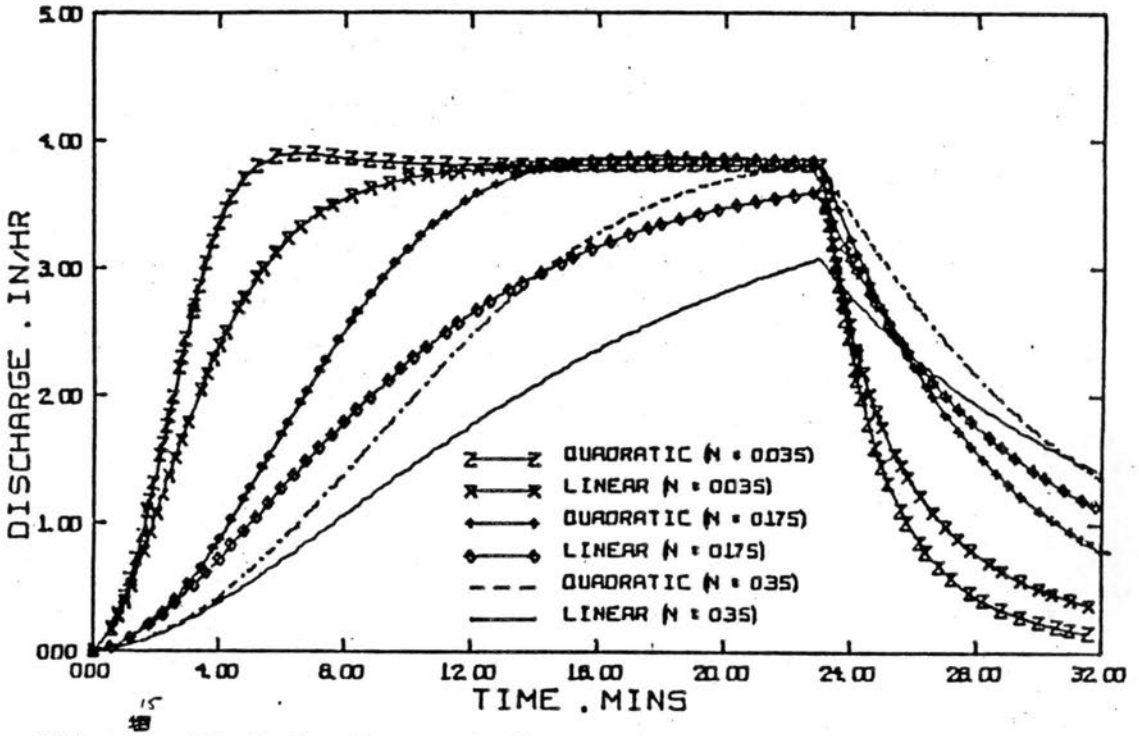

Figure 15. Effect of an increase in flow velocity on the error between solutions obtained by linear and quadratic interpolation functions for a turf surface After Ross.

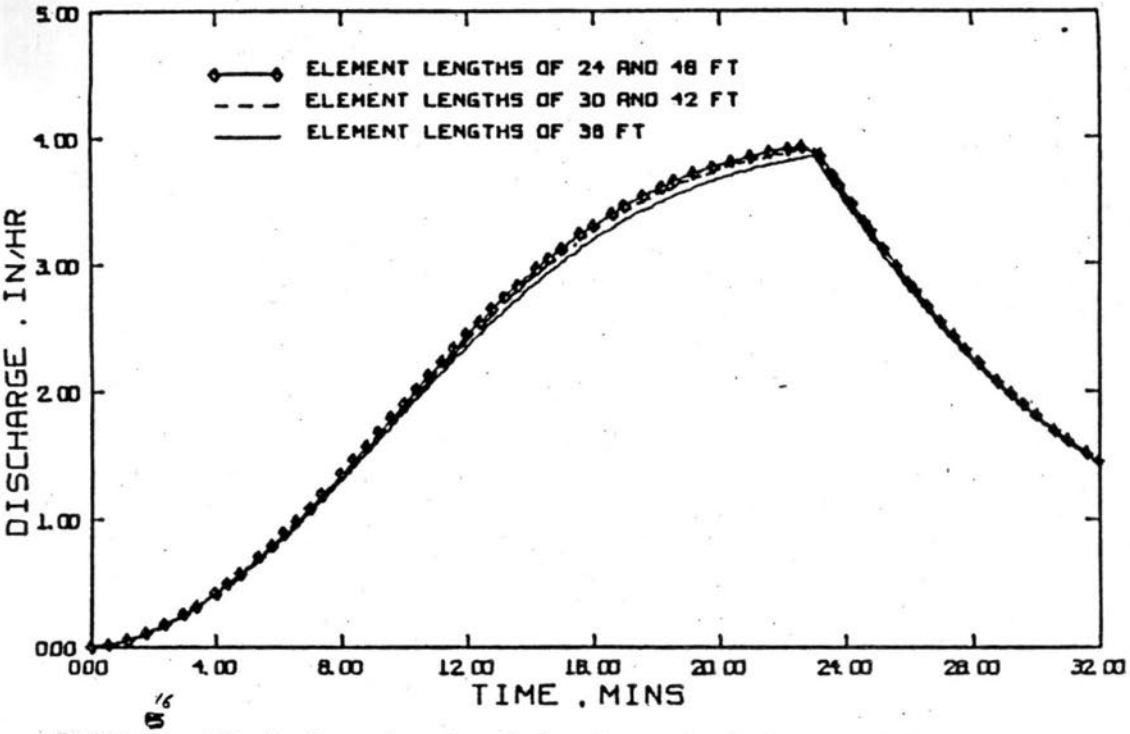

Figure 16. Effect of varying element lengths on the 2-element solution obtained for a turf surface. After Ross.

Conclusions and Recommendations

The following points can be infered from the study:

1- The finite element method seems to be an adequate suprior alternative method beside the other methods to solve and analyze the run-off problem.

2- The finite element method handles complex geometry, different boundary conditions. These properties represent a major advantage over the other techniques such as the finite difference method which has limited application in this direction.

3- The Galerkin's method of weighted residual applied in the study gives good results for both results for both the kinematic wave approximation and the complete dynamic approach.

4- The study showed that the kinematic wave approximation is a valid application on overland flow. This point has been verified by different researchers. The same approach was found to be applicable for most channels flow in small watersheds. It was found that kinematic wave approximation is not valid in relatively large rivers. This is due to the fact that the acceleration terms and the gradient term in the complete full dynamic equation (i-e $\frac{\partial u}{\partial t}$, $u\frac{\partial u}{\partial x}$, $\frac{\partial h}{\partial x}$) are more dominant and these values are larger compared to the gravitational and frictional terms. Therefore, the simulation to such rivers can be achieved through the dynamic wave formulation.

5- Study showed that the convergence of the solution might be affected by the size of the mesh. As the size decreases, i-e, the number of the elements increase, the solution converged. As a matter of fact if the finite element equations are written for every point in the flow domain, then we will get the exact solution. The approach of using more elements for the purpose of convergence is not warrented because of economic and time limitations. Another suprior approach in dealing with the problem of convergence is the using of the

higher-order approximation functions which proved to be effective in overland flow phase.

6- It was found that certain criterion for the time increment should be set in order to get a convergent solution. It was found that 20% the time founded by the Courant equation is necessary for a convergent solution using the kinematic wave approximation. For the complete momentum solution to converge, another time test criterion was adapted beside the Courant condition. The lesser value should be used in order to get a stable solution.

7- It was found that using equal element length verses using different element lengths has relatively no influence on the output solution.

The overland flow problem can be represented more accurately in two dimensions than in one dimension. This point is suggested for more research.

References

1- Al-Mashidani, G. and C. Taylor. "Finite element solutions of shallow water equations - surface runoff." Finite element methods in Flow problems, UAH Press, Huntsville, AL, 1974.

2- Desai, C.S., 1979. Elementary finite element method. Prentice-Hall, Inc., Englewood Cliffs, N.J.

3- Eagleson, P.S. "Dynamic hydrology" McGraw-Hill book company, 1971.

4- Henderson, F.M. Open channel Flow. The McGraw-Hill Book Co., Inc., New York, NY, 1971

5- Liggett, J.A. and D.A. Woolhiser, "the use of the shallow water equations in runoff computation" Proceeding of the third American Resources conference, San Francisco, Cal. NO. 8-10, 1967, PP. 117-126.

6- Lighthill, M.J. and G.B. Whitham, "On kinematic waves. I. Flood movement in long rivers" Proc. of the Royal Society of London. Vol. 229, May 1955, PP. 281-316.

7- Ross, B.B., 1978. A spatially responsive catchment model for predicting stormwater runoff from ungauged watersheds. Ph.D. Thesis, Va Polytech. Inst. State Univ., Blacksburg, Va.

8- Woolhiser, D.A. and J.A. Ligget, "Unsteady one dimensional flow over a plane - The rising hydrograph" water resources research Vol-3, NO.3, 1967, PP. 753-771.

9- Viessman, W., T.E. Harbaugh and J.W. Knapp. Introduction to hydrology. Intext educational publishers, New York, NY, 1972.